



UNIVERSIDADE D
COIMBRA

João Pedro Caria Vareda

**ENVIRONMENTAL CLEANING AND RECOVERY OF
HEAVY METALS VIA FUNCTIONALIZATION OF SILICA
AEROGELS**

PhD thesis in Chemical Engineering supervised by Professor Doctor Luísa Maria Rocha Durães and by Professor Doctor Artur José Monteiro Valente and submitted to the Department of Chemical Engineering of the Faculty of Sciences and Technology of University of Coimbra.

November 2021

Faculty of Sciences and Technology
University of Coimbra

Environmental Cleaning and Recovery of Heavy Metals via Functionalization of Silica Aerogels

João Pedro Caria Vareda

PhD thesis in Chemical Engineering supervised by Professor Doctor Luísa Maria Rocha Durães and by Professor Doctor Artur José Monteiro Valente and submitted to the Department of Chemical Engineering of the Faculty of Sciences and Technology of University of Coimbra.

November 2021



UNIVERSIDADE D
COIMBRA

Funding



This thesis was developed under the scope of two grants. Most of the work was conducted under the scope of the doctoral fellowship SFRH/BD/131280/2017 (2018-2021) with the workplan *Environmental Cleaning and Recovery of Heavy Metals via Functionalization of Silica Aerogels* granted by *Fundação para a Ciência e a Tecnologia* (FCT) funded by national funds and, when appropriate, co-funded by the European Commission through the European Social Fund.

This research was initiated with the grant from *Programa de Estímulo à Investigação 2015* with the project *AeroMCatch - Silica Aerogels for Remediation of Soils Contaminated with Heavy Metals* (Process No 141735; 2016-2017) funded by *Fundação Calouste Gulbenkian*.

I am grateful to the institutions for the grants received.



FUNDAÇÃO
CALOUSTE
GULBENKIAN

CENTRO 2020



PORTUGAL
2020



UNIÃO EUROPEIA
Fundo Social Europeu

Acknowledgments



I would like to acknowledge several people that had an impact on the development of this work.

My supervisor Luisa Durães for encouraging me to apply to scholarships and pursue a PhD, and for the mentorship along the years.

My supervisor Artur Valente for the many teachings and guidance.

To Marco Ferreira and Paulo Matos for accepting such challenging dissertation themes and contributing for this work.

Sílvia Gramacho for all the help with the atomic absorption spectroscopy analysis.

Pedro Santos for his help with the simulations and friendship.

To the friends at E01 for the joyful moments.

To my mother for supporting me.

Lastly, I acknowledge Elsevier, Springer Nature, the Royal Society of Chemistry, Taylor and Francis and MDPI for the right to reuse my published papers on this thesis.

Resumo



A poluição é um grave problema que pode conduzir a alterações irreversíveis, como a destruição de ecossistemas e perda de biodiversidade. Os metais pesados são os principais contaminantes de solos e águas subterrâneas na Europa. A sua principal fonte de emissão são atividades humanas, sendo as indústrias de extração e processamento de minérios as mais relevantes. Por serem poluentes não biodegradáveis, acumulam-se e a remediação de áreas contaminadas é difícil e nem sempre possível *in situ*. Desta forma, a preservação do meio ambiente passa pela minimização das emissões poluentes, sendo o tratamento de efluentes uma das estratégias para tal.

Nesta tese é estudada a remoção de cobre, chumbo, cádmio e níquel de água, através do processo de adsorção. Esta seleção recai na elevada importância destes quatro metais na sociedade atual, quer seja pela sua ampla utilização e valor económico, ou pelas elevadas toxicidade e emissões. O trabalho realizado foca-se no desenvolvimento de adsorventes para estes metais, através da síntese de aerogéis e xerogéis de sílica organicamente modificados e caracterização do processo de sorção dos metais por estes. Pretende-se desenvolver adsorventes que possam funcionar como uma solução transversal, removendo todos os metais contaminantes, mas também produzir soluções seletivas para cobre e níquel, devido ao seu valor económico.

Os adsorventes são sintetizados através da metodologia sol-gel, catalisada por ácidos e bases, sendo que a modificação da sua química de superfície é conseguida através de co-precusores organicamente modificados. Quando conveniente, a modificação dos grupos orgânicos dos precusores é feita *a priori* da síntese do adsorvente. A influência do processo de secagem, por extração com dióxido de carbono supercrítico ou por evaporação, nas propriedades do material final foi também avaliada. Os adsorventes foram alvo de caracterização física/estrutural, química e térmica.

Com o objetivo de remover todos os metais em estudo, a modificação das matrizes de sílica é feita através de grupos orgânicos contendo enxofre (tiol) ou azoto (p. ex. amina) como átomos dadores de electrões, dando origem à síntese de diferentes formulações. O estudo das matrizes modificadas com grupo tiol encontra-se no Capítulo 4 enquanto que o estudo das matrizes com

azoto encontra-se no Capítulo 5. A modificação da matriz de sílica conduz a uma diminuição de área de superfície específica. Quando as formulações contêm grupos amina, a sua secagem por evaporação densifica o material, levando a uma perda acentuada de porosidade e área de superfície específica, esta última podendo chegar a $2 \text{ m}^2 \text{ g}^{-1}$. A comparação com um aerogel não modificado revelou que a modificação da sílica é necessária para esta aplicação, pois o material não modificado apenas interagiu com chumbo (remoção para os restantes catiões $<9\%$ com uma concentração inicial de 50 mg L^{-1}). A generalidade das modificações verificou-se capaz de interagir com os metais em solução, sendo os grupos isocianurato e ureia as exceções (remoção $\leq 10\%$ com uma concentração inicial de catião 50 mg L^{-1} , exceto para chumbo). Os grupos amina são mais eficientes que os demais testados, tendo inclusivamente melhorado o desempenho sortivo de matrizes modificadas com tiol, mesmo em materiais de reduzida porosidade.

O estudo mais detalhado de formulações selecionadas revelou que processo de sorção é concluído em algumas horas e as interações com os catiões são fortes e dificilmente reversíveis. Foi selecionado o aerogel contendo aminas primárias e secundárias (A_A+3A) como o melhor adsorvente transversal para os catiões em estudo (capacidade de adsorção de Langmuir de 60 mg g^{-1} para cobre, 347 mg g^{-1} para chumbo, 83 mg g^{-1} para cádmio e 66 mg g^{-1} para níquel). O seu estudo em misturas binárias permitiu concluir que até seis horas de adsorção este material revela um comportamento seletivo para cobre (2.6 em relação a níquel e até 49 a cádmio). Assim o adsorvente A_A+3A é simultaneamente uma solução transversal e seletiva para cobre, sendo o resultado da adsorção controlado pelas condições operatórias. A sua regeneração por via química com ácidos é possível, mas conduz à perda parcial de características adsorptivas, para cerca de um terço da capacidade inicial. A recuperação do cobre dessorvido pode ser feita por eletrólise.

A modificação da matriz de sílica com certos ionóforos conduziu ao desenvolvimento de aerogéis seletivos. A introdução de azóis na sílica resultou num material que não interage com os catiões, não se verificando uma remoção significativa de cobre. Tal facto deve-se à inacessibilidade dos átomos dadores de electrões por parte dos catiões, sendo a distância entre estes (2.4 \AA) inferior ao raio hidratado dos catiões, devido a repulsão estérica dos grupos funcionais vizinhos e a repulsão electrostática. O adsorvente baseado num salen revelou propriedades estruturais semelhantes às de um aerogel mesmo após secagem evaporativa, devido a um encolhimento reduzido (10%), e tem uma acrescida afinidade para o níquel, sendo a sua capacidade remoção para este último superior e inalterada pela presença dos demais catiões. Apesar do modelo BET se ajustar melhor aos dados, de um ponto de vista estatístico, a existência de multicamadas de catiões não é plausível e o tipo de interações adsorvente-adsorvato é essencialmente definido pelo raio iónico dos catiões. A seletividade estimada revela que este adsorvente é duas vezes mais seletivo para níquel do que

para cobre e até 9 vezes para cádmio. Devido à forte interação com níquel a sua dessorção é muito limitada.

Assim, este trabalho permitiu demonstrar a elevada capacidade adsorptiva dos aerogéis de sílica modificados organicamente para metais pesados com presença relevante em efluentes de algumas indústrias, bem como em solos e águas, quando comparados com outros adsorventes comerciais ou em investigação. A assinalável versatilidade química da rede de sílica permite ainda adaptar facilmente a química de superfície destes materiais para obter soluções de remoção mais amplas ou seletivas, tirando cumulativamente partido da elevada porosidade e área de superfície dos aerogéis.

Abstract



Environmental pollution is a severe issue that might cause permanent changes, such as the destruction of ecosystems and loss of biodiversity. Heavy metals are the main pollutant in European soils and groundwater. Their main source are human activities, the most relevant being mining and ore processing. Their non-biodegradability causes accumulation in the environment and the remediation of contaminated sites is difficult and might not be possible to do *in situ*. Thus, the preservation of natural environments is dependent on minimizing pollutant emissions, with effluent treatment being one possible approach.

In this thesis the removal via sorption of copper, lead, cadmium and nickel from water is studied. These were selected due to their current relevance based on wide application, economic value, high toxicity and emissions. The focus of the work is the development of adsorbents for these metals, achieved by the synthesis of organically modified silica aerogels and xerogels, and the study of the sorption process. The goal is the development of a multipurpose solution, able to remove all pollutants, as well as producing selective copper and nickel adsorbents, due to high economic value of these metals.

The adsorbents are synthesized through acid-base catalyzed sol-gel chemistry. The surface chemistry modification is achieved by using precursors containing organic moieties of interest. When appropriate, the organic groups on the precursors are modified prior to the gel's synthesis. The effects of the drying stage, via supercritical fluids extraction with carbon dioxide or via evaporative drying, on the final material's properties are also assessed. The adsorbents are characterized structurally, chemically and thermally.

To remove all cations under study, the silica matrixes are modified with organic groups containing sulfur (thiol groups) or nitrogen (*e.g.*, amine) electron donor atoms, resulting in several different formulations. The study of silica matrixes modified with thiol groups is presented in Chapter 4 whilst the study of nitrogen modified matrixes is in Chapter 5. The modification of the silica matrix was found to reduce the specific surface area. Formulations containing amine groups are densified when dried by evaporation, severely decreasing porosity and surface area, the latter as low as $2 \text{ m}^2 \text{ g}^{-1}$. Comparing with pristine (non-modified) matrixes, it was revealed that the surface chemistry modification is required for this application, with the former only interacting with lead

(the removal for the remainder cations is <9% with a starting concentration of 50 mg L⁻¹). In general, the modified matrixes interact with the cations in solution, with isocyanurate and urea groups being notable exceptions (removal <10% with a starting cation concentration of 50 mg L⁻¹, except for lead). Amine groups are the most efficient of those tested, improving even the adsorptive performance of thiol modified sorbents, even on materials of reduced porosity.

The in-depth study of selected formulations revealed that the sorption takes a few hours, and the adsorbent-cation interactions are strong and not easily reversible. The aerogel containing primary and secondary amines (A₁A+3A) was chosen as the best multipurpose adsorbent (Langmuir adsorption capacity of 60 mg g⁻¹ for copper, 347 mg g⁻¹ for lead, 83 mg g⁻¹ for cadmium and 66 mg g⁻¹ for nickel). Its study with binary mixtures of cations revealed that it is selective for copper up to six hours of the adsorption process (selectivity of 2.6 in relation to nickel and 49 in relation to cadmium). Thus, A₁A+3A is both the multipurpose solution and the copper selective one, and the outcome of the adsorption is controlled by the operating conditions. Desorption of the cations from this material is possible with acids, but it leads to partial loss of the sportive performance, to a third of the original one. The recovery of desorbed copper can be achieved via electrodeposition.

The modification of the silica matrix with certain ionophores led to the synthesis of selective aerogels. The azole modification of the silica generated a material that interacts poorly with the cations; hence a significant removal of copper was not observed. This result was attributed to the possible inaccessibility of the azole groups in the matrix, as these are smaller (2.4 Å across) than the cations, due to steric hindrance of neighboring groups and electrostatic repulsion. The nickel selective, salen based adsorbent features aerogel-like characteristics (as it suffered a small shrinkage of 10% after evaporative drying) and has a high affinity for nickel. Its removal is the highest and unaffected by the presence of competing ions. Despite the BET model describing the data better, from a statistical point of view, the existence of cation multilayers is unlikely, and the aerogel-cation interactions are defined by the hydrated radius of the cation. Its estimated selectivity reveals that this adsorbent is twice as selective for nickel than for copper and 9 times than for cadmium. Due to the high affinity with nickel, its desorption is very limited.

This work allowed to demonstrate the high adsorptive performance of organically modified silica aerogels for heavy metals relevant in some industrial effluents, soil and water, when compared with other commercial or researched adsorbents. The great chemical versatility of the silica matrix also allowed to adapt its surface chemistry to obtain more general use or selective solutions, taking advantage of the high porosity and surface area of aerogels.

Table of Contents



Funding.....	i
Acknowledgments.....	iii
Resumo.....	v
Abstract	ix
Table of Contents	xi
List of Figures.....	xv
List of Tables	xix
List of Acronyms	xxiii
List of Symbols.....	xxv
Chapter 1 Introduction	1
1.1. Motivation	2
1.2. Goals	4
1.3. Thesis Structure.....	4
1.4. Dissemination of Results	5
Chapter 2 Heavy Metals in the Environment.....	7
2.1. Chemistry of Heavy Metals	8
2.2. Legislation for Heavy Metals.....	13
2.3. Heavy Metal Polluted Sites	16
2.3.1. Sites Affected by Mining Activity	17
2.3.2. Sites Affected by Industrial Activity.....	22
2.3.3. Other Sites.....	27
2.3.4. Portugal.....	29
2.4. Techniques for Removal of Heavy Metals from Aqueous Media	30
2.4.1. Overview of Heavy Metal Removal Techniques.....	31
2.4.2. Suitability of Removal Techniques for Real World Media.....	34
Chapter 3 Aerogels as Adsorbents of Heavy Metals	37
3.1. Sorptive Processes.....	38
3.1.1. Adsorption Mechanisms	39

3.1.2.	Adsorption Kinetics	40
3.1.3.	Adsorption Isotherms	41
3.1.4.	Adsorption Thermodynamic Parameters	43
3.1.5.	Desorption and Adsorbent Regeneration	43
3.2.	Heavy Metal Adsorbents in the Literature	44
3.3.	Silica Aerogels.....	52
3.3.1.	Synthesis via Sol-Gel Chemistry	53
3.3.2.	Properties and Applications	58
3.4.	Tailoring Aerogels as Heavy Metal Adsorbents	60
Chapter 4	Silica-Based Adsorbents with Thiol Groups.....	63
4.1.	Experimental Procedures.....	65
4.1.1.	Materials	65
4.1.2.	Preparation of Adsorbents	65
4.1.3.	Batch Adsorption Experiments	66
4.1.4.	Characterization of Materials	67
4.2.	Characteristics of the Adsorbents	68
4.3.	Adsorption Performance of Xerogel and Aerogel Counterparts	73
4.4.	Adsorption Kinetics	74
4.5.	Adsorption Isotherms	76
4.6.	Conclusion	80
Chapter 5	Silica-Based Aerogel Adsorbents with Nitrogen-Containing Groups.....	83
5.1.	Experimental Procedures.....	85
5.1.1.	Materials	85
5.1.2.	Preparation of Silica-based Adsorbents.....	85
5.1.3.	Batch Adsorption Experiments	86
5.1.4.	Desorption Tests and Metal Recovery	87
5.1.5.	Characterization of Materials	88
5.2.	Investigation on the Adsorption Performance Advantage of Amine Groups	88
5.3.	Effect of scCO ₂ on Surface Groups	91
5.4.	Synthesized Adsorbents and Characterization	92
5.5.	Preliminary Sorption Tests and Screening of Adsorbents.....	99
5.6.	Effect of pH and Adsorbent Dose on Adsorption	100
5.7.	Adsorption Kinetics	101
5.8.	Adsorption Isotherms	105
5.9.	Adsorption Thermodynamics	107
5.10.	Competitive Adsorption in Binary Mixtures	109

5.11.	Desorption and Recovery of Copper.....	113
5.12.	Conclusion	119
Chapter 6	Silica-Based Adsorbents Modified with Metal Ionophores	121
6.1.	Experimental Procedures.....	123
6.1.1.	Materials	123
6.1.2.	Preparation of Azole Modified Silica Aerogel	123
6.1.3.	Preparation of Schiff Base Modified Silica Aerogel.....	124
6.1.4.	Batch Adsorption Experiments	125
6.1.5.	Characterization of Materials.....	125
6.2.	Geometry Optimization of POPTMS and HSPTMS.....	126
6.3.	Azole Modified Silica Adsorbent.....	126
6.3.1.	Characteristics of the Adsorbent	126
6.3.2.	Adsorption Performance	129
6.4.	Schiff Base Modified Silica Adsorbent	131
6.4.1.	Schiff Base Reaction	131
6.4.2.	Characteristics of the Adsorbent	132
6.4.3.	Adsorption Performance	135
6.4.4.	Kinetics, Competitive Sorption and Selectivity	139
6.5.	Conclusion	142
Chapter 7	Final Conclusions and Future Work	145
References	149
Annex I	Distribution of Heavy Metals in Different Locations.....	175
Annex II	Copper and Nickel Ionophores.....	187
Appendix A	Thermogravimetric Data.....	203
Appendix B	Desorption Data	207
Appendix C	Simulation Details and Optimized Geometries Data.....	211

List of Figures



Figure 1 - Schematic representation of heavy metal emissions from ore extraction and processing.	2
Figure 2 - Speciation diagrams for the cations under study in the M^{2+} -OH system. M^{2+} refers to a divalent cation. $[M^{2+}]_{Total} = 1\text{mM}$ [34-37].	8
Figure 3 - Mechanisms of heavy metal cations transport through different natural media.	12
Figure 4 - Representation of different interactions that heavy metals can suffer in the soil and the process of phytoremediation. Soil particles designate all solid soil constituents.	12
Figure 5 - Evolution of the relative emissions of heavy metals across the EEA-33, indexed to 1990 [13].	13
Figure 6 - Photographs of some studied areas: (a) polluted streams in Yiyang; (b) mine tailing deposits in S. Francisco de Assis; (c) Lubumbashi river; (d) Coal mines around Qingshui River.	18
Figure 7 - Distribution of the heavy metals in Iberian Peninsula (a) in soils (quantities in mg kg^{-1}) and (b) in water (quantities in $\mu\text{g L}^{-1}$).	30
Figure 8 - Schematic representation of heavy metal laden aqueous effluents treatment processes: a) chemical precipitation; b) coagulation-flocculation; c) ion-exchange; d) adsorption; e) membrane filtration; f) electrodeposition.	33
Figure 9 - Evolution of the number of publications per year, according to the <i>Web of Science</i> database for the past fifteen years, in heavy metal adsorption and adsorbents. Search keywords: heavy metal* and sorption, adsorption, adsorbent, sorbent. Data obtained at 22/04/2021.	45
Figure 10 - Maximum adsorption capacity for heavy metal cations, according to the literature data reported in Table 19.	47
Figure 11 - Representation of the nanostructure of mesoporous silica aerogels. Reprint from [356] with permission from Elsevier.	55
Figure 12 - Representation of structural changes during aerogel drying stage and corresponding definition.	56
Figure 13 - Schematic representation of (a) a Schiff base ($R_1 \neq H$), (b) a crown ether and (c) a porphyrin.	61
Figure 14 - Photographs of M and AM xerogels (X) and aerogels (A).	69

Figure 15 - Microstructure of M and AM materials observed by FE-SEM with a 25kx magnification. 71

Figure 16 - Effect of pH on adsorption performance reported by (a) Dinh Du *et al.* [296] on amine functionalized MCM-41. Copyright 2019 Pham Dinh Du *et al.*; (b) Fan *et al.* [239] on disulfide bridged silica xerogel Reprint with permission from Springer Nature. 73

Figure 17 - Adsorption isotherms of (a) copper and (b) lead on AM counterparts. 74

Figure 18 - Sorption kinetics for (a) copper, (b) lead, (c) cadmium and (d) nickel on M and AM adsorbents. 75

Figure 19 - Sorption isotherms for (a) copper, (b) lead, (c) cadmium and (d) nickel onto M and AM adsorbents. 77

Figure 20 - SEM micrographs and approximate composition by EDS, assessed on the marked region, of adsorbent particles after adsorption: (a) Cu; (b) detail of Cu salts; (c) Pb; (d) detail of Pb salts; (e) Cd; (f) detail of Cd salts; (g) Ni; (h) detail of Ni salts. 79

Figure 21 - XRD patterns of the sample AM after adsorption of Cu and Pb. 80

Figure 22 - Isotherm curves for (a) copper and (b) lead adsorption on B and A xerogels. 89

Figure 23 - Kinetic curves for (a) copper and (b) lead adsorption on B and A xerogels. 90

Figure 24 - ¹³C CP-MAS NMR spectra for sample A_A. 91

Figure 25 - Photographs of the prepared modified aerogel and xerogel adsorbents. 92

Figure 26 - Morphology of the prepared aerogel samples (10kx magnification) and details for samples A_TRIS and A_U (30kx magnification). 95

Figure 27 - FTIR spectra for different nitrogen-containing groups modified xerogels and aerogels. 96

Figure 28 - Thermogravimetric curves for the nitrogen-modified aerogels: (a) weight loss; (b) sample weight temperature derivative. 98

Figure 29 - The effect of: (a) initial solution pH at $C_0 = 50 \text{ mg L}^{-1}$; (b) adsorbent dose at $C_0 = 500 \text{ mg L}^{-1}$ on heavy metals removal by aerogel A_A. 101

Figure 30 - Sorption kinetics for (a) copper, (b) lead, (c) cadmium and (d) nickel on amine modified materials. 103

Figure 31 - Sorption isotherms for (a) copper, (b) lead, (c) cadmium and (d) nickel on amine modified materials. 106

Figure 32 - Aspect of sample A_A+3A after sorption equilibrium with copper (top) and nickel (bottom). 107

Figure 33 - Effect of temperature on the adsorption performance of A_A+3A. 109

Figure 34 - Kinetic curves for the total sorption in binary mixtures (a) containing copper or (b) without copper onto A_A+3A. 110

Figure 35 - Kinetic curves for the sorption of individual cations, in binary mixtures, onto A_A+3A: (a) copper sorption; (b) lead sorption; (c) cadmium sorption and (d) nickel sorption. 111

Figure 36 - Effect of (a) contact time on the desorption of copper and (b) loaded particles concentration on the desorption of the metal ions.....	114
Figure 37 - FTIR spectra of A_A+3A before and after regeneration with 1M HCl	115
Figure 38 - Copper adsorption capacity by A_A+3A in adsorption/desorption cycles.....	116
Figure 39 - SEM micrographs from A_A+3A (left) and A_A+3A after copper adsorption, washing and drying in an oven (right) at 30kx.	117
Figure 40 - Copper deposition on the cathode.....	118
Figure 41 - Schematic representation of the POPTMS formation reaction.	123
Figure 42 - Schematic representation of the HSPTMS formation reaction.....	124
Figure 43 - ¹³ C CP-MAS spectra of sample P.....	127
Figure 44 - Photograph of adsorbent P (left) and microstructure at 20kx magnification (right).	128
Figure 45 - Copper and lead sorption isotherms for sample P.....	129
Figure 46 - Zeta potential of sample P (left) and copper removal (right) at different pH values.....	130
Figure 47 - Representation of the computed optimum structure of the hydrolyzed POPTMS co-precursor.	131
Figure 48 - ¹ H NMR spectra for salicylaldehyde, APTMS and HSPTMS.....	132
Figure 49 - Photograph (left) and micrograph at 30kx magnification (right) of the Schiff base modified aerogel.....	132
Figure 50 - Infrared spectrum of the Schiff base modified adsorbent.	134
Figure 51 - Adsorption isotherms onto adsorbent SI in single-metal solutions.	137
Figure 52 - Representation of the optimized structure of the hydrolyzed HSPTMS co-precursor.	139
Figure 53 - Adsorption kinetics for the total uptake in binary mixtures of (a) nickel and (b) copper.	140
Figure 54 - Adsorption kinetics for (a) nickel and (b) copper, isolated and in binary mixtures... ..	140
Figure II. 1 - Representation of molecular structures of selected copper ligands. Proposed functional groups responsible for cation interaction are presented in blue.	190
Figure II. 2 - Fluorescence spectra changes and images reported by (a) Bing <i>et al.</i> [416] and (b) Gündüz <i>et al.</i> [418].	193
Figure II. 3 - Copper ionophores applied to modify materials/membrane sensors and representation of proposed functional groups responsible for cation interaction (in blue).	194
Figure II. 4 - Representative nickel ligands. Proposed functional groups responsible for cation interaction are presented in blue.....	197
Figure II. 5 - Colorimetric detection of nickel and absorbance changes as reported by (a) Peralta-Domínguez <i>et al.</i> [423] and (b) Kang <i>et al.</i> [425].	199
Figure II. 6 - Representation of nickel ionophores used to prepare membrane sensors and proposed functional groups responsible for cation interaction (in blue).	200

Figure C. 1 - Representation of the constructed simulation box used in the optimization of POPTMS. Dimensions: 2.5370 nm × 3.1676 nm × 2.5814 nm. The box contains 663 water molecules..... 213

Figure C. 2 - Atom numbering in the POPTMS molecule..... 213

Figure C. 3 - Representation of the constructed simulation box used in the optimization of HSPTMS. Dimensions: 2.6520 nm × 3.1410 nm × 2.4120 nm. The box contains 632 water molecules..... 215

Figure C. 4 - Atom numbering in the HSPTMS molecule..... 215

List of Tables



Table 1 - Chemical form, health effects and common sources for heavy metals.....	9
Table 2 - Selected properties of the cations in solution.	11
Table 3 - Background concentration for heavy metals in soils and river water.....	13
Table 4 - Maximum concentration level (MCL) for heavy metals in drinking-water and their toxicity.	14
Table 5 - Recommended maximum concentration level for heavy metals in irrigation water.	15
Table 6 - Limit values for heavy metal concentration in agricultural soils, sludges for agricultural use and sediments.	16
Table 7 - Classes of the geoaccumulation index, according to Müller [118].	18
Table 8 - Comparison of water concentration against water quality standards.	19
Table 9 - Geoaccumulation indexes for soils affected by mines.....	20
Table 10 - Geoaccumulation indexes for sediments in sites affected by mines.	22
Table 11 - Heavy metal concentration in wastewaters from selected industries.	24
Table 12 - Comparison of water concentration against water quality standards in watercourses affected by industrial activities.	25
Table 13 - Geoaccumulation indexes for soils and sediments affected by industrial activities.	26
Table 14 - Comparison of water concentration against water quality standards in watercourses of sites affected by several sources of pollution.....	28
Table 15 - Geoaccumulation indexes for soils and sediments in sites affected by several sources of pollution.	29
Table 16 - Comparison of advantages and disadvantages of different treatment techniques for heavy metal laden liquid media [58, 170, 175].	34
Table 17 - Relevant sorption kinetic models for heavy metals.	40
Table 18 - Relevant sorption isotherm models for heavy metals sorbates.....	41
Table 19 - Adsorption capacity, whenever possible from the isotherm model, for heavy metals by different adsorbents in the literature.....	48
Table 20 - Typical properties of silica-based aerogels [341, 352, 354, 355, 361].	58
Table 21 - Applications for silica-based aerogels and respective properties of interest.....	59
Table 22 - Summary of the gelation conditions for the prepared adsorbents.	66

Table 23 - Structural properties for M and AM adsorbents.....	69
Table 24 - Theoretical and experimental percentages of C, H, N and S chemical elements in M and AM xerogel samples.....	72
Table 25 - Total and surface amine and mercapto groups on the xerogel adsorbents.....	72
Table 26 - Copper and lead uptake for AM aerogel and xerogel counterpart ($C_0 = 500 \text{ mg L}^{-1}$, 24 h).....	74
Table 27 - Adsorption model fit parameters for sorption kinetics on M and AM adsorbents.....	75
Table 28 - Adsorption model fit parameters for sorption isotherms on M and AM adsorbents..	76
Table 29 - Aerogel/xerogel functional groups and samples nomenclature.....	86
Table 30 - Summary of the adjusted condensation/gelation conditions for the synthesis of nitrogen-modified aerogels and xerogels.....	86
Table 31 - Adsorption models fit parameters for sorption isotherms on B and A xerogels.....	89
Table 32 - Adsorption model fit parameters for sorption kinetics on B and A xerogels.....	90
Table 33 - Removal efficiency of copper and lead on M and A adsorbents.....	91
Table 34 - Structural properties of the aerogel and xerogel modified adsorbents.....	93
Table 35 - Chemical composition of the samples modified with nitrogen-containing groups.....	97
Table 36 - Heavy metal removal efficiencies, in percentage, for different adsorbents. $C_0 = 50 \text{ mg L}^{-1}$, pH 5, 20 °C, 24 hours.....	100
Table 37 - Parameters of kinetic models for the fast/first step of the kinetic curves of the referred adsorbent-adsorbate systems.....	102
Table 38 - Fit parameters for sorption kinetics on the three selected amine modified materials.	104
Table 39 - Fit parameters for sorption isotherms on the three selected amine modified materials.....	105
Table 40 - Thermodynamic characterization of the adsorption process for aerogel A+3A.....	108
Table 41 - Fitting parameters of kinetic models for the total sorption on A_A+3A.....	109
Table 42 - Fitting parameters of kinetic models for the sorption of individual cations, in binary mixtures, on A_A+3A.....	110
Table 43 - Selectivity for the adsorption of cations on A_A+3A.....	112
Table 44 - Effect of the desorption agent on cation desorption from A_A+3A after three hours.....	114
Table 45 - Elemental composition of sample A_A+3A before and after regeneration with 1M HCl.....	115
Table 46 - Copper recovery by electrolysis.....	118
Table 47 - Physical/structural properties of sample P.....	127
Table 48 - Chemical composition of sample P.....	128
Table 49 - Isotherm adsorption models fit parameters for sorption on sample P.....	129
Table 50 - Physical/structural properties of the Schiff base modified aerogel.....	132
Table 51 - C, H and N content of the Schiff base modified aerogel.....	134

Table 52 - Fit parameters for the isotherm models and maximum uptake by Schiff base modified aerogel.....	137
Table 53 - Fitting parameters of the kinetic models for the total sorption onto SI in binary mixtures.	139
Table 54 - Fitting parameters of the kinetic models for the sorption of nickel and copper isolated and in the presence of interfering ions, onto SI.....	140
Table 55 - Selectivity coefficients of the Schiff base-modified aerogel.	142
Table I. 1 - Heavy metal concentration in watercourses of sites affected by mines (minimum and maximum values).	177
Table I. 2 - Heavy metal concentration in soils and sediments of sites affected by mines (minimum and maximum values).....	178
Table I. 3 - Heavy metal concentration in watercourses in sites affected by industries (minimum and maximum values).....	181
Table I. 4 - Heavy metal concentration in soils and sediments in sites affected by industries (minimum and maximum values).	182
Table I. 5 - Heavy metal concentration in watercourses in sites affected by several sources of pollution (minimum and maximum values).....	184
Table I. 6 - Heavy metal concentration in soils and sediments in sites affected by several sources of pollution (minimum and maximum values).	185
Table II. 1 - Selected studies where the interaction of ligands with copper and interferents is evaluated.....	191
Table II. 2 - Selected works containing selective modified adsorbents or ISE towards copper..	195
Table II. 3 - Selected studies where the interaction of ligands with nickel is evaluated.	198
Table II. 4 - Selected works containing nickel ISE.	201
Table A. 1 - Onset and end temperatures and mass loss for each thermal phenomenon in the aerogels of Chapter 5.....	205
Table B. 1 - Desorption of copper from A ₂ S ₂ O ₈ with different desorption agents.....	209
Table B. 2 - Heavy metal desorption from A ₂ S ₂ O ₈ after three hours with multiple desorption agents. Effect of concentration of the cation and regeneration agent.	210
Table C. 1 - Cartesian coordinates of the hydrolyzed POPTMS precursor.	214
Table C. 2 - Cartesian coordinates of the hydrolyzed HSPTMS precursor.	216

List of Acronyms



AAAPTMS	<i>N</i> 1-(3-trimethoxysilylpropyl)diethylenetriamine
AAS	atomic absorption spectroscopy
AIC	Akaike information criterion
APTMS	(3-aminopropyl)trimethoxysilane
BET	Brunauer–Emmett–Teller
BIC	Bayesian information criterion
CPMAS	cross polarization magic angle spinning
DW	drinking water
EDS	energy-dispersive X-ray spectroscopy
EDTA	Ethylenediamine tetraacetic acid
FE-SEM	field emission scanning electron microscopy
FTIR	Fourier transform infrared spectroscopy
GLYMO	(3-glycidyloxypropyl)trimethoxysilane
HSAB theory	hard and soft (Lewis) acids and bases theory
HSPTMS	(<i>E</i>)-2-(((3-(trimethoxysilyl)propyl)imino)methyl)phenol
IW	irrigation water
MCL	maximum concentration level
MTES	methyltriethoxysilane
MTMS	methyltrimethoxysilane
NMR	nuclear magnetic resonance spectroscopy
ORMOSIL	organically modified silica
POPTMS	1-(1 <i>H</i> -pyrazol-1-yl)-3-(3-(trimethoxysilyl)propoxy)propan-2-ol
TEOS	tetraethyl orthosilicate
TTMSI	tris[3-(trimethoxysilyl)propyl] isocyanurate
UPTMS	1-[3-(trimethoxysilyl)propyl]urea

List of Symbols



C	bulk concentration of adsorbate species in the liquid phase	mg L^{-1}
c	concentration of adsorbent in an adsorption experiment	g L^{-1}
C_{BET}	Brunauer-Emmett-Teller constant	
D	maximum adsorbed amount at a given step in the double exponential model	mg L^{-1}
D_{pore}	average pore size	nm
E	constant in the intraparticle diffusion model	mg g^{-1}
I_{geo}	geoaccumulation index	
K	formation constant	
k_1	first order rate constant	h^{-1}
k_2	pseudo-second order adsorption rate constant	$\text{g mg}^{-1} \text{h}^{-1}$
k_{D}	adsorption rate constant in the double exponential model	h^{-1}
K_{d}	adsorbate distribution coefficient	L g^{-1}
K_{F}	Freundlich constant	$\text{mg g}^{-1} (\text{L mg}^{-1})^{1/n_{\text{F}}}$
K_{H}	Henry constant	L g^{-1}
k_{IPD}	intraparticle diffusion rate constant	$\text{mg g}^{-1} \text{h}^{-0.5}$
K_{L}	Langmuir constant; equilibrium constant for the first adsorbate layer in the BET model	L mg^{-1}
K_{S}	equilibrium constant for the upper adsorbate layer in the BET model	L mg^{-1}
m	mass of adsorbent in an adsorption experiment	g
q	adsorbate uptake	mg g^{-1}

Environmental Cleaning and Recovery of Heavy Metals via Functionalization of Silica Aerogels

q_m	maximum adsorption capacity in the Langmuir model	mg g^{-1}
r	pore radius	m
$RE\%$	removal efficiency of adsorbed species	%
R_L	Langmuir separation factor	
S_{BET}	Brunauer-Emmett-Teller specific surface area	$\text{m}^2 \text{g}^{-1}$
T	temperature	$^{\circ}\text{C}$
t	time	h
V	volume of liquid phase in an adsorption experiment	L
V_{pore}	pore volume	$\text{cm}^3 \text{g}^{-1}$
a	selectivity	
a_{pot}	potentiometric selectivity	
γ	liquid surface tension	N m^{-1}
ΔG^0	adsorption standard Gibbs free energy variation	kJ mol^{-1}
ΔH^0	adsorption standard enthalpy variation	J mol^{-1}
ΔP	pressure gradient in the aerogel pores	Pa
ΔS^0	adsorption standard entropy variation	$\text{J mol}^{-1} \text{K}^{-1}$
θ	liquid contact angle	$^{\circ}$
ρ_b	bulk density	kg m^{-3}
ρ_s	skeletal density	kg m^{-3}

Chapter 1

Introduction



1.1. Motivation

Environmental pollution, a challenge currently faced by mankind, leads to significant and possibly irreversible changes in the Earth's ecosystems. Contamination by heavy metals, the main pollutants in European soils and groundwater, is an example of such: it has anthropogenic origin and humanity struggles to deal with it [1]. Evidences of the use of metal objects by humans date back to the 5th millennium BCE [2], previous to what is considered to be the start of the bronze age, when humans first used metals [3]. Nowadays, we still rely on metals to enable the continued development of society, with these being used as raw materials in different industries [4-6]. Though naturally occurring, through weathering of parent materials, and some being biologically essential (for example, copper and chromium are micro nutrients [7]), pollutant emissions raise the concentration of these elements in natural environments to dangerous concentrations [8, 9]. Non-essential heavy metals are toxic to living organisms, as are the essential ones at high concentrations [7].

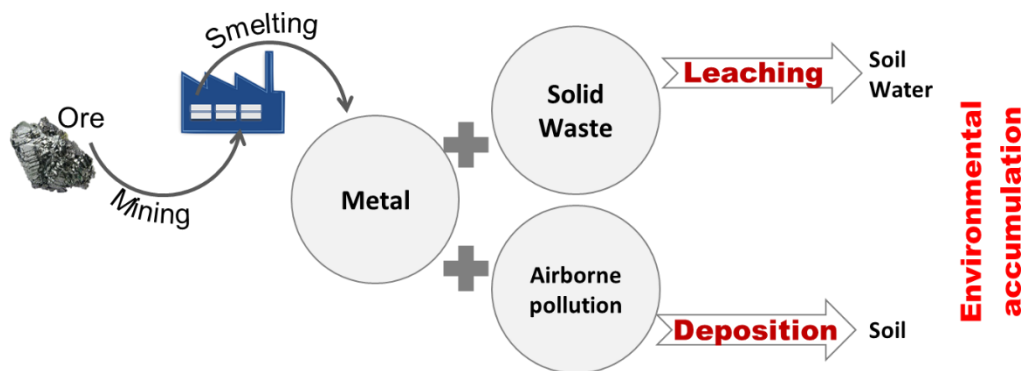


Figure 1 - Schematic representation of heavy metal emissions from ore extraction and processing.

After being released into the environment as solid, liquid and gaseous wastes, the heavy metals accumulate in soils and sediments due to different phenomena - Figure 1. Because of the dynamic equilibria within the ecosystems and between soil constituents themselves, heavy metals may be present in different phases such as the solid phase (immobilized contaminants) or dissolved in soil solution and watercourses (mobile contaminants) [9-12] and easily interchange between them. The latter form is the most dangerous because mobile species can leach *e.g.* to underground aquifers and be absorbed by living organisms.

Different methods for the decontamination of polluted sites, that are specific for soil, liquid, or gaseous media, have been proposed. Limitations in large scale implementation, economic viability and lack of restrictive legislation, hindered the application of solutions for the resolution of this issue via remediation of polluted media and/or rigorous treatment of effluents.

Copper, lead, cadmium and nickel feature high toxicity and are prone to human-made emissions and accumulation in the environment, as elaborated in Chapter 2. They are relevant resources in the majority of business sectors of contemporaneous societies [4, 6, 13].

Copper is the third most important metal by weight [14], its production is very high (estimated at 16 million tons yearly [5, 15]) and it is used in electrical equipment (60% of consumption), plumbing/construction, machinery, transport, coins, art, music instruments, kitchen utensils [6, 14] and to catalyze many reactions [16-18]. Copper is also a micronutrient in animals and plants.

Lead and its related compounds are very toxic [19]. Lead goods were used for many centuries, like the water pipes used in the Roman Empire [6]. In the USA lead water pipes are still a cause for concern in many places. Most recent uses of lead [19] have been banned: as gasoline additives, in solders, paint pigments and the EU plans to ban lead ammunition and fishing gear [20]. It is still used for lead-acid batteries and as radiation shields [6]. No biological functions are known [19].

Cadmium is highly toxic. It can be applied as a stabilizer in plastics, pigment in dyes, coating agents, accessories/jewelry, Ni-Cd rechargeable batteries and solar cells [21, 22], with the latter two contributing to impulse its use [22]. The EU has banned it from being used in plastics, paints and jewelry [23].

Nickel is ferromagnetic at room temperature [6] and an efficient catalyst [24]. It is used for the production of stainless steel (75% of its consumption [25]), alloys (Ni/Cr alloys are used for heating elements that withstand high temperatures, Ni/Fe and Ni/Al/Co alloys are used as magnets), nickel cast iron (jewelry, coins), corrosion-resistant coatings by electroplating and the production of batteries (nickel-metal hydride and Li-ion) [6, 26, 27]. Nickel is also important in biological processes, being a micronutrient for plants and cyanobacteria [27].

Due to the lack of best available materials, their accelerated production/consumption, mainly in China [25, 28], can cause their depletion in the next decades [5, 29]. Furthermore the exploration of more and lower grade ores, deeper deposits, mining in remote sites and keeping up with environmental standards, all necessary to satisfy the market, are projected to increase mining costs [5].

1.2. Goals

Copper, lead, cadmium and nickel are relevant, toxic and in risk of depletion. Many heavy metals are used as raw materials in different industries [4, 5] and have commercial value [5, 28], so minimizing their discharge has economic impact on businesses. Recovering metals via adsorption can become an effective way for avoiding their drainage and to make their consumption sustainable. There are also initiatives to achieve circular economy [30] in areas where metals are of paramount importance. Thus, the work developed in this thesis aims for:

- i) the removal of metal ions (copper, lead, cadmium and nickel) from contaminated aqueous environments, using functionalized silica gels as adsorbents;
- ii) recover valuable metal ions (copper and nickel) and regenerate the adsorbents, to enable their reuse and contribute to a sustainable growth of a metal-dependent society.

From the evaluated metals, only copper and nickel have increasing market value [5, 28] due to their high importance, reflected in increased demand and production [14, 15]. Therefore, only these two cations are economically viable to recover. Nevertheless, stock prices are sensitive to global events and copper's price has started to fall in 2019 [25] but is rebounding in 2020 [31]. In addition, the removal of cadmium and lead from aqueous media is of crucial relevance for ecosystems and global health due to their high toxicity.

The approach used to achieve the aforementioned goals encompasses the development of materials falling into two categories: a multipurpose solution, non-selective adsorbent, to enable the simultaneous removal of several heavy metals; the design of sorbents with selective affinities, allowing a selective and step-recovery of desired metals. The choice of adsorbent to implement at a given situation depends on the composition of the media being treated and the final purpose: recover relevant raw materials or simply comply with effluent discharge regulations. Accordingly, silica aerogels/xerogels functionalized with appropriate organic ligands are proposed as advanced adsorbents for the removal of heavy metals from polluted water environments. Both adsorbent and heavy metal are recovered with desorption and chemical/electrochemical methods, respectively.

1.3. Thesis Structure

The work presented in this thesis was developed through the period of two individual grants, *Prémio de Estimulo à Investigação* 2015 (AeroMCatch, 2016-2017) and FCT scholarship, (2018-2021).

The thesis is divided into seven chapters, briefly described below.

Chapter 1 frames the work developed in this thesis. It also describes its layout and compiles the different publications from the author from which the subsequent chapters are derived.

Chapter 2 features theory on heavy metals, their chemistry and a survey on pollution and treatment strategies associated with them.

Chapter 3 highlights the background on adsorptive processes, the synthesis of silica-based aerogels and a literature survey on adsorbents of heavy metals.

Chapter 4 presents the modification of silica-based xerogels and aerogels with thiol groups (accomplished under the scope of the AeroMCatch project) and their corresponding study as non-selective adsorbents through batch tests.

Chapter 5 presents the modification of silica-based aerogels with nitrogen-containing functional groups. Different functional groups are used to prepare several formulations. The impact of the synthesis methodologies on the materials properties are evaluated. Results on their adsorption performance, for single and binary cation mixtures, selectivity and regeneration are discussed. The recovery of the ions is investigated by various methodologies.

Chapter 6 reports the development of functionalized silica-based aerogel adsorbents modified by ionophores. The organically modified silica (ORMOSIL) adsorbents are prepared through the modification of the silica co-precursors. The samples are tested in single and binary mixtures, and selectivity and regeneration are evaluated.

Chapter 7 compiles the final conclusions and discusses perspectives for future work.

1.4. Dissemination of Results

The results obtained throughout the development of this PhD work were published in different journals, listed hereafter. The contents of the different chapters are mainly based on those.

Original Research papers:

Vareda, J. P.; Durães, L., Functionalized silica xerogels for adsorption of heavy metals from groundwater and soils. *Journal of Sol-Gel Science and Technology* 2017, 84, 400-408, 10.1007/s10971-017-4326-y.

Vareda, J. P.; Durães, L., Efficient adsorption of multiple heavy metals with tailored silica aerogel-like materials. *Environmental Technology* 2019, 40, 529-541, 10.1080/09593330.2017.1397766.

Lamy-Mendes, A.; Torres, R. B.; Vareda, J. P.; Lopes, D.; Ferreira, M.; Valente, V.; Girão, A. V.; Valente, A. J. M.; Durães, L., Amine Modification of Silica Aerogels/Xerogels for Removal of Relevant Environmental Pollutants. *Molecules* 2019, 24(20), 3701, 10.3390/molecules24203701.

Vareda, J. P.; Valente, A. J. M.; Durães, L., Silica Aerogels/Xerogels Modified with Nitrogen-Containing Groups for Heavy Metal Adsorption. *Molecules* 2020, 25, 2788, 10.3390/molecules25122788.

Review papers:

Vareda, J. P.; Valente, A. J. M.; Durães, L., Heavy metals in Iberian soils: Removal by current adsorbents/amendments and prospective for aerogels. *Advances in Colloid and Interface Science* 2016, 237, 28-42, 10.1016/j.cis.2016.08.009.

Durães, L.; Maleki, H.; Vareda, J. P.; Lamy-Mendes, A.; Portugal, A., Exploring the Versatile Surface Chemistry of Silica Aerogels for Multipurpose Application. *MRS Advances* 2017, 2, 3511-3519, 10.1557/adv.2017.375.

Vareda, J. P.; Lamy-Mendes, A.; Durães, L., A reconsideration on the definition of the term aerogel based on current drying trends. *Microporous and Mesoporous Materials* 2018, 258, 211-216, 10.1016/j.micromeso.2017.09.016.

Vareda, J. P.; Valente, A. J. M.; Durães, L., Assessment of heavy metal pollution from anthropogenic activities and remediation strategies: A review. *Journal of Environmental Management* 2019, 246, 101-118, 10.1016/j.jenvman.2019.05.126.¹

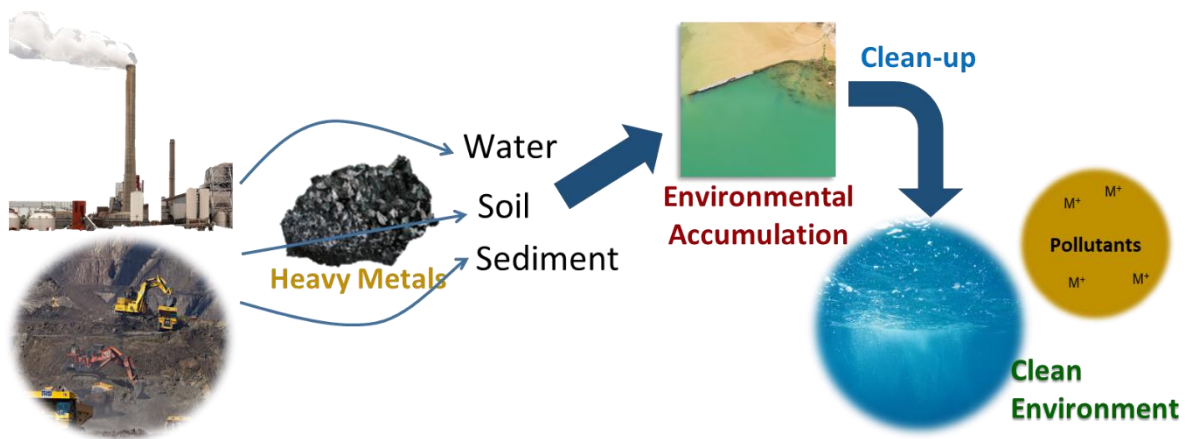
Vareda, J. P.; Valente, A. J. M.; Durães, L., Ligands as copper and nickel ionophores: Applications and implications on wastewater treatment. *Advances in Colloid and Interface Science* 2021, 289, 102364, 10.1016/j.cis.2021.102364.

Vareda, J. P.; García-González, C. A.; Valente, A. J. M.; Simón-Vázquez, R.; Stipetic, M.; Durães, L., Insights on toxicity, safe handling and disposal of silica aerogels and amorphous nanoparticles. *Environmental Science: Nano* 2021, 8, 1177-1195, 10.1039/D1EN00026H.

¹ Classified as *hot paper* and *highly cited paper* by the *Web of Science* platform.

Chapter 2

Heavy Metals in the Environment



The content of this chapter is based on the author's published works *Heavy metals in Iberian soils: Removal by current adsorbents/amendments and prospective for aerogels* and *Assessment of heavy metal pollution from anthropogenic activities and remediation strategies: A review*.

2.1. Chemistry of Heavy Metals

Heavy metal is a poorly defined term that refers to a group of elements with a density greater than 4 g cm^{-3} , including metals and metalloids like arsenic [32]. Table 1 summarizes typical forms and health effects of common heavy metals. Although there are several heavy metals (and metalloids) discussed in this chapter, only copper, lead, cadmium and nickel are under study in this thesis due to their significance as resources from which we are dependent, toxicity and environmental accumulation, as explained in Chapter 1.

The speciation of heavy metals plays a key role in their persistence in the environment; mobile forms can easily leach, spreading to different media, and are more bioavailable, being absorbed by living organisms [9-12]. Furthermore, some properties like toxicity are also dependent on the speciation - Table 1. The speciation curves for the heavy metals under study in this thesis in water are presented in Figure 2. In water, the ions can be solvated in multiple hydration spheres. Increasing the ionic radius, the charge density and the volume of the primary hydration sphere decreases [33]. Small primary hydration spheres have less dehydration energy and are therefore less stable. The ionic radius, charge density and hydration energy for the cations under analysis are reported in Table 2.

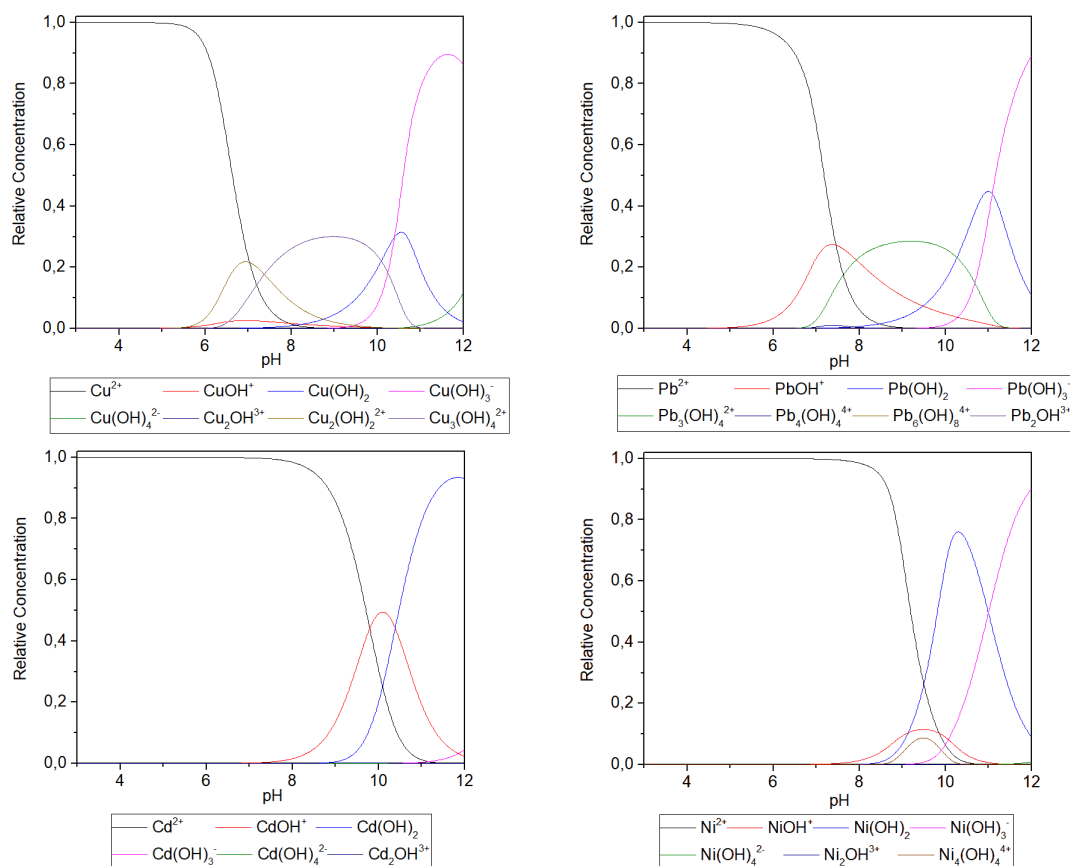








Figure 2 - Speciation diagrams for the cations under study in the M^{2+} -OH system. M^{2+} refers to a divalent cation. $[M^{2+}]_{\text{Total}} = 1 \text{ mM}$ [34-37].

Table 1 - Chemical form, health effects and common sources for heavy metals.

Heavy Metal	Chemistry	Effects on Human Health and Hazard Communication Pictograms	Common Sources	Ref.
Arsenic (As)	Occurs in -3, 0, +3 and +5 oxidation states. Most As is found as arsenate minerals. As(V) adsorbs more easily to sediments. In soils it predominates in anionic forms. As mobility increases with pH.	Carcinogenic, causes cardiovascular disease, development anomalies and neurologic disorders. 	Fossil fuel burning, pesticides, wood treatments, agriculture, medical and veterinarian uses, mining and ore processing.	[7, 10, 38]
Cadmium (Cd)	Occurs in 0 and +2 oxidation states. Found as carbonate and hydroxide at higher pH and as Cd(II) at low pH. In acid conditions, it has high mobility.	Negatively affects several enzymes, causes kidney malfunctions and bone disease. 	Impurity in phosphate fertilizers, detergents, petroleum products, biosolids, mining and ore processing.	[39-41]
Chromium (Cr)	Occurs in 0, +3 and +6 oxidation states. Cr(VI) is the most toxic and mobile oxidation state. Cr(III) is the preferred form at low pH. Its mobility is related to the soil's sorption characteristics. At high soil pH Cr(VI) becomes more leachable.	Causes allergic dermatitis and lung cancer. 	Releases from electroplating processes, disposal of Cr containing wastes, sewage treatment plants, mining and ore processing.	[10, 27]
Copper (Cu)	Occurs in 0, +1 and +2 oxidation states. Cu(II) is the most common and most toxic form. Copper solubility increases at pH 5.5. It usually complexes rapidly; after being introduced in the environment, it becomes immobilized.	Can cause anemia, damages to the liver and kidneys, stomach irritation. 	Fertilizers, sewage sludges, fuel combustion, mining and ore processing.	[14, 42, 43]
Mercury (Hg)	Occurs in 0, +1 and +2 oxidation states. Alkylated forms are also common and are the most toxic. Volatile in metallic form.	Changes enzymatic activity, causes kidney liver and neurological damage, Affects the reproductive system and is carcinogenic. 	Coal combustion, light bulbs production, chlor-alkali and vinyl chloride production, mining and ore processing.	[7, 10, 38]
Nickel (Ni)	Occurs in 0 and +2 oxidation states although others exist. Ni(II) is the most common form, exists at low pH and is leachable. At neutral or higher pH, Ni precipitates. It easily adsorbs to soil particles becoming immobilized.	Can cause dermatitis, lung, cardiovascular and kidney diseases and cancer. 	Nickel mining, fossil fuel combustion, metal processing industries.	[26, 27, 44]

Environmental Cleaning and Recovery of Heavy Metals via Functionalization of Silica Aerogels

Table 1 - Chemical form, health effects and common sources for heavy metals (concluded).



Heavy Metal	Chemistry	Effects on Human Health and Hazard Communication Pictograms	Common Sources	Ref.
Lead (Pb)	Occurs in 0 and +2 oxidation states. Pb(II) is the most common and reactive form. Forms low solubility compounds as pH increases.	Affects the kidneys, central nervous system, red blood cells. Causes development issues in children. 	Lead mining and smelting, coal burning, biosolids.	[10, 19, 45]
Zinc (Zn)	Occurs in 0 and +2 oxidation states being the latter the most common. It is bioavailable at high pH. Easily complexes or is sorbed.	Can cause damages to the brain, respiratory and gastrointestinal tracts and prostate cancer. 	Mining, waste combustion, steel processing, biosolids.	[42, 46, 47]

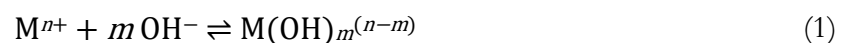
Table 2 - Selected properties of the cations in solution.

Heavy Metal	Ionic Radius /Å [48]	Hydrated radius/ Å [48]	Charge Density /C mm ⁻³ [49]	-Hydration Enthalpy ^a /kJ mol ⁻¹ [50]
Cadmium(II)	0.95	4.60	59	1807
Copper(II)	0.73	3.92; 4.56 ^b	116	2100
Lead(II)	1.19	5.08	32	1481
Nickel(II)	0.69	4.11	134	2105

^aFor the hydration of gaseous ions; ^bEquatorial and axial dimensions in Jahn–Teller distorted octahedron.

Because heavy metals are not degradable [9, 51], bioaccumulation and biomagnification occur throughout the food chain (being particularly important for humans, positioned at the top of their food chain), causing different diseases and poisoning [8, 9, 52]. Bioavailable and mobile forms of heavy metals are released by anthropogenic activities like mining, several industries, fossil fuel combustion and pesticide and biosolids use [8, 10, 53, 54]. Metal processing and mining contribute to 48% of the total release of contaminants by the European industrial sector [1]. Fertilizers contain, as impurities, trace amounts of heavy metals, such as Cd and Pb. In spite of being discontinued, some pesticides include Cu, Hg, Mn, Pb, Zn and As compounds [54]. The use of biosolids (manures, sewage sludge), rich in several nutrients, as fertilizers, also introduces Cd, Cr, Ni, Se and Mo into soils [54].

The distribution of heavy metals depends not only on the proximity to emission sources but also on the media being assessed. In ecosystems, heavy metals are found in soils (and its different components), sediments, water streams, air and biota, in mobile or immobilized forms, in a dynamic equilibrium [11, 54, 55] - Figure 3. The mass transfer between phases is controlled by reactions occurring with heavy metals as *e.g.* precipitation or dissolution, sorption by minerals or organic matter, ion exchange, complexation, biological fixation/mobilization, plant uptake and volatilization [7, 10, 55, 56]. These are affected by pH (Equation 1), temperature, amount of water, concentration of salts and organic matter, etc.. Soils with higher (basic) pH usually lead to the immobilization of heavy metals due to phenomena like adsorption or precipitation of insoluble salts ($m=n$, Equation 1) [57]. Oxides and organic matter can interact with heavy metals adsorbing/fixating them [55]. The dynamics of these pollutants in soils and its effect on the biota is further illustrated in Figure 4. Due to the aforementioned reasons, the concentration of heavy metals is different in soil, watercourses and river sediments.



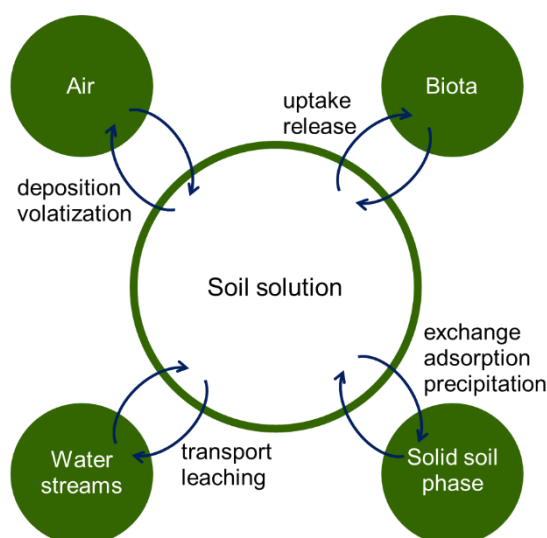


Figure 3 - Mechanisms of heavy metal cations transport through different natural media.

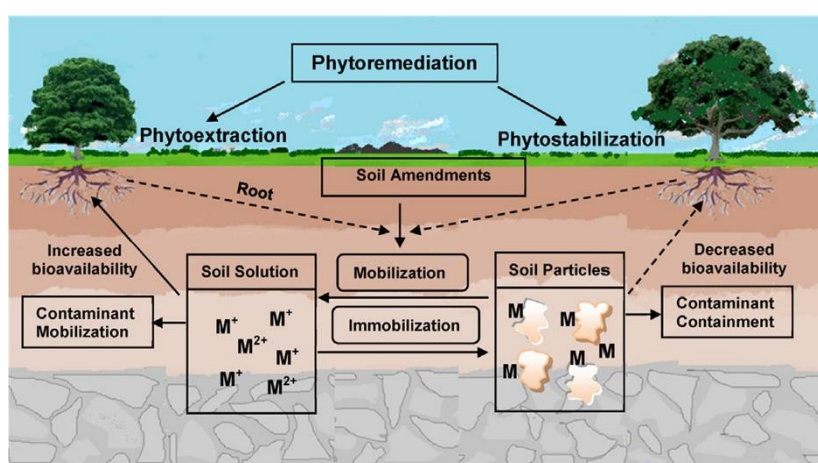


Figure 4 - Representation of different interactions that heavy metals can suffer in the soil and the process of phytoremediation. Soil particles designate all solid soil constituents.

Clean-up of polluted media has been widely studied and different strategies were proposed. In the case of aqueous media, chemical precipitation, adsorption and membrane processes can be employed [58] for this purpose. Strategies for this kind of medium are further discussed in Section 2.4.. For heavy metal contaminated soils and sediments there are several traditional physical-chemical decontamination methods [54, 59], and microbial activity and hyperaccumulator plants (phytoremediation, Figure 4) have also been widely discussed [60-64]. Economic viability and efficiency are key factors in determining the applicability of a remediation technique.

The background concentrations of heavy metals in soils (upper crust and surface soil) and river water, given by world averages, are reported in Table 3.

Table 3 - Background concentration for heavy metals in soils and river water.

Heavy Metal	Upper Crust ^a / mg kg ⁻¹ [10, 65]	Surface Soil ^a / mg kg ⁻¹ [10, 65]	River Water/ µg L ⁻¹ [10]
Arsenic	1.8	4.7	0.13 - 2.71
Cadmium	0.1	0.41	0.06x10 ⁻² - 0.61
Chromium	35	42	0.29 - 11.46
Copper	14	14	0.23 - 2.59
Lead	15	25	0.007 - 308
Mercury	0.07	0.07	--
Nickel	19	18	0.35 - 5.06
Zinc	52	62	0.27 - 27

^a Whenever the background concentration was dissonant between the references, the lowest value was selected as a conservative approach in order to assess polluted sites.

2.2. Legislation for Heavy Metals

As the effects of heavy metals became better known, particularly on human health, their usage has become more constrained. For example, mercury, lead and cadmium were banned, except for very specific applications, and their emissions are monitored. The evolution of the relative emissions of these elements in the last three decades can be found in Figure 5, using the emissions of 1990 as reference. This figure shows the effected of the imposed mitigation of these emissions. Limits in heavy metal concentration in different media, particularly in water, have been defined by government agencies to minimize the exposure of ecosystems to these toxic elements. However, not all governments share the same level of concern for this issue and, thus, some countries have more legislation than others. Nevertheless, the concentration limits for pollutants on natural media have become stricter. For example, the European Union imposes a maximum concentration of 0.5 µg m⁻³ for lead in air [66].

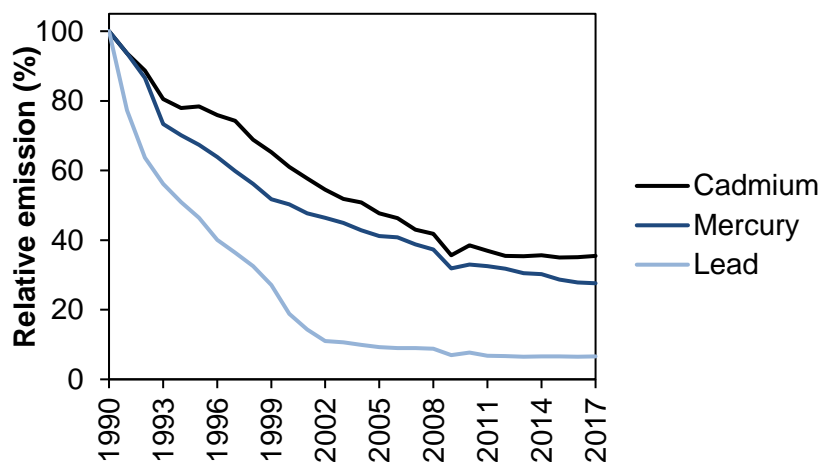


Figure 5 - Evolution of the relative emissions of heavy metals across the EEA-33, indexed to 1990 [13].

Safe drinking water is defined by the World Health Organization (WHO) [52] as not representing significant health risks over a lifetime of consumption. Table 4 presents the limit concentration of several heavy metals in drinking water, proposed by several entities, and their toxicity. For the sake of simplicity, when referring to the chemical symbol of metals, all the possible chemical compounds with the element are included.

Table 4 - Maximum concentration level (MCL) for heavy metals in drinking-water and their toxicity.

Heavy Metal	MCL in drinking water/ $\mu\text{g L}^{-1}$					Toxicity/ $\text{mg kg}^{-1} \text{bw}^{\text{a}}$	
	WHO ^b	EU ^c	USA ^d	Canada ^e	China ^f	PTWI ^{b,g}	LD50 ^h
As	10	10	10	10	10	withdrawn (0.0021 daily ⁱ)	41.0 [67]
Cd	3	5	5	5	5	0.025 monthly	5.2 [68] 88.0 [67]
Cr	50	25	100	50	50 ^j	--	--
Cu	2000	2000	1300	--	1000	0.500 daily ^k	5.6 [68] 584.0 [67]
Pb	10	5	15	10	10	withdrawn (0.025 ⁱ)	--
Hg	6	1	2	1	--	0.004	6.6 [68] 1.0 [67]
Ni	7	20	--	--	20	--	--
Zn	--	--	--	--	1000	1.0 daily ^k	20.2 [68]

^a Bodyweight; ^b World Health Organization [52]; ^c Council of the European Union [69]; ^d United States Environmental Protection Agency [70]; ^e Water and Air Quality Bureau - Healthy Environments and Consumer Safety Branch [71]; ^f Ministry of Health of China [72]; ^g Provisional tolerable weekly intake for humans; ^h Median lethal dose values obtained in mice or rats; ⁱ Former value; ^j Reported as hexavalent chromium; ^k Maximum tolerable intake.

From Table 4, we can verify that the values imposed by several governments are in accordance with the guideline values from WHO, despite the slow revisions of legislation. WHO hasn't limited the concentration for zinc in its 2017 guide, as they consider that there are no health concerns at levels found in drinking water. The European Commission has adopted in December 2020 a revised drinking water directive (the former is from 1998), that member states have until 2023 to transpose, in which the latest considerations from WHO are taken into account.

The MCL values shown in Table 4 are very low, being just a few $\mu\text{g L}^{-1}$ in most situations, evidencing the toxicity of these elements and the strictness of regulations. In fact, only copper and zinc are allowed to achieve a few mg L^{-1} . Complying with these low concentrations requires the employment of advanced treatment technologies, if the anthropogenic sources of pollution are significant.

Table 4 also shows toxicity values for the heavy metals under analysis. The Joint FAO/WHO Expert Committee on Food Additives - JECFA [73] proposes provisional tolerable weekly intake for these substances. Some of these values were withdrawn, as it was found that those

concentrations were not health-protective. The proposed values are all very low, evidencing the effects of bioaccumulation and the acute toxicity of these elements in humans. For mice or rats the median lethal dose values also evidences the acute toxicity of heavy metals [67, 68].

The regulation of pollutants concentration in drinking water is without a doubt a priority for governments. However, a few countries also enforce maximum concentrations for these pollutants in irrigation water (Table 5), driven by the need to control the concentration of heavy metals in food.

Table 5 - Recommended maximum concentration level for heavy metals in irrigation water.

Heavy Metal	Recommended maximum concentration level/ $\mu\text{g L}^{-1}$		
	FAO [74]	Portugal [75]	Canada [76]
As	100	100	100
Cd	10	10	5
Cr	100	100	8 Cr(VI) 5 Cr(III)
Cu	200	200	200 ^a
Pb	5000	5000	200
Hg	--	--	--
Ni	200	500	200
Zn	2000	2000	1000 (pH<6.5)

^a Value defined for cereals; 1.0 mg L^{-1} for tolerant crops.

It is worth noting that there is no directive defined by the European Council for the concentration of heavy metals in irrigation water. On the other hand, the values defined by FAO are just guidelines and have no legal binding.

The limits in Table 5 are generally less strict than the ones in Table 4, and the maximum recommended concentration is usually one order of magnitude greater than that of drinking water. Exceptions to this trend are the concentrations for copper and the one enforced by Canada for chromium. Moreover, values for irrigation water are stricter in Canada, where chromium, copper, lead and zinc concentrations are lower than the ones defined by FAO. The concentration for lead proposed by FAO is very high given that lead is a very toxic element. However, this may be related to the fact that lead binds very easily with organic and colloidal matter in the soil, with only a small fraction of it being soluble, hence, bioavailable. Furthermore, lead uptake by plants usually occurs through the roots, and its uptake and translocation by aerial parts of plants is reduced [77].

Legislation for other contaminated media, soils and sediments, is lacking in the majority of countries. However, the EU and Canada have legislation on contaminants in agricultural soils, which is summarized in Table 6. The European limit concentration in sludges for agricultural use as well as the Canadian legislation and US guidelines on sediments are also presented in Table 6.

The maximum limits for heavy metals in agricultural soils are meant to ensure that these can be cultivated, and crops do not absorb an excessive amount of these pollutants, remaining therefore edible. The current European directive is more permissive than its Canadian counterpart. For sediments, only Canada defined regulations, once again very strict. On this regard, USA only features guidelines.

Table 6 - Limit values for heavy metal concentration in agricultural soils, sludges for agricultural use and sediments.

Heavy Metal	Limit concentration / mg kg ⁻¹ dw ^a				
	Agricultural soils		Sludges for agriculture		Sediments
	EU ^b (soil pH 6≤pH<7)	Canada ^c	EU ^b	USA guideline ^{d,e}	Canada ^{f,g}
As	--	12	--	33.0	5.9
Cd	1 - 3	1.4	20 - 40	4.98	0.6
Cr	--	64	--	111	37.3
Cu	50 - 140	63	1000 - 1750	149	35.7
Pb	50 - 300	70	750 - 1200	128	35.0
Hg	1 - 1.5	6.6	16 - 25	1.06	0.170
Ni	30 - 75	45	300 - 400	48.6	--
Zn	150 - 300	200	2500 - 4000	459	123.0

^a Dry weight; ^b Council of the European Communities [78]; ^c Canadian Council of Ministers of the Environment [79]; ^d Ingersoll *et al.* [80]; National Oceanic and Atmospheric Administration's Office of Response and Restoration [81]; ^e Consensus-based probable effect level; ^f Canadian Council of Ministers of the Environment [82]; ^g Canadian Interim Sediment Quality Guideline.

2.3. Heavy Metal Polluted Sites

Several authors have assessed the distribution of heavy metals on different natural media. In this section the focus is given to the concentration on watercourses, soils and stream sediments. Samples in each study were collected in different locations of the studied area and at different moments. Furthermore, only sites considered in the original study as inside the influence area/downstream of the pollution source, when discriminated, were taken into account. It should be noted that, due to the anthropogenic sources of pollution and possible remediation strategies employed, the sites assessed in the literature may feature different degrees of pollution at the present time. In Section 2.3.1., the studies in which heavy metals were quantified in sites affected by mining activities and associated ore smelting are reviewed. On the other hand, in Section 2.3.2., studies evaluating the content of these pollutants in sites affected by industries, mainly metallurgical industries, are surveyed. Although mining and smelting can also be considered industrial activities, in this chapter a special focus is giving to these due to their pertinence for HM pollution, by being discussed separately. Section 2.3.3. highlights studies where the heavy metal concentration has been assessed in locations with multiple sources of pollution, caused by a number of combined factors

not directly associated with the exploration/use of HM. In Section 2.3.4. previous studies are assessed for the particular case of HM pollution in Portugal.

2.3.1. Sites Affected by Mining Activity

The distribution of heavy metals in locations related with mining activities was investigated in several studies and their concentrations are summarized in Annex I: Table I. 1 and I. 2. Figure 6 shows some photos of the studied locations. Sites of Ra mines were surveyed in Alto da Várzea [83] and Sra. das Fontes, Portugal [84]. In the Iberian Pyrite Belt, where Au, Zn and Pb are extracted, the bases of the rivers Odiel, Tinto [85] and Meca [86] were studied. Zinc-lead mines were studied in Assif El Mal, Morocco [87], in Rubiais, Spain [88], in Noyelles-Godault and Aubry, Douai area, France [89, 90] and in Kosovska Mitrovica, Kosovo [91]. In the U.K., abandoned mines where these two heavy metals were the main product were also studied [92]. The Příbram region, Czech Republic, has a history of Pb and Ag extraction and processing and has been intensively studied [93-95]. Coal exploration sites such as the Yongding river [96], the Sidney basin [97] and the Qingshui river basin in Beijing [98] have also been assessed. Gold extraction sites were also evaluated: Anka, Nigeria [99], where artisanal mining activities occurs, and in the legacy mining township of Maldon, Australia [100]. The Copperbelt, at the border of DR Congo and Zambia, is a region that is explored for Cu and Co and has been studied by many authors [101-105]. Several sites surrounding mines, mainly metal mines, were studied in China [106], including in Tongling [107], Xikuangshan [108], Yiyang county [109], Jishui river in Dexing [110] and Maba river in Shaoguan [111]. Other evaluated sites include the W mine of S. Francisco de Assis [112]; the Sør-Varanger region [113] at the Norwegian - Russian border, an area of great Fe and Ni ore exploration; the Ni and Cu mining region of Sudbury [102]; northern Namibia [104], where mines were explored for Pb, Zn, V, Cu, Li and Ge; Adrianópolis [114], where Pb mining and processing have occurred for several decades; As and Pb mining and smelting communities in Armenia [115]; the region of Villadossola in the Italian Alps [116], explored for Fe, Ni, Cu and Co sulphides and the Lot river basin, France [117], where Zn ore was processed.

To interpret the values presented in the previously mentioned studies, the relative concentration of heavy metals in water and the geoaccumulation index (introduced by Müller - Table 7) are presented in Table 8-10. In Table 8, the relative concentration of heavy metals from Annex I: Table I. 1 (maximum value) is compared to drinking-water (DW) and irrigation water (IW) standards defined by WHO and FAO, respectively. It is expected that the water from the evaluated watercourses is subject to treatment before being distributed to the public water supply. The comparison with drinking-water regulations enables one to estimate the appropriate treatment to be employed. In Table 9 and Table 10, the geoaccumulation index (I_{geo}) - Equation 2 [118] -

enabled to assess elemental contamination in soils/sediments of the sites surveyed in the literature. However, this index does not differentiate between accumulation of anthropogenic or lithogenic origin. As the original authors of each study seldom present I_{geo} , most values in Table 9 were calculated using the concentration in soil of Table I. 2 and the background upper crust values of Table 3.

$$I_{geo} = \log_2 \frac{C}{1.5 C_{background}} \quad (2)$$

The values of Table 10 are given in each original study.

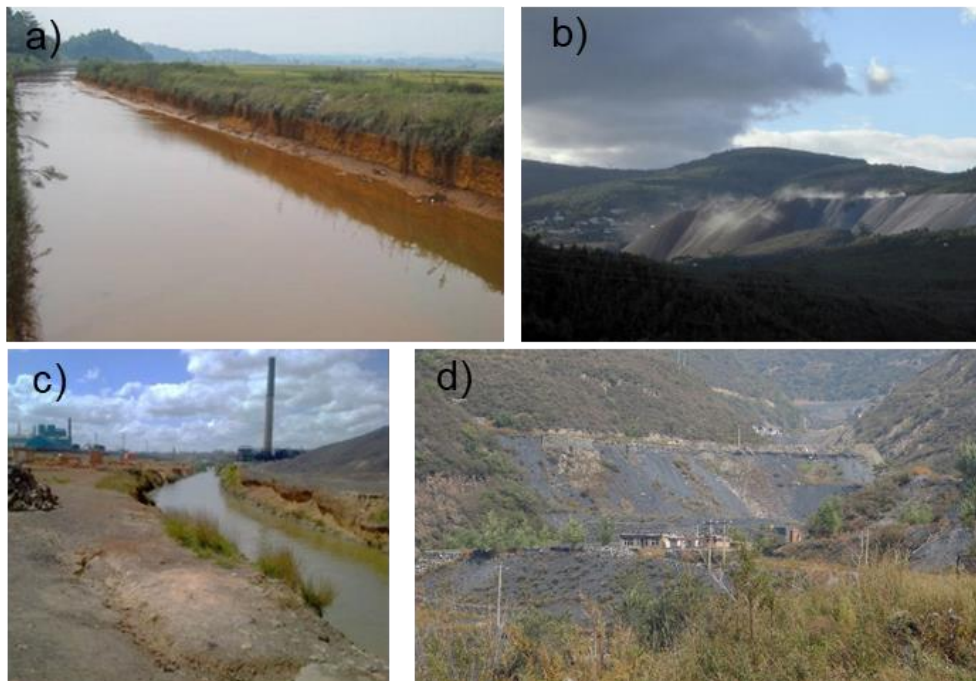


Figure 6 - Photographs of some studied areas: (a) polluted streams in Yiyang; (b) mine tailing deposits in S. Francisco de Assis; (c) Lubumbashi river; (d) Coal mines around Qingshui River.

Table 7 - Classes of the geoaccumulation index, according to Müller [118].

I_{geo}	I_{geo} class	Soil/Sediment Quality
$I_{geo} \leq 0$	0	Practically unpolluted
$0 < I_{geo} < 1$	1	Unpolluted to moderately polluted
$1 < I_{geo} < 2$	2	Moderately polluted
$2 < I_{geo} < 3$	3	Moderately to heavily polluted
$3 < I_{geo} < 4$	4	Heavily polluted
$4 < I_{geo} < 5$	5	Heavily polluted to extremely polluted
$I_{geo} > 5$	6	Extremely polluted

Table 8 - Comparison of water concentration against water quality standards.

Site [Ref.]	Standard ^a	Relative Water Concentration							
		As	Cd	Cr	Cu	Pb	Hg	Ni	Zn
Alto da Várzea, Portugal [83]	DW	3.28	1.43	0.16	0.04	5.07	--	1.54	--
	IW	0.33	0.43	0.08	0.39	0.01	--	0.05	0.01
S. Francisco Assis, Portugal [112]	DW	0.78	0.12	--	0.01	2.31	--	--	--
	IW	0.08	0.04	--	0.05	0.00	--	--	0.16
Iberian Pyrite Belt, Spain [85]	DW	360.40	706.33	7.78	111.35	160.70	--	1955	--
	IW	36.04	211.90	3.89	1114	0.32	--	68.41	341.75
Meca river, Spain [86]	DW	13.00	266.67	--	4.60	36.00	--	31.43	--
	IW	1.30	80.00	--	46.00	0.07	--	1.10	2.05
Assif El Mal, Morocco [87]	DW	--	--	--	0.66	6.40	--	5.43	--
	IW	--	--	--	6.60	0.01	--	0.19	2.99
Yongding River, China [96]	DW	--	--	0.03	0.00	0.04	--	1.14	--
	IW	--	--	0.01	0.01	0.00	--	0.04	0.02
Yiyang, China [109]	DW	--	13.33	13.20	0.05	3.00	--	85.71	--
	IW	--	4.00	6.60	0.45	0.01	--	3.00	2.05
Sidney basin, Australia [97]	DW	1.00	0.07	--	0.01	0.70	--	31.43	--
	IW	0.10	0.02	--	0.07	0.00	--	1.10	0.20
Anka, Nigeria ^b [99]	DW	1363.00	81.00	--	0.11	15.30	--	--	--
	IW	136.30	24.30	--	1.05	0.03	--	--	--

^a DW - Drinking Water; IW - Irrigation Water; ^b Values refer to mine discharge water.

Mercury was not evaluated in the cited works and no guideline from WHO exists for zinc. The values from Table 8 indicate that, in all the assessed cases, the water does not meet the drinking water criteria defined by WHO and, in some cases, neither the maximum recommended concentration from FAO for irrigation water. Despite that, there are several serious cases involving the large majority of metals. The concentration of As in mine discharge water in Anka [99] - an artisanal mining exploitation - is around 1400 times greater than the MCL, followed by the water at Iberian Pyrite Belt (360 times higher). It should also be stressed that significant relative values can also be found for cadmium (Iberian Pyrite Belt's rivers Tinto, Odiel and Meca) in relation to drinking water legislation. In fact, the Iberian Pyrite belt is the spot with higher concentration of metals, relatively to WHO's drinking water levels. River water in Yiyang, China, is also highly contaminated with Cd, Cr (*ca.* 13 times over the MCL for drinking water) and Ni (*ca.* 86-fold). On the other hand, the highly toxic Cr shows relatively low values in all places where it was quantified.

Table 9 - Geoaccumulation indexes for soils affected by mines.

Site [Ref.]	$I_{\text{geo soil}}$							
	As	Cd	Cr	Cu	Pb	Hg	Ni	Zn
Alto da Várzea, Portugal ^a [83]	4.65 -	--	-3.87 -	-1.04 -	-0.40 -	--	-3.07 -	<0.85
	5.59	--	-1.22	-0.24	0.82	--	-2.11	
Senhora das Fontes, Portugal ^a [84]	4.24 -	< 4.74	-2.32 -	< 2.13	-1.03 -	--	-1.55 -	-3.18 -
	7.12		0.83		1.12		2.06	1.04
S. Francisco Assis, Portugal ^a [112]	6.37	3.12	-0.47	2.96	1.38	--	-0.21	2.05
Rubiais, Spain ^a [88]	--	3.74 -	-4.13 -	0 - 2.93	1.03 -	0.93 -	-2.51 -	2.12 -
		9.31	-1.32		8.08	7.88	0.52	9.38
United Kingdom ^a [92]	--	<11.18	--	0.12 -	3.95 -	--	--	2.04 -
				1.88	10.89			9.42
Douai, France ^a [89]	--	-1.74 -	--	--	-1.53 -	--	--	-1.38 -
		10.99			7.91			8.64
Cultivated soils Douai, France ^a [90]	1.20 -	3.63 -	-0.59 -	-0.44 -	2.17 -	0.19 -	-1.57 -	0.94 -
	3.43	7.15	0.40	1.14	5.65	2.63	0.47	4.80
Litavka River valley, Czech Republic ^a [93]	--	4.32 -	--	--	-0.58 -	--	--	2.09 -
		8.81			7.71			6.81
Přibram, Czech Republic ^a [94]	5.54 -	-0.32 -	--	2.32 -	5.38 -	--	--	-2.30 -
	6.54	6.31		4.54	10.65			2.73
Přibram, Czech Republic ^a [95]	5.41 -	4.22 -	--	-0.81 -	3.36 -	--	--	1.69 -
	6.24	8.18		2.80	7.69			6.20
Sør-Varanger, Norway ^a [113]	-2.17 -	-0.58 -	-3.36 -	-1.08 -	-2.09 -	--	-1.68 -	-2.40 -
	2.19	4.27	0.12	5.74	2.66		6.03	3.39
Kosovska Mitrovica, Kosovo ^a [91]	-0.36 -	-0.58 -	-2.91 -	-1.22 -	0.60 -	-2.39 -	-1.91 -	-1.29 -
	10.50	8.29	4.39	6.25	10.60	6.71	6.51	7.27
Assif El Mal, Morocco ^a [87]	--	--	--	1.36 -	1.72 -	--	-2.57 -	2.77 -
				2.48	2.88		-0.88	4.71
Kolwezi, DR Congo [101]	-0.3 -	--	--	9.8 -	6.3 -	--	6.3 -	10.3 -
	4.5			19.8	13.9		13.4	18.9
Lubumbashi, DR Congo ^a [102]	2.89 -	2.58 -	--	9.11 -	-0.10 -	--	-2.25 -	1.19 -
	5.23	7.04		9.40	5.17		0.23	4.00
Lubumbashi, DR Congo [103]	4.5 - 6.0	--	--	10.3 -	9.0 -	--	5.1 - 6.5	10.5 -
				11.5	10.3			13.2
Copperbelt Province, Zambia ^a [104]	-1.67 -	-2.91 -	--	-2.86 -	-2.93 -	-4.25 -	--	-2.72 -
	4.98	3.06		10.81	4.22	1.89		2.82
Copperbelt Province, Zambia ^a [105]	<6.56	--	-5.04 -	-1.81 -	<4.48	-5.71 -	<2.21	<2.53
			3.50	10.96		2.07		
Northern Namibia ^a [104]	-1.52 -	-0.45 -	--	-2.77 -	-1.29 -	-4.79 -	--	-2.84 -
	9.78	11.73		7.89	8.50	5.39		6.96
Sudbury, Canada ^a [102]	-0.43 -	1.00 -	--	1.31 -	-0.32 -	--	0.92 -	-1.29 -
	4.09	3.74		5.98	2.97		5.81	0.14
Tongling, China ^a [107]	--	2.98 -	-0.89 -	1.26 -	0.88 -	--	-1.76 -	0.16 -
		7.44	1.56	5.23	3.91		0.39	3.28
Xikuangshan, China ^a [108]	1.05 -	-0.58 -	--	-1.18 -	-2.45 -	--	--	-0.59 -
	7.03	9.77		4.07	4.86			6.03
Beijing, China [98]	--	0.4 - 3	-1.7 -	-1.0 -	-1.1 -	--	-1.1 -	-1.2 -
			-0.3	0.2	2.1		0.5	-0.3
Dexing, China ^a [110]	1.89 -	1.74 -	0.19 -	0.47 -	0.83 -	--	-0.51 -	-0.10 -
	6.28	4.12	0.86	4.35	4.58		0.90	2.53
Yiyang, China ^a [109]	--	1.42 -	-1.18 -	0.09 -	-0.03 -	--	-1.02 -	0.23 -
		6.14	0.07	3.36	1.73		0.50	2.63

^a Values calculated based on the concentration reported in the original research and the average upper crust concentration (Table 3).

Table 9 - Geoaccumulation indexes for soils affected by mines (concluded).

Site [Ref.]	I_{geo} soil							
	As	Cd	Cr	Cu	Pb	Hg	Ni	Zn
China [106]	-5.70 -	-1.41 -	-4.70 -	-7.36 -	-2.55 -	-1.71 -	-1.34 -	-3.59 -
	6.06	8.85	1.24	6.54	7.36	9.05	4.0	7.68
	(~1.0)	(~4.0)	(~-0.5)	(~1.2)	(~2.0)	(~1.8)	(~0.5)	(~1.2)
Maldon, Australia ^a [100]	2.81 -	-2.32 -	-1.19 -	-0.58 -	-0.91 -	-0.07 -	-2.03 -	-1.83 -
	6.10	1.30	0.12	1.49	1.76	6.42	-0.31	2.07
Adrianópolis, Brazil ^a [114]	--	3.66 -	-2.56 -	1.44 -	3.38 -	--	-0.79 -	0.45 -
	--	7.20	-0.92	5.41	8.75	--	0.43	3.52
Alaverdi, Armenia ^a [115]	3.15 -	--	--	--	-1.32 -	--	--	--
	8.62	--	--	--	7.36	--	--	--
Akhtala, Armenia ^a [115]	1.74 -	--	--	--	-0.58 -	--	--	--
	6.68	--	--	--	9.12	--	--	--
Villadossola, Italy ^a [116]	0.97 -	1.00 -	-0.25 -	0.42 -	0.51 -	--	0.34 -	-0.58 -
	1.18	3.12	0.94	1.78	2.03	--	0.63	0.88

^a Values calculated based on the concentration reported in the original research and the average upper crust concentration (Table 3).

The values from Table 9 confirm that the soils surrounding the studied mines are very polluted - most maximum I_{geo} values reveal heavy or extreme pollution. However, the spatial distribution of heavy metals in those sites is very uneven. It is worth noting that in some cases the area under study is vast. The elements being explored at the site are present in high concentrations in the soil, as expected. The I_{geo} reveals that the most polluted sites, with a majority of the quantified metals causing extreme pollution, are the old mine sites in U.K., Příbram, Kosovska Mitrovica, Kolwezi, Lubumbashi, northern Namibia, Xikouangshan and the two mining regions of Armenia. The analysis of the studies at the Douai smelter reveals that the pollution effectively spreads to the surrounding cultivated soils. Surrounding the smelter, the soils are extremely polluted with Cd, Pb and Zn, a trend that is also verified in the agricultural soils nearby. The latter, are also moderately to heavily polluted with Hg and heavily polluted with As. The various mine sites studied in China [106] show uncontaminated locations within the studied areas, as well as areas where extreme pollution is found, with the exception of Cr and Ni. This is the result of uncontaminated sample collection locations in the study area and the very different mining areas under analysis.

The I_{geo} values for sediments shown in Table 10 are much lower than those found on Table 9. However, the pollution found in sediments follows the trend of soil. Lead pollution is more significant in sediments than in soils from Sra. das Fontes and river water from Yongding and Maba rivers. It seems that these sediments tend to preferably bind Pb. In the Lot River, heavy metal pollution in sediments is of at least class 4, according to Müller's classification - Table 7, with copper being the exception.

Table 10 - Geoaccumulation indexes for sediments in sites affected by mines.

Site [Ref.]	I_{geo} sediments							
	As	Cd	Cr	Cu	Pb	Hg	Ni	Zn
Alto da Várzea, Portugal [83]	2 - 6	--	0 - 1	0	0 - 2	--	0	0
Senhora das Fontes, Portugal [84]	2 - 4	--	0 - 1	0 - 1	0 - 2	--	0 - 1	0 - 1
Lot River, France [117]	--	-1.0 - 8.0	--	-1.0 - 2.5	-1.0 - 4.2	--	--	-1.0 - 5.6
Yongding River, China [96]	--	--	-1.67 - 0.04	-1.80 - 0.24	-1.17 - 1.88	--	-1.69 - 0.81	-1.06 - 0.62
Maba river, China [111]	0.66 - 6.36	2.90 - 8.34	-1.0 - 0.0	-0.58 - 5.01	-0.56 - 4.96	2.23 - 5.56	-0.6 - 1	0.09 - 5.62
Kolwezi, DR Congo [101]	-0.5 - 5.1	--	--	10.9 - 21.7	6.4 - 13.5	--	5.6 - 11.4	10.3 - 13.8
Lubumbashi, DR Congo [103]	--	--	--	9.8 - 12.3	8.3 - 15.6	--	5.2 - 7.6	10.8 - 15.8
Anka, Nigeria ^a [99]	2.63	--	0.62	2.29	3.67	--	--	--

^a Values refer to mine sediments.

From the analysis of the referred works, I observe that mining activities release significant amounts of heavy metals to the environment, polluting the surrounding areas. In some cases, a mixture of different elements is found together in the extracted ores. Soils and surface sediments reveal extreme pollution in many cases and, in general, they are significantly polluted. These contain oxides and hydroxides, clays and organic matter in their compositions, which are able to bind cations, retaining the heavy metal contaminants. It can also be concluded that pollutants do not diffuse quickly to the surrounding areas, which is also dependent on the size of the study site. Water from watercourses can also be very polluted due to these activities. In spite of more water quality regulations being enforced, and wastewaters being treated, there are still sites whose river water is very contaminated and inappropriate for irrigation or human consumption.

2.3.2. Sites Affected by Industrial Activity

In this section, studies assessing the heavy metal loadings of the surrounding areas of industrial facilities and complexes are surveyed. Table I. 3 and Table I. 4 in Annex I show the concentrations of heavy metals found in the referred literature. Table 11 summarizes the concentration of heavy metals in selected industrial wastewaters.

The distribution of heavy metals in locations affected by different kinds of industrial facilities were reviewed, with particular importance being given to metallurgical plants. In Portugal, the Esmoriz-Paramos lagoon [119] and the Estarreja chemical complex [120, 121] were assessed. In the U.K. the surroundings of a Pb-Zn smelter in Avenmouth [92] and in Prescott [122], where a Cu rod-dolling plant is operating, were studied. In Spain the industrialized city of Huelva [123] was

studied and in Bazoches-les Gallérandes, France, the surroundings of a Pb-recycling plant were assessed [124]. Sites of several industrial areas in Vojvodina [125] and Smederevo [126], Serbia, were evaluated. In Veles, Macedonia, the surroundings of a deactivated Pb and Zn smelter plant was studied [127]. The pollution of two industrialized cities in China, Wuxi [128] and Yixing [129], was assessed, as well as the contamination caused by former metallurgical complexes in South Korea [130] and Monterey, Mexico [131].

In a similar way, several authors have studied the heavy metal content in water streams that receive wastewaters and provide drinking water for populations. These can receive large amounts of industrial - metallurgical, petrochemical, oil industries and dyeing, agricultural and domestic effluents, sometimes untreated. In the case of the site analyzed in Taiwan [132], effluent discharges are also from technological and science parks, hospitals and original equipment manufacturers.

The composition of reported industrial effluents [132-145], summarized in Table 11, come from industries including dyeing, electroplating, rolling and pickling, and steel processing. In some of the aforementioned works, the effects of applying these wastewaters for the irrigation of crops were evaluated.

Table 11 reveals that most effluents are not treated and the discharged wastewaters feature high concentrations of heavy metals. This is particularly noticeable in some electroplating wastewaters [133-136], in some industrialized areas [137-139] and even in wastewaters used for irrigation [145]. The receiving media are not likely able to accommodate the continuous discharge and as such, become contaminated. This is very relevant when the receiving media are rivers, which provide drinking water to populations and irrigation water for crops, or soils that accumulate the contaminants input. In Jiangsu [133] and in Delhi [139], the high concentration of heavy metals in discharged wastewaters leads to dangerous high concentrations in the receiving media. In Titagarh [145], the use of wastewaters as irrigation waters causes heavy pollution of the soils. The issue of poorly treated effluents calls for more environmental policies and regulation enforcement and supervision by the governments.

Table 12 presents the relative heavy metal concentration in the evaluated watercourses and Table 13 shows the I_{geo} for soils and sediments. Mercury was not assessed in the watercourses of Table 12.

Table 11 - Heavy metal concentration in wastewaters from selected industries.

Site [Ref.]	Concentration In Wastewater / mg L ⁻¹							
	As	Cd	Cr	Cu	Pb	Hg	Ni	Zn
Electroplating wastewater [133]	--	b.d.l.	28.1	6.40	b.d.l.	--	9.73	1.34
Electroplating wastewater [140]	--	--	0.06 ^a	0.26	--	--	0.06	0.008
Electroplating wastewaters [134]	--	--	2.6 - 6.0	2157.3 - 15560.3	--	--	40.8 - 245.4	2.1 - 12.5
Electroplating wastewater [141]	--	0.011 - 0.015	0.073 - 0.113	--	--	--	0.904 - 0.966	4.55 - 4.97
Electroplating wastewater [135]	--	--	35.9	3.2	8.6	--	1.3	505.0
Electroplating wastewater for Cu(II) [136]	--	--	--	43.3	--	--	11.7	--
Raw wastewater from engineering plant [137]	--	--	1779.8	79.8	0.4	--	--	38.43
Industrial wastewaters [138]	--	0.1 - 0.9	1.9 - 3.9	1.9 - 6.7	0.3 - 0.9	--	1.4 - 4.4	--
Chlor-alkali industry wastewater for Hg(II) [136]	--	0.6	--	--	3.2	9.9	--	--
Delhi industrial area [139]	--	b.d.l. - 0.9	b.d.l. - 319	b.d.l. - 48	b.d.l. - 326	--	b.d.l. - 40	b.d.l. - 16
Industries from Ondo, Nigeria [142]	b.d.l. - 1.23	b.d.l.	b.d.l. - 0.04	b.d.l. - 0.044	b.d.l.	b.d.l. - 3.00	b.d.l. - 1.20	b.d.l.
Discharges to Ismailia Canal, Egypt [143]	--	0.017 - 0.026	--	0.035 - 0.042	--	--	0.021 - 0.027	0.053 - 0.060
Taichung industrial and technological parks, Taiwan [132]	--	b.d.l. - 0.0008	b.d.l. - 0.030	b.d.l. - 0.721	b.d.l. - 0.0004	--	b.d.l. - 0.295	b.d.l. - 0.255
Wastewater used in irrigation [144]	--	b.d.l. - 0.23	b.d.l. - 0.82	b.d.l. - 1.54	b.d.l. - 0.37	--	b.d.l. - 0.37	b.d.l. - 1.25
Wastewater used in irrigation [145]	--	b.d.l. - 0.06	b.d.l. - 0.81	0.07 - 6.30	b.d.l. - 7.50	--	b.d.l. - 4.20	0.21 - 4.30

b.d.l. - below detection limit; ^a Defined as Cr(VI) content.

Table 12 - Comparison of water concentration against water quality standards in watercourses affected by industrial activities.

Site [Ref.]	Standard ^a	Relative Water Concentration							
		As	Cd	Cr	Cu	Pb	Hg	Ni	Zn
Esmoriz-Paramos lagoon, Portugal [119]	DW	--	--	0.00	0.02	3.80	--	--	--
	IW	--	--	0.00	0.15	0.01	--	--	0.35
Tigris river, Turkey [146]	DW	--	0.00	--	0.05	0.00	--	57.14	--
	IW	--	0.00	--	0.46	0.00	--	2.00	0.07
Karoon river, Iran [147]	DW	--	--	2.37	0.04	--	--	17.43	--
	IW	--	--	1.18	0.35	--	--	0.61	--
Khoshk river, Iran [148]	DW	--	60.00	11.00	0.03	13.00	--	28.57	--
	IW	--	18.00	5.50	0.30	0.03	--	1.00	1.37
Yamuna river, India [149]	DW	--	6.67	0.16	--	--	--	30.00	--
	IW	--	2.00	0.08	--	--	--	1.05	--
Yamuna river, India [150]	DW	--	144.33	39.66	8.82	111.21	--	392.59	--
	IW	--	43.30	19.83	88.21	0.22	--	13.74	14.26
Yamuna river, India [139]	DW	--	66.67	2.20	0.08	36.00	--	151.43	--
	IW	--	20.00	1.10	0.75	0.07	--	5.30	0.06
Patancheru, India [151]	DW	11.65	--	0.94	--	1.38	--	7.73	--
	IW	1.17	--	0.47	--	0.00	--	0.27	0.18
Kasimpur, India [152]	DW	--	--	2.00	0.43	--	--	1.71	--
	IW	--	--	1.00	4.30	--	--	0.06	0.15
Gomti river, India [153]	DW	--	0.00	6.32	0.02	8.60	--	26.57	--
	IW	--	0.00	3.16	0.23	0.02	--	0.93	0.08
Gomti river, India [154]	DW	--	0.00	0.11	0.00	3.90	--	2.43	--
	IW	--	0.00	0.06	0.00	0.01	--	0.09	0.02
Karnaphuli River, Bangladesh [155]	DW	5.39	6.11	2.25	--	2.75	--	--	--
	IW	0.54	1.83	1.12	--	0.01	--	--	--
The Luan River Basin, China [156]	DW	--	0.37	1.79	0.01	1.51	--	1.99	--
	IW	--	0.11	0.89	0.15	0.00	--	0.07	0.09
Jiangsu, China [133]	DW	--	--	17.08	2.25	--	--	542.86	--
	IW	--	--	8.54	22.50	--	--	19.00	0.18
Taichung, Taiwan [132]	DW	--	0.00	1.05	0.03	0.04	--	4.71	--
	IW	--	0.00	0.52	0.31	0.00	--	0.17	0.01

^a DW - Drinking Water; IW - Irrigation Water.

Table 13 - Geoaccumulation indexes for soils and sediments affected by industrial activities.

Site [Ref.]	I_{geo} soil							
	As	Cd	Cr	Cu	Pb	Hg	Ni	Zn
Estarreja^a, Portugal [120]	9.17	2.87	-5.45	2.66	3.59	10.02	-4.15	1.09
Estarreja^a, Portugal [121]	0.10 - 7.62	--	--	--	--	-1.81 - 7.02	--	-2.29 - 1.35
Huelva^a, Spain [123]	1.72 - 9.58	0.09 - 6.94	-3.01 - 1.09	3.68 - 8.90	1.61 - 7.93	--	-2.25 - 0.77	-0.06 - 5.92
Bazoches-les Gallérandes^a, France [124]	0.16 - 3.38	--	-1.76 - 0.82	-2.41 - 0.70	-2.65 - 6.42	--	-1.94 - 0.52	-3.29 - 0.16
Avenmouth^a, U.K. [92]	--	8.51	--	2.94	6.27	--	--	5.54
Prescot^a, United Kingdom [122]	2.74 - 5.73	4.74 - 8.20	--	3.13 - 5.74	3.79 - 4.68	--	--	0.24 - 1.17
Vojvodina^a, Serbia [125]	-0.51 - 3.09	0.26 - 2.24	-2.25 - 1.89	-1.69 - 2.74	-1.49 - 1.64	-2.39 - 2.34	-2.25 - 1.10	-1.96 - 3.30
Smederevo^a, Serbia [126]	--	0.55 - 4.94	-12.36 - 1.13	-1.56 - 3.12	-0.17 - 2.64	--	0.49 - 2.58	-3.22 - 0.94
Veles^a, Macedonia [127]	-1.05 - 5.35	1.00 - 11.97	-1.63 - 5.10	-0.93 - 6.34	-0.79 - 9.38	-3.39 - 6.84	-1.96 - 4.40	-1.83 - 8.44
Varanasi^a, India [144]	--	1.87 - 5.88	-1.97 - 3.69	-3.04 - 3.28	-5.61 - 0.98	--	-3.83 - 0.27	-2.45 - 2.31
Titagarh^a, India [145]	--	7.21 - 8.41	1.17 - 1.86	0.07 - 2.99	2.14 - 2.90	--	0.65 - 2.23	1.22 - 1.87
Wuxi^a, China [128]	1.87 - 3.03	-5.64 - 1.30	-0.99 - 0.87	0.35 - 2.85	-0.40 - 2.85	-0.67 - 1.34	--	-1.39 - 2.51
Yixing^a, China [129]	--	-0.74 - 1.30	-0.28 - 0.37	-0.46 - 0.86	0.66 - 1.25	--	--	--
South Korea^a [130]	5.56 - 14.62	--	--	2.08 - 10.38	3.05 - 12.41	--	--	3.33 - 5.67
Monterey^a, Mexico [131]	5.40 - 11.13	<11.16	--	<5.11	3.24 - 10.45	--	--	2.05 - 7.30
I_{geo} sediments								
Khoshk river, Iran [148]	--	-2.1 - 2.15	0.1 - 1.25	0.4 - 2.05	2.1 - 4.8	--	0.10 - 0.48	0.24 - 1.8
Karnaphuli River, Bangladesh [155]	6.3 - 8.3	-3.0 - -0.49	11.1 - 13.2	--	8.0 - 10.0	--	--	--
The Luan River Basin, China [156]	--	0.17 - 3.1	0.2	-3.0 - 0.8	-1.4 - 0.9	--	-2.9 - 1.0	-0.9 - 1.4

^a Values calculated based on the concentration reported in the original research and the average upper crust concentration (Table 3).

Table 12 shows that the analyzed water does not meet, in many situations, the criteria for drinking water or even irrigation water. Cd, Cr and Ni are very relevant in these watercourses. The Yamuna river is the most contaminated watercourse in Table 12. It can be seen that the concentrations of heavy metal cations are quite high; for example, for Cd and Pb it can reach values higher than 100 times the drinking water limit and almost 400 times higher for Ni. The drinking water guideline is also largely exceeded in the Khoshk river and in Jiangsu by at least two orders of magnitude. In fact, Ni concentration found in Jiangsu is 543-fold that of the limit.

The soils in the sites summarized in Table 13 feature significant contamination of heavy metals. Similarly to Table 9, the minimum I_{geo} reveals the existence of uncontaminated sites within the studied area. However, in this table, this value can also reveal cases of severe pollution [130, 131, 145]. The most polluted soils are found in Huelva, Avenmouth, Prescott, Veles, South Korea and Monterey, showing that the problem is not specific for a given country. Some of the maximum I_{geo} values in these locations are twice the value used to define extreme pollution, revealing serious pollution. Chromium is not very relevant in the reported sites, with the exception of Veles and Varanasi. On the other hand, Hg concentration in soils is more relevant, causing extreme pollution in Estarreja and Veles. As, Cd, Cu, Pb and Zn are also shown to cause significant levels of pollution in many of the sites under focus. These results reveal that remediation is mandatory in places where metallurgical industries are located.

In terms of sediment contamination, Karnaphuli River is the most polluted out of Table 13. In this river, extreme pollution is caused by all quantified elements with the exception of cadmium. In the Khoshk river, pollution is mainly due to Pb, being Cd and Cu also significant. In contrast, the sediments from the Luan River Basin do not feature relevant pollution, except in the case of Cd.

2.3.3. Other Sites

In this section, the distribution of heavy metals in locations where the heavy metal pollution cannot be attributed to a single source, hence existing multiple sources of heavy metal pollution. Table I. 5 and I. 6 in Annex I show the concentrations of heavy metals found in each cited study.

The pollution in watercourses and their sediments was evaluated in: Dil Deresi, a small stream that flows into Izmit bay, Turkey [157]; Tembi River, Iran [158]; Zarrin-Gol River, Iran [159]; Korotoa river, Bangladesh [160]; Songhua river, China [161]; and Monte Alegro watercourse in Ribeirão Preto, Brazil [162]. The pollution in these locations is described as due to a variety of factors including industrial, domestic and hospital wastewaters, agriculture and runoffs from landfills. In a similar way, the sediments of the Gulf of Taranto, Italy [163] were also analyzed, which receive pollutants from steel industries, oil refineries and the region's rivers.

In Alicante, Spain, the heavy metal content of agricultural soils was evaluated [164, 165]. Similarly, several cities in China were evaluated with the same purpose by Chen *et al.* [166], who studied Xi'an city, and by Cheng *et al.* [167] who surveyed 31 metropolises. The sources of pollution were natural sources but also traffic and industrial activities.

Table 14 presents the relative heavy metal concentration in the evaluated watercourses and Table 15 presents the I_{geo} for soils and sediments.

Table 14 - Comparison of water concentration against water quality standards in watercourses of sites affected by several sources of pollution.

Site [Ref.]	Standard ^a	Relative Water Concentration							
		As	Cd	Cr	Cu	Pb	Hg	Ni	Zn
Dil Deresi, Turkey [157]	DW	29.00	5.00	2.20	0.05	37.00	--	--	--
	IW	2.90	1.50	1.10	0.47	0.07	--	--	2.05
Tembi river, Iran [158]	DW	--	116.67	11.60	0.36	191.00	--	118.57	--
	IW	--	35.00	5.80	3.55	0.38	--	4.15	0.26
Korotoa river, Bangladesh [160]	DW	9.20	7.33	2.52	0.06	6.40	--	10.14	--
	IW	0.92	2.20	1.26	0.60	0.01	--	0.36	--
Songhua river, China [161]	DW	0.38	--	0.36	0.02	2.80	--	--	--
	IW	0.04	--	0.18	0.19	0.01	--	--	0.20
Monte Alegro watercourse, Brazil [162]	DW	--	0.02	0.01	0.00	1.88	--	--	--
	IW	--	0.01	0.01	0.03	0.00	--	--	0.01

^a DW - Drinking Water; IW - Irrigation Water.

Table 14 clearly shows that on these sites the pollution in watercourses is significant. Despite not being affected by a single source of pollution, several anthropogenic factors, like agriculture, industries and road traffic can end up creating significant pollution in water. Tembi river features the most polluted waters, with Cd, Pb and Ni concentrations being 100 times over the limit for drinking-water. The concentration in Dil and Korotoa river, also exceeds the drinking water limit by up to one order of magnitude depending on the cation. In Songhua river and Monte Alegro watercourse, heavy metal contamination is not relevant.

The I_{geo} values reported in Table 15 reveal that, in contrast with the conclusions of sections 2.3.1. and 2.3.2., the soils are not significantly polluted. This is due to the lack of a major source of heavy metal pollution. In the Alicante region [164, 165], for example, only Cd pollution is relevant. As the studied area covers agricultural soils, the Cd contamination is most likely due to fertilizers. In China, soil pollution is greater and relevant: in Xi'an city all quantified elements reveal relevant pollution and in China's metropolises [167] Cd, Pb and Hg are the most significant.

The geoaccumulation index for sediments in Table 15 reveals two contrasting situations: Korotoa river is relevantly polluted for all quantified elements, while in Zarrin-Gol River and the Gulf of Taranto, the sediments are not polluted regarding the quantified elements.

Table 15 - Geoaccumulation indexes for soils and sediments in sites affected by several sources of pollution.

<i>I_{geo} soil</i>								
Site [Ref.]	As	Cd	Cr	Cu	Pb	Hg	Ni	Zn
Segura river valley ^a , Spain [164]	--	0.00 -	-1.32 -	-0.38 -	-1.34 -	--	-0.80 -	-1.22 -
		2.55	0.30	0.54	0.62		0.17	0.05
Alicante ^a , Spain [165]	--	1.18	-0.99	0.10	0.02	--	-0.45	-0.56
Xi'an city ^a , China [166]	0.20 -	--	--	0.01 -	-0.18 -	--	-0.54 -	-0.52 -
	2.43			2.02	2.80		1.58	2.58
China [167]	-1.05 -	-0.59 -	-1.12 -	-0.53 -	-0.78 -	-0.75 -	-1.18 -	-0.97 -
	0.27	2.90	-0.02	0.63	1.59	3.13	-0.11	0.68
<i>I_{geo} sediments</i>								
Gulf of Taranto, Italy [163]	--	--	<0	<0	<0	--	<0	<0
Korotoa river, Bangladesh [160]	-1.2 -	0.51 -	0.39 - 2.1	-0.53 -	0.72 -	--	-0.42 -	--
	3.1	3.9		1.2	1.9		1.7	
Zarrin-Gol River, Iran [159]	-0.87 -	--	-2.15 -	--	--	--	-3.34 -	-2.44 -
	0.62		-1.43				-2.79	-1.84

^a Values calculated based on the concentration reported in the original research and the average upper crust concentration (Table 3).

2.3.4. Portugal

With the intent of giving particular focus to the pollution found nationally, in this section the previously discussed studies performed in Portugal are recompiled. Studies on national sites are scarce and focused on some specific, more problematic sites: Estarreja [120, 121] and Esmoriz-Paramos lagoon [119] - industrial sites; Alto da Várzea [83], Senhora das Fontes [84] and S. Francisco de Assis [112] - mine sites. The highest concentration of these metals, for soils and water, and the study sites' location are illustrated in Figure 7.

As discussed previously, and as is highlighted in Figure 7, the sites studied in the literature reveal extensive pollution levels for several heavy metals. Arsenic and zinc in soils are very relevant in these locations as is zinc in water. However, for water, lead is most worrying, due to its low maximum accepted concentration. It can be concluded that the wastes from the mining and industrial activities are significant and pollute the surrounding areas for long periods of time.

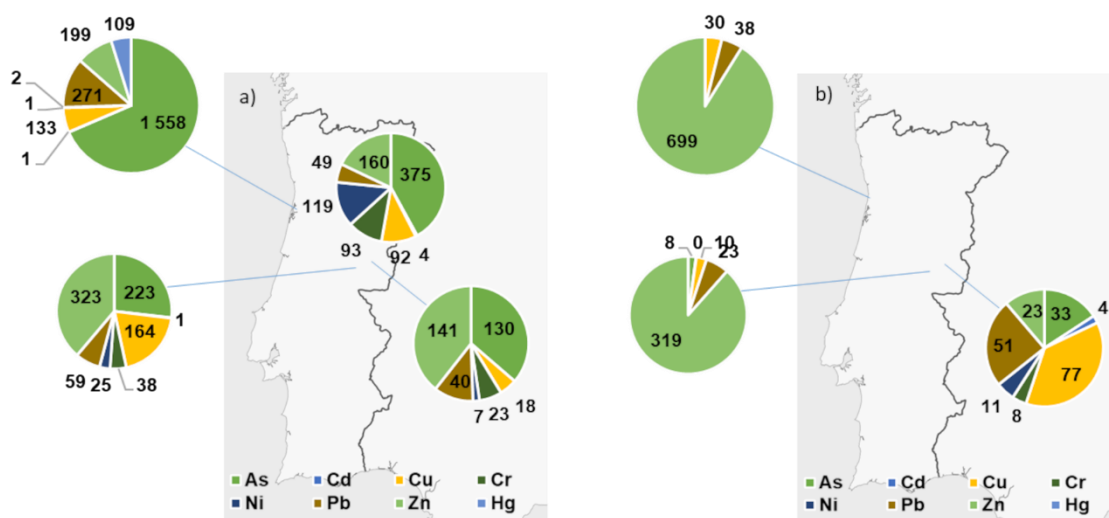


Figure 7 - Distribution of the heavy metals in Iberian Peninsula (a) in soils (quantities in mg kg⁻¹) and (b) in water (quantities in µg L⁻¹).

2.4. Techniques for Removal of Heavy Metals from Aqueous Media

Getting clean drinking water is essential and so water purification has been implemented by humans since ancient times [168]. The people settled in the Indus river valley (as early as 5500 BCE) filtered water with charcoal and used alum for purification. Ancient Egyptians also applied alum and used seeds from *Moringa oleifera* to purify water. In Ancient Greece, Hippocrates designed the so-called Hippocratic sleeve and Aristotle experimented with wax as a filter and proposed distillation to obtain clean water [168]. Recently, the discovery of zeolites in a reservoir in Tikal, a Maya city, presents evidence for the oldest zeolite water purification system, functional ~2200 years ago [169]. The authors concluded that the zeolites were deliberately brought to the city and placed in the reservoir to form a water purification system that had to be replaced following floods.

In addition, in order to comply with regulations, wastewaters and water destined for human consumption have to be treated. Removal of heavy metals from these can be achieved by several processes, from the most simple - chemical precipitation, to highly efficient membrane or electrochemical processes.

Section 2.4.1. presents an overview on the different processes used to remove heavy metals from liquid media. A schematic representation of each of these processes is presented in Figure 8. Section 2.4.2. discusses the suitability of the techniques described, given the values presented in Section 2.3..

2.4.1. Overview of Heavy Metal Removal Techniques

Different strategies used to remove heavy metal cations from liquid media are briefly discussed in this section. Table 16 summarizes the advantages and disadvantages of different processes.

Chemical precipitation is the most employed strategy and is the simplest [58, 170]. By adding a precipitation agent to the effluent, the cations react to form insoluble species that precipitate from solution. Typically, this occurs by hydroxide precipitation, using agents like lime to raise the effluent's pH. Metal hydroxides are amphoteric, so their solubility increases at low and high pH values. As a result, each ion has its own optimal pH for precipitation, value at which other salts can become more soluble. For practical purposes, the optimum pH range for the precipitation of all metals is 8.5-9. Sulfides can also be used as precipitation agents (*e.g.* pyrite), as the metal sulfides have lower solubility than the corresponding metal hydroxides. In this case, the dissolution of the sulfide agent generates H₂S and the metal cations precipitate at acidic conditions. Neutralizing the medium to avoid exposure to the toxic H₂S is crucial [58, 170, 171]. The precipitates are separated by filtration or sedimentation. Chemical precipitation generates a large volume of sludges (metal hydroxide sludges are considered low density sludges), with costly treatment and disposal. Besides, this method leads to higher concentration of salts in the wastewater which does not meet the criteria for its disposal [58, 170-172]. Coagulation and precipitation agents can be simultaneously used to enhance the treatment efficiency [58]. SUEZ's sells commercial polymer precipitation agents as the *MetClear* product line [173].

Coagulation and flocculation can also be employed to remove heavy metals as well as suspended matter [58, 170, 174]. Adding coagulants like aluminum or ferrous sulfate, leads to the destabilization of colloids into aggregates. Flocculation uses polyelectrolytes to bind particles into large agglomerates. Widely used flocculants include polyferric sulfate, aluminum sulfate and polyacrylamide. The agglomerates can afterwards be removed by sedimentation and filtration.

Membrane filtration technologies can also be employed to remove heavy metals [58, 170, 175]. Ultrafiltration (UF) membranes have pores larger than hydrated cations and low molecular weight solutes. Thus, to retain dissolved heavy metals, surfactant micelles that bind to cations or polymers that form complexes with them are added to the effluent, producing structures that are retained by the membrane [58, 170, 175-178]. Nanofiltration (NF) can be an alternative for some cations like nickel, chromium and arsenic. The membranes used are charged and their unique steric (size exclusion) and electrical (Donnan exclusion) effects allow the membrane to reject charged solutes smaller than the membrane's pores [170, 175]. Reverse osmosis (RO) can also be used for this purpose. By applying pressure, the semi-permeable membrane used in this process is able to

reject the majority of dissolved contaminants. It is shown that this technique is able to retain most heavy metals [58, 170, 175].

Ion exchange uses porous solids to reversibly exchange ions between the resin (solid phase) and the effluent under treatment (liquid phase). The ions are exchanged for similar ones and electroneutrality is maintained [179]. Generally inorganic zeolites or polymeric resins are used. To remove heavy metals, cation-exchange resins must be chosen: two common types are the strongly acidic featuring sulfonic groups and the weakly acidic resins, featuring carboxylic groups. Selective resins are available making this process suitable to recover valuable metals [58, 170, 180]. This process is known to generate good results at reasonable costs. Lanxess's *Lewatit* product family includes ion exchangers for heavy metals [181-183], and Dow, Dupont and Rohm and Haas also sell multiple solutions.

Electrochemical methods are also an option to remove heavy metals from water [58, 170, 175] and are typically associated with metallurgical industries. Electrodialysis is a membrane process in which ionized species exchange through charged membranes by applying electric potential. The charged species move across the electrodialysis cell, passing through cation and anion exchangers as they are attracted to the anode or cathode, and are concentrated in the concentrate stream (brine) [184]. Electroplating is a process in which a cation is reduced to a zero-valence state, at the surface of a substrate, by applying electric current [185]. Thus, the ion is reduced in a non-spontaneous reaction, at the expense of energy. This process is also called electrochemical deposition. The substrate at which the metal deposits acts as the cathode of the electrolytic cell, connected to the negative pole. Both electrodes can be an inert or the anode can be sacrificial [186]. When the ion is at the cathode/electrolyte interface, it is stripped of its hydration shell, adsorbed, reduced to an atom and then nucleation and crystal growth occur [185]. It is considered a "clean" process and is useful to recover valuable cations. Employing the same electrolytic cell and adjusting the electric tension applied, the process can be used in a selective way for a multitude of species.

Adsorption is another process used for the removal of heavy metals from liquid media [58, 170, 175, 187, 188]. In this process, the adsorbate present in the liquid phase, net accumulates at the surface of the solid phase - adsorbent. Adsorption is already employed as an additional step to remove organic and inorganic contaminants, down to acceptable levels, in water and wastewater treatment [189]. The efficiency of the process is intimately related to the adsorbent's properties - surface area or active sites, selectivity and kinetics. With the appropriate adsorbent, high efficiencies and fast kinetics can be obtained, while cheap adsorbents can make the process more viable. The variety of adsorbents developed [190], ensure versatility, efficiency, simplicity in design and operation and possible selectivity to the technique [191, 192]. Conventional commercial adsorbents

include clinoptilolite, bentonite, montmorillonite and activated carbon [188]. *Metsorb* from Graver Technologies is an example of engineered commercial adsorbent [193].

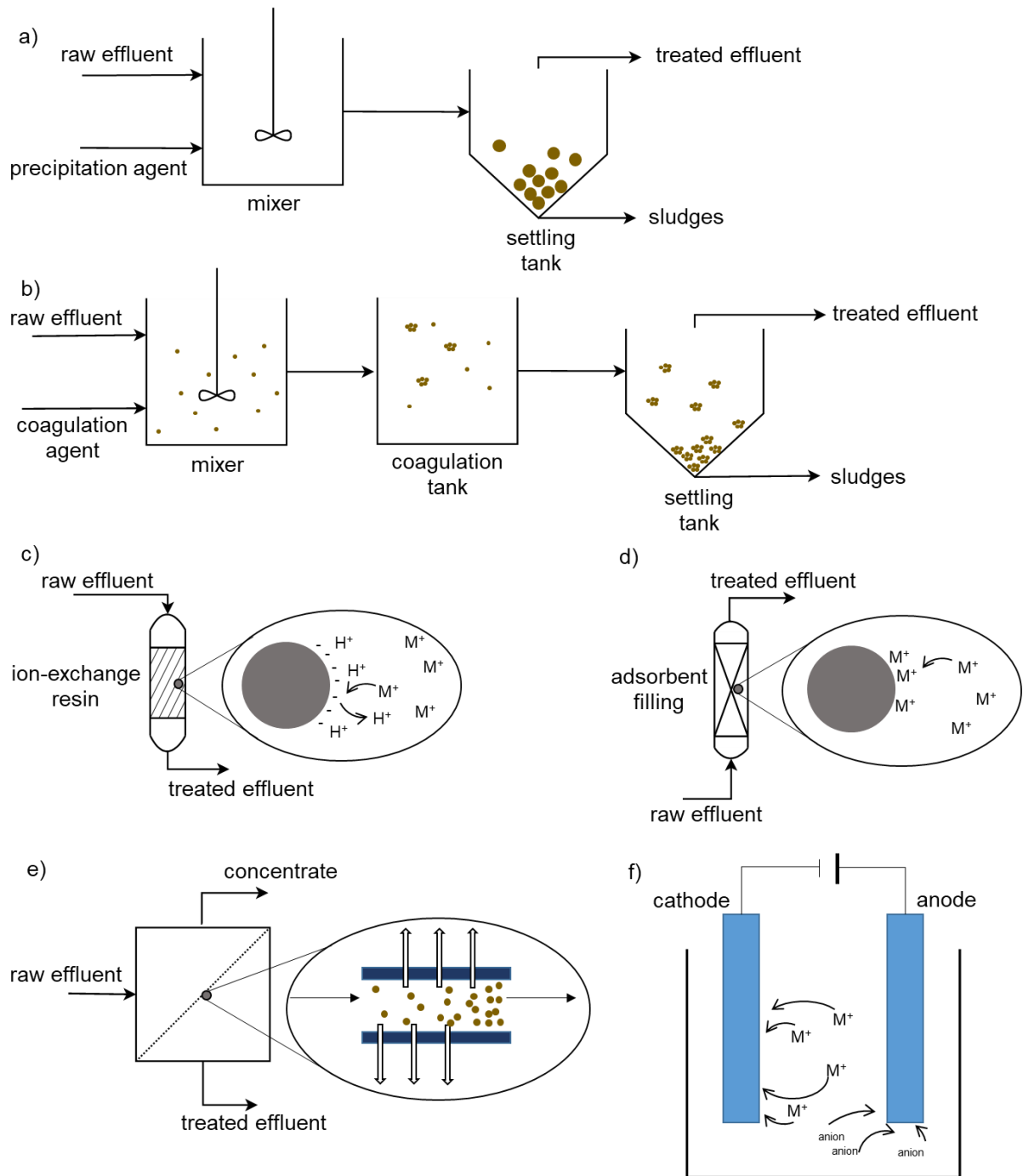


Figure 8 - Schematic representation of heavy metal laden aqueous effluents treatment processes: a) chemical precipitation; b) coagulation-flocculation; c) ion-exchange; d) adsorption; e) membrane filtration; f) electrodeposition.

Table 16 - Comparison of advantages and disadvantages of different treatment techniques for heavy metal laden liquid media [58, 170, 175].

Process	Advantages	Disadvantages
Chemical Precipitation	Low cost Low energy requirements Simple design/operation Safe operation	Production of high volume of sludge High cost for sludge disposal High consumption of precipitant agent Increasing difficulty in meeting disposal standards
Coagulation-Flocculation	Reduced time to settle suspended solids Improved sludge settling	Sludge production High cost for sludge disposal
Membrane Filtration	Small space requirement High efficiency Low pressure of operation (UF) High rejection rate (RO)	High operation cost Membrane fouling High pressure operation (RO) High energy consumption (RO)
Ion Exchange	No sludge production High removal capacity Fast kinetics Can be selective	Not all resins are adequate Resins have to be regenerated Treatment of regeneration solution High cost
Electrochemical	Selective separation High efficiency No sludge production	High cost High energy consumption
Adsorption	Simple design and operation Low initial cost High efficiency Low-cost adsorbents available Can be selective	Efficient adsorbents can be expensive Loaded adsorbent needs disposal/regeneration

2.4.2. Suitability of Removal Techniques for Real World Media

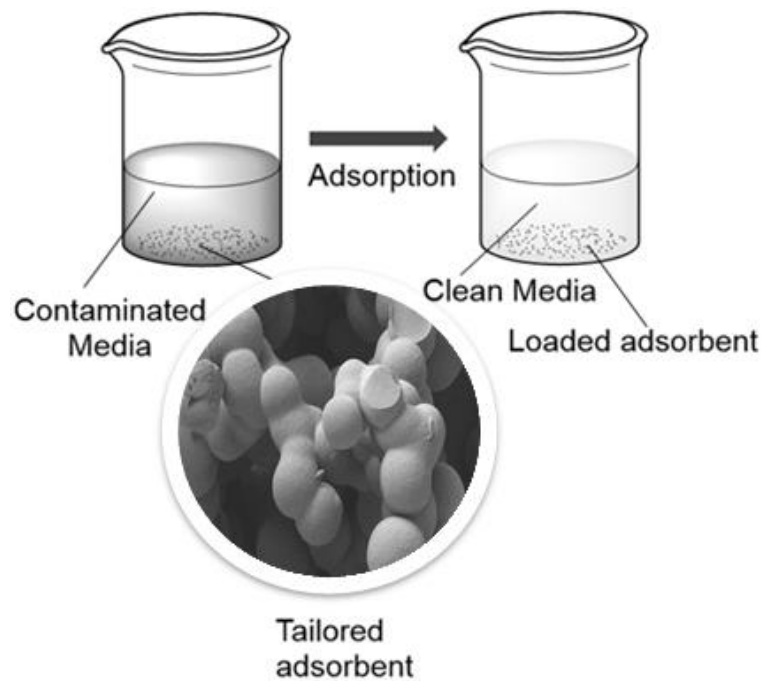
Section 2.3. reveals that the concentration of heavy metals in the water from watercourses in real world polluted sites is usually less than a mg L^{-1} . These concentrations are low, and thus, further treatment in order to comply with legislation is a difficult task. A possible and sustainable approach is to use cleaning processes that work well with low concentrations and achieve high efficiencies. In these cases, membrane filtration, ion exchange and adsorption processes can work with low initial concentrations and achieve high efficiency, generating very low concentrations in the output stream. Membrane filtration is expensive, its operation is not simple and membranes suffer from fouling among other drawbacks. Ion exchange is simple in design and operation and the resins are regenerable; however, it becomes costly when treating large amounts of effluent at low concentrations and the cations in the regenerating effluent are sent for treatment - normally chemical neutralization. Adsorption can be economically viable as it is of simple design and operation if the right adsorbent is used. An adsorbent that allows the process to achieve high efficiency and is inexpensive [194] makes this process a serious contender for efficient and economically viable solution to purify heavy metal laden water, even at higher concentrations. The loaded adsorbent needs to be properly disposed, which brings additional costs, but similarly to ion exchange, some adsorbents can be regenerated. A more expensive adsorbent that can be

regenerated can be more useful than a disposable adsorbent. Chemical precipitation aided with coagulants and high amounts of lime could also achieve very low final concentrations. However, this result is more difficult to achieve and occurs at the expense of major amounts of precipitation and coagulation agents, increasing costs and producing high volume of sludges that are expensive to treat and dispose of. In sum, in this situation, adsorption with reasonable cost and regenerable adsorbents seems the most inexpensive approach to purify the water from natural watercourses in order to be adequate for human consumption.

Some watercourses feature higher concentrations of heavy metals ($\sim 200 \text{ mg L}^{-1}$ of Cu and $\sim 700 \text{ mg L}^{-1}$ of Zn [85]; $\sim 13 \text{ mg L}^{-1}$ of As [99]; 11 mg L^{-1} of Pb and 27 mg L^{-1} of Ni [150]), as do the effluents from Table 11. These are very high when compared to drinking or irrigation water standards; nevertheless, these concentrations are still well within the concentration range for which the treatment techniques are capable of working efficiently [170, 176, 194-196]. For these situations, the techniques discussed previously are all applicable, with the same limitations. For the specific case of metallurgy industries, the possibility to recover the heavy metals is a key challenge, as these are used as raw materials. Ion exchange resins [180] and adsorbents [191, 192] can be selective, allowing to recover the desired cations, which gives an economical advantage to these two techniques. The sludges produced from chemical precipitation impair the recovery and reuse of those cations. For the cases of the effluents evaluated by John *et al.* [134] and Frank *et al.* [137], since one of the pollutants features extremely high concentrations ($>1000 \text{ mg L}^{-1}$), chemical precipitation becomes the most suited strategy. However, polymer enhanced ultrafiltration has also shown to be effective in very high concentrations [176], although much costly. Electrochemical processes are very expensive but for the case of metallurgical and surface treatment industries these can be adequate since the high operation cost is offset by the value of recovering high amounts of metal. These processes can also be selective, increasing the reusability of the recovered cations.

Chapter 3

Aerogels as Adsorbents of Heavy Metals



Part of the content of this chapter is based on the author's published works *Heavy metals in Iberian soils: Removal by current adsorbents/amendments and prospective for aerogels*, *A reconsideration on the definition of the term aerogel based on current drying trends*, *Assessment of heavy metal pollution from anthropogenic activities and remediation strategies: A review*, *Ligands as copper and nickel ionophores: Applications and implications on wastewater treatment* and *Insights on toxicity, safe handling and disposal of silica aerogels and amorphous nanoparticles*.

3.1. Sorptive Processes

Adsorption is a process in which a chemical species in a fluid phase (liquid or gas) net accumulates at the surface of a solid [197, 198]. The solid - adsorbent - and the chemical species in the fluid phase - adsorbate - become attached by physical or chemical interactions, due to unbalanced forces, reducing the surface free energy [199]. Sorption, on the other hand, is generally used to describe the initial penetration and dispersal of a sorbate into a solid matrix; the term includes adsorption, absorption, incorporation into microvoids and cluster formation [200].

The adsorption process comprises several steps: mass transport of the adsorbate in the bulk of the fluid phase; diffusion of adsorbate in the film at the solid-fluid interface; pore diffusion of the adsorbate through the adsorbent and surface reaction where the interactions between adsorbent and adsorbate take place [201].

In the adsorption of species from liquid phases, the amount of species adsorbed q_t (mg g^{-1}) at moment t is related to the bulk concentration of the species in the liquid phase C_t (mg L^{-1}), and can be calculated using Equation 3,

$$q_t = \frac{V(C_0 - C_t)}{m} \quad (3)$$

where V represents the volume of liquid phase (L), m the mass of adsorbent (g) and C_0 is the initial concentration of the adsorbate solution (mg L^{-1}). As time approaches infinity the adsorption equilibrium is achieved: $q_t = q_e$ and $C_t = C_e$.

The amount of species adsorbed can also be quantified as a removal efficiency in percentage (RE%) - Equation 4.

$$RE\% = \frac{C_0 - C_e}{C_0} \times 100 \quad (4)$$

The analysis of equilibrium, kinetics and thermodynamic parameters of adsorption processes allows the comprehension of the interactions between the adsorbent and adsorbate.

3.1.1. Adsorption Mechanisms

The removal of heavy metals via adsorption can be due to different phenomena like surface precipitation, surface complexation, cation exchange, cation- π interactions, Coulomb forces, van der Waals forces or hydrogen bonding, which are the sorption mechanisms [202-206]. The hydration sphere of the cation has been shown to be important for the adsorption process, with the loss of water molecules occurring during the binding process to the surface - inner-sphere complexation [33, 207-209]. In fact, the dehydration of the cation can act as a driving force for the adsorption process [33, 207-209]. Outer-sphere complexation occurs when the hydration shell of the cation is maintained, and the adsorbent-adsorbate interactions occur *via* hydrogen bonding or are of long-range electrostatic nature [210].

The sorption type (chemisorption or physisorption) can be inferred from information provided by the isotherm and kinetic models and confirmed by the thermodynamic parameters. However, these two types of sorption are limit situations; in real processes, a combination of chemical and physical interactions (hybrid scenario) is more probable. Physical adsorption is nonspecific and the formation of adsorbate multilayers at the surface of the adsorbent can occur; it is rapid, reversible and only significant at low temperatures. Chemisorption involves high heat of adsorption, is specific and only occurs in monolayers. In general, it involves transfer of electrons to form bonds between the adsorbent and adsorbate (mainly ionic and covalent), thus, irreversible [199, 211]. From a thermodynamic point of view, physical adsorption involves low enthalpy changes ($< 20 \text{ kJ mol}^{-1}$) while for chemisorption the enthalpy change is typically bigger than 80 kJ mol^{-1} .

The adsorption of metal ions from aqueous media is generally controlled by the adsorbent's surface chemistry and surface area or by precipitation reactions [202]. It is known that the interaction of Lewis bases modified adsorbents with the heavy metal cations may be explained by the Pearson acid-base concept (hard and soft (Lewis) acids and bases, HSAB theory). This interaction occurs in the form of coordination bonds, surface complexation mechanism, found in previous studies [205, 206, 212-217]. When surface precipitation is a dominant mechanism the adsorption isotherms features a characteristic vertical shape, having similar equilibrium concentrations for different initial concentrations [202].

3.1.2. Adsorption Kinetics

The adsorption kinetics evaluates the effect of contact time between adsorbate and adsorbent, allowing to obtain the rate constant of adsorption processes. It also gives insight on the type and mechanism of adsorption, information that is complemented with the one obtained from the isotherm models. The kinetic model reveals which phenomena of the adsorption process is the slowest, therefore identifying the mechanism [201].

The sorption kinetic models used in this work, including those most relevant for heavy metals [218] in their differential and integrated forms, are summarized in Table 17.

Table 17 - Relevant sorption kinetic models for heavy metals.

Model	Differential Form	Integrated Form
Pseudo-First Order	$\frac{dq_t}{dt} = k_1(q_e - q_t)$ (5)	$q_t = q_e(1 - e^{-tk_1})$ (6)
Pseudo-Second Order	$\frac{dq_t}{dt} = k_2(q_e - q_t)^2$ (7)	$q_t = \frac{q_e^2 k_2 t}{q_e k_2 t + 1}$ (8)
		$q_t = q_0 + \frac{q_e^2 k_2 t}{q_e k_2 t + 1}$ (9)
Double Exponential Model	$\frac{dq_t}{dt} = \frac{D_1 k_{D1}}{c} e^{-k_{D1}t} - \frac{D_2 k_{D2}}{c} e^{-k_{D2}t}$ (10)	$q_t = q_e - \frac{D_1}{c} e^{-k_{D1}t} - \frac{D_2}{c} e^{-k_{D2}t}$ (11)
Intraparticle Diffusion	--	$q_t = k_{IPD}t^{0.5} + E$ (12)

The pseudo-first order equation (Equation 5), also called Lagergren's first order rate equation [219], is used to describe adsorption in heterogeneous systems and is likely the oldest rate of adsorption model for liquid-phase systems [201]. The appropriate boundary conditions for integration of the equation are $q(t=0)=0$ and $q(t=\infty)=q_e$. k_1 is the first order rate constant (h^{-1}), t is the time (h) and q is the sorbate uptake (mg g^{-1}). The equation shows that the adsorption process is only dependent on the sorbate concentration - diffusion-controlled process [201, 220].

The pseudo-second order equation (Equation 7), also known as Ho and McKay equation [221], is usually the most suitable to describe the adsorption of heavy metals. It is integrated with the same boundary conditions of Equation 5. The parameter k_2 is the pseudo-second order adsorption rate constant ($\text{g mg}^{-1} \text{h}^{-1}$) and it depends on the operating conditions [201]. Equation 9 presents a more generic form of the equation, modified pseudo-second order model, in which q_0 represents an initial sorption, which can be explained by an initial boost sorption. This equation reveals that the surface reaction limits the overall kinetics. As such, it is shown that chemisorption is the rate limiting step in the adsorption process; this can be easily justified by a monolayer or

multilayer sorption or by irreversible sorption/desorption cycles. It is accepted that the surface reaction is of second order with respect to the number of available active sites [201].

The double exponential model (Equation 10) [222] describes a two-step kinetic adsorption process, where the adsorption starts with a fast step (step 1) and then progresses slowly towards equilibrium (step 2). In this equation, k_D (h^{-1}) is the adsorption rate constant (in general, related with the diffusivity), D_i (mg L^{-1}) represents the maximum adsorbed amount at step i and c is the concentration (g L^{-1}) of adsorbent in the test [223]. If k_{D1} is much greater than k_{D2} the equation can be simplified by assuming that the term corresponding to the rapid step is null. This model usually describes diffusion limited processes, with the fast step being associated with external diffusion and the slow step with intraparticle diffusion, but it can also describe adsorbents with two types of active sites on their surface, in which case this model is used as two-site model and does not describe a diffusion limited process [223].

The intraparticle diffusion model of Equation 12 was presented by Weber and Morris and is based on Fick's 2nd law equation [224, 225]. It states that the adsorbate uptake is proportional to the square root of time. k_{IPD} ($\text{mg g}^{-1} \text{h}^{-0.5}$) is the rate constant and depends on the diffusion coefficient, and E (mg g^{-1}) is a constant shown to be correlated to the boundary layer thickness [224].

3.1.3. Adsorption Isotherms

Adsorption isotherms evaluate the effect of the initial concentration of adsorbate and provide information about the mechanism, surface properties and degree of affinity towards sorbates [226]. These models apply to experimental data obtained at equilibrium conditions.

The most important sorption isotherms for heavy metals removal [218] and others used in this work are summarized in Table 18.

Table 18 - Relevant sorption isotherm models for heavy metals sorbates.

Model	Equation
Langmuir	$q_e = \frac{q_m K_L C_e}{1 + K_L C_e}$ (13)
	$R_L = \frac{1}{1 + K_L C_0}$ (14)
Freundlich	$q_e = K_f C_e^{1/n_F}$ (15)
BET (Brunauer–Emmett–Teller)	$q_e = \frac{q_m K_L C_e}{(1 - K_S C_e)(1 - K_S C_e + K_L C_e)}$ (16)
Langmuir-Henry	$q_e = \frac{q_m K_L C_e}{1 + K_L C_e} + K_H C_e$ (17)

The Langmuir isotherm [227] (Equation 13) is the most common model. It considers a homogenous surface of the adsorbent where adsorption occurs at specific sites, active sites, that are identical and equivalent and accommodate only one molecule of sorbate per site - monolayer adsorption [198, 228]. Thus, it is assumed that chemisorption is behind the adsorbate-adsorbent interactions. In this equation, K_L ($L\ mg^{-1}$) is the Langmuir constant, and q_m ($mg\ g^{-1}$) is the maximum adsorption capacity.

One can evaluate if the adsorption is favorable or not by calculating the separation factor (Equation 14). The value of R_L indicates that adsorption is irreversible when its value is zero, favorable for $0 < R_L < 1$, linear when its value is one, or unfavorable for $R_L > 1$.

The Freundlich sorption isotherm (Equation 15) [229], describes the adsorption on heterogeneous surfaces [198]. The Freundlich constant, K_F ($mg\ g^{-1} (L\ mg^{-1})^{1/n_F}$), indicates the relative adsorption capacity of the adsorbent, and $(1/n_F)$ is the heterogeneity factor, approaching zero with heterogeneous surfaces. The heterogeneity factor also gives information on the adsorption type - chemisorption occurs when this factor is smaller than one while multilayer adsorption occurs when it is greater than one. If the heterogeneity factor is one, the equation is reduced to Henry's law. The Freundlich equation is empirical and has no thermodynamic grounds [198].

The BET (Brunauer–Emmett–Teller) isotherm model [230] describes multilayer adsorption and was initially conceptualized for the sorption of gaseous species. The BET theory assumes that the first layer is Langmuir-like, and so it is reduced to the Langmuir equation when there is only one sorbed layer; that the upper layers have equal heat of adsorption and adsorption/desorption rates and are therefore equal among themselves [231, 232]. It can be expressed for liquids (Equation 16) [231], in which q_m represents the monolayer sorption capacity ($mg\ g^{-1}$), K_L is the equilibrium constant for the first adsorbate layer (Langmuir constant, $L\ mg^{-1}$), and K_S is the equilibrium constant for the upper layers. C_{BET} is equal to K_L divided by K_S .

The Langmuir-Henry model (Equation 17) combines both the Langmuir and Henry isotherms [200], describing sorption both at active surface sites and by the dissolution of the sorbate inside the porous matrix. K_L is the Langmuir constant and has the same meaning as in the Langmuir isotherm ($L\ mg^{-1}$), and K_H is the Henry constant ($L\ g^{-1}$).

3.1.4. Adsorption Thermodynamic Parameters

The analysis of thermodynamic adsorption parameters allows to get further understanding of the process, namely the nature of the sorbate-sorbent interactions.

The calculation of the thermodynamic parameters of adsorption requires the estimation of the adsorption equilibrium constant at different temperatures. While not the most rigorous approach, the equilibrium constant is commonly estimated testing only one adsorbate concentration at each temperature and using the distribution coefficient, K_d (L g^{-1}), Equation 18 [233, 234]. The adsorption standard Gibbs free energy variation (kJ mol^{-1}) is calculated with Equation 19 [233]. The adsorption standard entropy ($\text{J mol}^{-1} \text{K}^{-1}$) and enthalpy (J mol^{-1}) variations are estimated via fitting using a modified van't Hoff equation, Equation 20.

$$K_d = \frac{q_e}{C_e}, \quad (18)$$

$$\Delta G^0 = -RT \ln K, \quad (19)$$

$$\ln K = \frac{\Delta S^0}{R} - \frac{\Delta H^0}{RT}, \quad (20)$$

The modified van't Hoff equation assumes that the standard enthalpy and entropy changes are constant in the considered range of temperatures. The spontaneity of the process in the standard conditions is evaluated by the standard Gibbs free energy variation. The standard enthalpy change indicates if the sorption process is exothermic, endothermic or athermic, being entropy driven *i.e.* $|\Delta H^0| < |T\Delta S^0|$, in the latter cases [208, 209]. The adsorption enthalpy also indicates the strength of adsorbent-adsorbate interactions, increasing with its value (in modulus), hence chemisorption is associated with high heats of adsorption ($> 80 \text{ kJ mol}^{-1}$) [234]. Low entropy variations reveal that there are no significant changes in the disorder of the system during the adsorption at the interface between phases [234].

3.1.5. Desorption and Adsorbent Regeneration

Desorption is the reverse process of adsorption and both occur simultaneously, as the process is dynamic [235]. However, extensively desorbing the sorbates is necessary to regenerate the adsorbent. When the loaded adsorbent is placed in a solution, the adsorption/desorption dynamic process resumes, and desorption agents favor the desorption reaction. This is not always easy and is dependent on the nature of sorbate-sorbent interactions. Solutes adsorbed by physical

interactions and ion exchange are easily desorbed. When cation- π interactions are responsible for the adsorption, the adsorbates are potentially desorbed in natural environments, while adsorbates sorbed by surface complexation are not easily desorbed [204].

When physical adsorption occurs, higher temperatures and low pressures favor the desorption of sorbates, while chemisorption is usually irreversible [235]. When the sorbate-sorbent interactions are very strong, desorbing species may result in/require the destruction of the sorbent and/or of the sorbate [236]. This impedes the reutilization of adsorbents but may be required to recover valuable sorbates or treat materials loaded with dangerous pollutants.

Acids are commonly used for desorption procedures of metals [237-240]. Because metal cations in solution act as Lewis acids, the hydrolysis of their hydrated species ($M(H_2O)_n^{z+}$) results in the release of hydronium ions to the solution and new hydrated species ($M(H_2O)_{n-1}(OH)^{(z-1)+}$) are formed [34]. In an acidic, low pH media, hydrolysis is prevented. Hydronium ions have high affinity for Lewis bases active surface groups, and at $pH < pK_a$ of surface ligands, they protonate the latter. The pH dependent surface charge is the reason why at $pH < pK_a$ of surface ligands, adsorption of metal cations is not favored [241]. Acids can also degrade the sorbent, releasing the sorbate. Bases, also frequently used as desorption agents [242-244], can increase the solubility of the metal ion, by the formation of metal hydroxides [34-37]. As such, the adsorption/desorption equilibrium is dislocated toward the presence of cations in solution. Furthermore, these species are also not easily sorbed. Bases are corrosive and can also promote desorption by the degradation of the adsorbent.

3.2. Heavy Metal Adsorbents in the Literature

The versatility, efficiency and low cost of the adsorption process has spiked the interest for this process, already widely used, and hundreds of new adsorbents and natural materials have been researched for their heavy metal removal capabilities. These facts are evidenced by the increasing number of publications in recent years on heavy metal adsorption - Figure 9. Engineered materials developed as higher efficiency adsorbents can be synthesized with controlled porosity and/or surface chemistry, among other properties, to ensure interaction with adsorbates and maximize their performance.

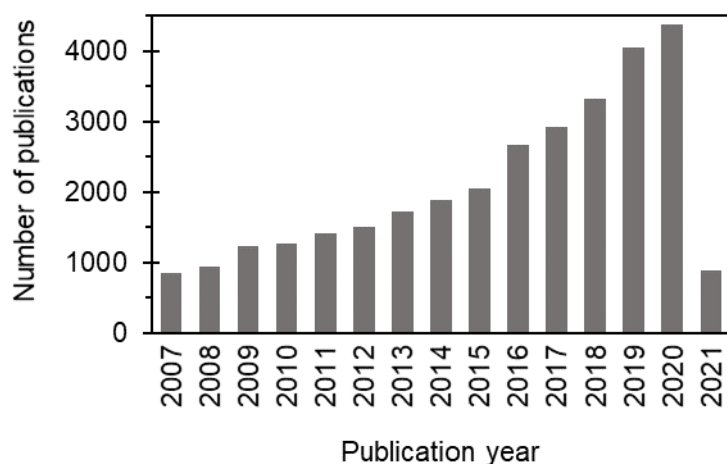


Figure 9 - Evolution of the number of publications per year, according to the *Web of Science* database for the past fifteen years, in heavy metal adsorption and adsorbents. Search keywords: heavy metal* and sorption, adsorption, adsorbent, sorbent. Data obtained at 22/04/2021.

The types of adsorbents used for heavy metals include natural materials and their derivatives, polymers, carbon adsorbents, mesoporous silicas and aerogels. Selected works using these adsorbents are briefly discussed below and their adsorption capacities, for the cations under focus in this thesis, are summarized in Table 19 and represented (maximum values only) in Figure 10.

Natural adsorbents include zeolites, clay materials, natural polymers and organic wastes. Zeolites are crystalline aluminosilicate minerals that occur naturally but can also be synthesized [245]. These have been investigated for the purpose of adsorbing heavy metals in their natural state [246-249], after modification [249-251] and as synthetic zeolites [248, 252-254]. Clays are natural materials that combine hydrous aluminosilicates - clay minerals - with metal oxides and organic matter. Unmodified clay minerals [251, 255-257], synthetic ones [258, 259] and modified/engineered minerals [240, 260-262] can be used for the adsorption of metal ions from water. Natural polymers such as chitin and chitosan have also been successfully employed as heavy metal adsorbents in their natural form [263, 264] or in composite adsorbents [191, 265-267]. Hokkanen *et al.* [244] developed an aminated micro fibrillated cellulose for this purpose. Organic waste materials, such as sawdust [268] and engineered materials from such wastes [269] were equally tested with this goal. Biochars are produced from organic wastes and can be used as adsorbents [270-273]. More complex materials, such as an aminothiourea chitosan modified magnetic biochar composite are also reported as heavy metal adsorbents [274].

Engineered adsorbents are based on a wide range of materials. These can be based on iron nanoparticles [275, 276], titania nanoparticles [277], synthetic polymers [278-280], polymer sponges [281] and polymer hydrogels [282]. An aminopropyl functionalized H-RUB-18 (sodium silicate) was developed by Macedo *et al.* [283].

Carbon-based adsorbents have also been employed to adsorb metal cations. Carbon nanotubes (CNTs) [284-286] and activated carbon [270, 287-289] were studied by some authors. Hayati et al. [290, 291] studied the adsorption properties of a poly(amidoamine)/CNT composite, while a magnetic graphene oxide grafted polymaleicamide dendrimer was developed by Ma *et al.* [292].

Mesoporous silicas are very interesting materials that are widely studied as adsorbents. Nanoparticles such as functionalized Santa Barbara Amorphous (SBA) [293], Mobil Composition of Matter (MCM) [205, 216, 294-297], PVA/amine MCM-41 composite [298] and other [299] were developed for this purpose. Furthermore, modified silica gels [300-305] and other mesoporous silicas were tested [242, 306, 307] for the same purpose. Amine modified mesoporous silica particles were tested by Hao *et al.* [308, 309], Allothman *et al.* [238] and Chen *et al.* [310]. A silica-cellulose nanofibrils composite was developed by Agaba *et al.* [311], while a PVA/SiO₂ composite nanofiber membrane [312] and cross-linked PVA/NH-SiO₂ beads [313] were also reported. Nonporous sulfonic acid functionalized silica microspheres were prepared and tested by Qu *et al.* [314].

For the adsorption of heavy metals, silica aerogels [315-319], cryogels [320], xerogels [239], organic aerogels [321-324], other types of inorganic aerogels [325, 326] and carbon aerogels [327, 328] were developed and tested. Composite aerogels like carboxylated magnetic cellulose aerogels have also been developed [329].

Furthermore, some adsorbents were developed with the goal of being selective for a particular heavy metal cation [213, 330-339]. To achieve such goal, these adsorbents were modified with ionophores, as discussed in more detail in Section 3.4..

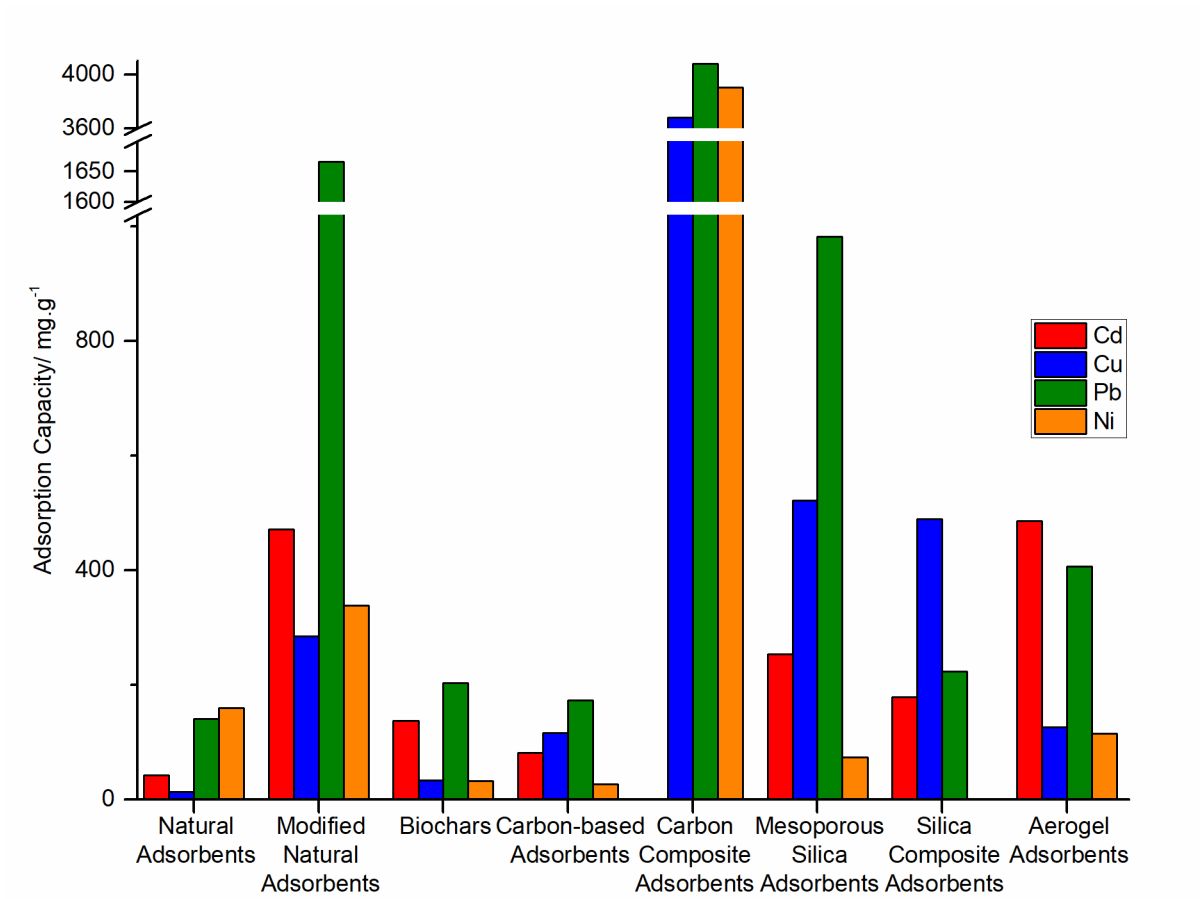


Figure 10 - Maximum adsorption capacity for heavy metal cations, according to the literature data reported in Table 19.

Table 19 - Adsorption capacity, whenever possible from the isotherm model, for heavy metals by different adsorbents in the literature.

Material	Adsorption capacity/ mg g ⁻¹				Ref.
	Cd	Cu	Pb	Ni	
Clinoptilolite	--	9.0	--	--	[246]
Clinoptilolite	--	12.7	--	--	[247]
Chabazite	--	11.4	--	--	[247]
Natural zeolite	4.6	5.9	--	2.0	[248]
Natural zeolite	4.0	--	59.4	--	[249]
Mg-zeolite	36.9	15.2	58.5	--	[250]
Fe (III) modified zeolite	66.2	--	213.3	--	[249]
Ca modified zeolite	1.1	--	55	--	[251]
Zeolite from fly ash	--	82.7	--	--	[252]
Zeolite X from kaolin	92.6	43.8	213.4	24.9	[253]
Synthetic zeolite	50.8	50.5	--	20.1	[248]
Synthetic zeolite A	185.5	--	--	--	[254]
Bentonite	5.0	--	55	--	[251]
Kaolinite	--	10.8	--	1.7	[255]
Montmorillonite	--	7.6	--	12.9	[256]
Beidellite	42.0	--	83.3	--	[257]
Nano hydroxyapatite	142.9	--	1000.0	40.0	[258]
Synthetic hydroxyapatite	--	--	--	14.5	[259]
Expanded perlite	--	1.9	--	--	[260]
Chitosan/ hydroxyapatite composite	--	--	909	--	[261]
Carboxymethyl cellulose / hydroxyapatite composite	--	--	625	--	[261]
Amine modified saponite	--	--	--	148.5	[240]
Methylene bisacrylamide-co-acrylic acid/bentonite composite	416.7	222.2	1666.7	270.3	[262]
Chitin from silkworm chrysalides	--	--	32.0	61.2	[263]
Chitosan from silkworm chrysalides	--	--	141.1	52.8	[263]
Chitosan	--	--	--	159.1	[264]
Chitosan-MAA nanoparticles	1.8	--	11.3	0.9	[191]
Chitosan coated PVC beads	--	87.9	--	120.5	[265]
Cross-linked magnetic chitosan particles	--	126.6	--	66.2	[266]
Poly Ethyleneoxide/chitosan nanofiber membrane	232.3	285.1	214.8	338.6	[267]
Amine modified micro fibrillated cellulose	471.6	200.2	--	159.9	[244]
Citric acid modified sawdust	12.8	15.1	48.5	9.8	[268]
Orange peel/Iron oxide composite NP	71.4	--	--	--	[269]
Jarrah biochar	--	4.4	--	--	[270]
<i>Sida hermaphrodita</i> biochar	35.7	33.3	--	--	[271]
<i>Tectona grandis</i> biochar	--	--	--	32.9	[272]

Table 19 - Adsorption capacity, whenever possible from the isotherm model, for heavy metals by different adsorbents in the literature (continued).

Material	Adsorption capacity/ mg g ⁻¹				Ref.
	Cd	Cu	Pb	Ni	
<i>Amorphophallus konjac</i> biochar	137.6	--	202.8	--	[273]
Aminothiourea chitosan modified magnetic biochar composite	93.7	--	--	--	[274]
Nano zerovalent iron	769.2	--	--	--	[275]
Aminated iron oxide nanoparticles	75.2	--	170.4	--	[276]
Poly(amidoamine) functionalized TiO ₂	288.0	312.0	301.0	--	[277]
Perfluorous conjugated microporous polymer	--	--	808.2	--	[278]
β -cyclodextrin polymer	136.4	164.5	196.4	--	[279]
Polyazomethineamide	--	470.7	452.1	462.3	[280]
PEI-grafted gelatin sponge	79.9	--	80.6	--	[281]
Gum ghatti-Grafted poly(acrylamide-co-acrylonitrile) hydrogel	--	203.7	384.6	--	[282]
Aminopropyl functionalized H-RUB-18	--	133.4	--	118.0	[283]
Acidified MWCNTs	--	25.0	91.0	--	[284]
CNTs	--	--	102.0	--	[285]
Oxidized MWCNT	22.3	--	--	--	[286]
Ethylenediamine-functionalized MWCNTs	21.7	--	--	--	[286]
Activated carbon	--	6.8	--	--	[270]
Activated carbon	33.6	24.1	22.8	27.0	[287]
Steam activated carbon	81.6	116.0	173.6	--	[288]
<i>Typha angustifolia</i> derived activated carbon	48.1	--	61.7	--	[289]
Poly(amidoamine)/CNT composite	--	3677	4080	3900	[290, 291]
Magnetic graphene oxide grafted polymaleicamide dendrimer	--	--	181.4	--	[292]
Sinapinaldehyde modified SBA-15	--	--	33.6	--	[293]
N-N dimethyldodecylamine modified MCM-41	191.1	278.9	267.3	--	[205]
N-N dimethyldodecylamine modified MCM-48	175.4	259.2	238.3	--	[205]
Thiol-functionalized MCM-41	--	37.8	110.7	--	[216]
Chitosan-functionalized MCM-41-A	--	--	90.9	--	[294]
Melamine-based dendrimer amines magnetic MCM-48	114.1	125.8	127.2	--	[295]
Aminopropyl modified MCM-41	14.1	--	64.2	--	[296]
Diethylenetriamine modified MCM-41	--	--	77.5	58.5	[297]
PVA/amine MCM-41 composite	46.7	--	--	--	[298]
Mercapto modified SiO ₂ NP	4.8	--	10.4	--	[299]
EDTA functionalized silica gel	--	79.4	--	74.0	[300]
4-phenylacetophynone 4-aminobenzoylhydrazone functionalized silica gel	--	0.8	--	0.8	[301]

Table 19 - Adsorption capacity, whenever possible from the isotherm model, for heavy metals by different adsorbents in the literature (concluded).

Material	Adsorption capacity/ mg g ⁻¹				Ref.
	Cd	Cu	Pb	Ni	
Thiourea-diamine functionalized silica gel	--	79.4	--	--	[302]
Poly(amidoamine) functionalized silica gel	--	104.6	--	--	[303]
Carboxyl functionalized silica gel	43.8	50.8	--	31.9	[304]
Thioglycolic acid functionalized silica gel	--	21.0	--	17.6	[305]
L-Proline functionalized mesoporous silica	--	--	21.9	--	[242]
EDTA functionalized mesoporous silica	5.5	--	7.2	--	[306]
EDTA functionalized mesoporous silica	71.4	49.5	147.1	--	[307]
Amino-functionalized mesoporous silica		138.5	982.1		[308]
Amino-functionalized mesoporous silica	192.2	148.7	592.6	--	[309]
Di-amine functionalized mesoporous silica	253.0	522	--	--	[238]
Melamine-amine functionalized aluminum mesoporous silica	--	--	147.5	--	[310]
Silica-cellulose nanofibrils composite	130.5	--	157.7	--	[311]
PVA/SiO ₂ composite nanofiber membrane	--	489.1	--	--	[312]
Cross-linked PVA/NH-SiO ₂ beads	--	--	67.6	--	[313]
Sulfonic acid functionalized silica microspheres	179	93	223	--	[314]
Amine functionalized silica aerogel	--	47.6	--	27.7	[315]
Amine functionalized silica aerogel	35.7	--	45.5	--	[316]
Mercapto functionalized silica aerogel	--	51.0	--	--	[317]
Mercapto functionalized silica aerogel	200.0	83.3	250.0	--	[318]
Amine functionalized silica aerogel particles	--	--	407.0	--	[319]
Bis-amine bridged silica cryogel	--	77.0	276.0	--	[320]
Disulfide bridged silica xerogel	36.0	19.5	66.3	--	[239]
Poly(methacrylic acid-co-maleic acid) grafted nanofibrillated cellulose aerogel	134.9	--	165.8	115.6	[321]
Polybenzoxazine aerogel	--	1.5	0.3	--	[322]
Nanocellulose/polyethylenimine crosslinked aerogel	485.4	--	--	--	[323]
Cellulose Nanofibrils aerogel	--	16.7	94.9	--	[324]
Calcium alginate aerogel	244.6	126.8	--	--	[325]
Sodium alginate/graphene oxide aerogel	--	98.0	267.4	--	[326]
Carbon aerogel	--	--	34.7	2.8	[327]
Carbon aerogel	15.5	--	34.7	--	[328]
Carboxylated magnetic cellulose aerogels	--	73.6	--	--	[329]

The works summarized in Table 19 do not use the same experimental conditions and thus they cannot be compared directly. In addition, some of the materials were tested only for a few cations. Nevertheless, it is clear that the several types of adsorbents employed in the literature are

adequate to remove heavy metals and show the versatility and potential efficiency of the adsorption process.

The results from Table 19 and Figure 10 reveal that natural adsorbents have, in general, low adsorption capacities, particularly if these are used as obtained. Common widely available adsorbents, belonging to this category such as clinoptilolite [246] and bentonite [251], are shown to have little efficiency despite being very cheap. This capacity increases when natural materials are modified or engineered: modified and synthetic zeolites [248-254], composite and synthetic clay minerals [240, 258-262]. Natural polymers chitin and chitosan [263, 264] are better adsorbents than the previously referred materials, but these too increase their performance by being modified [191, 244, 265-267]. Furthermore, the valorization of organic matter wastes via the production of biochar also generated better adsorbents than unmodified natural materials, with a reduced cost [270-273].

It is clear from Table 19 and Figure 10 that engineered materials are more efficient than unmodified natural adsorbents. However, these are also more expensive and less available. Carbon-based adsorbents achieve higher adsorption capacities [290-292] when prepared properly: activated carbons show heavy metal adsorption capacities similar to those of unmodified natural materials [270, 287, 289], but can be enhanced if prepared in certain conditions [288]. Mesoporous silicas have been extensively studied and most synthesis conditions generate good results [205, 238, 295, 308]. Other metal nanoparticles [276, 277] and polymers [279, 280] reported are also good candidates. Aerogels are still not very researched for this application, but promising results have also been reported for these materials [318-321, 325].

For engineered materials, their composition, particularly their surface chemistry, greatly affects the performance of the adsorbent, meaning that the modification of the material is a key factor to its performance. The functionalization of these materials is achieved by modifying their surface with Lewis base ligands. Examples of such are amine (primary, secondary or tertiary), melamine, chitosan, thiol, thiourea, EDTA (ethylenediamine tetraacetic acid) and acidic groups, which are based on N, S or O donor atoms. Zeolites are modified differently, with iron oxide and magnesium.

The balance between the adsorbent cost and its removal capacity is still unresolved: smaller amounts from an engineered adsorbent can adsorb the same pollutant as high amounts of natural, low efficiency adsorbents. The cost of smaller equipment allied with small amounts of adsorbent may be more cost effective. Therefore, an economic evaluation is needed for each case. The ability to reuse the adsorbent is critical in the economic viability of an adsorbent at the commercial scale.

From this literature survey it becomes clear that despite the many materials reported for this application, improving existing solutions, none is yet to become a commercial success. This is

partially due to the synthesis complexity, making the final material very costly. Thus, it is still necessary to conduct more research on heavy metal adsorbents, to find a more viable solution for large scale applications. Aerogels could be part of a solution as the extreme porosity and high specific surface areas are the prime features of an adsorbent. Moreover, the modifiable surface chemistry makes these materials more versatile and allows the exploration of many possibilities of functional groups. However, environmental applications for these materials are still scarce, although modified silica materials are promising. The introduction of functional groups, active for adsorption, in the aerogel matrix usually negatively impacts its structural properties [315, 316, 319]. As such, not only are the functional groups important but so are the synthesis procedures, as different chemical systems and functionalization methods can yield different macroscopic properties to the materials with the same modifying groups [315, 316, 319, 320].

The limitations found in the literature make room for more research on the subject, particularly in aerogels for heavy metal adsorbents. As such, the goal of this thesis addresses such lacunas.

3.3. Silica Aerogels

Aerogels are nanostructured materials with unique properties such as high surface area, porosity, insulation performance and low density. The term was introduced by Kistler [340], when he developed a methodology that allowed to dry gels without collapsing their structure. Gels are solid materials made of two phases: a solid crosslinked three dimensional matrix and a liquid [341]. The IUPAC definition of aerogels “gels comprised of a microporous solid in which the dispersed phase is a gas” [342] is controversial in the scientific community as it excludes mesopores and macropores from these materials [341, 343-352]. Definitions for aerogels have been proposed by several authors, however none has received a consensual backing from the scientific community. These state that the drying of the material must not impact its structure, implying that only supercritical dried materials are regarded as aerogels. Most recently, it was proposed that “aerogels are highly porous nanostructured solid materials derived from gels, in which the pores' filling phase is a gas and whose properties/structure are not significantly affected by the removal of swelling agents” [353]. It is then advised to evaluate the extent of changes caused to a monolith dried under subcritical conditions and determine their significance.

Silica aerogels are the most studied ones since silicon provides better control of the steps of the sol-gel synthesis. In fact, silicon has lower partial positive charge than transition metals [354], leading to lower, more manageable rates of the hydrolysis and condensation reactions.

3.3.1. Synthesis via Sol-Gel Chemistry

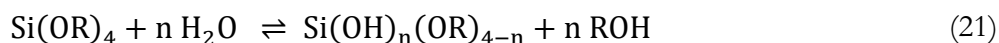
Sol-gel technology is a simple, economic and reliable method for the preparation of nanostructured materials, in particular metal and metalloid oxides. It involves the transition from a liquid to a sol and then to a gel, hence the name. An inorganic matrix composed by interconnected uniform particles of reduced dimensions is obtained through a series of polymerization reactions in solution at low temperatures [341, 354, 355]. Sol-gel technology allows the manipulation of the surface chemistry of the manufactured products, hence aerogels can be tailored for several applications [341]. The starting materials of this methodology are metal or metalloid precursors. Salts, alkoxides, oxides, hydroxides, complexes, amines and acylates can be used as precursors provided that they are soluble in the desired solvent. The most common silica precursors are alkoxides, the ones used in this work [341, 354].

Sol-gel technology can be divided into the following steps: sol formation, gelation, gel aging, gel washing, gel drying and densification (the latter is not used in this work) [341, 355]. A more detailed discussion on these steps will be done in the following subsections.

Hydrolysis, Condensation and Gelation

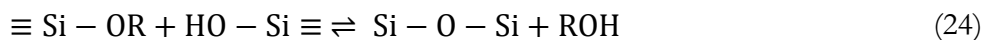
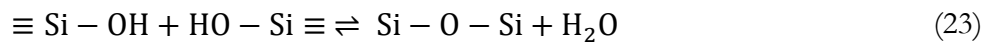
A sol (colloid) is a suspension in which the dispersed phase particles are smaller than 1000 nm. The sol formation step comprises the hydrolysis and condensation of the precursors [355].

In the case of alkoxide precursors, in the hydrolysis step, the precursor reacts with water, releasing an alcohol molecule and a hydrolyzed species. A general hydrolysis reaction for an orthosilicate (tetrafunctional alkoxide) and a trifunctional alkoxide are shown in Equations 21 and 22, respectively. The lone electron pairs from water's oxygen perform a nucleophilic attack on the silicon atom [354] and the hydrolysis reaction is initiated. The amount of water added to the mixture influences the extent of this reaction. To guarantee complete hydrolysis, a certain amount of water is required, so, the amount of water added to the system acts as a process parameter [341, 355].



Condensation is the step where the sol is formed. The hydrolyzed precursors react with each other, releasing water molecules and creating siloxane bonds ($\equiv\text{Si-O-Si}\equiv$), Equation 23. Condensation can also occur between a hydrolyzed and a non-hydrolyzed alkoxide, with the release

of an alcohol molecule - alcohol condensation, Equation 24. At this stage, nucleation occurs, starting the growth of primary particles that form the disperse phase of the sol [341, 355].



Tetrafunctional silicon alkoxides feature a very slow gelation kinetics due to the small partial positive charge of silicon, as already referred [354]. In fact, the hydrolysis and condensation steps are so slow that each one can be controlled independently. Thus, these reactions are catalyzed using acids or bases. Acid catalysts accelerate the hydrolysis reaction in comparison to condensation. In these conditions, the hydrolysis reaction occurs through a different mechanism, electrophilic attack on the oxygen atom of the alkoxide group [341]. At low pH values, the silica particles tend to form more ordered and linear chains with lower degree of branching [352]. Thus, the obtained gel is reversible, being easily dispersed in solution [341]. Basic catalysts accelerate condensation and polycondensation reactions resulting in denser silica particles with low microporosity and branched chains [352]. Two-step acid-base catalysis generates similar results [341, 352, 354, 355].

During gelation, the condensation reactions are extended to the entire sol, in a process similar to a polymerization, hence the name polycondensation. Hydrolysis and condensation are considered complete. At this stage the 3D structure of the gel is formed, occupying the entire volume of the sol. Primary particles start to aggregate onto secondary particles which themselves aggregate onto crosslinked chains in a pearl-necklace type structure (Figure 11). The moment when gelation occurs is identified by an abrupt increase in sol viscosity. The gelation of the mixture is favored by a change in its pH, induced by the addition of a catalyst, as already mentioned [355].

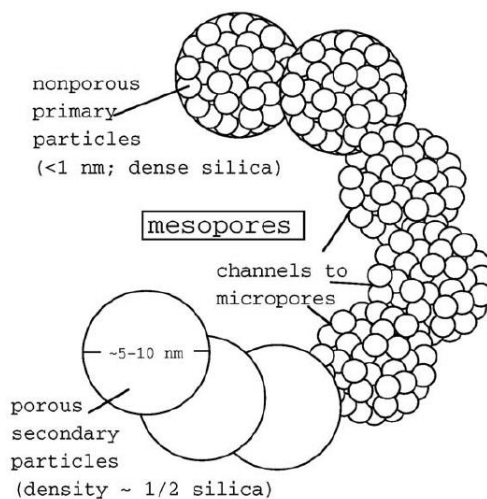


Figure 11 - Representation of the nanostructure of mesoporous silica aerogels. Reprint from [356] with permission from Elsevier.

Gel Aging

Gel aging strengthens the gel network through thickening of the connection points (necks) between the secondary particles, and Ostwald ripening. The thickening of necks occurs by mass diffusion throughout the liquid and precipitation of silica in this zone [352, 355]. This phenomenon is due to different solubility values alongside the particle's surface, with solubility being low in the convex area of the necks due to the negative curvature [352]. The Ostwald ripening mechanism consists in the dissolution of smaller particles, which reduces their number, and reprecipitation onto larger particles, helping the growth of the network [341, 355]. Syneresis, which also occurs in the aging process, consists in the expelling of liquid from the network due to its slight contraction, induced by its strengthening [354].

Aging can occur in the mother solution itself or in a specifically prepared solution which can contain more precursor to further strengthen the solid structure. Temperature, aging time and solution pH are controlled in this step to optimize the desired results [352].

Gel Washing and Drying

Gel washing allows to remove byproducts, catalysts and unconverted reactants from the gel's network. It can also be used to exchange solvents which is useful to many drying approaches.

The drying step consists in the removal of the liquid phase from the gel, replacing it with air. Gel drying can be achieved by three main processes: evaporative drying (at ambient pressure or vacuum conditions), supercritical drying and freeze drying [341, 352, 355]. Because each one of the previous approaches causes different changes in the porous structure of the gel, specific names are traditionally given to a gel dried by each one of them: evaporative dried gels are called xerogels,

supercritically dried gels are aerogels and freeze dried gels are cryogels [355]. This classification was overcome as monoliths with minimal impact can be obtained with all of these strategies and should be called aerogels, Figure 12.

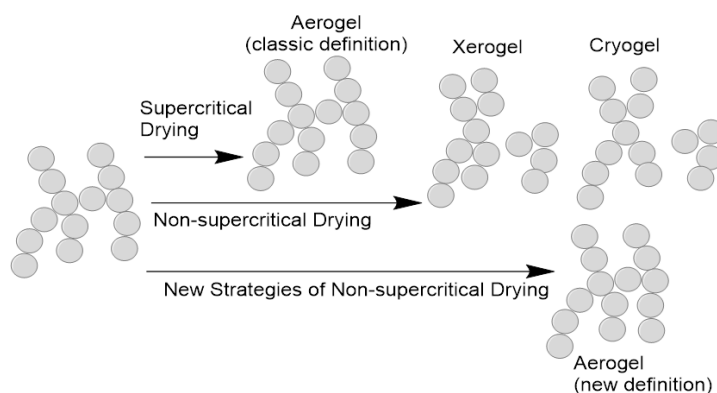


Figure 12 - Representation of structural changes during aerogel drying stage and corresponding definition.

Evaporative drying is achieved by evaporating the liquid phase by increasing the temperature or, in less frequent cases, using vacuum. In this process, large pressure gradients form between the liquid phase and vapor in the nanometer sized pores of the gel - Young-Laplace equation, Equation 25,

$$\Delta P = \frac{2\gamma\cos\theta}{r} \quad (25)$$

where γ is the liquid surface tension, θ is the contact angle and r is the pore's radius. As the liquid evaporates from the pores (emptying them), the shape of the meniscus changes, decreasing its curvature radius and increasing the pressure gradient [357]. At the same time the capillary forces create large stresses in the gel's solid structure, which eventually causes both the pores and the structure to collapse. The capillary stresses bring surface silanol groups closer. These groups create more siloxane bridges that irreversibly shrink the structure, leading to its densification. The capillary forces become more significant with increasing adhesion between the liquid phase and solid structure. Therefore, xerogels have a high tendency to break, shrink and become more dense [341, 355]. To overcome the limitations of this technique, different strategies were investigated, in order to obtain aerogel-like materials by ambient pressure drying. All these strategies consist in minimizing the capillary forces (Equation 25) by reducing the liquid-solid interaction and include: silica surface modification with nonpolar groups (increases contact angle with polar solvents), use of non-polar solvents with low surface energy and use of additives capable of reducing surface tensions (reduces γ) [355].

In order to avoid the collapse of the gel caused by evaporation of the solvent, the drying stage can be performed in supercritical conditions, bypassing the critical point of the solvent. This was the approach used by Kistler when producing the first aerogel. The high temperature supercritical drying (HTSCD) re-emerged in the 1970s followed by the low temperature supercritical drying (LTSCD) or supercritical fluids extraction with CO₂, in the 1980s [341].

In high temperature supercritical drying, the gel and a suitable solvent are placed in an autoclave and both pressure and temperature are risen beyond the solvent's critical point. Under these conditions the solvent is in its supercritical state, meaning that each molecule can move freely, and surface tensions cease to exist. The solvent is vented out of the autoclave at constant temperature, until atmospheric pressure is reached [341]. When using organic solvents, the high temperatures required to reach the critical point can lead to rearrangements in the gel's structure and esterification on the gel's surface, making it temporarily hydrophobic (in the case of being derived from orthosilicates and therefore hydrophilic) [352].

In the low temperature supercritical drying approach, carbon dioxide is pumped into an autoclave containing the gel to extract the solvent. This method requires the solvent to be soluble in supercritical CO₂. Carbon dioxide can be pumped in liquid state, flushing the solvent at high pressure. Afterwards the temperature is risen, residual solvent is dissolved, and the supercritical fluid is vented out to complete the procedure. Carbon dioxide may also be pumped into the autoclave as a supercritical fluid, dissolving the organic solvent in the gel as it passes through the sample [358].

When using methanol, ethanol or 2-propanol as solvent, high temperature supercritical drying would need to occur at temperatures above 240 °C (critical temperature of these alcohols) whereas for low temperature supercritical drying, 40 °C is enough (the critical temperature of carbon dioxide is 31 °C) [359]. This operating temperature is important when there are organic groups in the sample because many organic functional groups degrade at relative low temperatures. This is the case when gels derive from trifunctional alkoxysilanes, gels are reinforced by polymers or additives/surfactants are used. Furthermore, high temperature can lead to restructuring of the silica skeleton [352].

In freeze drying, the triple point is bypassed by freezing and then sublimating the solvent under vacuum. This technique is generally only applied when the solvent is water due to its more accessible melting point. Currently, alcohols are becoming more accessible as new freeze dryers capable of reaching lower temperatures are released to market [360]. Unlike supercritical drying, this approach does not guarantee the formation of monoliths [355]. This is a direct result of the expansion of water as it freezes, that collapses the porous structure.

3.3.2. Properties and Applications

Silica-based aerogels are highly porous materials that are lightweight, good thermal and sound insulators, feature high specific surface area and reduced pore size. Nevertheless, they are usually fragile showing poor mechanical properties [355]. In fact, native silica aerogels are brittle and although thermally resistant they are moisture sensitive. Table 20 summarizes some typical properties of silica aerogels.

Table 20 - Typical properties of silica-based aerogels [341, 352, 354, 355, 361].

Bulk density	0.03 - 0.35 g cm ⁻³
Porosity	90 - 99%
Specific surface area	100 - 1000 m ² g ⁻¹
Mean pore diameter	5-100 nm
Thermal conductivity	0.015 - 0.1 W m ⁻¹ K ⁻¹
Refraction index	1.0 - 1.08

For many applications, native silica aerogels are not very adequate: moisture sensitivity affects the longevity of the material, their fragility means poor machinability, and these are obtained from expensive drying techniques to prevent the collapse of the structure. Thus, silica aerogels are usually modified or reinforced to optimize the most important properties in each application. Silica aerogels can be tailored via sol-gel technology by changing, for example, the silica precursors, which allows the addition of new properties to the resulting materials. When modifying the gel with organic groups by using an organically modified silane, the resulting gel is called ORMOSIL (organically modified silica). These co-precursors can also be used to reinforce the final material, increasing mechanical properties. With proper co-precursor mixtures, translucent, hydrophobic, flexible or electric insulation aerogels can be produced [355].

Due to their very interesting properties, the use of silica aerogels has been proposed for dielectric materials, catalyst supports, building and space environment insulators, chemical sensors, hydrophobic coatings, nuclear waste confinement, adsorbents and as drug carriers [341, 352, 354, 355, 362-368]. Table 21 shows several of the proposed applications and respective properties of interest for silica-based aerogels.

Table 21 - Applications for silica-based aerogels and respective properties of interest.

Property	Application
Thermal insulator; withstands high temperatures; lightweight.	Construction (super insulator); appliances insulation; space technology.
Lightweight; high specific surface area.	Support for catalysts, insecticides, propegol; chemical sensor; filtrating medium; adsorbent; drug carriers.
Translucid to visible light; low refraction index.	Cherenkov detectors; optical systems; daylighting; glazing; optical fibers.
Low sound speed.	Sound insulator.
Elastic; lightweight.	Cosmic dust collector.

For many of these applications, the toxicity of the used materials is of concern. Aspects such as crystallinity, aggregation state and surface chemistry influence the toxicity of nanoforms towards any organism [369, 370]. Crystalline forms of silica are known to be toxic. Silicosis, an occupational disease, but also other respiratory and systemic illnesses are due to the inhalation of breathable particles [369, 371]. Workplace regulations limit the concentration of airborne silica particles [372, 373] and, when handling silica particles/dusts, adequate personal protective equipment should be used [374]. It is consensual that amorphous silica does not cause this disease, as it is more soluble and its dissolution in water produces non-toxic products, hence, can be eliminated from the organism [375-378]. As the dissolution of nanomaterials usually implies their degradation, the less soluble the more toxic, in the long-term, they are [376, 379]. However, acute toxicity can be caused by exposure to soluble nanoforms [379]. The toxicity of silica particles is associated with the presence of silanol groups, but also siloxane and silica-derived radicals in the surface [369, 370, 380] capable of releasing reactive oxygen species to the exposed cells [369-371]. The existing silanol groups in mesoporous amorphous silica are much less available to cells than in crystalline, non-porous clavated silicas [381].

Biocompatibility studies [382-392] found that silica and silica-composite aerogels have generally good cytocompatibility. These have also been researched for biomedical applications [363, 381-383, 387-395]. Furthermore, several authors concluded, by studying different amorphous silica nanoparticles (which can be correlated to the structural units of silica aerogels) - nonporous and porous and with different surface chemistry - that these are also not ecotoxic for a large majority of organisms that includes plants [396, 397], soil microorganisms [398, 399] and both marine [397, 400, 401] and freshwater species [397, 402, 403]. Nevertheless, it was observed that smaller particles are more toxic.

3.4. Tailoring Aerogels as Heavy Metal Adsorbents

There are several characteristics sought for a good adsorbent, such as high surface area and porosity, stability (mechanical, chemical and thermal), high adsorption capacity, fast kinetics, low cost, availability and reusability [199]. Activated carbon and zeolites are very popular adsorbents.

The application of aerogels in polluted media has been proposed due to their high specific surface area, low pore size, and ability to introduce specific functional groups via sol-gel chemistry. So, aerogels can act as adsorbents removing several contaminants from polluted media. In fact, silica-based aerogels have been tested for the removal of organic pollutants and heavy metals from aqueous environments [11, 237, 404, 405].

There are three different approaches that can be used to modify the surface chemistry of aerogels: using precursors to add organic functional groups of interest, co-precursor synthesis, the functional groups are added prior to gelation; in liquid phase silylation, the functional groups are added after gelation and prior to gel drying, via reaction of a liquid precursor mixture with the solid gel; and in vapor phase silylation, the functional groups are added via chemical vapor deposition after supercritical drying of the alcogel [355, 406, 407]. Silylation is commonly used to hydrophobized monoliths as a way to reduce capillary forces prior to evaporative drying [406]. In this thesis the co-precursor method is used. When necessary, the desired organic group is obtained by modifying a commercial co-precursor, before sol-gel chemistry.

For the particular case of heavy metals there are several aspects to take under consideration. It is necessary to use appropriate ligands in the solid to remove these ions. The ligand's pK_a and stability constant of the metal-ligand complex also play a key role [408]. In the liquid phase, the speciation of the metal cation in solution (affected by counterions and pH) and the existence of interfering ions are also of utmost importance. In fact, the metal ion can be found in a form not available for adsorption and as a result no removal of the pollutant is achieved. The pH of the solution affects both the speciation of the metal ion (Figure 2) and the ligand in the adsorbent, that can be positively charged due to adsorption of hydronium ions at $pH < pK_a$ and so, competitive adsorption and charge repulsion occur. Lewis bases such as ligands containing nitrogen, oxygen, phosphor and sulfur electron donor atoms are capable of interacting with the metal cations [409, 410]. In fact, many materials compiled in Section 3.2. were modified with these donor atoms.

Some ligands interact selectively with cations, favoring the complexation of one over the remainder. These ligands are the so-called ionophores and are commonly used to prepare chemosensors (that generally produce a response measurable by fluorescence or in the UV-vis region) or ion sensing membrane electrodes but have also been used to modify adsorbents [213, 330-339, 411-483].

Both for copper and nickel, Schiff bases, crown ethers and porphyrins are the most common families of molecules used as ionophores. These types of molecules are generally multidentate and based on the presence of nitrogen or oxygen donors. Schiff bases are considered a subclass of imines and are obtained by a condensation reaction of a primary amine and a carbonyl precursor, like an aldehyde [484-486]. A schematic representation of a Schiff base is depicted in Figure 13(a). Schiff bases can be multidentate and include N and O, P or S donor atoms. These ligands can also be acyclic or macrocyclic. Salens are a type of symmetrical tetradentate Schiff base, with two nitrogen and two oxygen donor atoms, that have catalytic and medical applications [487, 488].

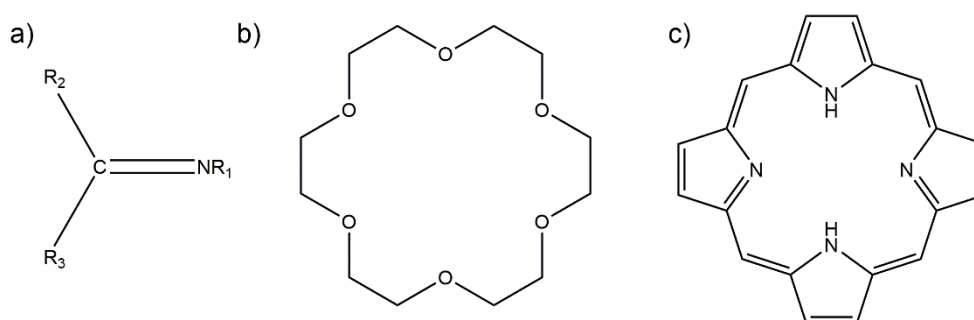


Figure 13 - Schematic representation of (a) a Schiff base ($R_1 \neq H$), (b) a crown ether and (c) a porphyrin.

Crown ethers are macrocyclic polyethers, Figure 13(b) [342, 489, 490]. Besides the oxygen donors, crown ethers can also be substituted with sulfur and nitrogen donors [490, 491]. There is generally an ethyl or propyl chain in between each donor atom but aromatic rings are also possible. Crown ethers are capable of strongly binding some cations [489], coordinated at the center of the ring by the inward facing oxygen donors.

Porphyrins are macrocycles composed of four pyrrole subunits connected via methine bonds [492, 493]. Porphin, the simplest porphyrin is represented in Figure 13(c). Porphyrins and their derivatives are ligands found in biological systems: hemes chelate iron and chlorophylls chelate magnesium [493, 494]. Other biological molecules, derived from porphyrins, are known to chelate other metals such as nickel. Porphyrins-based materials are used as chemosensors [495].

The aforementioned molecules, as macrocycles, strongly bind cations, and in particular dications, at the center of the ring, due to the presence of the donor atoms. So, its size, the amount and the type of donor atoms in the molecule, as well as other factors, will affect its selectivity towards a particular cation.

A literature survey of copper and nickel ionophores, ions whose recovery is relevant in this thesis, is presented and discussed in Annex II.

Of particular relevance are the studies that report the development or the modification of adsorbents with copper ionophores (Table II. 2). Ebraheem *et al.* [338] developed a polymeric resin based on an oxime and performed adsorption tests. Based on the obtained distribution coefficients, it is visible that the resin binds preferably with copper, being selective for this element. Other authors have also prepared modified resins [330-332] based on azoles. In these works, the adsorption by the resins under competitive conditions is clearly selective towards copper (over nickel, cobalt, zinc and cadmium) in a good range of pH values. Some azole derivatives are more selective than others: a copper selectivity of 9 (in relation to the second most adsorbed ion) at pH 3.4 [332] and a maximum of 2.5% of ligand sites occupied by interferents [330] are reported. Modified adsorbents, selectively responsive for copper, in comparison to other tested cations are also reported [213, 333, 334]. The selectivity was shown to vary according to pH. Dudler *et al.* [335] studied the stability constant of an azacrown ether. The authors found that the ligand's binding is much stronger with copper than with other cations, a result also found in other studies [411, 412]. This result is still valid with the modified silica adsorbent containing this ligand, that was shown not to remove cobalt, zinc or nickel in the presence of copper. Azacrown ethers were also used to modify chitosan [336], resulting in a selective adsorption of copper in comparison to cadmium and lead. The amine modified silica gel prepared by Im *et al.* [337] was shown to be selective in mixtures of copper, cadmium and zinc. Polyethyleneimine grafted diatomaceous earth particles were capable of uptaking nearly the entirety of copper from a 1000 mg/L solution, while only 10% of nickel was removed [339]. Other cations (aluminum, iron, magnesium, calcium and manganese) had smaller uptakes than nickel. A mesoporous silica modified with a Schiff base, resulted in a material that selectively adsorbed copper over a wide range of cation interferents [496].

To the best of my knowledge, no works based on modifying aerogel adsorbents with nickel ionophores are reported, and adsorbents with these are scarce [497-499]. Table II. 4 compiles works where nickel ionophores are used to prepare membrane electrodes.

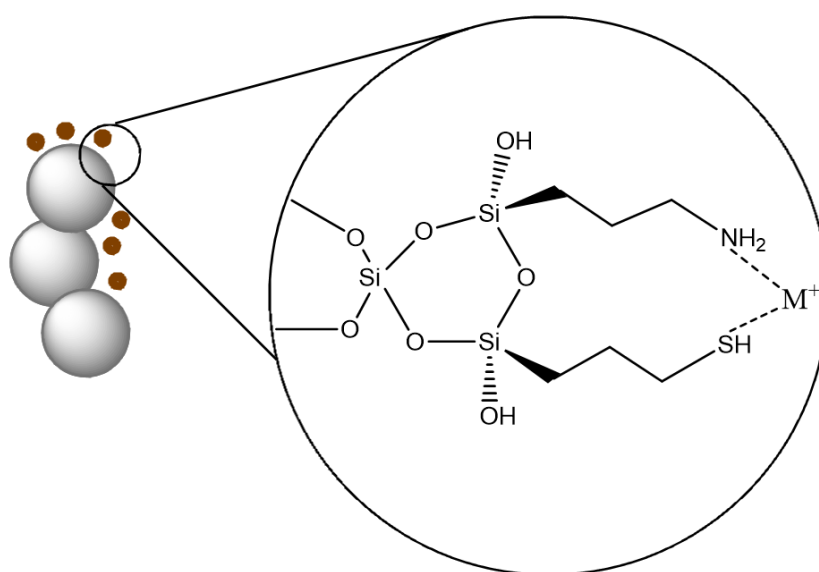
The ligands studied in this thesis, for the development of silica-based aerogels as adsorbents for the removal of heavy metals in contaminated water, are thiol, amine, urea and isocyanurate groups. For the development of selective ORMOSIL adsorbents, azole ionophores (for copper) and salen ionophores (for copper and nickel) were investigated.

In this work the selectivity between species was evaluated by the ratio of their individual molar uptake, as described in Equation 26.

$$\alpha_{A,B} = \frac{q_{eA}}{q_{eB}} \quad (26)$$

Chapter 4

Silica-Based Adsorbents with Thiol Groups



The content of this chapter is based on the author's published works *Functionalized silica xerogels for adsorption of heavy metals from groundwater and soils* and *Efficient adsorption of multiple heavy metals with tailored silica aerogel-like materials*.

Summary

The work comprised in this chapter reports the development of tailored silica based xerogels, for the decontamination of heavy metal polluted environments via an immobilization strategy. The adsorbents remove and immobilize the cationic heavy metals found on aqueous environments. Thiol groups were selected to modify the silica materials due to their capability of interacting with the cations in solution. In addition, primary amine groups were also used in one adsorbent (AM), that features both amine and mercapto groups (adsorbent with double functionalization), which is not common. The developed materials were characterized and their performance on the sorption of copper, cadmium, lead and nickel was studied through batch adsorption tests. The comparison between aerogel and xerogel counterparts of both formulations revealed that materials derived from formulation M have very similar properties, while AM aerogels have very different structural properties from their xerogels counterparts. Nevertheless, a screening of the adsorption performance with copper and lead revealed that both counterparts perform identically. Thus, only the xerogels are fully studied as adsorbents. The adsorbent with both amine and thiol groups presented higher cation uptake, which was attributed to the amine groups. The equilibrium and kinetic studies suggest that, in general, the sorption of the cations is due to chemisorption, most likely through a surface complexation mechanism.

4.1. Experimental Procedures

4.1.1. Materials

Tetraethyl orthosilicate (TEOS, 98%, *Sigma-Aldrich*), methyltriethoxysilane (MTES, 99%, *Sigma-Aldrich*), (3-mercaptopropyl)trimethoxysilane (MPTMS, 95%, *Sigma-Aldrich*), (3-aminopropyl)trimethoxysilane (APTMS, 97%, *Sigma-Aldrich*) were used as silica sources. Methanol ($\geq 99.8\%$, *VWR*), ethanol ($\geq 99.8\%$, *Sigma-Aldrich*), oxalic acid anhydrous ($> 97\%$, *Sigma-Aldrich*) and ammonium hydroxide (25% wt, *Sigma-Aldrich*) were used as solvents and catalysts for sol-gel chemistry. All reactants were used as received. For the cation solutions, copper(II) sulfate pentahydrate ($> 98\%$, *Sigma-Aldrich*), lead(II) nitrate ($\geq 99.0\%$, *Sigma-Aldrich*), cadmium(II) nitrate tetrahydrate ($> 99\%$, *Sigma-Aldrich*), nickel(II) nitrate hexahydrate (crystals, *Sigma-Aldrich*) were used. Hydrated salts were dried in an oven (100 °C) until constant weight prior to utilization. For the back titrations, hydrochloric acid (37%, *Sigma-Aldrich*), sodium hydroxide ($>98\%$, *Sigma-Aldrich*), phenolphthalein 1% solution, sodium thiosulfate pentahydrate ($>99.5\%$, *Sigma-Aldrich*), sodium tetraborate decahydrate ($>99.5\%$, *Sigma-Aldrich*), iodine (resublimed, *Acros Organics*) and potassium iodide (100%, *VWR*) were used without further purification. High purity water was used in all the procedures.

4.1.2. Preparation of Adsorbents

The syntheses were conducted *via* a one-pot approach, using different co-precursors. Formulation M (functionalized with mercapto groups) was prepared with TEOS, MTES and MPTMS in a 30:40:30 mol% proportion, while formulation AM (functionalized with amine and mercapto groups) used TEOS, MTES, MPTMS and APTMS in a 10:60:10:20 molar percentage, respectively. A greener solvent for sol-gel chemistry, ethanol, was tested for both formulations but only formulation M could generate an alcogel within a convenient time (less than 24 hours). Thus, methanol was used as solvent for formulation AM. The silica precursors were mixed, under stirring, with the solvent (ethanol for formulation M and methanol for AM) and an aqueous solution of the acid catalyst (0.1 M oxalic acid). After 24 hours of hydrolysis, the basic catalyst (10 M ammonium hydroxide) was added to the mixture. The molar proportions of Si:solvent:acid water:basic water are 1:12:4:4 in formulation M and 1:25:4:4 in formulation AM. The resulting sol was homogenized, poured into appropriate molds, and aged. Table 22 summarizes the aging and registered gel times for the formulations. All the synthesis steps were conducted at 27 °C.

Table 22 - Summary of the gelation conditions for the prepared adsorbents.

Formulation	Aging Time /days	Gelation Time
M	5	1 h
AM	5	30 min

The aged M and AM alcogels were washed with a flow of hot methanol at high pressure (~ 130 bar). Then, they were dried in an oven using different temperature cycles (60 °C for 48 h; 100 °C for 3 h). For comparison purposes, the alcogels were dried via supercritical fluids extraction with CO₂ to obtain aerogels (washing step with solvent followed by continuous flow of scCO₂ at pressures up to 150 bar at 50 °C) [500]. The aerogels and xerogels were compared to evaluate the impact of the drying approach in the specific surface area and removal capabilities. To test as adsorbents, xerogels and aerogels were milled and sieved, selecting only the particles with a size between 75 and 250 μm .

4.1.3. Batch Adsorption Experiments

Metal aqueous solutions were prepared at pH 5. The powdered adsorbent and the metal solution were mixed in a test flask and shaken (rotating shaker) at speed setting 16 (*REAX 20, Heidolph Instruments*) and 20 °C. All tests were conducted using an adsorbent concentration of 2 g L⁻¹. When the test ends, the solution is filtered, and the cation concentration in solution is determined via flame atomic absorption spectroscopy with an acetylene-air flame (*Perkin Elmer 3000*).

Adsorption capacity (q_t or q_e if equilibrium is reached, mg g⁻¹) and the removal efficiency (RE%) were calculated using Equations 3 and 4, respectively, as described in Section 3.1.. Adsorption models were fitted to the data using non-linear regression (Levenberg Marquardt algorithm). The models used are described in Section 3.1.. The quality of the fits was assessed using Akaike Information Criterion (AIC) and Bayesian Information Criterion (BIC) [501].

Batch equilibrium tests were performed by changing the adsorbate concentration from 10 to 500 mg L⁻¹ and conducted for 24 h. For batch kinetic tests, contact times ranged from 5 min to 6 hours, with an adsorbate concentration of 200 mg L⁻¹ for copper and lead, 20 mg L⁻¹ for cadmium and 50 mg L⁻¹ for nickel. The concentrations were selected based on the pollution found on Iberian soils and the goals of the *AeroMCatch* project. The loaded adsorbent (for equilibrium tests only) was filtered, washed with water, dried at 60 °C and stored for further analysis.

4.1.4. Characterization of Materials

The adsorbents were characterized in terms of structural properties, microstructure, hydrophobicity and chemical composition.

Structural characterization and microstructure observation

Bulk density (ρ_b , kg m⁻³) of the adsorbents was obtained by weighting portions of sample and assessing its volume: by measuring geometrically regular pieces in the three axes, or by liquid displacement in the case of some xerogels, due to randomness of particle shapes. Skeletal density (ρ_s) was obtained from fine powdered samples by helium pycnometry (*Accupyc 1330, Micrometrics*). Porosity was calculated by Equation 27 applying both the bulk and skeletal densities of the sample. The BET (Brunauer-Emmett-Teller) specific surface area (S_{BET} , m² g⁻¹) was determined using nitrogen adsorption at 77 K (*ASAP 2000, Micrometrics*). The average pore size was calculated with Equation 28, where V_{pore} is obtained from Equation 29. The microstructure of the samples was observed with a field-emission scanning electron microscope, FE-SEM (*Merlin Compact/VPCCompact FESEM, Zeiss, Carl Zeiss Microscopy*), after coating them with a conductive layer of gold by physical vapor deposition during 30 seconds.

$$\text{Porosity (\%)} = \left(1 - \frac{\rho_b}{\rho_s}\right) \times 100 \quad (27)$$

$$D_{\text{pore}} = \frac{4V_{\text{pore}}}{S_{\text{BET}}} \quad (28)$$

$$V_{\text{pore}} = \frac{1}{\rho_b} - \frac{1}{\rho_s} \quad (29)$$

Chemical characterization

Static contact angle measurements (sessile drop technique) were performed on pellets of compressed powdered samples (*OCA 20, Dataphysics*) using high purity water. C, H, N and S content of powdered samples was determined by elemental analysis (*EA 1108 CHNS-O, Fisons*) in order to verify the incorporation of the amine and mercapto groups into the silica structure. Silicon cannot be quantified via this technique and oxygen was shown to be incorrectly assessed in silica aerogels [502]. For comparison with the experimental results, different theoretical hypotheses were considered for the condensation of the precursors. These theoretical scenarios assume that the hydrolysis of precursor molecules is complete, and all precursor molecules react to form the gel backbone. The non-condensed hydroxyl groups at the ends of the network were not considered.

The different scenarios vary in the number of hydroxyl groups that are left unreacted, per precursor molecule, hence ranging from a complete condensation to an incomplete condensation where 2 hydroxyl groups are left unreacted per precursor molecule. Quantification of total amine and mercapto groups was done using elemental analysis results and surface groups were assessed by back titration, following reported procedures [503, 504]. The elemental composition of loaded adsorbent samples was estimated with energy-dispersive X-ray spectroscopy, EDS (*X-Max^N Silicon Drift EDS Detector, Oxford Instruments*). Crystal structures at the surface of the loaded adsorbent were studied by X-ray diffraction, XRD (*X'Pert, Philips*) using a θ - 2θ geometry (parallel beam), an accelerating voltage of 40 kV and a current intensity of 35 mA. The cobalt anticathode features $K\alpha_1$ and $K\alpha_2$ wavelengths of 0.178896 and 0.179285 nm, respectively.

4.2. Characteristics of the Adsorbents

The typical aspect of the xerogels (X) of both formulations, M and AM (Table 22), as well as their aerogel (A) counterparts for comparison, are shown in Figure 14.

For both formulations, the gels shrink and crack when dried via APD. The AM xerogel is more translucent than the M xerogel, which is related to the presence of amine groups in the AM formulation. These groups establish hydrogen bonding with ammonia, water and the alcohol leading to higher shrinkage during drying. In comparison, the aerogel samples did not shrink significantly; monolithic portions are obtained and are clearly white and opaque. Nevertheless, aerogels were difficult to dry with $scCO_2$ due to the retention of alcohol and water by hydrogen bonding to amine moieties. Regarding shrinkage, formulation M does not shrink significantly when dried by APD, relatively to the supercritical drying.



Figure 14 - Photographs of M and AM xerogels (X) and aerogels (A).

Table 23 shows the adsorbents density, porosity, specific surface area, pore volume and average pore size. Aerogel counterparts were also assessed for comparison purposes.

Table 23 - Structural properties for M and AM adsorbents.

Sample	Bulk density ^a /g cm ⁻³	Porosity /%	S_{BET} /m ² g ⁻¹	V_{pore} /cm ³ g ⁻¹	D_{pore} /nm
Aerogel M	0.83	25	702 ± 12	0.302	1.7
Xerogel M	0.85	23	678 ± 7	0.271	1.6
Aerogel AM	0.16	86	329 ± 3	5.262	64
Xerogel AM	1.04	14	2.2 ± 0.1	0.130	237

^a Values measured by liquid displacement and should be considered indicative.

Nitrogen adsorption measurements in silica aerogels are found to be difficult [505, 506], as even stiff samples contract and expand, influencing the adsorption of nitrogen, during the course of the analysis. In addition, this analysis is mostly limited to the mesopores size range, struggling to properly quantify micropores and most part of macropores. Consequently, specific surface area via BET model is correctly assessed but the quantification of pore volume is not accurate. Furthermore, the BJH (Barrett-Joyner-Halenda) theory to assess the pore size distribution does not apply well to aerogels due to the predominance of non-cylindrical pores. As such, pore volume was calculated through a relation between bulk and skeletal densities of the material, as explained before.

Table 23 reveals that the xerogels from formulation M have a very high specific surface area, not very different from the ones obtained for the aerogel of the same formulation. The monoliths

have small pores and are mostly microporous. This porous feature justifies the so high surface area. In fact, both counterparts are very similar and for this reason, I concluded that the xerogels can be seen as aerogel-like materials. In relation to formulation AM the situation is completely different. The amine groups affect the sol-gel process in a way the thiol groups do not, and the former cause an increase in the secondary silica particle sizes and consequent decrease in surface area [507]. The xerogels have a very low specific surface area, even when measured with a higher amount of material, suggesting that this adsorbent is non-porous/macroporous and with low amount of meso or micropores. Given the obtained average pore diameter, the sample is essentially macroporous which reduced its porosity and surface area greatly, two orders of magnitude lower than its aerogel counterpart. It can be seen that formulation AM generates a much higher porosity than formulation M, by comparing the aerogels from both formulations.

The morphology of the samples was assessed by FE-SEM and is shown in Figure 15. The microstructure of the xerogels is compact, with very small pores, which is again indicative of a significant shrinkage of the gel during APD, as already mentioned. The images reveal a meso and microporous texture on both adsorbents. However, for formulation AM, a small surface area was obtained despite this sample appearing to be porous in this SEM analysis, and very similar to sample M regarding this feature. The result of the surface area, not in agreement with the SEM analysis, may possibly be justified as follows: i) as this formulation has several organic moieties, there is a possibility of having a high amount of closed pores, and ii) the higher amount of MTES and lower content of TEOS in this formulation can make it more flexible and prone to volume variation during nitrogen adsorption measurement, thus giving inaccurate results by this technique. By comparison, the aerogel counterparts are clearly very porous, and their different microstructure is highlighted: A_M features small pores (slightly larger than the xerogel), while A_AM features lots of macropores.

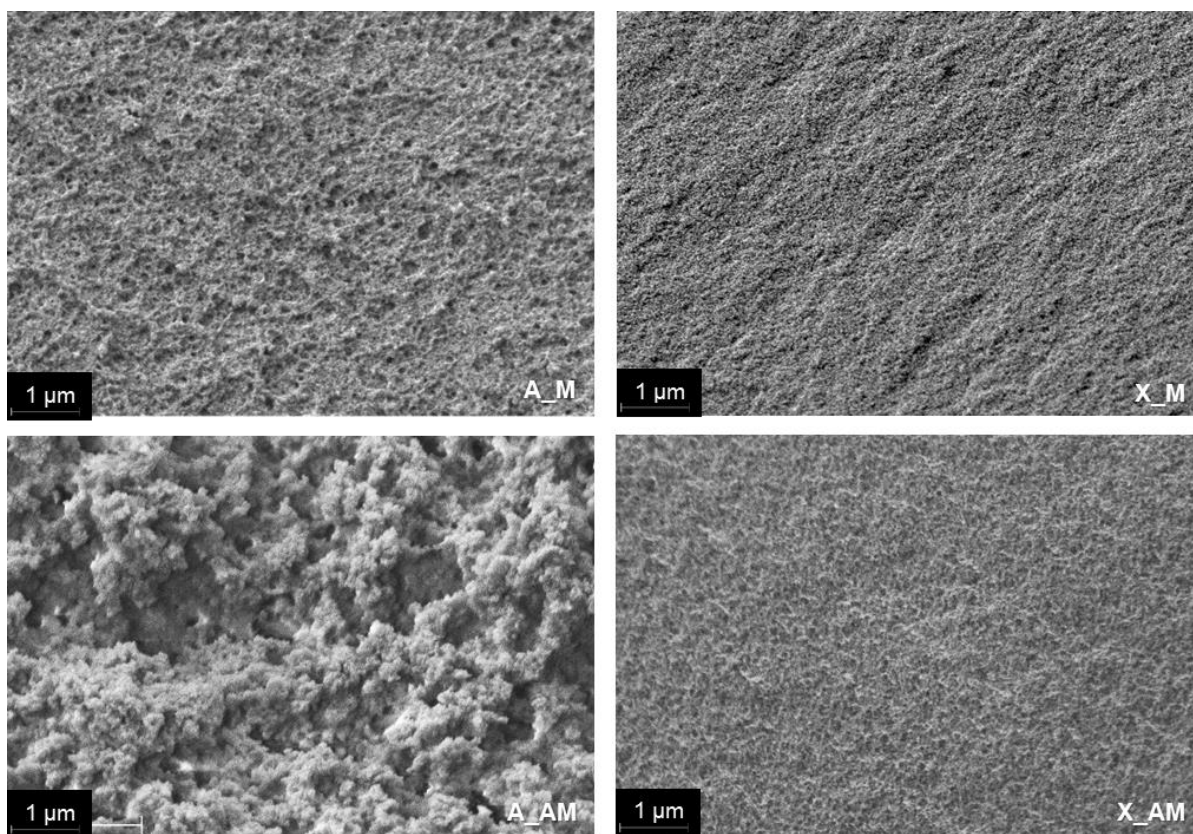


Figure 15 - Microstructure of M and AM materials observed by FE-SEM with a 25kx magnification.

The hydrophobicity of the samples is important to prevent them from degrading by exposure to moisture (a behavior typical of native silica aerogels), as these materials are meant to be tested in aqueous media. A contact angle of $124 \pm 14^\circ$ was obtained for adsorbent X_M and $147 \pm 11^\circ$ for adsorbent X_AM. It is evident that formulation AM is clearly more hydrophobic than formulation M, which was expected due to the different proportion of hydrophobic methyl groups added from MTES. Both formulations reveal hydrophobicity ($\theta_c > 90^\circ$), which ensures their non-degradability when exposed to moisture. The materials were immersed in water to test their degradation. It was found that, after 15 days of contact with water the gels did not show visual signs of degradation.

The results from elemental analysis provide valuable information not only about the incorporation of the amine and thiol groups in the prepared adsorbents but also on the extent of the sol-gel reactions (incomplete or complete condensation) and are presented in Table 24.

Table 24 - Theoretical and experimental percentages of C, H, N and S chemical elements in M and AM xerogel samples.

Xerogel	Hypothesis	wt% C	wt% H	wt% N	wt% S
M	Complete condensation	18.8	4.0	0.0	11.6
	Incomplete condensation 1 OH	17.0	4.7	0.0	10.5
	Incomplete condensation 2 OH	15.5	5.3	0.0	9.5
	Experimental	19.6	4.1	0.3	9.6
AM	Complete condensation	22.2	5.1	3.5	4.0
	Incomplete condensation 1 OH	20.0	5.7	3.1	3.6
	Incomplete condensation 2 OH	18.2	6.2	2.8	3.2
	Experimental	18.5	4.8	3.3	3.7

For formulation M, the experimental mass percentages corresponding to carbon and hydrogen are closer to the theoretical values of complete condensation. There is also some trace amount of nitrogen probably due to residues of the ammonia catalyst. The amount of sulfur in the sample is somewhat lower than predicted. These results suggest that the mixture that composes formulation M has undergone complete (or near complete) condensation but probably not all the MP-TMS could link to the silica backbone. For formulation AM, the carbon, nitrogen and sulfur experimental percentages reveal an incomplete condensation, when compared to theoretical hypothesis, between complete condensation and 2 OH, but uncertain. Hydrogen is the only element that does not follow this trend, but its low atomic weight gives rise to higher inaccuracy. So, it can be concluded that, in general, for this formulation the sol-gel reactions were not complete.

Table 25 presents the total and surface functional groups relevant for heavy metal adsorption (*i.e.*, amine and mercapto) quantified via elemental analysis and back titration, respectively.

Table 25 - Total and surface amine and mercapto groups on the xerogel adsorbents.

Xerogel	Total groups by elemental analysis (mmol g ⁻¹)			Surface groups by back titration (mmol g ⁻¹)		
	Amine	Mercapto	Sum	Amine	Mercapto	Sum
M	--	2.99	2.99	--	0.231 ± 0.000	0.23
AM	2.08	1.15	3.23	0.71 ± 0.01	0.207 ± 0.003	0.92

The amount of total functional groups is in line with the composition of the prepared sol. Furthermore, the total amount of functional groups, quantified via elemental analysis is similar in both adsorbents - Table 25. This was expected, as these were prepared with the same total molar percentage (30%) of these groups. Table 25 shows that the amount of surface groups is much lower than the total amount of groups present throughout the sample, meaning that not all functional groups seem to be accessible for adsorption. Furthermore, it appears that not all thiol groups added to formulation M xerogels are actually available at the surface of the adsorbent, as the quantified amount of surface groups does not significantly vary between formulation M (with 30%) and

formulation AM (with 20%). It should be noted that the quantification via back titration is limited because it relies on the ability of the analyte to react with the functional groups. This is of course influenced by the adsorbent's morphology/homogeneity, high hydrophobicity, contact time and mixing level.

4.3. Adsorption Performance of Xerogel and Aerogel Counterparts

The pH of the starting adsorbate solutions was shown to be within a range for which the adsorption of these heavy metals is maximized for different adsorbents, since the cations are available in solution (in free state - Figure 2) for adsorption [8, 10, 315, 508, 509]. It is worth noting that at low pH values, competitive adsorption occurs between hydronium and metallic ions and the active sites become positively charged, while at high pH values precipitation of metal hydroxides can induce high removals. Figure 16 represents the effect of the initial pH on the adsorption performance of different adsorbents [239, 296]. Faghihian *et al.* [315] reports a similar behavior to that of Figure 16a) on an amine functionalized silica aerogel.

To select between aerogel and xerogel counterparts to use as adsorbents, the adsorption performance of both aerogel and xerogel counterparts of formulation AM were tested for copper and lead. These results can be found on Table 26 and Figure 17. These two cations were selected to screen the adsorbents due to their high concentration on soils in the Iberian Peninsula, relevant in the *AeroMCatch* project. Since formulation M generates counterparts with very similar properties, in this case the xerogel was selected as is easier and less expensive to produce.

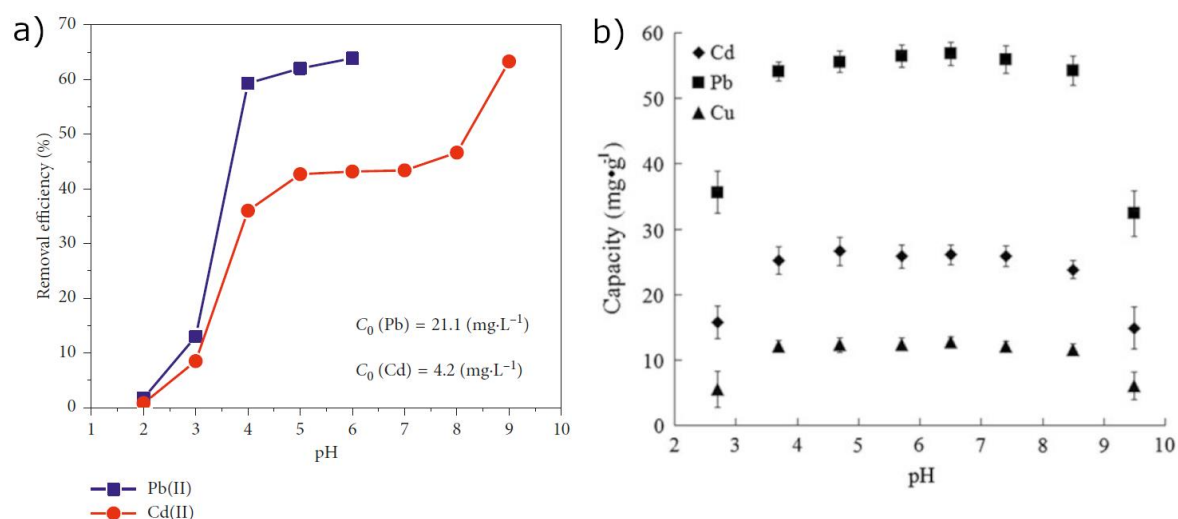


Figure 16 - Effect of pH on adsorption performance reported by (a) Dinh Du *et al.* [296] on amine functionalized MCM-41. Copyright 2019 Pham Dinh Du *et al.*; (b) Fan *et al.* [239] on disulfide bridged silica xerogel Reprint with permission from Springer Nature.

Table 26 - Copper and lead uptake for AM aerogel and xerogel counterpart ($C_0 = 500 \text{ mg L}^{-1}$, 24 h).

Sample	Copper q_e (mg g^{-1})	Lead q_e (mg g^{-1})
Xerogel AM	140 ± 1	125 ± 35
Aerogel AM	117 ± 3	165 ± 2

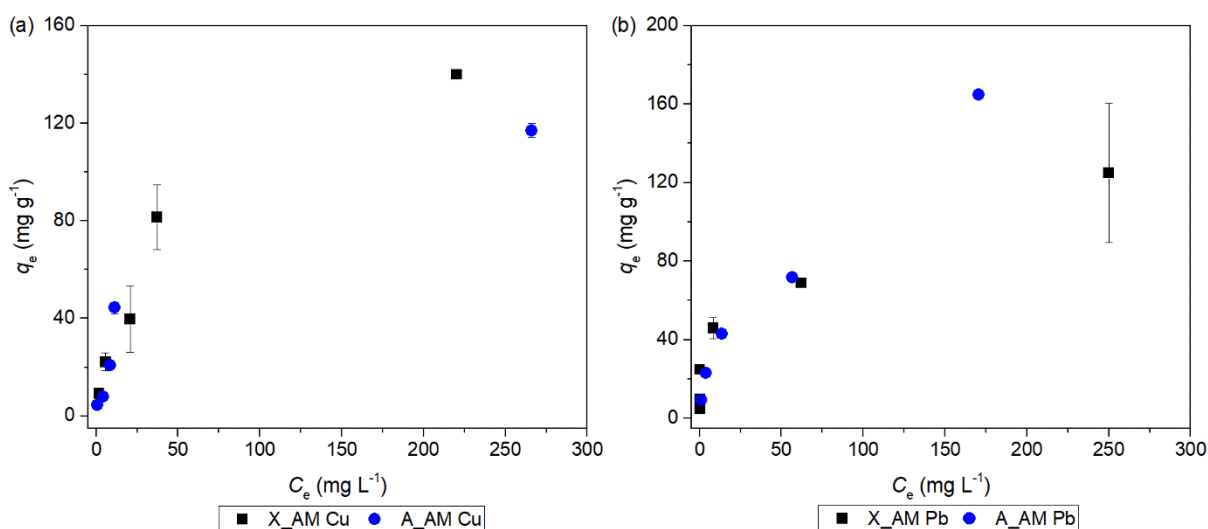


Figure 17 - Adsorption isotherms of (a) copper and (b) lead on AM counterparts.

Table 26 and Figure 17 clearly shows that the AM aerogel and xerogel counterparts are not very different when it comes to their heavy metal removal performance. This happens despite the clear different structural properties between counterparts of this formulation. This confirms that the surface area obtained for the AM xerogels is not reliable. In addition, the adsorbents used in the adsorption tests were milled and sieved, and this may have attenuated the difference of the specific surface areas when compared to those measured by N_2 adsorption in monolithic portions of sample. The grinding step possibly also enhanced the exposure of the functional groups to the metals. Thus, the number of functional groups accessible to the metals in solution did not have a limiting effect even with the structural changes originated by the drying conditions. As such, the xerogels were the selected material type for these adsorbents, making their production cheaper and easier. From herein, in this chapter, for the sake of simplicity, the designation X is not used for the adsorbents as all samples are xerogels.

4.4. Adsorption Kinetics

To interpret the results of the kinetic tests, kinetic models were fitted to the data regarding the sorption of Cu(II) , Pb(II) , Cd(II) and Ni(II) onto M and AM xerogels. These are shown in Table 27 and Figure 18. For the sake of simplicity, only the best model is represented in the graphs.

Table 27 - Adsorption model fit parameters for sorption kinetics on M and AM adsorbents.

	Pseudo-first order (PS1)				Pseudo-second order (PS2)				Exp. q_e /mg g ⁻¹
	k_1 /h ⁻¹	q_e /mg g ⁻¹	AIC ^a	BIC ^b	k_2 /g mg ⁻¹ h ⁻¹	q_e /mg g ⁻¹	AIC ^a	BIC ^b	
M Cu	7.3	58.0	33.1	20.4	0.278	60.2	32.2	19.6	66.8
AM Cu	17.5	68.8	28.5	15.9	0.454	71.7	19.1	6.4	81.5
M Pb	8.5	23.7	23.0	14.9	0.441	26.1	20.3	12.1	40.7
AM Pb	1.8	30.3	25.3	17.2	0.056	34.8	20.8	12.6	68.9
M Cd	10.9	6.4	21.2	-4.0	3.4	6.7	17.0	-8.2	7.7
AM Cd	3.1	4.8	-2.6	-15.2	0.7	5.5	0.0	-12.6	3.4
M Ni	38.7	10.3	1.6	-6.5	9.7	10.5	-5.7	-13.8	10.6
AM Ni	9.9	10.6	7.0	-5.6	1.8	11.0	-0.8	-13.4	15.2

^a Akaike Information Criterion (AIC); ^b Bayesian Information Criterion (BIC).

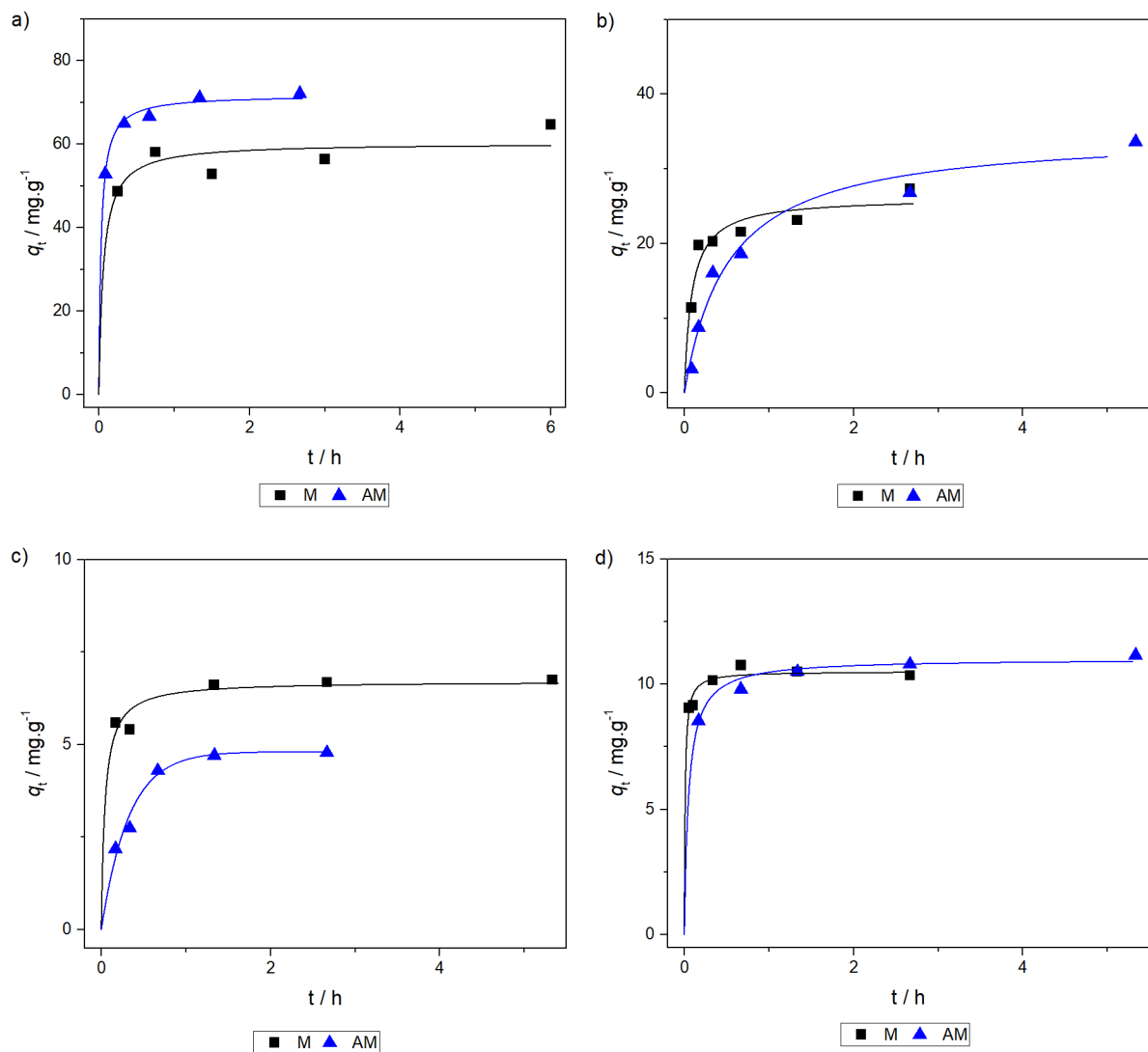


Figure 18 - Sorption kinetics for (a) copper, (b) lead, (c) cadmium and (d) nickel on M and AM adsorbents.

Figure 18 shows that the adsorption process occurs in one step, is fast in the beginning for all situations and equilibrium is usually reached after one hour. In some cases though, the equilibrium is not completely reached after a few hours and so the adsorption process continues

slowly. The results in Figure 18 and Table 27 show that the sorption kinetics usually follows the pseudo-second order model, meaning that the process is limited by the surface reactions. Consequently, chemisorption is most likely occurring. The exception to this trend occurs for the adsorption of cadmium onto AM, situation in which the adsorption seems to be controlled by the bulk concentration as evidenced by the fitting quality of the pseudo-first order model. For the case of M-Cu system, both quality criterion (AIC and BIC) are very similar and so both models describe the data properly [510, 511]. The pseudo-second order model was chosen because it was in agreement with the respective isotherm (Section 4.5.), suggesting a chemisorption mechanism [512].

4.5. Adsorption Isotherms

The adsorption isotherm curves of the four studied metals are represented in Figure 19. For the sake of simplicity, only the best fitting model is represented in the graphs. The fitting parameters are compiled in Table 28. It is clear that both adsorbents interact very well with the tested cations, achieving better uptakes than most silica-based materials in Table 19. Formulation AM generated xerogels that adsorb more of these ions than the ones of formulation M (experimental q_e values in Table 28), despite the measured much lower surface area for AM xerogels when compared to M xerogels.

Table 28 - Adsorption model fit parameters for sorption isotherms on M and AM adsorbents.

	Langmuir model				Freundlich model				max q_e exp /mg g ⁻¹
	$q_{\max}/$ mg g ⁻¹	$K_L \times 10^3/$ L mg ⁻¹	AIC a	BIC b	$1/n_F$	$K_F /$ mg g ⁻¹ (L mg ⁻¹) ^{1/n_F}	AIC a	BIC b	
M Cu	109.8	26.4	44.4	36.3	0.3	17.7	30.6	22.5	99.3
AM Cu	172.5	20.0	39.5	26.9	0.5	12.3	44.3	31.6	139.9
M Pb	52.2	25.0	34.2	26.1	0.3	8.0	31.0	22.8	48.0
AM Pb	127.3	36.3	51.2	43.0	0.3	20.2	41.8	33.7	125.0
M Cd	150.3	4.9	27.1	18.9	0.6	2.8	21.1	12.9	91.5
AM Cd	1060	0.41	28.9	16.2	1.0	0.48	30.0	17.3	109.3
M Ni	112.8	4.0	20.6	8.0	0.6	1.7	26.0	13.4	67.1
AM Ni	90.2	12.9	24.1	15.9	0.5	5.1	38.5	30.4	72.7

^a Akaike Information Criterion (AIC); ^b Bayesian Information Criterion (BIC).

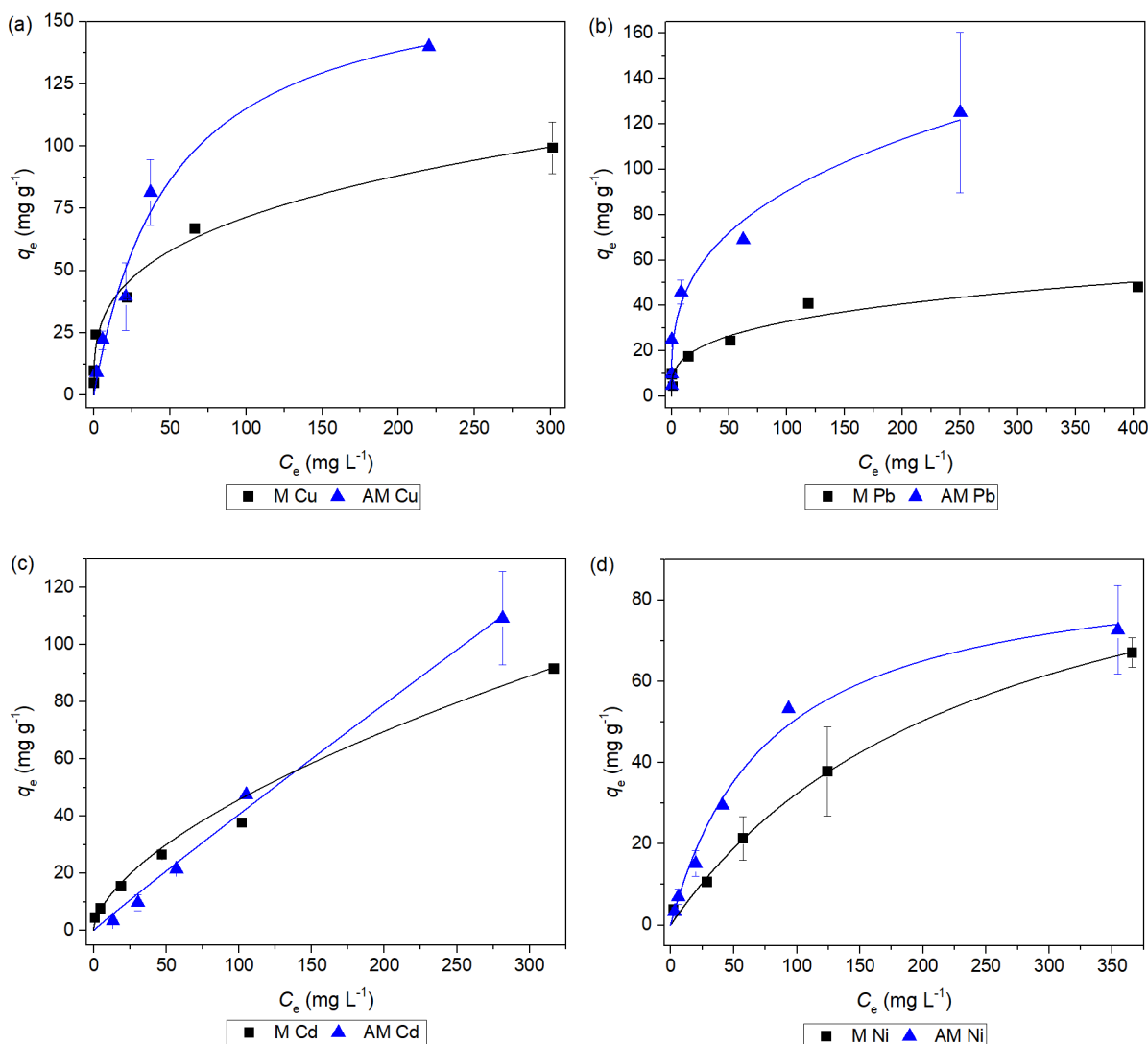


Figure 19 - Sorption isotherms for (a) copper, (b) lead, (c) cadmium and (d) nickel onto M and AM adsorbents.

The interaction of the xerogels with the cations is explained by different models depending on the adsorbate. Copper removal by adsorbent M is modeled by the Freundlich equation (Equation 15), whilst for AM the Langmuir model (Equation 13) shows the best fit. Lead and cadmium sorption follows the Freundlich trend for both adsorbents, while nickel sorption is modeled by the Langmuir isotherm. To most of these cases, in the evaluated concentration range, the obtained parameters reveal that monolayer sorption prevailed, as even the Freundlich equation shows that cooperative sorption does not occur. Thus, it can be hypothesized that the adsorption is due to the interaction at active surface sites, the surface thiol and amine groups [205, 206, 212-217], with chemisorption (inner-sphere complexation) likely behind the adsorbent-adsorbate interactions. The notable exception to this conclusion is the case of cadmium sorption with adsorbent AM, for which Figure 19(c) shows a linear trend - Henry's law. Although the AIC and BIC criteria suggest that the Langmuir model fitted better to the experimental points, the obtained Langmuir parameters do not make much physical sense. It seems that there are no specific

adsorbent-adsorbate interactions in this situation, and the observed removal is due to the presence of the solid adsorbent and the filling of its pores with the liquid phase.

The results obtained with the several cations do not allow to draw a conclusion regarding the homogeneity of the adsorbents' surface: it can be considered homogenous, when the Langmuir model fits to the data, or with different degrees of heterogeneity, when the Freundlich model fits better the data, with a higher heterogeneity in the interactions with lead - Table 28.

The K_L (for nickel) and K_F (for lead) values shown in Table 28 reveal a bigger affinity of adsorbent AM for the adsorbates, which translates into higher metal uptakes. In fact, AM adsorbent is more efficient than adsorbent M, even if marginally. This is consistent with the predictions by the HSAB theory: for copper and lead the presence of the amine groups made the adsorbent much more efficient for these borderline (hardness between 8 and 9 eV [409]) acids. For the remaining situations, the mercapto groups seem to be the ones that interact preferably with the cations, as the adsorption capacities did not increase significantly with the addition of the amine groups. This interaction between adsorbent and adsorbate occurs in the form of coordination bonds, by a surface complexation mechanism, as found in previous studies [205, 206, 212-217]. A different silica material, featuring both mercapto and amine groups, did not show the adsorption performance obtained by these new adsorbents [513].

The loaded adsorbent from the isotherm studies (only for adsorbent AM and for a metal concentration of 500 mg L^{-1}) was collected, dried and its microstructure and approximate chemical composition was investigated by FE-SEM and EDS. The microstructure and elemental chemical compositions of the particles are presented in Figure 20. This figure reveals visible structures in the surface of the adsorbent particles. For copper and lead these cover the majority of the surface forming a sort of layer. EDS reveals that these structures are where the heavy metal is located. This observation could be explained by the metal precipitation on the surface of the solid particles when the aerogel is being dried after being recovered from the adsorption experiment. If this is not the case, the SEM micrographs reveal that precipitation also comes into play during the sorption process [204, 514]. The amount of metal adsorbed should not be visible in SEM images and it could be very hard to quantify via EDS. Furthermore, although the test parameters (most importantly pH) are optimized not to favor precipitation, the mechanism of removal is always hard to determine. For every metal analyzed, the morphology of the crystals is different, which is expected.

In copper and lead loaded AM samples, the xerogels' surface was coated by a significant amount of metal precipitates. To have an insight on their origin, these samples were analyzed by XRD. The XRD patterns for copper and lead loaded adsorbent are found in Figure 21. Crystalline

phases associated with copper and lead salts were found, evidencing that these structures are likely to be precipitates formed during sample drying.

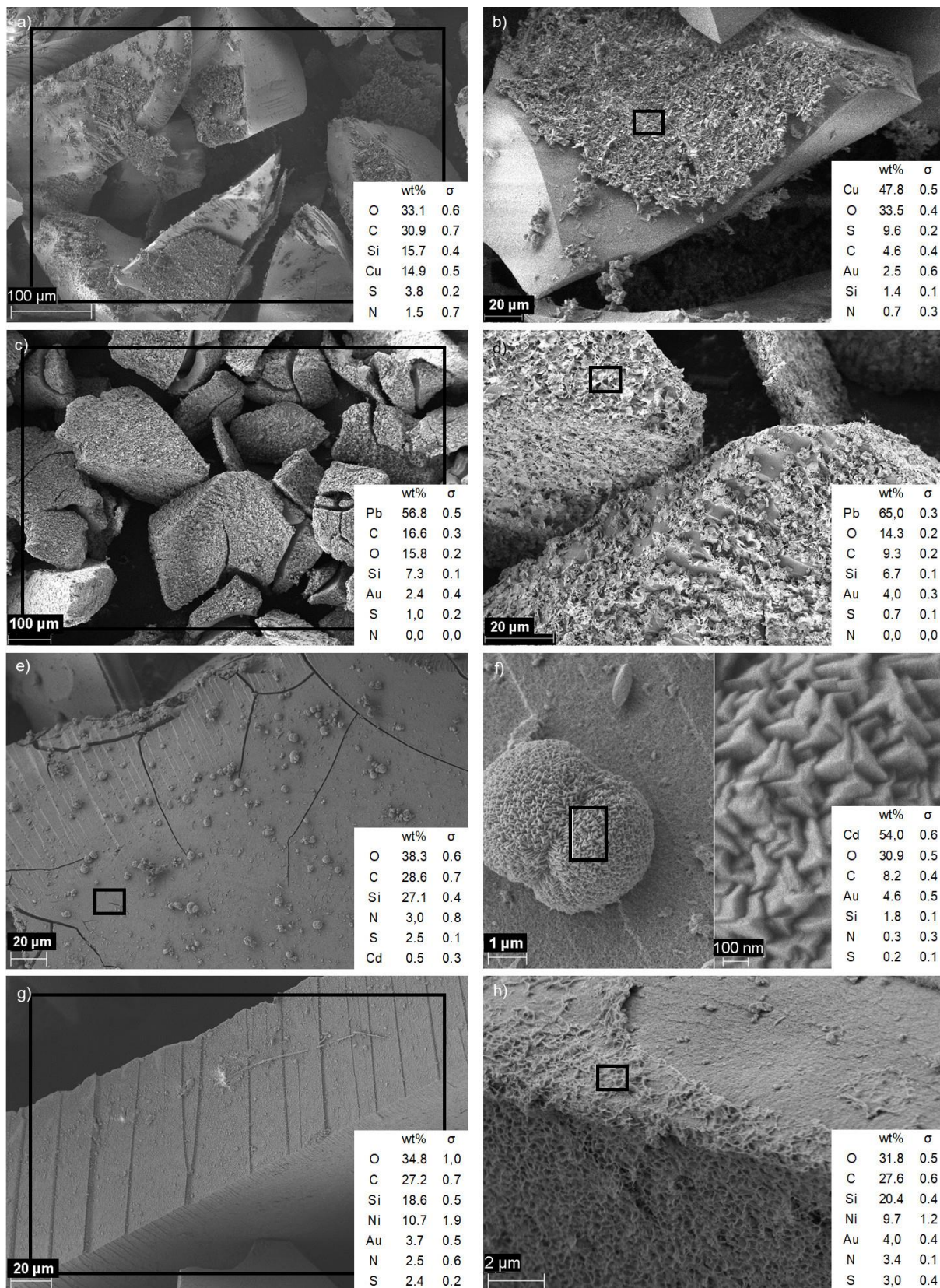


Figure 20 - SEM micrographs and approximate composition by EDS, assessed on the marked region, of adsorbent particles after adsorption: (a) Cu; (b) detail of Cu salts; (c) Pb; (d) detail of Pb salts; (e) Cd; (f) detail of Cd salts; (g) Ni; (h) detail of Ni salts.

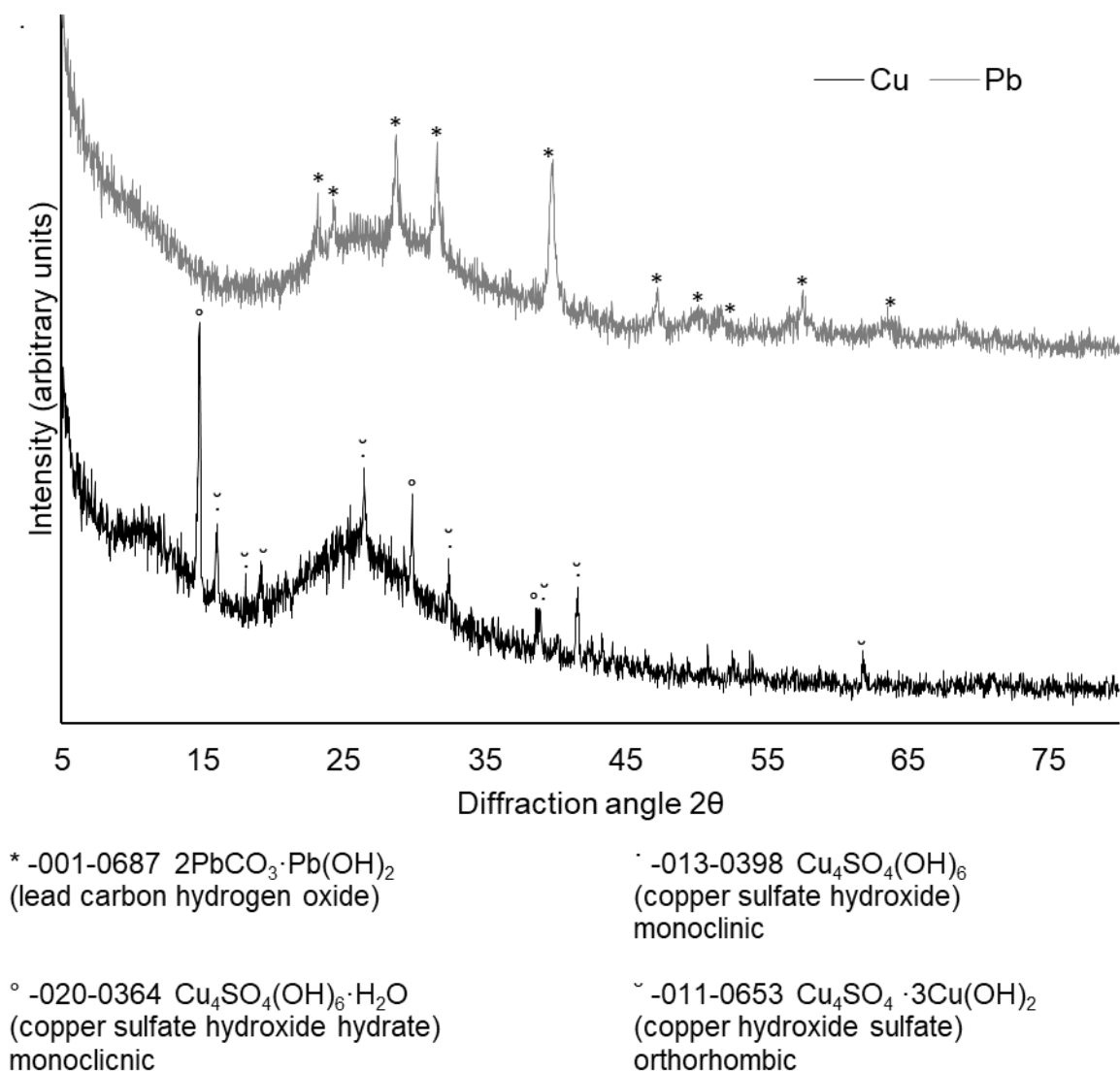


Figure 21 - XRD patterns of the sample AM after adsorption of Cu and Pb.

4.6. Conclusion

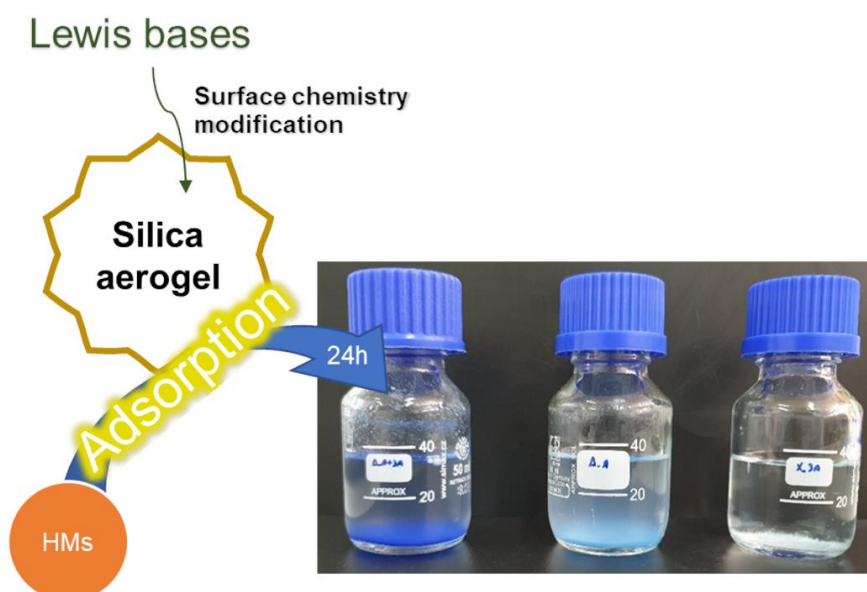
Two different formulations were prepared and studied on this Chapter: formulation M, with thiol groups (sulfur electron donor atom) and formulation AM, with both thiol and amine groups (sulfur and nitrogen electron donor atoms). The introduction of the Lewis bases in the matrix of silica aerogels successfully allowed them to interact with dissolved cations and adsorb them.

The amine groups in the silica matrix increased adhesion forces between the gel's solid and liquid phases, resulting in the densification and collapse of the xerogel sample, compared to its aerogel counterpart. The differences in physical and structural properties did not significantly affect the adsorption capacity of both counterparts of this formulation. The surface chemistry modification with thiol groups did not cause major variations in structural properties between aerogel and xerogel counterparts.

The xerogels of both formulations were thus studied in more detail through kinetic and equilibrium adsorption tests. The sorption of the cations is fast, as equilibrium is usually achieved after one hour. Apart from the sorption of Cd onto AM, the process seems to be controlled by the surface reaction. The batch equilibrium studies revealed that adsorbent AM sorbs more cation than adsorbent M across a wide range of concentrations, and that this process occurs as a monolayer. It is also suggested that there is more affinity for AM than M, which leads to believe that amine groups (or nitrogen electron donors) are more efficient in this application than thiol groups. Lastly, the adsorption process occurs by the complexation of the cations on active surface sites that correspond to the Lewis bases functional groups.

Chapter 5

Silica-Based Aerogel Adsorbents with Nitrogen-Containing Groups



Part of this chapter is based on the author's published works *Amine modification of silica aerogels/xerogels for removal of relevant environmental pollutants* and *Silica Aerogels/Xerogels Modified with Nitrogen-Containing Groups for Heavy Metal Adsorption*.

Summary

The work presented in this chapter is focused on the synthesis of silica-based aerogels and xerogels modified with different nitrogen containing groups. Given the conclusion found in the previous chapter, the efficiency of nitrogen electron donors is further investigated by using an amine modified silica matrix and comparing it with adsorbent M and a material with no Lewis base functional groups. This investigation led to the study of more functional groups, namely primary amines, secondary amines, urea and isocyanurate. The goal is to assess the importance of the functional group on the usability of silica-based aerogels as heavy metal adsorbents rather than solely evaluating the fitness of one modified material.

The structural effect of the amine modification of silica on ambient pressure dried gels is already known from the previous chapter, and so, in this chapter supercritical drying and its impact on the materials' surface chemistry is also evaluated.

The non-modified and the differently modified silica-based aerogels and xerogels are characterized and the sorption performance of the counterparts of the different formulations is evaluated in preliminary adsorption tests and discussed. The effect of different test conditions on the batch adsorption of the cations is also evaluated. Three samples are selected, and their sorption behavior of cations is studied in depth with single cation solutions. Competitive adsorption with binary mixtures is also evaluated with selected samples.

It is verified that the aerogel adsorbent with the combined amine precursors, containing primary and secondary amines, performs the best in single-cation solutions. However, the estimated thermodynamic adsorption parameters reveal weak interactions between aerogel and cations. When tested in binary mixtures this sample showed selective towards copper, and its selectivity is maximized at six hours of contact time. Copper can be desorbed from this sample successfully, however, this procedure degrades the matrix which in turn decreased the adsorption performance after one regeneration cycle. Thus, an adsorbent that can remove multiple cations in solution (multipurpose solution) or selectively remove copper and enable its recovery was obtained.

5.1. Experimental Procedures

5.1.1. Materials

Methyltriethoxysilane (MTES, $\geq 99\%$, *Sigma-Aldrich*), tetraethylorthosilicate (TEOS, 98%, *Sigma-Aldrich*), (3-aminopropyl)trimethoxysilane (APTMS, $\geq 97\%$, *Sigma-Aldrich*), N1-(3-trimethoxysilylpropyl)diethylenetriamine (AAAPTMS, technical grade, *Sigma-Aldrich*), 1-[3-(trimethoxysilyl)propyl]urea (UPTMS, 97%, *Sigma-Aldrich*) and tris[3-(trimethoxysilyl)propyl]isocyanurate (TTMSI, $> 95.0\%$, *Fluorochem*) were used as silica sources. Methanol (99.8%, *VWR International*) and ethanol ($\geq 99.8\%$, *Fisher*), anhydrous oxalic acid ($\geq 99\%$, *Sigma-Aldrich*) and ammonium hydroxide (25% NH_3 in H_2O , *Sigma-Aldrich*) were used as solvents and catalysts for sol-gel chemistry. Heavy metal solutions were prepared using copper(II) sulfate pentahydrate ($> 98\%$, *Sigma-Aldrich*) (for the study in 5.2 only), copper(II) nitrate hemipentahydrate (*p.a.*, *Chem-Lab*), lead(II) nitrate ($\geq 99.0\%$, *Sigma-Aldrich*), cadmium(II) nitrate tetrahydrate ($\geq 99.0\%$, *Sigma-Aldrich*) and nickel(II) nitrate hexahydrate (crystals, *Sigma-Aldrich*). Nitric acid (65%, *Fisher*) was used to adjust the solutions' pH. Hydrochloric (*analytical grade*, 37%, *Fisher*) and nitric acids and sodium hydroxide (*pellets*, *EKA Chemicals*) were chosen as desorption agents. All reactants were used as received. High purity water was used whenever needed.

5.1.2. Preparation of Silica-based Adsorbents

Six different formulations were prepared, mixing different co-precursors. These, as well as their nomenclature is described in Table 29.

Organically modified silica aerogels (denoted by A) and xerogels (denoted by X) were prepared by mixing the precursors in methanol and, then an aqueous oxalic acid solution (0.1 M) is added to enhance the hydrolysis of precursors. This solution is maintained in an oven at 27 °C during 24 h. Subsequently, an aqueous ammonium hydroxide solution is added to the previous mixture and the sol is left to gel and age. Gelation time varies from a few minutes to a couple of hours. The Si:solvent:acid water:basic water ratios were kept at 1:12:4:4. To prepare aerogels, gelation and aging occurred in cylindrical polypropylene molds and the samples were washed with hot ethanol followed by supercritical drying with CO_2 (5 g min^{-1} at 150 bar and 50 °C for 60 min). To prepare xerogels, the alcogels were dried in an oven at 60 °C for three days. The condensation/gelation conditions were adjusted to obtain cohesive gels. These conditions are summarized in Table 30, along with the registered gel times. To be used as adsorbents, xerogels and aerogels are milled and sieved, selecting only the particles with a size between 75 and 250 μm .

Table 29 - Aerogel/xerogel functional groups and samples nomenclature.

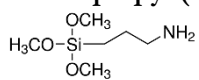
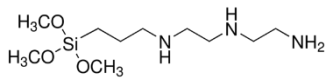
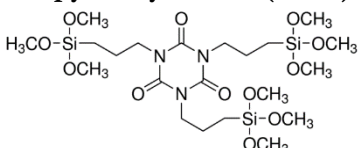
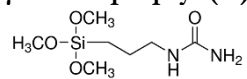
Functional Groups	Molar Composition (%) of the Precursor System ^(a)	Xerogel	Aerogel
Ref. material (without N-containing groups)	62.5%MTES/37.5%TEOS	X_B	A_B
3-Aminopropyl (A) 	50%MTES/30%TEOS/20%APTMS	X_A	A_A
Propyl diethylenetriamine (3A) 	50%MTES/30%TEOS/20%AAAPTMS	X_3A	A_3A
3-Aminopropyl (A) + propyl diethylenetriamine (3A)	50%MTES/30%TEOS/10%APTMS /10%AAAPTMS	X_A+3A	A_A+3A
Propyl isocyanurate (TRIS) 	50%MTES/30%TEOS/20%TTMSI	X_TRIS	A_TRIS
γ-Ureidopropyl (U) 	50%MTES/30%TEOS/20%UPTMS	X_U	A_U

Table 30 - Summary of the adjusted condensation/gelation conditions for the synthesis of nitrogen-modified aerogels and xerogels.

Formulation	[Base] /M	Aging Time /days	Gelation Temperature/°C	Gelation Time
B	1	6	27	2 h
A	1	6	27	10 min
3A	1	1	60	30 min
A+3A	1	6	27	30 min
TRIS	10	6	60	20 min
U	10	6	27	2 h

5.1.3. Batch Adsorption Experiments

The powdered adsorbent and the cation solution are mixed in a test flask, that is shaken in a rotating stirrer at speed setting 16 (*REAX 20, Heidolph Instruments*) or, in a *ProBlot 6* Hybridization Oven (*Labnet International*), for the case of the thermodynamic tests. When the test ends, the solution is filtered, and the concentration of the filtrate is determined by flame atomic absorption spectroscopy (AAS) with an acetylene-air flame (*939 AAS, Unicam*).

Adsorption capacity (q_t or q_e if equilibrium is reached, mg g^{-1}), removal efficiency (RE%) and model fitting were computed in the way described in Section 4.1.3..

Initial screening of adsorbents (Sections 5.2. and 5.5.) was performed at pH5, with an adsorbent dose of 2 g L^{-1} , at $20 \text{ }^\circ\text{C}$ and 24 h of contact time, for equilibrium tests, or as a function of time for kinetic tests. Commercial activated carbon (activated charcoal suitable for cell culture,

Sigma-Aldrich) was also tested for comparison purposes. Afterwards, the effect of different test parameters on the adsorption performance was studied using A_A adsorbent: initial adsorbate solution pH was varied between 4 and 5 and adsorbent concentration ranged from 2 to 10 g L⁻¹. pH 4 and 2 g L⁻¹ of adsorbent concentration were selected for the subsequent experiments. Three adsorbents were selected to study in depth with batch isotherm and kinetic tests (A_A, X_3A, A_A+3A).

Batch equilibrium tests were performed by changing the adsorbate concentration from 20 to 500 mg L⁻¹ and conducted for 24 h. For batch kinetic tests, contact times ranged from 1 min to 24 hours, with an adsorbate concentration of 200 mg L⁻¹. These tests were conducted at 20 °C. Thermodynamic tests were conducted with the same 200 mg L⁻¹ adsorbate concentration, and with a temperature range of 25-45 °C for 24 hours on adsorbent A_A+3A. The loaded adsorbent (for equilibrium tests only) was filtered, washed with water, dried at 60 °C and stored.

The effect of different adsorbates was also assessed with binary mixtures of cations, of equal mass concentration of 100 mg L⁻¹, in batch kinetic tests. Contact times ranged from 5 min to 24 hours. The selectivity (α) between the different cations was calculated by the ratio of the molar uptake capacity, using Equation 26.

5.1.4. Desorption Tests and Metal Recovery

The desorption of cations from A_A+3A and this aerogel's regeneration were studied. The tests were conducted by shaking (rotating shaker) the loaded adsorbent in the desorption solution. The desorption agents tested were hydrochloric acid, nitric acid and sodium hydroxide. Initial tests were conducted with a particle concentration of 6.7 g L⁻¹ and a desorption solution concentration of 0.5 and 1 M. These desorption experiments were conducted for 3 hours. To quantify the effect of the test parameters on the desorption efficiency, higher contact times (6, 15 and 24 h) and a higher volume of desorption solution (particle concentration of 2.2 g L⁻¹) were also studied. Heavy metals concentrations in the desorption solution were determined by AAS.

For adsorption/desorption cycles of copper, after sorption, the loaded adsorbent was regenerated with 1 M HCl, washed thoroughly and dried. The process was repeated until adsorption performance dropped considerably. Recovery of copper from the HCl solution was achieved via electrodeposition (*Axiomet AX-3005ds*), using an electric potential of 2.4 V and two graphite electrodes. The process lasted a total of 40 minutes, with the cathode being cleaned every 10 minutes. Recovery was calculated using copper concentration in solution determined by AAS.

The composition of the regenerated adsorbent was studied by FTIR and elemental analysis.

5.1.5. Characterization of Materials

The adsorbents were characterized in terms of structural properties, microstructure, and chemical composition. These were assessed as already described in Section 4.1.4..

To evaluate the effect of supercritical carbon dioxide on the surface groups of the materials, solid state NMR was used to assess the formation of carbamate groups in sample A_A. Solid NMR experiments were performed in a *NEO-750 (Bruker)* spectrometer equipped with a T3 solid probe (operating at a proton resonance frequency of 750 MHz and using a zirconia rotor of an outer diameter of 3.2 mm). Carbon chemical shifts were referenced to the carbon methine signal of solid adamantane at 28.92 ppm. The ^{13}C Cross Polarization Magic Angle Spinning (1D ^{13}C CPMAS) experiment was calibrated with a glycine sample. The 1D ^{13}C CPMAS spectrum of the samples was carried out with a contact time of 2 ms. During cross polarization, the field strength of the carbon pulse was set constant to 49.7 kHz and that of the ^1H pulse was applied with 51 kHz with a linear ramp (ramp70100.100 in the *Bruker* library). The inter-scan relaxation delay was 2 s, the MAS rate was 20 kHz. Heteronuclear decoupling during acquisition of the FID was performed with SPINAL-64 with a proton field strength of 108.6 kHz. The number of scans was 2048 and the total measurement time of the spectrum was *ca.* 1 h.

Infrared spectra (*FT/IR 4200, Jasco*) of the samples were obtained by using KBr pellets, with a wavenumber range from 4000 to 400 cm^{-1} , 128 scans and a resolution of 4 cm^{-1} . Thermogravimetric analysis (*TG 209F3, NETZSCH*) was performed in a nitrogen environment from ambient temperature to 1000 $^{\circ}\text{C}$ and a heating rate of 10 $^{\circ}\text{C min}^{-1}$.

5.2. Investigation on the Adsorption Performance Advantage of Amine Groups

Overall, the analysis of the materials in Chapter 4 allowed to conclude that amine groups are in fact very efficient in adsorbing heavy metals, as it was indicated by the HSAB theory and verified by the superior efficiency of the AM adsorbent. However, it should be stressed that these did not seem to be advantageous in all situations studied in the previous chapter, as the performance improved marginally for some cases. Although, if the amine groups weren't able to interact with all the previously tested cations, reducing the thiol groups from 30 to 10% would cause a serious decrease in sorptive performance of AM, which did not occur. In order to investigate the sorptive performance of amine groups towards metallic cations, two new formulations were introduced: A and B, described in 5.1.2.. A and B xerogels were tested with copper and lead to understand the efficiency of amine over thiol groups. The results are shown in Table 31 and 32 and Figure 22 and 23.

The two prepared adsorbents led to contrasting results: formulation B removes very small amounts of pollutant (when used for copper, the adsorption follows a random pattern), while adsorbent A has very high affinity towards the cations. Because formulation B has no Lewis bases functional groups, besides silanol, it was not expected to uptake cations in a significant amount. The isotherm analysis confirmed this prediction, validating the utmost importance of the presence of amine groups in the prepared adsorbent. The highest amount of adsorbed copper and lead on adsorbent A is, curiously, the same in mass (Table 31). However, the adsorbent does not interact similarly with both cations. In fact, assuming that the most relevant interactions occur between the metal ions and the amine non-bonding electrons, the charge density of Pb(II) is much lower than that of Cu(II) as a consequence of their ionic radii (Table 2), making lead more easily sorbed.

For the adsorption of copper, the Freundlich isotherm described the data better than the Langmuir model. On the other hand, the Langmuir model fits the lead adsorption more accurately in the absence of amine groups, while the Freundlich equation is more appropriate for adsorbent A (Table 31). Both models (considering the obtained parameters) suggest that chemisorption is the mechanism characterizing both pollutants. The Freundlich model reveals that adsorbent A is fairly heterogeneous and that the interactions toward lead are stronger, suggested by K_F values.

Table 31 - Adsorption models fit parameters for sorption isotherms on B and A xerogels.

	Langmuir model				Freundlich model				max q_e exp /mg g ⁻¹
	q_{max} /mg g ⁻¹	$K_L \times 10^3$ /L mg ⁻¹	AIC a	BIC b	$1/n_F$	K_F /mg g ⁻¹ (L/mg) ^{1/n}	AIC a	BIC b	
B Cu	c)	c)	c)	c)	c)	c)	c)	c)	14.8
A Cu	137.5	25.3	43.9	35.8	0.4	14.5	21.9	13.8	124.2
B Pb	24.9	78.5	34.6	9.4	0.3	5.6	38.9	13.7	24.0
A Pb	128.5	96.9	56.8	48.7	0.2	45.7	50.5	42.3	124.2

^a Akaike Information Criterion (AIC); ^b Bayesian Information Criterion (BIC); c) The adsorption capacity is negligible or residual.

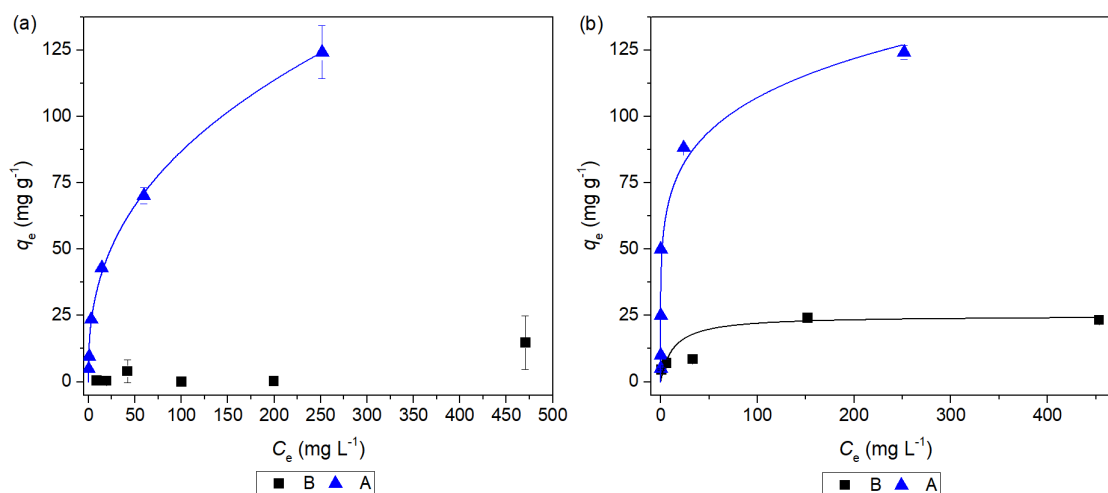


Figure 22 - Isotherm curves for (a) copper and (b) lead adsorption on B and A xerogels.

Because the adsorption of copper with sample B is residual, no kinetic test was done for this case. For the adsorption of lead with xerogel B, the pseudo-second order model was selected, to be in agreement with the isotherm result since AIC and BIC indicate that both models seem to be appropriate [510, 511]. Furthermore, when silica aerogels [315, 515] or ordered mesoporous silica [205] are used for different pollutants, the adsorption process is usually described by the pseudo-second order model. The pseudo-second order model fitted to the data the best in the remaining situations. For A and B's adsorption of copper and lead, the process is fast at the beginning, but the equilibrium is not reached, in the time range considered, which can justify the significant differences between the experimental and model equilibrium uptake. These results have some similarities with those obtained for M and AM adsorbents. This observation can be an indication that the amine groups became less available for adsorption after an initial uptake, hence the process becomes slower. In lead removal, adsorbent A has a significantly lower value of k_2 than B.

Table 32 - Adsorption model fit parameters for sorption kinetics on B and A xerogels.

	Pseudo-first order (PS1)				Pseudo-second order (PS2)				Exp. q_e /mg g ⁻¹
	k_1 /h ⁻¹	q_e /mg g ⁻¹	AIC	BIC	k_2 /g mg ⁻¹ h ⁻¹	q_e /mg g ⁻¹	AIC	BIC	
A Cu	1.8	17.4	18.2	5.6	0.10	20.6	13.8	1.2	70.2
B Pb	20.2	23.7	2.7	-9.9	2.2	24.3	3.7	-8.9	24.0
A Pb	1.3	25.8	20.1	11.9	0.04	32.7	15.8	7.8	88.2

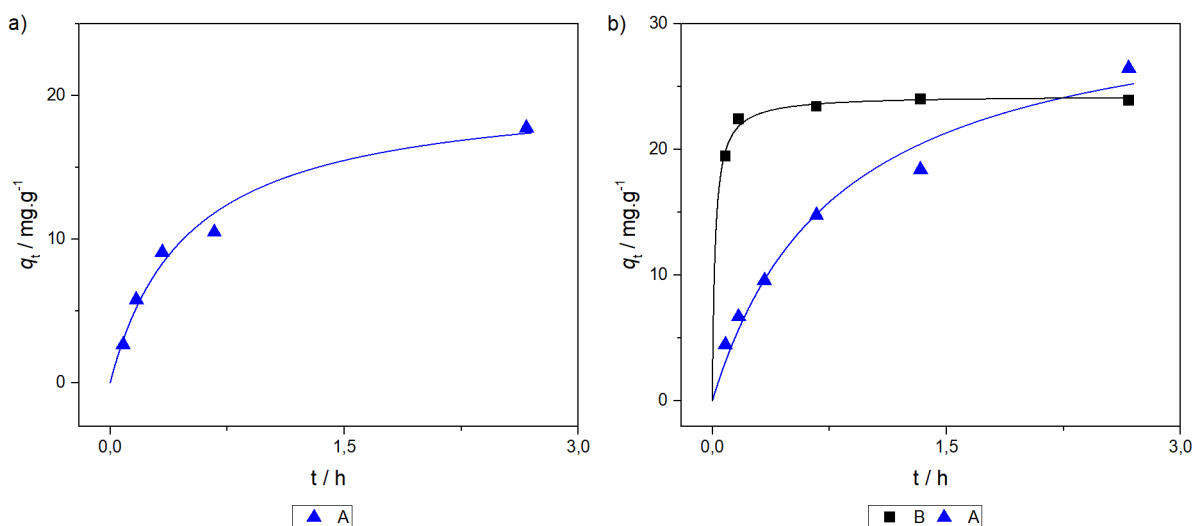


Figure 23 - Kinetic curves for (a) copper and (b) lead adsorption on B and A xerogels.

From the equilibrium and kinetic studies, it is clear that amine groups are very efficient in removing the tested heavy metals. With amine groups only, a high removal was obtained for copper and lead. Table 33 compares the removal of copper and lead by M and A adsorbents. These results show that only 20% of amine groups are more effective than 30% of thiol groups in this

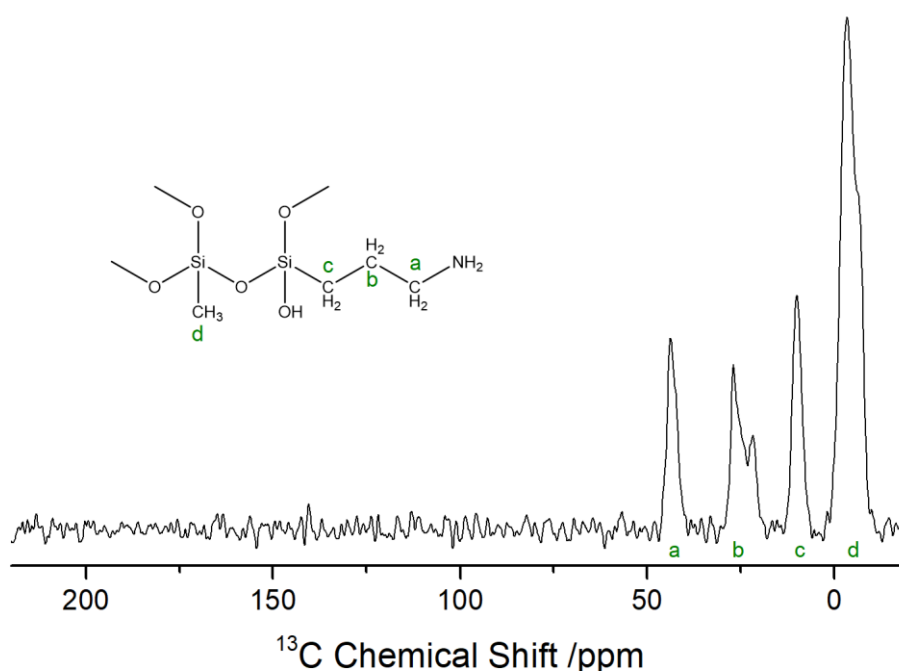
application, with adsorbent A having better removals in all evaluated initial concentrations. It can be concluded that amine groups are, in fact, better than thiol ones for the adsorption of these cations, and that a small amount of these groups is sufficient to achieve interesting results. As such, amine groups are further studied in this chapter.

Table 33 - Removal efficiency of copper and lead on M and A adsorbents.

	Removal Efficiency (%)		
	$C_0 = 50 \text{ mg L}^{-1}$	$C_0 = 100 \text{ mg L}^{-1}$	$C_0 = 200 \text{ mg L}^{-1}$
M Cu	97 ± 1	78.3 ± 0.7	66.8
A Cu	94.1 ± 0.4	86.0 ± 0.5	70 ± 3
M Pb	70 ± 6	48.9 ± 0.0	40.7
A Pb	100.0 ± 0.0	100.0 ± 0.0	88.2 ± 0.5

5.3. Effect of scCO_2 on Surface Groups

Carbamates are formed from the reaction of carbon dioxide and amines at low temperatures [516]. In fact, adsorption of CO_2 with amine modified materials at temperatures close to that of the critical point of carbon dioxide is reported elsewhere [516-518]. As such, during supercritical drying with CO_2 , the formation of carbamates is a possibility and would require an additional step of regeneration of amine groups in the adsorbent via desorption of CO_2 . The formation of carbamates was studied by solid state ^{13}C CP-MAS NMR for sample A_A and its result is shown in Figure 24.

Figure 24 - ^{13}C CP-MAS NMR spectra for sample A_A.

As it is revealed by Figure 24, the only peaks visible in the ^{13}C CP-MAS spectra are associated with the methyl (-3.6 ppm) and aminopropyl (9.8, 27 and 43 ppm) groups, and there is no peak associated with the carbamate bond (~ 150 ppm) [519]. Thus, it can be concluded that the supercritical drying methodology employed does not alter the adsorbent's surface chemistry and can be used to produce aerogels with nitrogen-containing groups.

5.4. Synthesized Adsorbents and Characterization

Photographs from the synthesized aerogels and xerogels are depicted in Figure 25. The differences observed from the analysis of different samples are mainly due to the aerogel and xerogel counterparts. All xerogels have shrunk considerably and feature a semi-translucid, glassy aspect. Samples X_B, X_TRIS and X_U did not break into small fragments, retaining some monolithic structure. Formulation 3A has generated aerogels that differ significantly from the remaining ones. In fact, these were the most difficult gels to dry using supercritical carbon dioxide (scCO_2). The remaining aerogels are very similar and completely white.

It was observed that the introduction of amine functional groups on the solid matrix hindered the solubility of the liquid phase of the gel on scCO_2 . This was attributed to a higher retention of water (weakly soluble in scCO_2 at low temperatures [520]) via hydrogen bonding. This situation has been overcome by employing long washing steps on the gel.

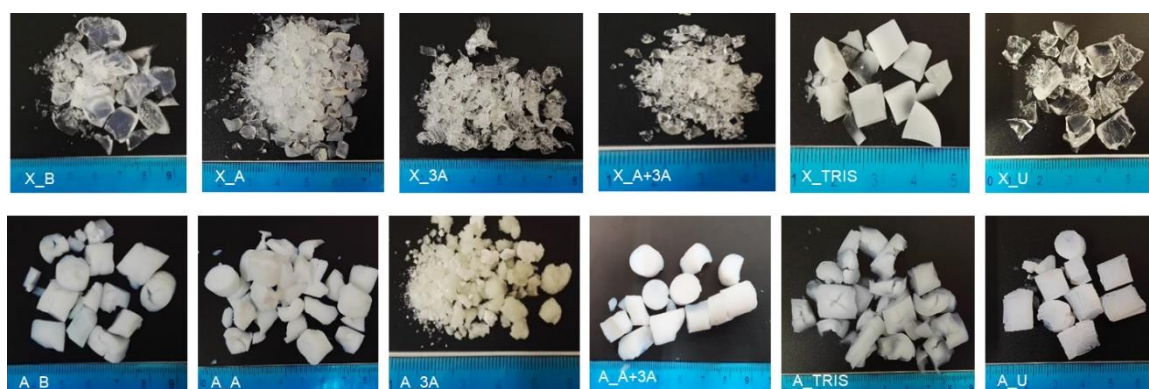


Figure 25 - Photographs of the prepared modified aerogel and xerogel adsorbents.

The visual differences revealed by Figure 25 are further complemented by the physical properties reported in Table 34. In a general way, aerogels are one order of magnitude lighter and more porous. It was not possible to report all properties of samples X_3A and X_U, in particular those related with surface area and porosity, due to the lack of reliability of the obtained data. The contraction of aerogels during nitrogen adsorption [506], could have inhibited the exposure of pores, in particular for these samples of complex and closed structure. Additionally, these samples

could be mainly microporous and with low surface areas, limiting its assessment given the test conditions [521, 522]. The difficulty in obtaining the porosity value in sample X_U comes from the limited way of approximating bulk density, being overestimated.

The presence of a primary amine or isocyanurate groups in samples A_A/A_A+3A and A_TRIS, respectively, did not alter the bulk density, porosity and pore volume greatly in comparison with sample A_B. On the other hand, the introduction of any functional group led to a decrease in the specific surface area, due to an increase in the average pore size. This is associated with the catalytic effect of amine groups in sol-gel chemistry, giving longer secondary particles [507]. Aerogel samples A_3A and A_U differ significantly, in regard to the properties presented in Table 34, from the remainder samples. As previously mentioned, sample A_3A did not retain its porous structure during drying, hence justifying the reduced porosity observed. Sample A_U is denser and less porous than the majority of modified aerogel samples. This could be due to the urea groups that also catalyze sol-gel reactions and can generate hydrogen bonds through the nitrogen or oxygen atom of these groups.

Table 34 - Structural properties of the aerogel and xerogel modified adsorbents.

Formulation		Bulk density ^a /g cm ⁻³	Porosity /%	S _{BET} /m ² g ⁻¹	V _{pore} /cm ³ g ⁻¹	D _{pore} /nm
B	Xerogel	1.07	24	761 ± 9	0.2	1
	Aerogel	0.141	90	1006 ± 15	6.4	25
A	Xerogel	1.41	3	27.9 ± 0.1	0.02	4
	Aerogel	0.13 ± 0.03	87 ± 3	573 ± 5	7 ± 2	45 ± 13
3A	Xerogel	1.30	7	b)	0.05	-
	Aerogel	0.7 ± 0.3	48 ± 19	14.2 ± 0.2	0.7 ± 0.5	182 ± 135
A+3A	Xerogel	1.12	23	3.07 ± 0.05	0.2	268
	Aerogel	0.19 ± 0.02	86 ± 2	256 ± 3	4.5 ± 0.6	70 ± 9
TRIS	Xerogel	1.14	16	634 ± 13	0.1	1
	Aerogel	0.13 ± 0.02	88 ± 2	451 ± 11	7 ± 1	59 ± 10
U	Xerogel	1.42	c)	b)	c)	-
	Aerogel	0.43 ± 0.05	67 ± 4	398 ± 7	1.6 ± 0.3	16 ± 3

^a Values for some xerogels were obtained with liquid displacement and should be considered indicative. b) Non-reliable result from nitrogen adsorption. c) Residual porosity, since the skeletal and bulk densities show similar values.

Figure 26 shows the scanning electron micrographs for the different aerogels. The samples can be divided into two contrasting groups: samples A_B, A_A and A_A+3A are clearly porous, while A_3A, A_TRIS and A_U show a much more closed featureless structure, being A_3A the more compacted one. Samples of the first group feature the expected microstructure for silica aerogels. They show a porous matrix formed by aggregated secondary silica particles of very small

size. The remaining samples are mainly microporous, and their microstructure is similar to that of modified xerogels described in Chapter 4.

The introduction of the propylamine groups in the silica backbone (sample A_A) seemed to have little change in the microstructure of the aerogels (Table 34 and Figure 26), when compared to the reference sample. However, this is not the case with formulation 3A that includes the functional groups containing three amines (one primary and two secondary), which affected significantly the properties of this formulation. This can be possibly explained by the size of the organic group in the silane, that may induce less ramified structures due to increased steric hindrance and slower hydrolysis [355, 523], and/or due to the presence of three amine groups, which may extensively catalyze the condensation reactions [507]. Formulation A+3A shows properties in-between the former two, as expected. Sample A_TRIS has high surface area and pore volume, not that different from sample A_A (Table 34), but the micrograph reveals a structure that seems less porous than the latter. Nevertheless, a great number of small pores, that seem uniform in size, are visible in the surface of the sample (see the inset in Figure 26). With formulation U, the propylurea groups led to the second most closed structure (less porous), right after sample A_3A, in agreement with results of Table 34.

The chemical composition of the adsorbent samples was studied by infrared spectroscopy - Figure 27 - and elemental analysis - Table 35.

The samples' FTIR spectra shown in Figure 27 reveal the typical silica matrix expected for silica aerogels and xerogels [524]. The bands at ~ 443 , 554, 778, 932 (shoulder), 1047 and 1130 cm^{-1} , are attributed to bending vibrations of siloxane bonds, SiO_2 defects, symmetric stretching of siloxane bonds, stretching of silanol bonds and the two vibrational modes of asymmetric stretching of siloxane bonds, respectively. All formulations have very similar spectra, as they are based on nearly similar silica backbone and the different functional groups contain the same covalent bonds, in most cases. The main bands related to the functional groups are visible at ~ 720 (shoulder), 831 (shoulder), 1273-1470, 1560-1645, 1668 and $2850\text{-}2975\text{ cm}^{-1}$, that are ascribed to the deformation of methylene groups, stretching of silicon-carbon bonds, bending of methylene and methyl groups, bending of primary and secondary amines, stretching of carbonyl bonds and stretching of methylene and methyl groups, respectively. Despite amine and hydroxyl bonds generating bands in the same region of the spectra, the $1500\text{-}1650\text{ cm}^{-1}$ region of the spectra is different between formulation B and the other formulations, evidencing the presence of N-containing groups in the functionalized samples.

Samples were immersed in water for 15 days to test their degradation. Only some xerogel samples fragmented onto smaller pieces. FTIR analysis showed no quantifiable degradation of the materials by water.

5. Silica-Based Aerogel Adsorbents with Nitrogen-Containing Groups

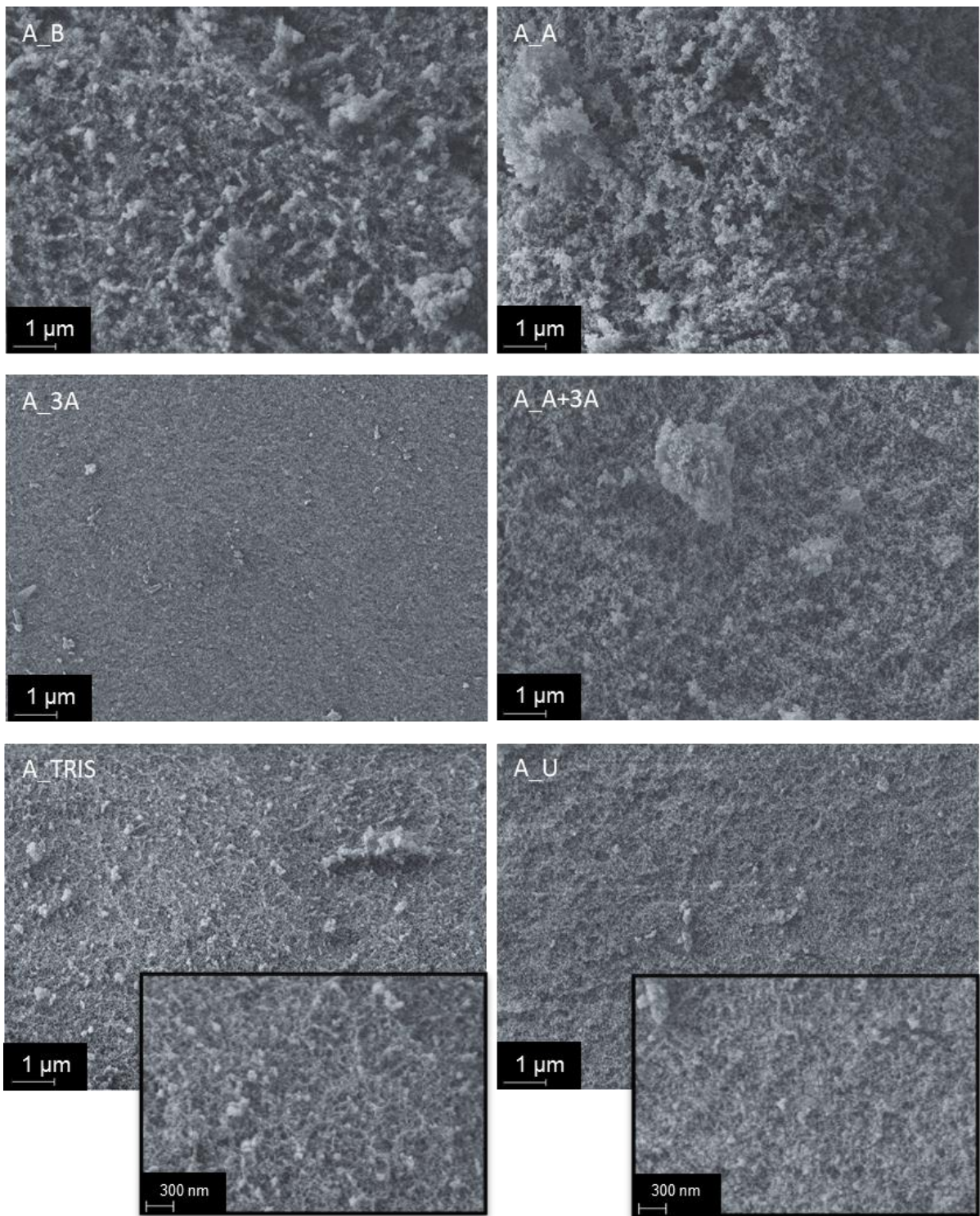


Figure 26 - Morphology of the prepared aerogel samples (10kx magnification) and details for samples A_TRIS and A_U (30kx magnification).

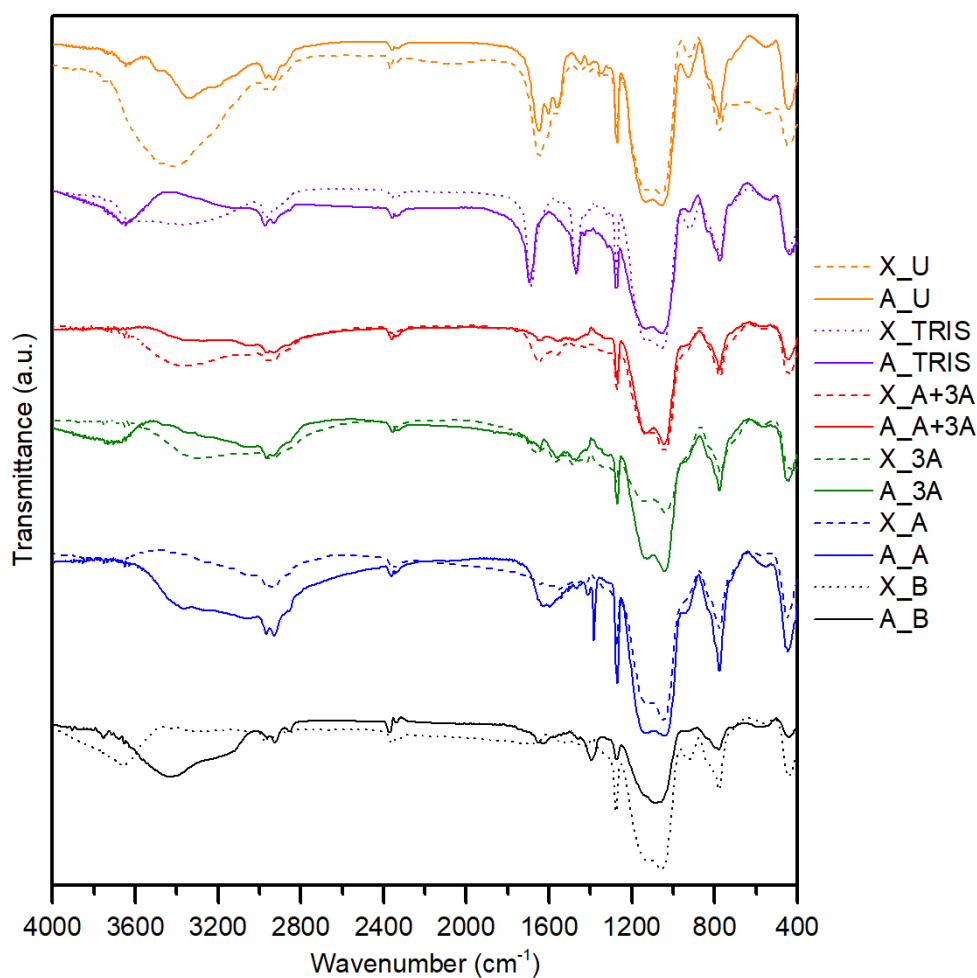


Figure 27 - FTIR spectra for different nitrogen-containing groups modified xerogels and aerogels.

For comparison with the experimental results from elemental analysis, different theoretical hypotheses were considered for the condensation of the precursors. These theoretical scenarios assume that the hydrolysis of precursor molecules is complete, and all precursor molecules react to form the gel backbone. The different scenarios vary in the number of unreacted hydroxyl groups, per precursor molecule, hence ranging from a complete condensation to an incomplete condensation where it is assumed that two hydroxyl groups are left unreacted in each molecule.

The elemental analysis data reveal in some cases (samples A_B, A_A, X_TRIS, A_TRIS and A_U) that the content of carbon is greater than that predicted by the theoretical scenarios. This can be attributed to the fact that hydrolysis was not complete (hence methoxy or ethoxy groups still exist in the silica backbone) or to the possible heterogeneity of the sample, with the quantification occurring in portions where some precursors are more prominent. In fact, Itagaki *et al.* [525] showed that the precursors tend to condense with similar species in some situations, and so phase segregation of condensed precursor species can occur. Analyzing the carbon content, most samples are between the values of complete condensation and incomplete condensation with one hydroxyl group remaining per precursor molecule. This is in general corroborated by the results

5. Silica-Based Aerogel Adsorbents with Nitrogen-Containing Groups

of N content. However, the analysis of the N content of formulation B reveals that, despite being washed, aerogels still have ammonia catalyst residues, contributing to some uncertainty. For the case of samples of formulations 3A and A+3A, the nitrogen content seems to suggest the more incomplete condensation scenario, which is not in agreement with the carbon result (Table 35).

Table 35 - Chemical composition of the samples modified with nitrogen-containing groups.

Formulation	Sample/Hypothesis	wt% C	wt% H	wt% N
B	Complete condensation	11.6	2.9	-
	Incomplete condensation 1 OH	10.2	3.9	-
	Incomplete condensation 2 OH	9.1	4.7	-
	Experimental Xerogel	11.9	3.5	0.6
	Experimental Aerogel	15.4	4.1	0.89
	A	Complete condensation	18.0	4.2
Incomplete condensation 1 OH		16.0	5.0	3.4
Incomplete condensation 2 OH		14.4	5.6	3.1
Experimental Xerogel		15.3	4.5	3.3
Experimental Aerogel		19.6	4.9	3.7
3A		Complete condensation	25.1	5.7
	Incomplete condensation 1 OH	22.9	6.2	8.4
	Incomplete condensation 2 OH	21.0	6.6	7.7
	Experimental Xerogel	22.2	5.9	7.9
	Experimental Aerogel	22.1	5.6	7.1
	A+3A	Complete condensation	21.9	5.0
Incomplete condensation 1 OH		19.8	5.6	6.1
Incomplete condensation 2 OH		18.0	6.1	5.6
Experimental Xerogel		19.1	5.5	6.0
Experimental Aerogel		21.0	5.1	5.5
TRIS		Complete condensation	19.8	3.5
	Incomplete condensation 1 OH	18.0	4.2	3.2
	Incomplete condensation 2 OH	16.1	4.9	2.9
	Experimental Xerogel	20.4	4.1	3.8
	Experimental Aerogel	22.0	4.4	3.8
	U	Complete condensation	19.0	4.1
Incomplete condensation 1 OH		17.1	4.8	6.1
Incomplete condensation 2 OH		15.6	5.3	5.6
Experimental Xerogel		17.1	4.4	5.6
Experimental Aerogel		21.4	4.9	6.5

The thermal stability of the aerogel samples is presented in Figure 28 and additional information is reported in Appendix A. The nitrogen-containing groups modified samples feature two degradation phenomena, with the degradation occurring continuously. Sample A_B is an exception, featuring four different thermal degradation phenomena. It can also be verified that samples modified with nitrogen groups lose more mass, associated with the presence of more organic groups in the structure.

In sample A_B the first two degradation stages (onset temperatures of 55 and 152 °C) correspond to the evaporation of residual solvent, ammonia residues and adsorbed water, totaling approximately 4.2% of weight lost. Phenomena with onset temperatures of 340 and 536 °C are associated with the first and second stages of the degradation of methyl groups, respectively [507]. The modified samples start losing mass at approximately 50 °C (onset temperature), except for A_TRIS and A_U (onset temperature of 90 and 135 °C, respectively) corresponding to the evaporation of residual solvent and adsorbed water. In sample A_U this phenomenon ends at a higher temperature and is responsible for a substantial higher mass loss (20%) than the corresponding phenomenon in the remaining samples (12% for sample A_3A and ~3% for the remainder). This must be the result of the degradation of the urea groups [526]. The final thermal degradation phenomenon causes most of the lost weight (up to 30%) and is due to the degradation of the nitrogen-containing and methyl groups. In these samples, this phenomenon starts at a lower temperature in samples that contain secondary amines (~350 vs 440 °C, onset temperature) and the two stages of degradation of methyl groups are not visible.

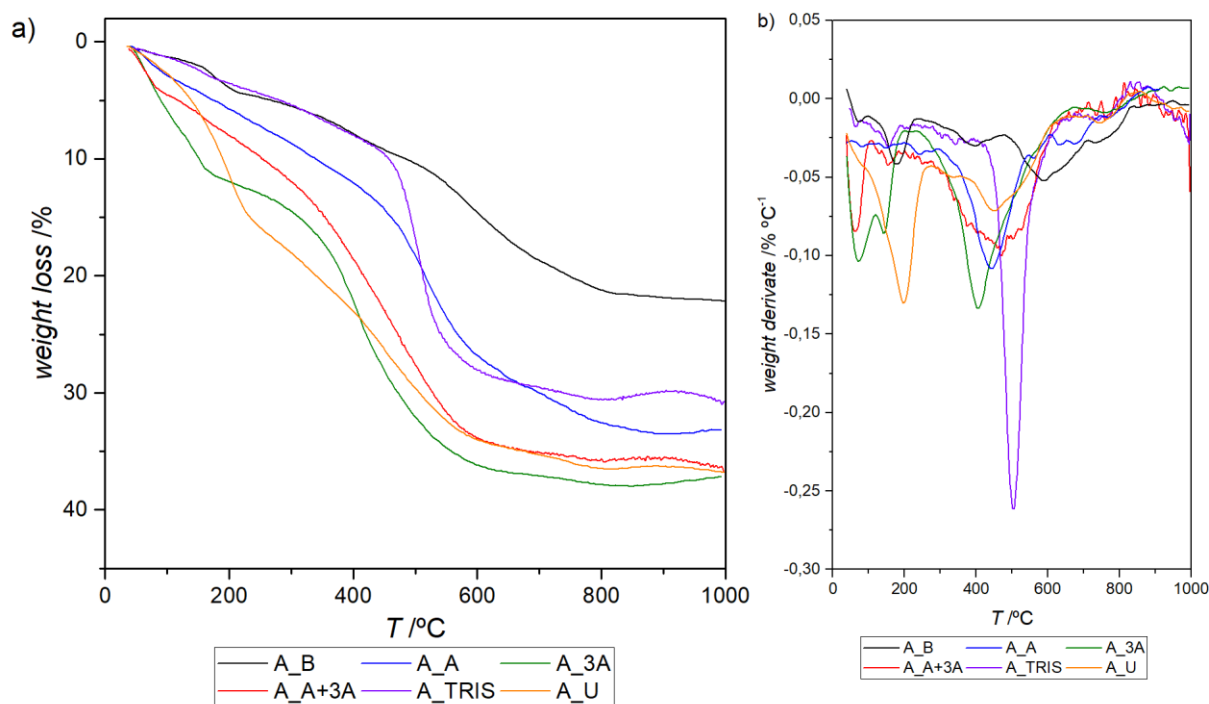


Figure 28 – Thermogravimetric curves for the nitrogen-modified aerogels: (a) weight loss; (b) sample weight temperature derivative.

5.5. Preliminary Sorption Tests and Screening of Adsorbents

Preliminary tests were conducted with every sample described in Table 29 to assess which ones were the most viable for the removal of different heavy metals. The results from this screening, based on two replicates, are presented in Table 36. A concentration of 50 mg L⁻¹ of the cations was used for these tests.

The obtained results show that activated carbon, considered as a standard adsorbent, is not a viable material for the removal of the tested cations, showing removal efficiencies below 20% - Table 36. On the other hand, the materials of formulation B do not interact well with the cations, apart from lead which has considerable removal efficiencies at the tested concentration. In fact, lead is fairly removed by all materials, compared to the other cations, because lead has the lowest charge density of the four, and thus has the less stable hydration sphere, being more labile [33, 209]. The removal of lead could be due to silanol groups, featured in all silica-based adsorbents or to non-specific processes like electrostatic interactions with the negatively charged [527, 528] silica surface. Despite having functional groups containing electron donor atoms, *i.e.* Lewis bases, the results obtained with aerogels and xerogels of formulations TRIS and U are nearly similar to those of formulation B. In fact, these three formulations do not show a good performance (except for lead), even when compared with activated carbon. This is a consequence of the hindering of active surface sites, in modified samples, towards the metal ions. This can be justified by the limitations in the adsorbent's microstructure/physical properties (formulation U) or by the absence of functional Lewis base groups at the surface of the adsorbent (formulation TRIS). As the isocyanurate ring is enclosed by three silicon atoms with sol-gel reactive groups, it is not so available on the surface of silica particles - contrary to what happens with the remaining precursors. The materials from formulations A, 3A and A+3A show better adsorption performances. Samples X_3A and A_3A are analogous in terms of structural properties (Table 34) and adsorption performance (Table 36). Samples A_A and A_A+3A perform better and more consistently across the four tested cations when compared to their xerogel counterparts and the remaining formulations. While for copper and lead, the lower surface area and porosity of the xerogels does not inhibit the adsorption process (suggesting that the active sites are accessible in the xerogels), this is not the case for cadmium and nickel. Because all cations are fairly similar in size, the surface heterogeneity or a different adsorption mechanism for the latter cations may explain these results.

The initial screening of the adsorption performance of the samples allows to conclude that A_A and A_A+3A are good adsorption candidates for the studied heavy metals. X_3A also performs fairly well and was also selected for being easier to obtain than its aerogel counterpart.

Table 36 - Heavy metal removal efficiencies, in percentage, for different adsorbents. $C_0 = 50 \text{ mg L}^{-1}$, pH 5, 20 °C, 24 hours.

Sample	Copper Removal (%)	Lead Removal (%)	Cadmium Removal (%)	Nickel Removal (%)
X_B	9 ± 2	45 ± 1	0.9 ± 0.2	7
A_B	8.7 ± 0.8	64 ± 12	a)	2.3 ± 0.2
X_A	13 ± 9	61 ± 3	6 ± 4	4.2 ± 0.8
A_A	98.6 ± 0.2	99.51 ± 0.01	98.75 ± 0.00	67 ± 2
X_3A	59.0 ± 0.2	98.9 ± 0.3	6.1 ± 0.9	12
A_3A	33.4 ± 0.7	97 ± 3	11 ± 2	3 ± 2
X_A+3A	64.7 ± 0.1	78 ± 15	27 ± 1	22 ± 3
A_A+3A	59.4 ± 0.1	93 ± 2	95.0 ± 0.7	64.0 ± 0.4
X_TRIS	10 ± 4	34.0 ± 0.3	a)	a)
A_TRIS	9 ± 2	52 ± 5	3 ± 2	a)
X_U	5.2 ± 0.5	38 ± 3	1.8 ± 0.3	a)
A_U	9	39 ± 7	3.0 ± 0.8	a)
AC	22 ± 1	19 ± 4	9 ± 1	6

a) No removal was observed.

5.6. Effect of pH and Adsorbent Dose on Adsorption

The effect of pH and adsorbent dose on the adsorption performance was studied using sample A_A. The results are presented in Figure 29. To evaluate the effect of the initial solution's pH, a starting concentration of 50 mg L^{-1} of cation and 2 g L^{-1} of adsorbent were used. The results in Figure 29a show that only copper adsorption significantly decreases by the pH decreasing to 4. Nickel shows the opposite trend, while for lead and cadmium the pH variation effect was not significant, and the detection limit was sometimes achieved. pH of 4 was chosen to guarantee that no metal ion hydroxides are formed. The adsorption performance of non-modified silica materials (A_B) was not impacted by the change to pH 4 (copper removal of $9 \pm 10\%$, lead removal of $63 \pm 19\%$, cadmium removal of $6 \pm 1\%$ and nickel removal of $5 \pm 3\%$).

At pH 4 and with a starting concentration of 500 mg L^{-1} , the removal of the metal ions was quantified as a function of the adsorbent dose - Figure 29b. As expected, the greater the mass of adsorbent the greater the mass of pollutant that can be removed. At the highest mass of adsorbent very significant amounts of cations were removed; in particular it can be observed an almost complete removal of lead and cadmium. Although at a high pollutant concentration, high removals are only expected with greater adsorbent doses, a small dose of 2 g L^{-1} was selected in this work to obtain adsorption isotherms and kinetic curves since wastewaters typically feature low concentrations of these pollutants due to high dilution.

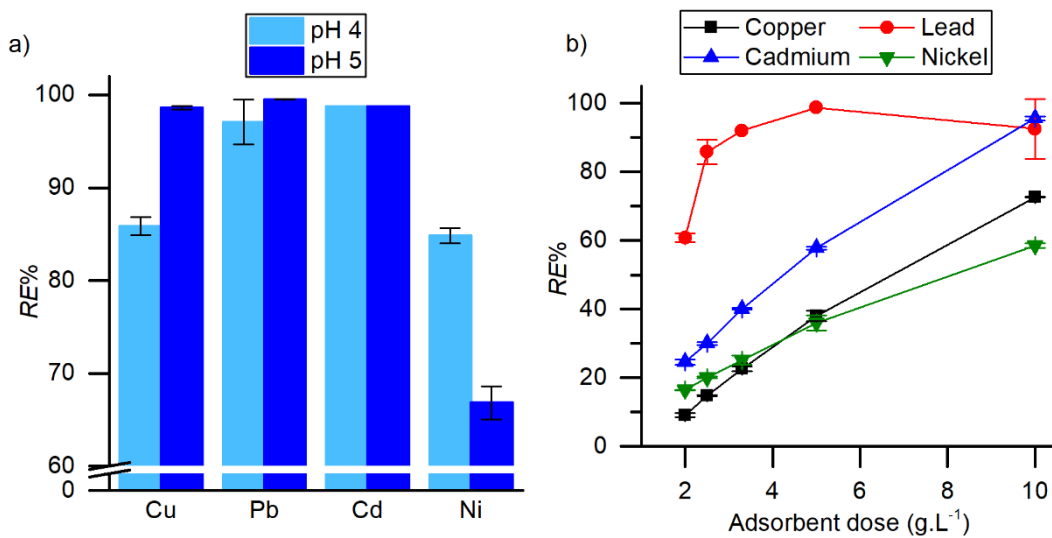


Figure 29 - The effect of: (a) initial solution pH at $C_0 = 50 \text{ mg L}^{-1}$; (b) adsorbent dose at $C_0 = 500 \text{ mg L}^{-1}$ on heavy metals removal by aerogel A_A.

5.7. Adsorption Kinetics

Adsorption kinetics were studied for adsorbents A_A, X_3A and A_A+3A. Kinetic models were fitted to data from kinetic tests and the results are shown in Figure 30 and Table 38. For the sake of simplicity, only the best model is represented in the graphs. The selection of the kinetic models was not solely based on Akaike's and Bayesian Information Criteria, as these are often in disagreement: BIC suggests that the double exponential model (DEM) is usually the best model, while AIC penalizes this model severely for having too many parameters for the number of data points, even when it is clearly the most adequate (see Figure 30). The kinetic tests reveal two different situations: the adsorption process occurs in two-steps (DEM model) or in one, being controlled by the rate of sorption phenomena at the adsorbent surface (pseudo-second order (PS2) model). This result was also observed in other functionalized silica materials [223]. The DEM model generally assumes that the steps are diffusion limited but it has also been shown that this model can describe adsorbents with two types of active sites present [223], situation in which the process is not limited by diffusion.

To understand the nature of the adsorbent-adsorbate interactions in the sorption process, when its kinetics is described by the double-exponential model, the points corresponding to the first step (fast step) were described using a surface reaction model, pseudo-second order, and a diffusion describing model, intraparticle diffusion. The results of this analysis are compiled in Table 37.

Table 37 - Parameters of kinetic models for the fast/first step of the kinetic curves of the referred adsorbent-adsorbate systems.

	Intraparticle Diffusion Model				Pseudo-Second Order			
	k_{IPD} /mg g ⁻¹ h ^{-0.5}	E /mg g ⁻¹	AIC	BIC	$k_2 \times 10^3$ /g mg ⁻¹ h ⁻¹	q_e / mg g ⁻¹	AIC	BIC
A_A Cu	13.4	11.1	39.3	26.7	4767	26.4	25.7	13.1
X_3A Cu	10.1	3.3	28.3	15.7	997.3	13.5	12.8	0.1
X_3A Pb	41.3	6.3	45.9	20.7	566.6	36.6	26.4	1.2
A_A Cd	17.4	3.8	29.1	16.4	455.5	21.7	26.4	13.7
X_3A Ni	8.0	2.3	34.5	9.4	1461	10.5	15.0	-10.2

The results of Table 37 clearly show that the kinetics of adsorption in the fast step is not limited by diffusion, with the pseudo-second order model fitting the data. Hence, it can be said that chemisorption is the limiting phenomena for the adsorption process in this step. The DEM model is mostly observed with adsorbent X_3A, which has little porosity and features two different kinds of active sites: primary and secondary amines. However, it is also the best model to describe the kinetics of A_A with copper and cadmium. In these situations, a clear two-step mechanism is observed. By looking for a mechanism, it can be hypothesized that the observed kinetic curve is due to the existence of multiple types of active sites, with different accessibilities and surface reaction rates. The slow step can be attributed to the interaction of the metal ions with other groups on the adsorbent, such as silanol, whilst the fast one is due to the interactions with the primary amine groups.

The interactions of A_A+3A with lead seem to be controlled by the bulk concentration as evidenced by the pseudo-first order model. For the remaining situations, the sorption kinetics is limited by the surface reactions, meaning that chemisorption is most likely occurring (model PS2). It is worth noticing that adsorbent A_A+3A, which also features different types of active sites, does not have its behavior modeled by the DEM equation. Furthermore, it behaves differently than A_A meaning that the secondary amine groups are still somewhat accessible. It is possible that due to its extensive porous structure, diffusion occurs quickly, and the functional groups are very accessible, interacting fast and in one step.

5. Silica-Based Aerogel Adsorbents with Nitrogen-Containing Groups

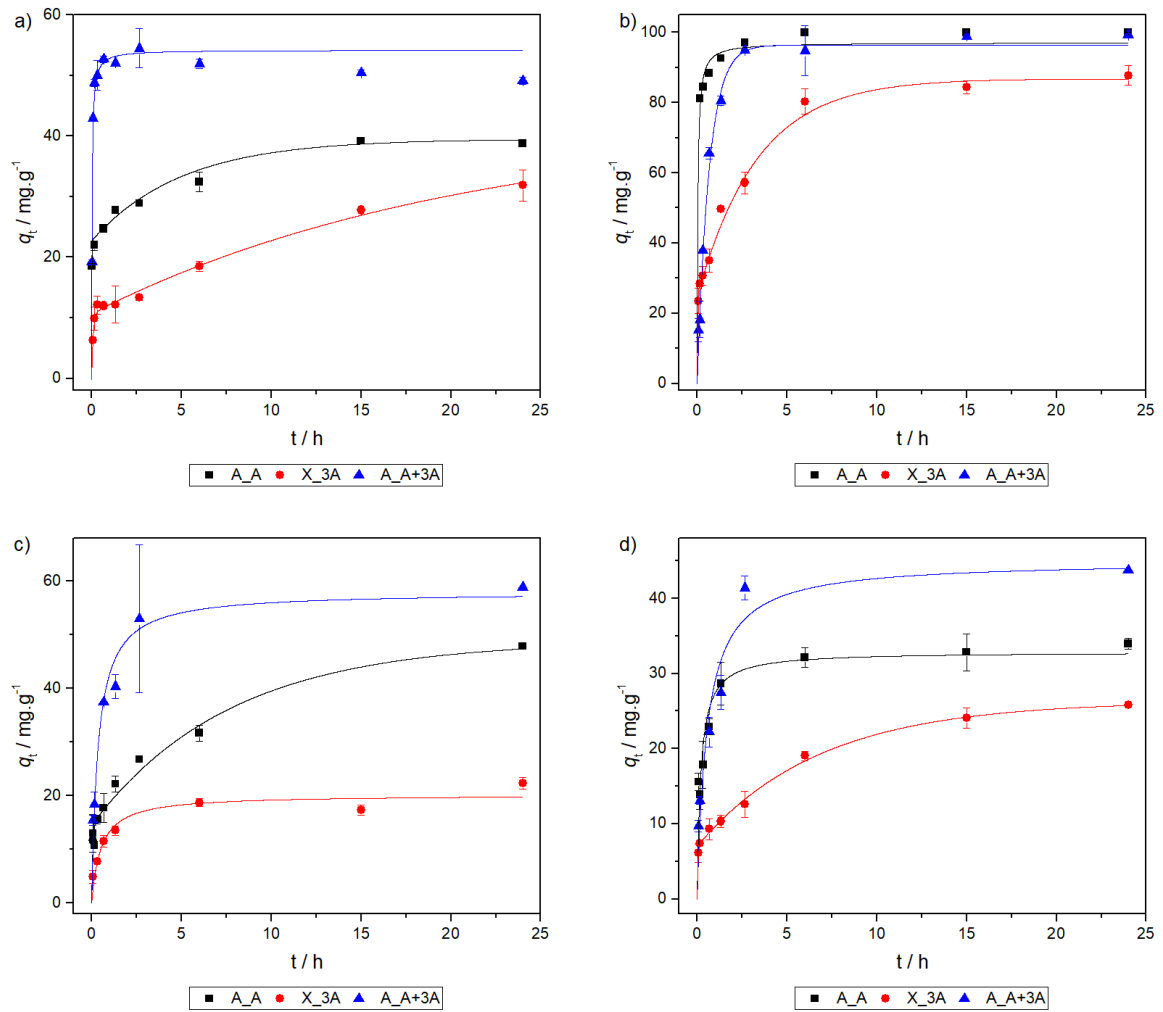


Figure 30 - Sorption kinetics for (a) copper, (b) lead, (c) cadmium and (d) nickel on amine modified materials.

Environmental Cleaning and Recovery of Heavy Metals via Functionalization of Silica Aerogels

Table 38 - Fit parameters for sorption kinetics on the three selected amine modified materials.

	Pseudo-first order (PS1)				Pseudo-second order (PS2)				Double-exponential model (DEM)						Exp. q_e /mg g^{-1}	Best Model	
	k_1 / h^{-1}	q_e / mg g^{-1}	AIC	BIC	$k_2 \times 10^3$ /g mg $^{-1}$ h $^{-1}$	q_e / mg g^{-1}	AIC	BIC	D_1 /mg L $^{-1}$	k_{D1} /h $^{-1}$	D_2 /mg L $^{-1}$	k_{D2} /h $^{-1}$	q_e / mg g^{-1}	AIC			BIC
A_A Cu	27.6	30.9	42.7	38.5	1866	31.5	39.5	35.3	45.3	102	33.6	0.18	39.5	51.2	10.3	44.0	DEM
X_3A Cu	0.43	26.8	43.5	40.4	36.3	27.2	39.8	36.7	21.7	11.8	63.2	4.8×10^{-2}	42.3	31.6	5.4	46.3	DEM
A_A+3A Cu	23.8	517	19.2	15.0	713	54.2	16.3	12.1	87.2	32.5	18.3	4.1	52.9	49.1	8.3	47.5	PS2
A_A Pb	11.2	93.3	34.5	26.4	261	97.1	26.3	18.1	161	23.4	39.1	0.73	100.0	68.7	-14.8	94.3	PS2
X_3A Pb	0.87	80.4	56.8	53.7	16.1	85.9	50.9	47.3	124	0.32	49.3	26.8	86.8	52.6	26.4	82.7	DEM
A_A+3A Pb	1.5	96.4	28.0	23.8	18.4	106.4	37.7	33.5	191	1.5	2.2	400	96.5	71.1	30.2	89.6	PS1
A_A Cd	0.93	36.9	44.5	40.3	29.0	41.5	40.1	35.9	28.6	16.0	68.7	0.14	48.9	64.0	23.2	47.9	DEM
X_3A Cd	1.3	19.2	22.2	16.4	96.4	20.2	18.0	12.3	1.1×10^5	4.8×10^{-6}	28.3	1.8	5.3×10^4	99.7	16.2	30.0	PS2
A_A+3A Cd	1.9	53.0	36.8	28.6	48.1	58.0	28.5	20.3	68.6	0.56	48.7	7.3	59.2	--	--	58.9	PS2
A_A Ni	3.1	31.4	33.5	29.3	150	32.9	26.4	22.2	24.2	4.9×10^9	42.0	1.1	33.1	52.8	12.0	44.4	PS2
X_3A Ni	0.38	23.9	32.1	27.9	21.8	26.1	29.2	25.0	38.6	0.15	14.1	21.5	26.3	35.7	-5.1	25.8	DEM
A_A+3A Ni	1.1	42.7	32.7	24.5	40.3	45.0	29.4	21.2	17.8	25.9	71.6	0.67	44.7	--	--	43.8	PS2

5.8. Adsorption Isotherms

Adsorption isotherm curves for adsorbents A_A, X_3A and A_A+3A are represented in Figure 31. For clarity, only the best fitting model is represented in the graphs. The fit parameters are compiled in Table 39. Figure 31 and Table 39 show that the Langmuir equation is the best model in most of the cases. This suggests that the surface of the adsorbents can be considered homogeneous and that the adsorption process is due to the interaction at active surface sites - the amine functional groups. This result was expected, as it was previously obtained in Chapter 4, and corroborates the predictions from the hard and soft acids and bases theory. Furthermore, it has been proposed that multiple amine groups are involved in the complexation of a cation [205, 313, 529]. Notable exceptions to this trend are obtained for the systems: A_A with nickel and X_3A with copper. In the first situation the model that best fits to the data is the Freundlich model, suggesting that the interactions with this cation occur differently than in other situations, and the adsorbent surface cannot be considered homogeneous. In the second situation, an L4 isotherm is observed [199], which is characterized by the existence of two plateaus due to the development of a new surface where adsorption can occur. Thus, the second plateau indicates the saturation of the new surface and the complete saturation of the adsorbent. This could be due to the reorientation of previously sorbed species, leading to partial uncovering of the adsorbent surface [199]. The isotherm for each plateau is given in Table 39. It is suggested that the Langmuir model fits each plateau better.

Table 39 - Fit parameters for sorption isotherms on the three selected amine modified materials.

	Langmuir model				Freundlich model				Max. Exp.
	q_{\max} /mg g ⁻¹	$K_L \times 10^3$ /L mg ⁻¹	AIC	BIC	1/n _F	K_F /mg g ⁻¹ (L/mg) ^{1/n}	AIC	BIC	q_e /mg g ⁻¹
A_A Cu	43.5	2683	28.3	22.5	0.1	22.9	35.2	29.4	47.6
X_3A Cu	105.1	6.8	30.7	22.5	0.6	2.3	36.8	28.6	129.8
	131.0	236	a)	a)	0.1	35.2	a)	a)	
A_A+3A Cu	60.4	24.4	32.6	26.8	0.3	8.1	42.6	36.8	55.7
A_A Pb	183.3	116	52.1	46.4	0.3	42.7	61.5	55.7	172.1
X_3A Pb	110.6	52.4	44.2	38.5	0.3	19.9	55.6	49.8	99.9
A_A+3A Pb	346.9	16.9	25.7	17.5	0.7	10.0	28.6	20.5	171.8
A_A Cd	54.0	66.7	41.9	36.1	0.2	14.9	46.6	40.9	51.2
X_3A Cd	102.4	2.9	21.0	12.8	0.7	0.9	23.1	14.9	47.0
A_A+3A Cd	82.9	50.7	40.9	35.2	0.3	17.1	43.5	37.8	81.9
A_A Ni	68.2	34.6	41.4	35.6	0.3	10.5	32.2	26.4	68.2
X_3A Ni	69.2	4.2	22.4	9.8	0.6	1.5	29.2	16.5	42.0
A_A+3A Ni	65.6	21.5	31.0	25.2	0.4	7.7	39.6	33.8	61.3

a) Values without significance.

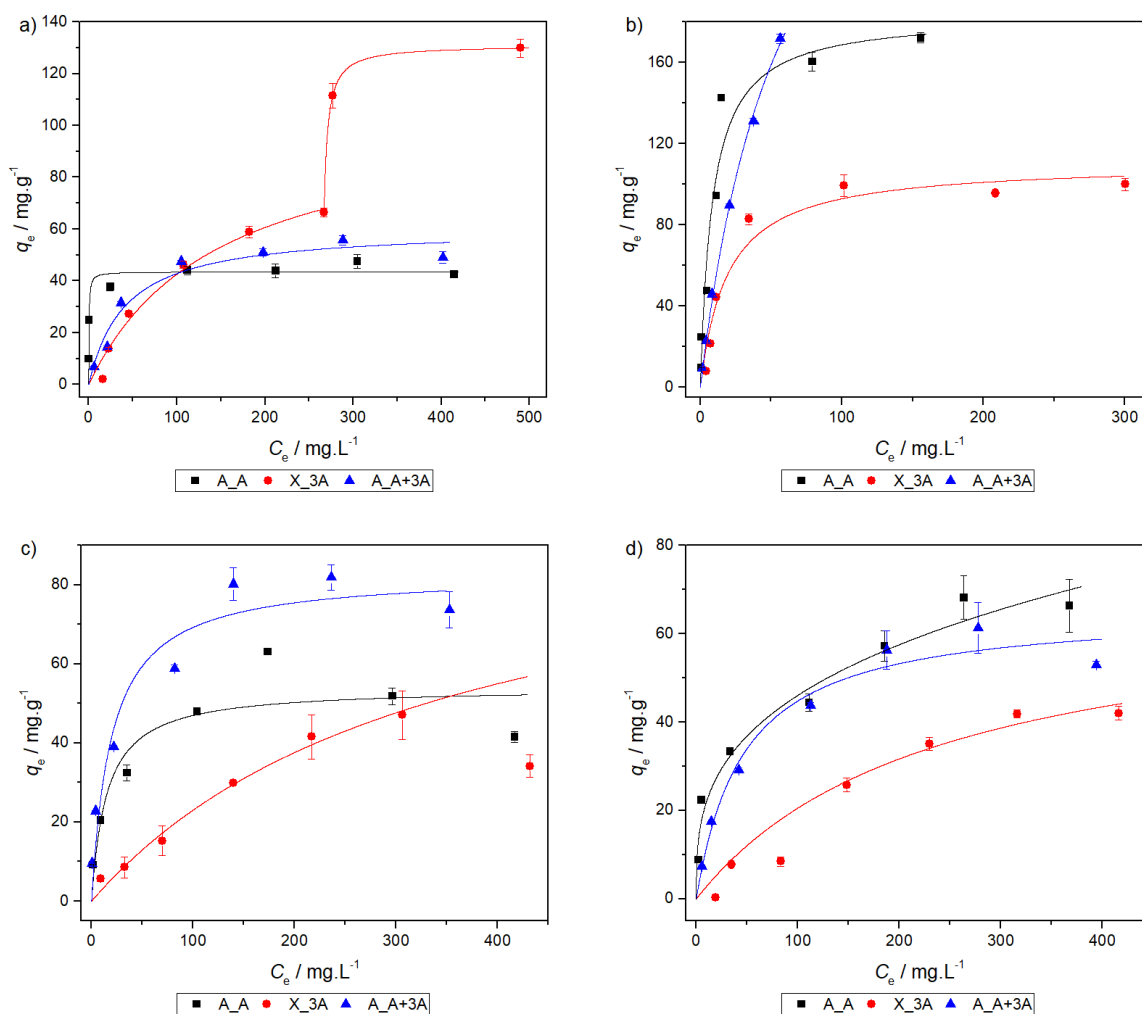


Figure 31 - Sorption isotherms for (a) copper, (b) lead, (c) cadmium and (d) nickel on amine modified materials.

Although the different adsorbents have similar behaviors, adsorbent A_A+3A is found to be the best out of the three evaluated in depth, for the majority of the situations. When adsorbing nickel and copper, the aerogel became colored, exhibiting a green or blue color, respectively, as shown in Figure 32. This was shown to be associated with cation complexation [205].

One finding is that the sorption of copper is lower in the materials presented in this chapter, compared to the ones from Chapter 4. The difference seems to be on the anion, as copper nitrate is less sorbed than copper sulfate [530], as was observed with A_A at different concentrations at pH4 and 5 (data not shown). When compared to the adsorbents compiled in section 3.2., adsorbent A_A+3A is better than natural minerals and zeolites, and its performance is among the best for modified silicas, including aerogels.

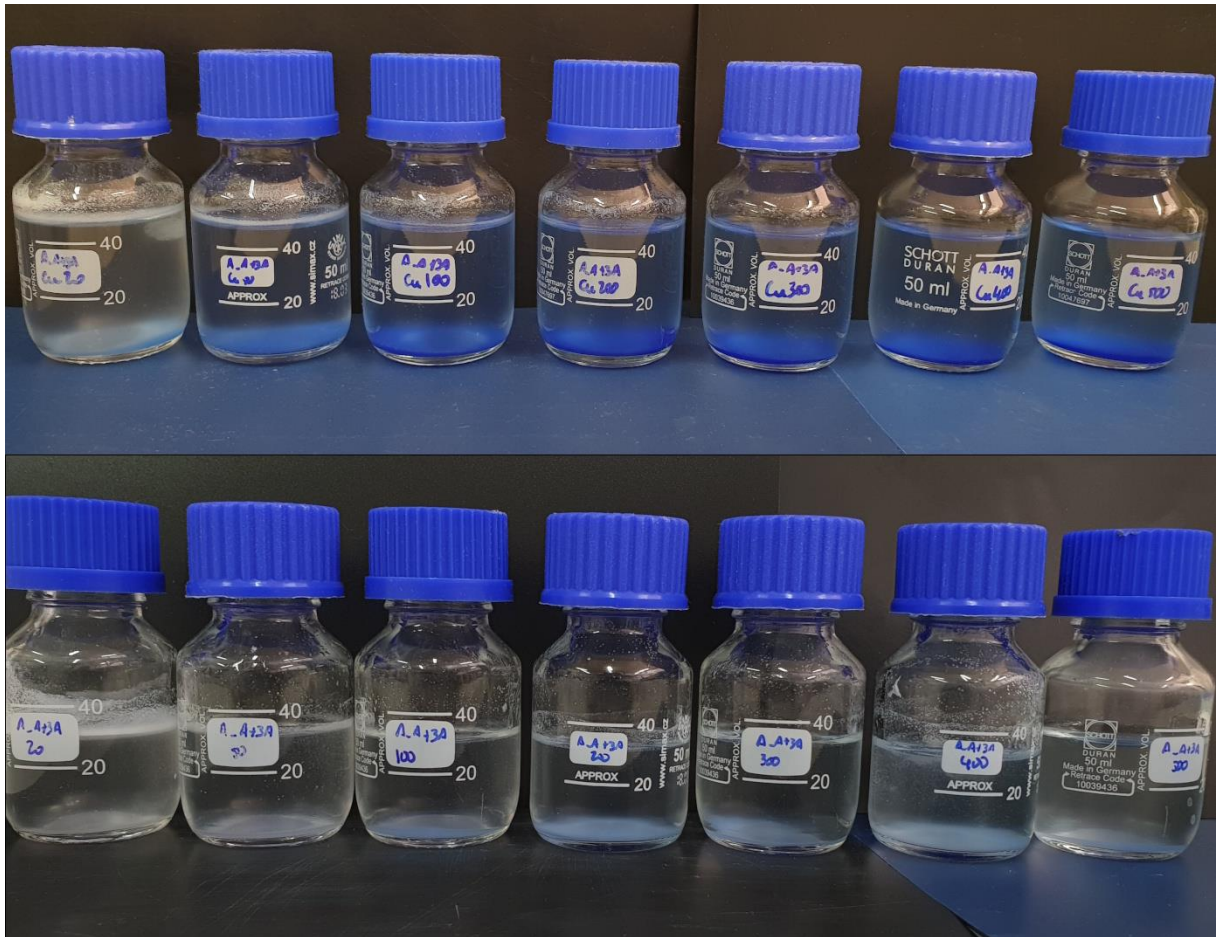


Figure 32 - Aspect of sample A_A+3A after sorption equilibrium with copper (top) and nickel (bottom).

5.9. Adsorption Thermodynamics

The adsorption capability of aerogel A_A+3A was studied with varying temperature, and its results are summarized in Table 40 and Figure 33. The standard Gibbs energy, enthalpy and entropy changes of adsorption were estimated as described in Section 3.1.4..

By the analysis of the standard Gibbs energy change, for all metal ions, the adsorption process is spontaneous. However, although for lead and cadmium the adsorption stability becomes higher by increasing the temperature, for copper and nickel only slightly variations of the Gibbs energy are observed. This can be justified by an athermic adsorption process (*i.e.*, K_d is independent on temperature as observed for nickel) or by a entropy-enthalpy compensating effect [531]. Another possible justification, by comparing the thermodynamic functions of nickel(II) and copper(II), is related with the configuration of hexahydrate complexes; while the $\text{Ni}(\text{H}_2\text{O})_6^{2+}$ has a symmetrical octahedron configurations, the hexa-coordinated copper(II) shows a Jahn-Teller distortion; consequently the shortest distance Cu-O(H_2O) is smaller than the distance Ni-O(H_2O) (1.96 and 2.055 Å, respectively [48]) and thus the ability of copper to interact with the adsorbent is higher, through a mechanism that has been proposed in the literature [529]. Looking to the thermodynamic function values shown in Table 40, it can be concluded that the enthalpy change

of sorption increases in the order $\text{Cu(II)} < \text{Cd(II)} < \text{Pb(II)}$. This is in close agreement with the effect of the metal ion radii (r_i): 0.73, 0.95 and 1.19 Å, respectively [48]; *i.e.* the interaction adsorbate-adsorbent is higher by increasing the charge density of metal ions. This also indicates that the interactions are of electrostatic nature. However, for Cd(II) and Pb(II) the sorption is characterized by an endothermic process and only for Cu(II) the sorption is slightly exothermic, suggesting that the sorption interaction between metal ions and the adsorbent is weak [532, 533]. This also explains the dependence of the Gibbs energy change of copper and nickel ($r_i = 0.69$ Å [48]) with the temperature, since the stability of hydration shell is higher and, consequently, these metal ions are the less labile [209]. This is in line with the entropy variation values for the different metal ions; in fact, the water loss from the hydration sphere of more labile metal ions plays a major role in driving the adsorption process [209].

Table 40 - Thermodynamic characterization of the adsorption process for aerogel A+3A.

Cation	Temperature / °C	K_d /L g ⁻¹	ΔG^0 /kJ.mol ⁻¹	ΔH^0 /kJ.mol ⁻¹	ΔS^0 /J.mol ⁻¹ .K ⁻¹	R^2
Copper	25	0.409	-8.07 ± 0.07	-19 ± 3	-36 ± 9	0.956
	30	0.326	-7.64 ± 0.06			
	35	0.278	-7.4 ± 0.1			
	40	0.267	-7.37 ± 0.02			
	45	0.250	-7.3 ± 0.1			
Lead	25	2.14	-15.10 ± 0.08	225 ± 18	805 ± 58	0.987
	30	17.2	-20.6 ± 0.4			
	35	16.6	-20.9 ± 0.5			
	40	160	-27 ± 1			
	45	859	-32 ± 4			
Cadmium	25	0.080	-5.4 ± 0.2	62 ± 4	226 ± 14	0.985
	30	0.124	-6.6 ± 0.1			
	35	0.161	-7.4 ± 0.1			
	40	0.240	-8.6 ± 0.1			
	45	0.410	-10.13 ± 0.00			
Nickel	25	0.238	-6.54 ± 0.08	a)	a)	a)
	30	0.250	-6.8 ± 0.2			
	35	0.232	-6.69 ± 0.04			
	40	0.258	-7.1 ± 0.2			
	45	0.263	-7.24 ± 0.03			

a) Adsorption performance does not change with temperature - Figure 33.

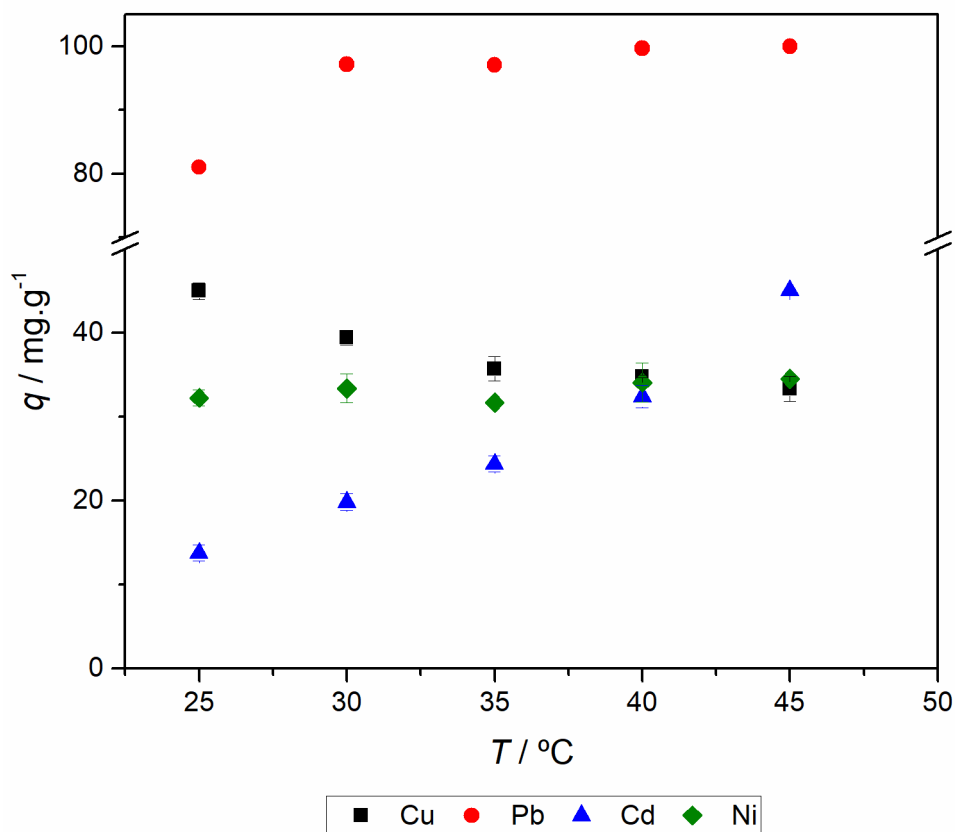


Figure 33 - Effect of temperature on the adsorption performance of A_A+3A.

5.10. Competitive Adsorption in Binary Mixtures

The adsorbent A_A+3A was also studied with binary mixtures of cations to evaluate the behavior of the sorption onto the adsorbent under competitive conditions. The results of the total (sum) uptake are displayed in Figure 34 and Table 41, while the kinetic curve of each individual component are presented alongside its isolated result in Figure 35 and Table 42.

Table 41 - Fitting parameters of kinetic models for the total sorption on A_A+3A.

	Pseudo-first order				Pseudo-second order			
	$k_1/$ h^{-1}	$q_e \times 10/$ $mmol g^{-1}$	AIC	BIC	$k_2/$ $g mmol^{-1} h^{-1}$	$q_e \times 10/$ $mmol g^{-1}$	AIC	BIC
Cu+Pb	1.8	7.1	-53	-57	3.1	7.8	-58	-62
Cu+Cd	13.9	7.0	-47	-55	76.1	7.2	-45	-54
Cu+Ni	18.8	9.1	-27	-40	54.9	9.3	-26	-39
Pb+Cd	4.4	4.7	-36	-44	16.7	5.0	-45	-53
Pb+Ni	8.8	6.9	-40	-46	24.4	7.2	-51	-57
Ni+Cd	3.4	5.5	-30	-42	16.3	5.7	-38	-50

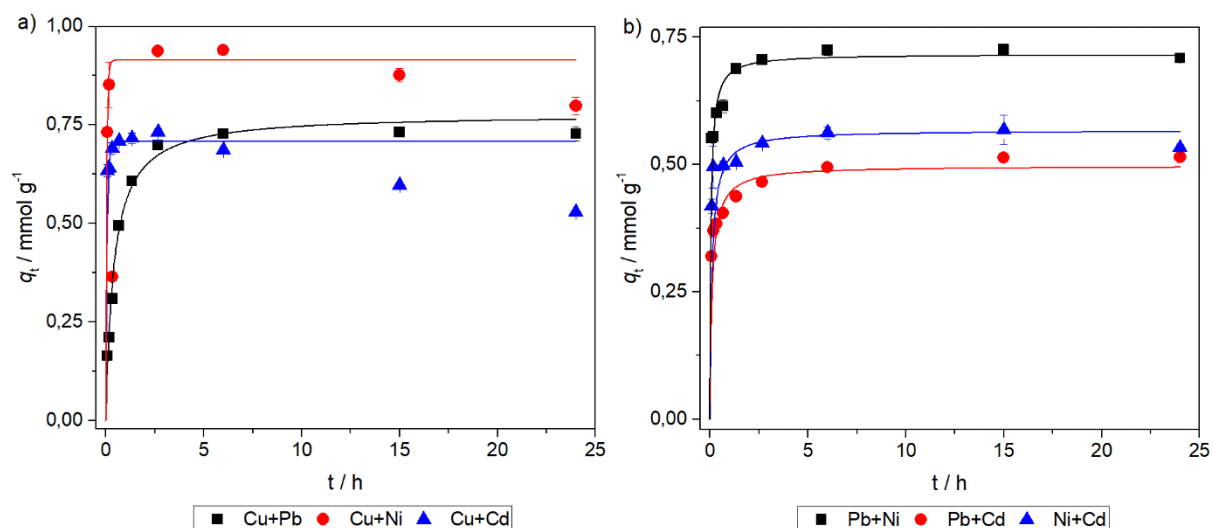


Figure 34 - Kinetic curves for the total sorption in binary mixtures (a) containing copper or (b) without copper onto A_A+3A.

The total adsorption of the binary mixtures on A_A+3A is generally explained by the pseudo-second order model. However, for the Cu+Cd and Cu+Ni mixtures the pseudo-first order model seems to be slightly better. These results suggest that despite the cations being mixed, the sorption phenomenon is still due to the active surface amine groups. The process is very fast, as the equilibrium is usually attained in less than three hours.

Table 42 - Fitting parameters of kinetic models for the sorption of individual cations, in binary mixtures, on A_A+3A.

	Pseudo-first order				Modified pseudo-second order				
	k_1 / h^{-1}	$q_e / \text{mg g}^{-1}$	AIC	BIC	$k_2 / \text{g mg}^{-1} \text{h}^{-1}$	$q_0 / \text{mg g}^{-1}$	$q_e / \text{mg g}^{-1}$	AIC	BIC
Cu	0.83	30.2	19	14	0.0325	a)	33.2	18	12
Cu (w/ Pb)	1.7	43.4	15	11	0.0468	a)	47.8	18	14
Cu (w/ Cd)	21.7	41.9	20	15	1.2	a)	43.1	9	3
Cu (w/ Ni)	0.87	44.4	25	16	0.0241	a)	48.6	31	23
Pb	5.2	48.7	33	29	0.165	a)	51.4	25	21
Pb (w/ Cu)	b)	b)	b)	b)	b)	b)	b)	b)	b)
Pb (w/ Cd)	12.5	48.3	22	17	0.46	a)	50.2	9	4
Pb (w/ Ni)	6.3	47.1	32	26	0.217	a)	49.7	22	17
Cd	4.8	29.3	28	22	0.23	a)	31.4	19	13
Cd (w/ Cu)	b)	b)	b)	b)	b)	b)	b)	b)	b)
Cd (w/ Pb)	1.5	28.8	24	16	0.257	17.9	14.7	-8	-17
Cd (w/ Ni)	b)	b)	b)	b)	b)	b)	b)	b)	b)
Ni	7.5	26.1	17	9	0.571	a)	27.1	9	1
Ni (w/ Cu)	1.1	16.1	15	7	0.098	a)	17.2	7	-1
Ni (w/ Pb)	10.4	27.1	15	9	0.83	a)	28.0	5	-1
Ni (w/ Cd)	4.6	28.4	22	13	0.29	a)	29.9	14	5

a) Neglectable value; b) Adsorption does not follow a kinetic trend.

The individual kinetic curves presented in Figure 35 reveal different behaviors for the tested cations. Copper sorption is enhanced by the presence of competing ions, in a synergistic effect [534]. The same behavior is reported by Afolabi *et al.* [535] when both copper and lead are mixed with a concentration of 55 mg L^{-1} each. This could be due to the increased ionic strength favoring copper adsorption, as shown with NaNO_3 [536, 537]. After six hours, copper sorption in mixtures decreases, possibly due to a decrease in available active surface sites and the high concentration of interferent cation, in relation to copper. The latter leads to increased competition for free active sites and possible partial copper release [538], resulting in higher removal of the interferent (Figure 35b) and d)). Lead sorption is only affected by the presence of copper, situation in which lead sorption seems to occur after copper reached equilibrium. Cadmium's sorption is highly affected by the interference of copper and nickel and does not follow a kinetic trend. Similarly to lead, the sorption of nickel by A_A+3A is only affected by copper.

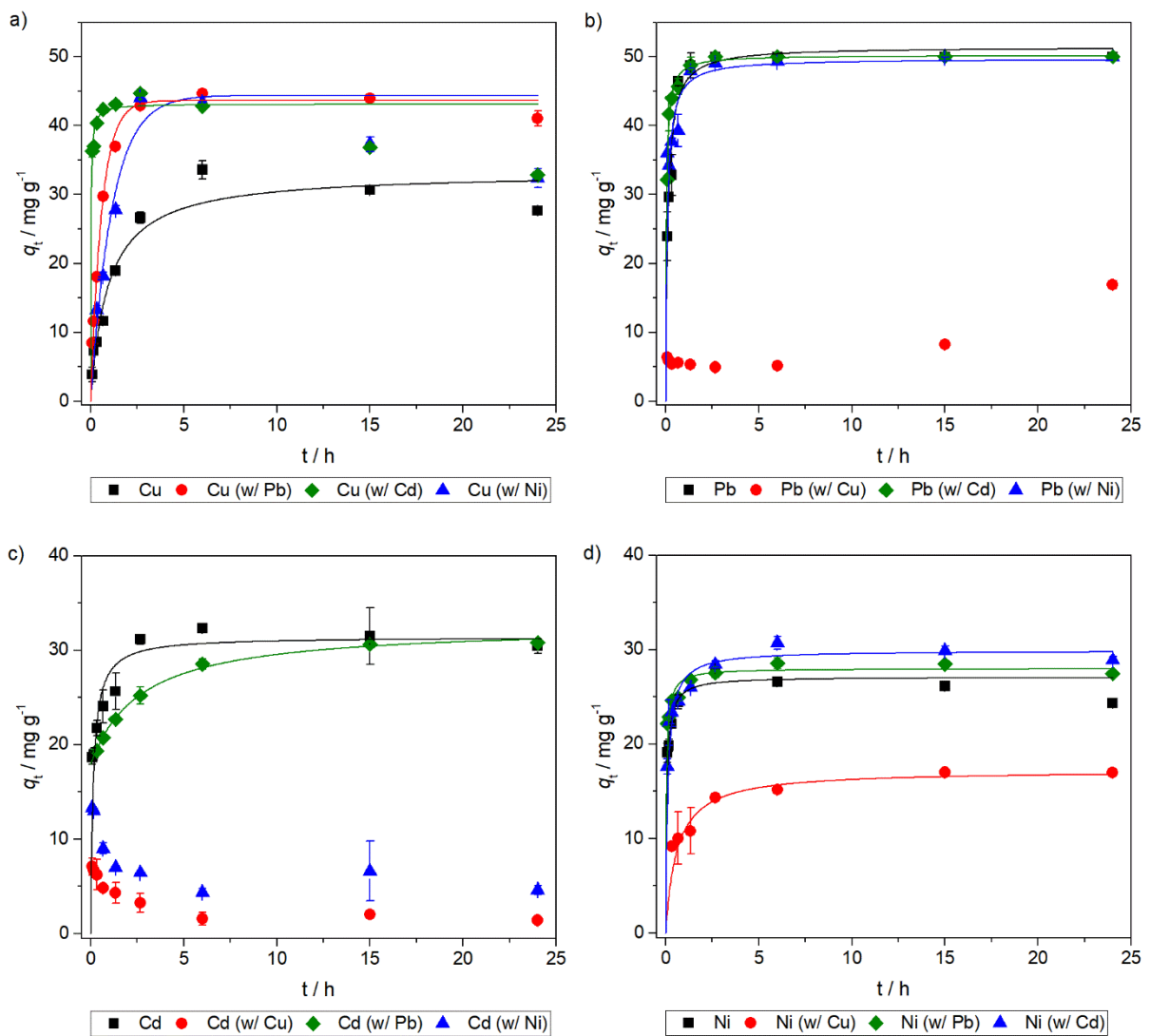


Figure 35 - Kinetic curves for the sorption of individual cations, in binary mixtures, onto A_A+3A: (a) copper sorption; (b) lead sorption; (c) cadmium sorption and (d) nickel sorption.

The results from Table 42 reveal that the adsorption of the cations does not follow a single kinetic model. The sorption kinetics of copper is only explained by the pseudo-first order model when mixed with lead or nickel. Its sorption also increased in these situations, compared to copper isolated. From Figure 35b) and d) it is observed that the sorption of these competing ions is reduced but progresses slowly over time. It can be speculated that diffusion is limiting the sorption of copper for different reasons: the interfering ions have reduced uptake and thus, as time progresses, the concentration of copper decreases but that of the interferent has little change; the sorption of interferents changes the surface of the adsorbent, enabling higher uptake of copper. In all remaining situations, the pseudo-second order model described the data better, in agreement with what was found when these ions were studied separately.

Figure 35 evidences that A_A+3A has a preference for sorbing copper, when compared to the other three cations. This result was unexpected, as this adsorbent was not developed with the purpose of being selective. Figure 35a) also shows that after six hours, copper sorption tends to decrease slightly as competing ions reach the sorption equilibrium. Thus, in order to maximize the removal of copper from a mixture using this material, the adsorption process cannot be longer than six hours. The obtained selectivities, calculated after six hours, using Equation 26, are presented in Table 43.

Table 43 - Selectivity for the adsorption of cations on A_A+3A.

	$\alpha_{Cu,i}$	$\alpha_{Pb,i}$	$\alpha_{Cd,i}$	$\alpha_{Ni,i}$
Cu	-	0.04	0.02	0.4
Pb	28.1	-	1.1	2.0
Cd	48.9	1.0	-	13.5
Ni	2.6	0.5	0.1	-

Table 43 further evidences that A_A+3A is selective for copper, in relation to the other studied metals. The only other situation where a clear selectivity is observed is of nickel in relation to cadmium. It is worth noting that because the mixtures are of equal mass, the molar concentration of lead in the cation solution is small. Thus, even though virtually all lead was removed from solution, except when this was mixed with copper, the selectivities towards lead are low.

5.11. Desorption and Recovery of Copper

Pertinent results for screening the desorption agents used on adsorbent A_A+3A are found in Table 44. All tests are present in Appendix B.

It was observed that, after adsorption, a significant amount of adsorbent particles could not be recovered by filtration. Likewise, a perceptible mass of adsorbent was lost following the desorption procedure and thus, all desorption agents' concentrations could not be compared.

The results of Table 44 show that NaOH leads to sample degradation. The silica was likely dissolved. At a 0.5 M desorption solution concentration, the performance of both acids was comparable. HCl at 1M concentration led to the best desorption results among the different conditions. With copper, almost all cation was recovered, while cadmium and nickel have the lowest recoveries. In other modified mesoporous silicas in the literature, nitric acid [237, 319], hydrochloric acid [238, 239, 539] and EDTA [308, 309] were used to effectively desorb cations. Nevertheless, desorption is not always achievable even when adsorbent-adsorbate interactions are not so strong: this is the case of the cation exchange sorption by the zeolite reported by Panayotova *et al.* [540].

The effect of the contact time with HCl 1M was evaluated with copper (as it is of interest to recover), while the amount of acid used for desorption (in other words, the concentration of adsorbent particles in the desorption procedure) was tested with the remaining ions (3 h), whose metal recovery was small. These results are presented in Figure 36. This figure reveals that in three hours the desorption procedure is complete, and there are no significant changes in the copper desorption for longer times. Thus, a virtual complete desorption of copper is not attainable. Figure 36b) shows that increasing the acid volume (decreasing the particle concentration) only benefited lead desorption as the remaining elements are less desorbed. Thus, the desorption of cadmium and nickel is not very extensive and recovering these cations by using the discussed methodology is not viable.

Table 44 - Effect of the desorption agent on cation desorption from A₁A+3A after three hours.

Cation	Isotherm Initial Concentration /mg L ⁻¹	Desorption Agent	Desorption /%	Sample Degradation
Cu	100	HCl 0.5 M	18.4	-
Cu	200	HCl 1M	57.6	-
Cu	100	HNO ₃ 0.5 M	21.1	-
Cu	200	HNO ₃ 1 M	32.4	-
Cu	100	NaOH 0.5 M	5.5	+
Cu	200	NaOH 1 M	75.1	+
Pb	100	HCl 0.5 M	29.6	-
Pb	200	HCl 1M	61.1	-
Pb	100	HNO ₃ 0.5 M	53.6	-
Pb	200	HNO ₃ 1 M	66.1	-
Pb	100	NaOH 0.5 M	59.6	+
Pb	200	NaOH 1 M	81.3	+
Cd	100	HCl 0.5 M	24.4	-
Cd	200	HCl 1M	27.5	-
Cd	100	HNO ₃ 0.5 M	30.8	-
Cd	200	HNO ₃ 1 M	15.7	-
Cd	100	NaOH 0.5 M	0.1	+
Cd	200	NaOH 1 M	2.0	+
Ni	100	HCl 0.5 M	23.5	-
Ni	200	HCl 1M	17.3	-
Ni	100	HNO ₃ 0.5 M	14.7	-
Ni	200	HNO ₃ 1 M	8.6	-
Ni	100	NaOH 0.5 M	23.3	+
Ni	200	NaOH 1 M	21.9	+

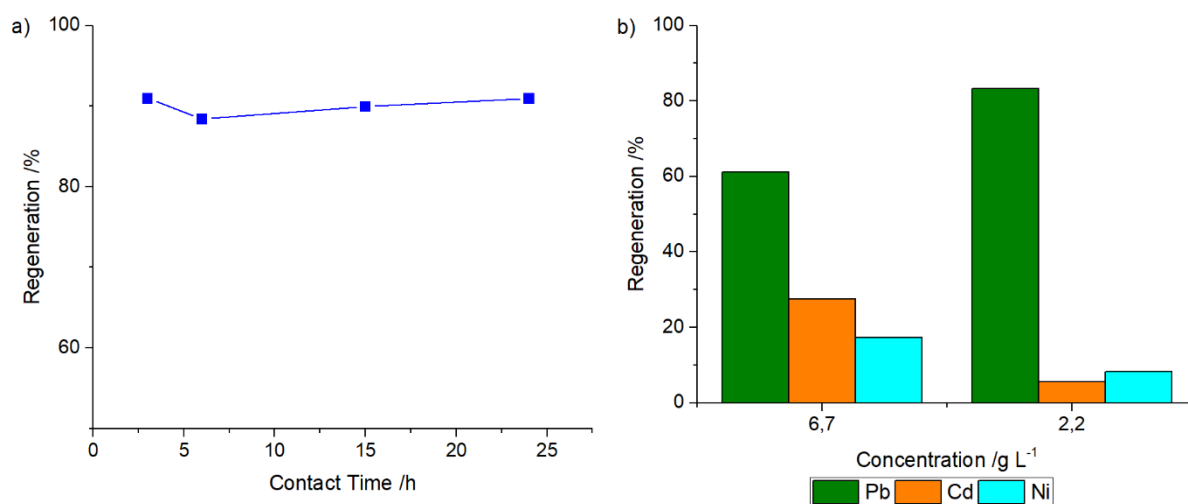


Figure 36 - Effect of (a) contact time on the desorption of copper and (b) loaded particles concentration on the desorption of the metal ions.

The adsorption of the cations on this adsorbent was implied to be due to chemisorption, so their desorption should be difficult, due to the strong nature of the adsorbent-adsorbate interactions, and the degradation of the adsorbent may be necessary. This was in fact observed with sodium hydroxide, although high cation desorption was not obtained with this procedure. To

evaluate the extent of the degradation caused by hydrochloric acid on A_A+3A, the FTIR spectra and the elemental composition of the regenerated adsorbent were assessed and are shown in Figure 37 and Table 45, respectively.

Table 45 - Elemental composition of sample A_A+3A before and after regeneration with 1M HCl.

Sample	wt% C	wt% H	wt% N
Aerogel	20.98	5.14	5.52
Regenerated Aerogel	13.84	4.79	4.28

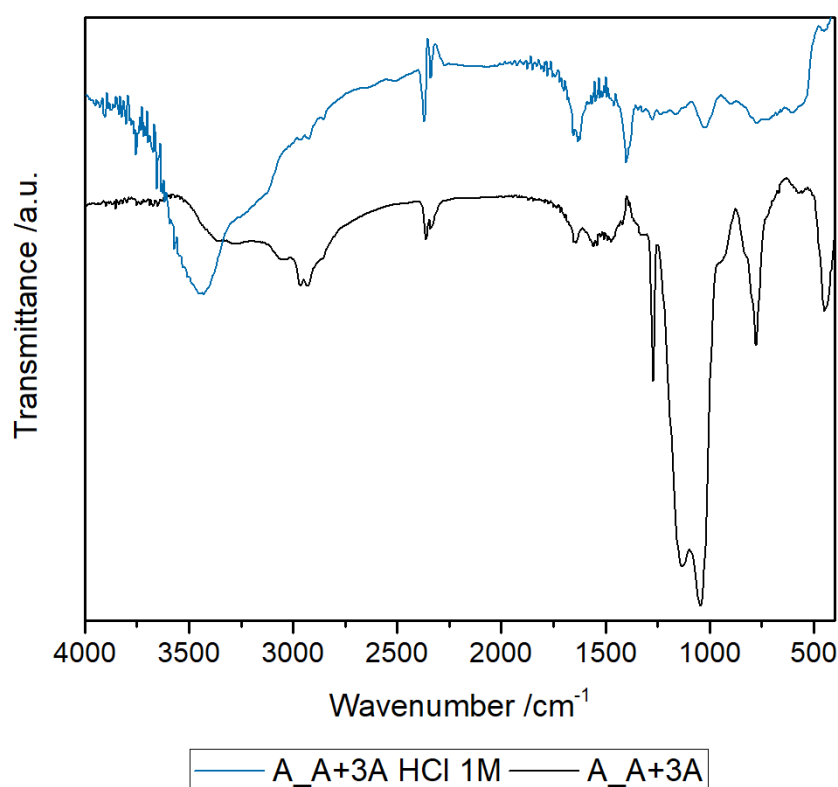


Figure 37 - FTIR spectra of A_A+3A before and after regeneration with 1M HCl.

Figure 37 and Table 45 reveal that the regeneration with HCl alters the aerogel matrix. Bands associated with the silica network and silicon-carbon bonds are now poorly defined. This result is backed up by the elemental analysis that shows a decrease in the weight of carbon, nitrogen and hydrogen. Thus, these analyses show that the desorption procedure occurs with the degradation of the adsorbent impairing its reuse.

Adsorption/desorption cycles of copper onto A_A+3A were studied. The results are presented in Figure 38. It is visible that after one regeneration with HCl, the adsorbent did not feature the same adsorption capacity, that dropped to a third in the second adsorption cycle. After every adsorption cycle, copper desorption was always successful ($111 \pm 8\%$ in the first cycle;

$74 \pm 4\%$ in the second cycle), and the adsorbent went from blue to white. The desorption value higher than a 100% can be due to the precipitation of copper inside the gel's pores, upon drying, due to the copper solution in the pores not being easily washed. Given the strong copper-aerogel interactions and the matrix degradation by HCl found previously, the loss of performance was expected: the desorption of the strongly sorbed cation comes at the expense of degrading the adsorbent, preventing its reuse. These reasons are also evoked in the literature [238].

The SEM images from Figure 39 give further insight on the adsorption performance of the aerogel after regeneration. The silica matrix became very compact after being dried in an oven, which negatively affects the adsorption of cations. Thus, I can conclude that the adsorbent is not fully regenerable, but copper can be recovered by degrading the aerogel. In other amine modified mesoporous silicas, the sorption capacity decreased slightly for chromium [237]; decreased about 30% after four regenerations for copper [238]; decreased less than 10% for copper and lead after ten uses [308]; less than 5% after six uses [309] and about 20% for lead cations after five cycles [319] or nine cycles [539]. In the bis-amine bridged silica cryogel introduced by Duan *et al.* [320], copper adsorption-desorption cycles revealed that the performance of the adsorbent was almost identical after three cycles. A similar result was obtained with a disulfide bridged silica xerogel, where after three cycles, the sorption of copper, lead and cadmium decreased 12% [239]. These results are in clear contrast with the one obtained in this thesis.

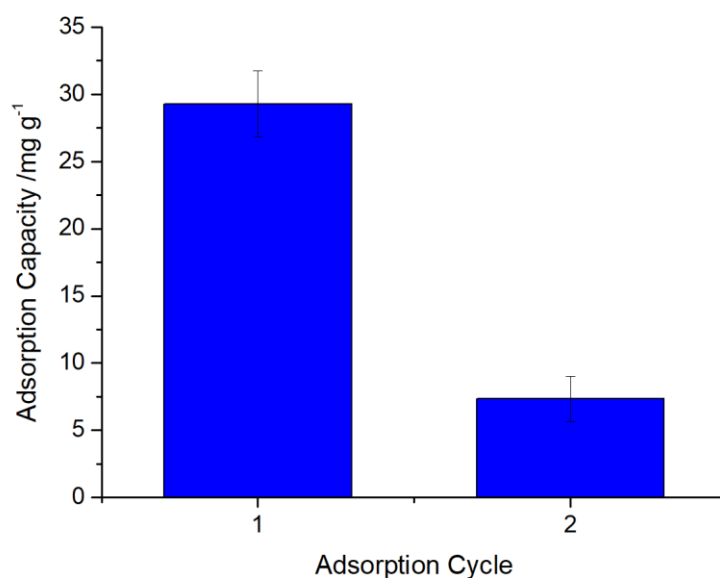


Figure 38 - Copper adsorption capacity by A₂A+3A in adsorption/desorption cycles.

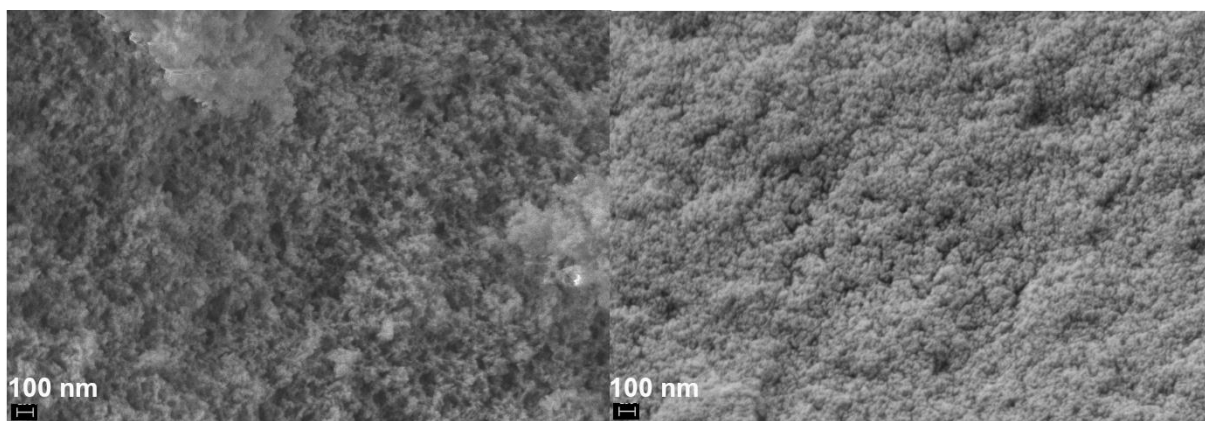
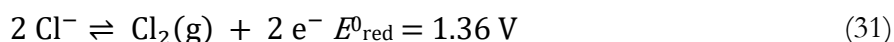
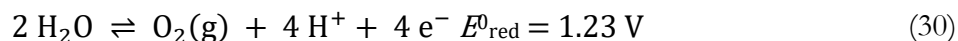


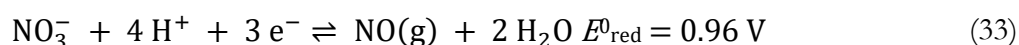
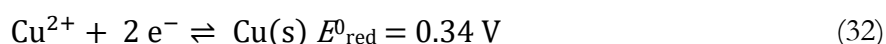
Figure 39 - SEM micrographs from A_A+3A (left) and A_A+3A after copper adsorption, washing and drying in an oven (right) at 30kx.

The recovery of copper from a 1 M HCl solution was investigated by electrodeposition and the results are shown in Table 46. Solutions of copper nitrate in HCl and the desorption solution from the first cycle were used to test the viability of this approach. The proposed oxidation and reduction semi-reactions (aqueous state omitted for simplicity) that can occur in the electrolytic cell are:

Anode



Cathode



With the applied electric potential of 2.4 V, and taken into account the overpotential, all of the reactions from Equations 30 to 33 are promoted, as there is an excess potential applied. The standard electromotive force necessary to reduce cupric ions and oxidize chloride is of 1.02 V, the highest out of the possible combinations considered. Thus, competing reactions are bound to occur with the experimental conditions applied, decreasing the efficiency of copper reduction. Experimentally, it was observed that the cathode gets covered with copper, noticeable by its color (Figure 40), and a gas is formed at the anode - chlorine, as can be confirmed by its smell. Thus, it can be stated that the reaction that occurs in the electrodeposition process is, most probably, represented in Equation 34.



Figure 40 - Copper deposition on the cathode.

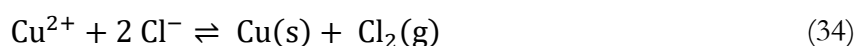


Table 46 - Copper recovery by electrolysis.

Sample	C_0 /mg L ⁻¹	Recovery / %
Solution 100 mg L ⁻¹	100	15 ± 6
Solution 200 mg L ⁻¹	200	16 ± 4
Desorption Cycle 1	100 ± 17	18 ± 9

The current generated by the power supply was very weak (~1 mA), which limited the reduction of copper. Thus, much longer times would be necessary to recover more copper. It was observed that with a higher starting concentration it was easier to reduce copper, as the cathode was visibly more covered in copper. The 200 mg L⁻¹ solution has similar recovery as the 100 mg L⁻¹ one, which could mean that the amount of copper reduced is proportional to the concentration. Electrolysis is viable to recover cations from solution and more suitable conditions can certainly generate better results. When testing the desorption solution, the electrodeposition of copper behaved similarly but the result shows more variability. It is possible that this solution has more compounds, namely moieties from the degradation of the aerogel, that affect the copper species in solution, the electrical conductivity of the media, and the chemical reduction itself.

5.12. Conclusion

The different studies presented in this chapter allowed to draw many conclusions. Amine groups are indeed excellent for the sorption of metallic cations and the conditions used in supercritical drying do not induce changes in surface chemistry via the formation of carbamates. Thus, several formulations with differential Lewis base functional groups, containing nitrogen donor atoms, were developed and studied in depth.

As it was expected given the results from the previous chapter, the xerogel counterparts of the different formulations prepared suffered densification during drying hence, aerogels are one order of magnitude lighter and more porous. The initial screening of adsorbents revealed that aerogel counterparts are generally better adsorbents and that only primary and secondary amine groups are efficient for the intended application. It was found that pH4 is more favorable for the adsorption of the studied metals, in agreement with their speciation diagrams.

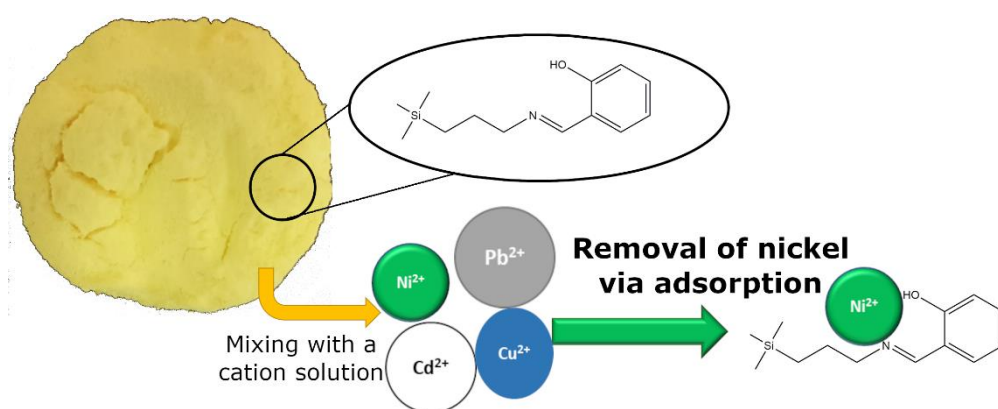
The in-depth study of the best samples (A_A, X_3A and A_A+3A) revealed that the Langmuir trend is verified in almost all cases and that the kinetic process can either reach equilibrium very fast or in a two-stage process depending on the adsorbate-adsorbent pair. These two stages may be attributed to the presence of two types of active sites in some of the materials. The isotherm and kinetic models suggest, in most situations, that the prepared adsorbents removed the cations by chemisorption.

Thermodynamic tests with the A_A+3A adsorbent reveal the spontaneous nature of the adsorption process, being observed that it is exothermic for copper, endothermic for lead and cadmium and athermic for nickel.

Competitive adsorption with binary mixtures revealed that A_A+3A is selective towards copper. In fact, copper is about three times more sorbed than nickel and about 50 times more than cadmium. The remaining cations do not seem to compete with copper until the latter's concentration in solution is very low. Desorption experiments were not able to desorb the cations significantly, except copper using a 1M solution of HCl, whose recovery occurred at the expense of the degradation of the adsorbent. This degradation impaired the adsorption capacity of A_A+3A after regeneration. Electrodeposition tests allowed the partial recovery of copper from solution, being a suitable process to recover valuable ions. Testing higher electrodeposition times would allow to recover more copper.

Chapter 6

Silica-Based Adsorbents Modified with Metal Ionophores



Summary

The work described in this chapter is focused on the synthesis of silica-based aerogel/xerogels modified with metal ionophores. To prepare the selective ORMOSIL adsorbents, azole (copper ionophores) and salen (copper and nickel ionophores) groups were investigated. These ionophore families were selected based on their availability, given the analysis of the survey presented in Annex II.

The incorporation of the ionophore ligands in the matrix is achieved by the modification of the organic group of commercial silica alkoxides, that is later used in a co-precursor method. The modifications are confirmed by NMR and the adsorbents' physical and chemical features are characterized.

The performance of the materials is investigated with batch equilibrium tests, and their selective behavior is latter assessed by kinetic curves with single and binary mixtures of cations.

The adsorbent modified with an azole ionophore showed a lackluster adsorption performance, possibly due to steric hindrance from atoms neighboring the azole ring and electrostatic repulsion between the two phases. The salen modified adsorbent showed an enhanced affinity for nickel, the cation with the highest removal. The interactions between the salen group and the hydrolyzed cations seem to be determined by the latter's radius (or its size relative to the distance between the electron donor atoms in the salen). This material showed a clear selectivity for nickel, when in mixtures, and the removal of this metal was unaffected by interferences.

6.1. Experimental Procedures

6.1.1. Materials

As silica sources, methyltriethoxysilane (MTES, $\geq 99\%$), methyltrimethoxysilane (MTMS, 98%), tetraethylorthosilicate (TEOS, 98%), (3-aminopropyl)trimethoxysilane (APTMS, $\geq 97\%$) and (3-glycidyloxypropyl)trimethoxysilane (GLYMO, 98%) were purchased from *Sigma-Aldrich* and used as received. 1H-pyrazole (98%, *Alfa Aesar*) and salicylaldehyde (*pa*, *Merck*) were used to modify the silica matrixes with ionophore groups. Anhydrous oxalic acid ($\geq 99\%$, *Sigma-Aldrich*) and ammonium hydroxide (25% NH_3 in H_2O , *Sigma-Aldrich*) were purchased as sol-gel chemistry catalysts. Methanol (99.8%, *VWR*) and ethanol ($\geq 99.8\%$, *Fisher*) were used as solvents. Deuterated methanol (CD_3OD , 99.8%), dimethyl sulfoxide (DMSO-d_6 , 99.8%) and 3-(trimethylsilyl)propionic acid sodium salt (TMSP, 98%) were purchased from *Eurisotop* and used as solvents and internal reference for liquid NMR spectroscopy. Heavy metal solutions were prepared using copper(II) nitrate hemipentahydrate (*p.a.*, *Chem-Lab*), lead(II) nitrate ($\geq 99.0\%$, *Sigma-Aldrich*), cadmium(II) nitrate tetrahydrate ($\geq 99.0\%$, *Sigma-Aldrich*), nickel(II) nitrate hexahydrate (crystals, *Sigma-Aldrich*). High purity water was used whenever needed. Nitric acid (65%, *Fisher*) or sodium hydroxide (*pellets*, *EKA Chemicals*) was used to adjust the pH of solutions.

6.1.2. Preparation of Azole Modified Silica Aerogel

Modification of GLYMO co-precursor

The modification of the silica matrix with an azole ligand was achieved by modifying the organic group in a silicon alkoxide precursor with pyrazole. Through the reaction of the epoxide and pyrazole [330, 541], an azole modified silica precursor (POPTMS, 1-(1H-pyrazol-1-yl)-3-(3-(trimethoxysilyl)propoxy)propan-2-ol) was obtained, as schematically represented in Figure 41.

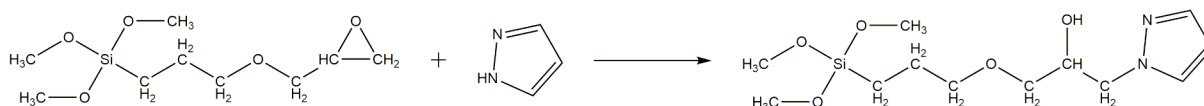


Figure 41 - Schematic representation of the POPTMS formation reaction.

GLYMO and pyrazole were dissolved in methanol with a 10 mol% excess of the ligand. This mixture, labelled as 1, was stirred until homogenization and left to react in an oven for 24 hours at 60 °C.

Synthesis of azole modified silica aerogel (formulation P)

The ORMOSIL aerogels were prepared by diluting MTMS and TEOS in methanol and hydrolyzing them (0.1 M oxalic acid). After a full day, this mixture (2), was mixed with the so-called mixture 1 and stirred. After being stirred for hydrolysis of the POPTMS, the basic catalyst (1 M ammonium hydroxide) was added under stirring. These steps were carried out at 27 °C. The sol was gently stirred until gelation (~1 h) at 60 °C and was aged for four days at this temperature. The Si:solvent:acid water:basic water molar ratios in the sol were kept at 1:12:4:4 and the silica co-precursors were mixed in an 50 MTMS/30 TEOS/20 POPTMS molar percentage. Aged gels were demolded and washed by being immersed in hot ethanol for two days, with ethanol being changed every day. The alcogels were dried via supercritical fluids extraction with CO₂, (5 g min⁻¹ at 150 bar and 50 °C for 60 min).

6.1.3. Preparation of Schiff Base Modified Silica Aerogel

Modification of APTMS co-precursor

The addition of a Schiff base functional group to the silica matrix was achieved by modifying the organic group in a silicon alkoxide precursor. The reaction between the primary amine of APTMS and salicylaldehyde was promoted [542, 543] resulting in a hemi-salen modified silica precursor (HSPTMS, (E)-2-(((3-(trimethoxysilyl)propyl)imino)methyl)phenol), according to the reaction shown in Figure 42.

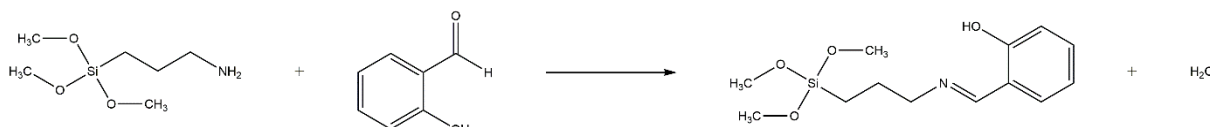


Figure 42 - Schematic representation of the HSPTMS formation reaction.

APTMS and salicylaldehyde were mixed in methanol with a 10 mol% excess of salicylaldehyde. This mixture, labelled as 3, was stirred until homogenization and left to react in an oven for 24 hours at 27 °C. The mixture turned yellow instantly, indicating the formation of the hemi-salen.

Synthesis of Schiff base modified silica aerogel (formulation SI)

To prepare silica aerogels with the HSPTMS precursor, MTES was diluted in methanol and hydrolyzed by adding a 0.1 M oxalic acid aqueous solution. After a full day, the hydrolyzed MTES, mixture 4, was mixed with the so-called mixture 3 and stirred. After a couple of minutes, TEOS

and then the basic catalyst (1 M ammonium hydroxide aqueous solution) were added. All sol-gel steps were carried out at 27 °C. The Si:solvent:acid water:basic water molar ratios in the sol were kept at 1:12:4:4 and the silica co-precursors were mixed in an 50/35/15 molar percentage for MTES, TEOS and HSPTMS respectively. Gelation and aging occurred in an oven at 27 °C for six days. Aged gels were demolded and washed by being immersed in hot ethanol (50 °C) for a total of six days, with ethanol being changed every day. Finally, the gel monoliths were dried in an oven for three days at 60 °C.

6.1.4. Batch Adsorption Experiments

The adsorption tests were conducted in the same way as described in the previous chapters. The powdered adsorbent (75-250 µm) and the cation solution are mixed in a test flask, that is shaken in a rotating stirrer at speed setting 16 (*REAX 20, Heidolph Instruments*). When the test ends, the solution is filtered, and the concentration of the filtrate is determined by flame atomic absorption spectroscopy with an acetylene-air flame (*939 AAS, Unicam*).

Batch equilibrium tests were performed by changing the adsorbate concentration from 20 to 500 mg L⁻¹ and conducted for 24 h. For batch kinetic tests, contact times ranged from 5 min to 24 hours, with an adsorbate concentration of 100 mg L⁻¹ per cation in solution. These tests were conducted with an adsorbent dose of 2 g L⁻¹ at pH 4 and 20 °C (for azole modified adsorbent) or 25 °C for the Schiff base modified adsorbent. The selectivity of the materials was evaluated with the kinetic tests of binary mixtures.

The adsorption of copper on the azole modified adsorbent was studied at pH 4 up to 7.

To test the viability of recovering the nickel sorbed to SI, a desorption test was performed with HCl and HNO₃ on nickel loaded particles (from the isotherm studies with a starting concentration of 100 mg L⁻¹). The loaded adsorbent was shaken with a 1 M solution of the desorption agent for three hours.

6.1.5. Characterization of Materials

The adsorbents were characterized in terms of structural properties, microstructure, and chemical composition following the procedures described in Sections 4.1.4. and 5.1.5..

The modification with the azole ligand was studied in sample P by solid state ¹³C CP-MAS NMR, as described in Section 5.1.5.. Zeta potential measurements of aqueous suspensions of this powdered sample, at different pH values, were carried out by electrophoretic light scattering (*Zetasizer NanoZS ZN 3500, Malvern Instruments*). Previous to the measurements, an aqueous

suspension of the sample (0.1%, w/v) was dispersed in an ultra-sound bath for 10 minutes and the pH was adjusted by the addition of HCl or NaOH. The measurements were conducted in triplicate.

The formation of HSPTMS was investigated by using NMR (Avance III, Bruker, ^1H spectra collected at 400 MHz and ^{13}C spectra collected at 100 MHz). For this analysis, HSPTMS was obtained directly via evaporation of the solvent. ^1H and ^{13}C spectra for both reactants and the resulting product were obtained by dissolution in deuterated methanol. The analysis of the ^{13}C spectrum did not contribute with more information than the ^1H spectrum analysis and thus, it is not shown. Linear shrinkage of the Schiff base modified adsorbent was calculated from the change in diameter of the dried sample and the gelation mold.

6.2. Geometry Optimization of POPTMS and HSPTMS

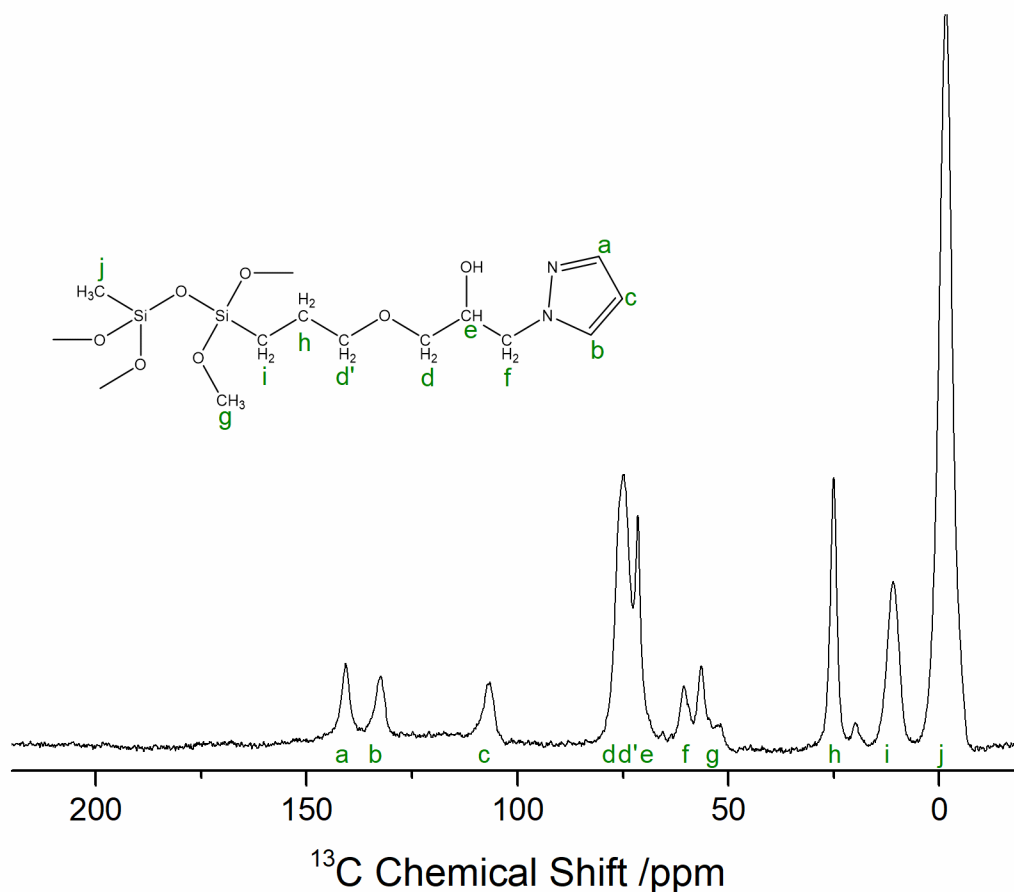
To provide insight on the interactions with the different ions, the geometry of hydrolyzed POPTMS and HSPTMS in water was computed. The system was composed of a box with the precursor molecule surrounded by water molecules, with full periodic boundary conditions. Additional details are given in Appendix C. The simulation was conducted in CP2K software v7.1 [544] using the Geometry, Frequency, Noncovalent, eXtended Tight Binding (GFN-xTB) with the DFT-D3 dispersion correction [545, 546] as electronic model. *Visual Molecular Dynamics* was used as the visualization software.

6.3. Azole Modified Silica Adsorbent

6.3.1. Characteristics of the Adsorbent

The modification of the silica network with the azole ionophore, and the resultant chemical composition were investigated via NMR. The ^{13}C CP-MAS spectra of sample P is shown in Figure 43.

The NMR spectra clearly shows that the azole ligand is present in the silica matrix and that it is chemically attached to the silica backbone, via the expected reaction presented in Figure 41. Furthermore, it seems that the modification of GLYMO is fairly complete, as no peaks associated with the epoxide group are observable. The methyl groups from MTMS co-precursor are also identifiable in the spectra, alongside methoxide groups, indicating that the hydrolysis was not complete.

Figure 43 - ^{13}C CP-MAS spectra of sample P.

The physical properties of sample P are summarized in Table 47. Its aspect and microstructure are depicted in Figure 44 and its elemental composition is given in Table 48.

Table 47 - Physical/structural properties of sample P.

Bulk density / g cm^{-3}	Porosity /%	S_{BET} / $\text{m}^2 \text{g}^{-1}$	V_{pore} / $\text{cm}^3 \text{g}^{-1}$	D_{pore} / nm
0.36 ± 0.05	74 ± 4	205 ± 2	2.1 ± 0.4	40 ± 8

The aspect of sample P is very similar to ORMOSIL aerogels and is alike to the adsorbents presented in Chapter 5. This sample is dense for an aerogel (considering the common values), and this results in a porosity that is lower than that of other aerogel adsorbents developed in this thesis. Nevertheless, the SEM micrograph reveals a very porous aerogel, as confirmed by the pore volume and specific surface area.

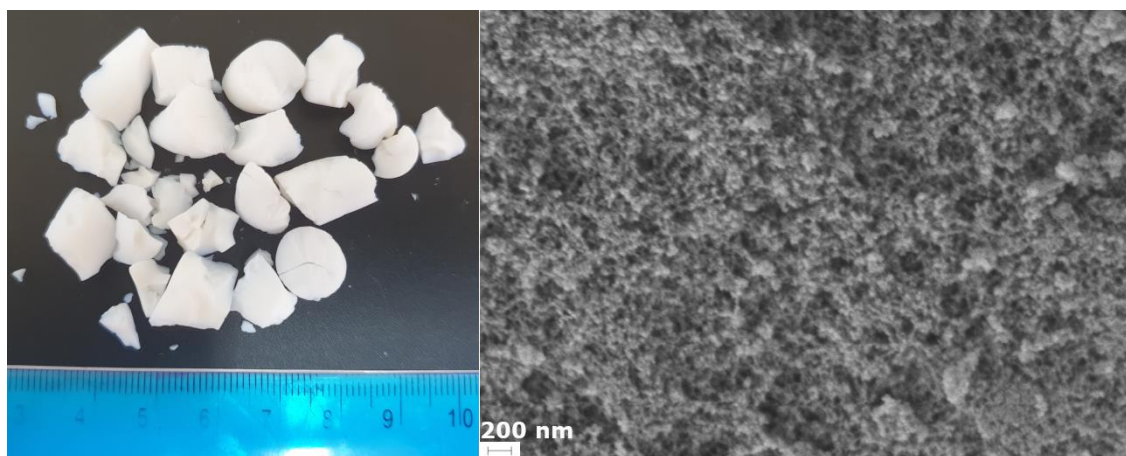


Figure 44 - Photograph of adsorbent P (left) and microstructure at 20kx magnification (right).

In terms of chemical composition, the NMR analysis reported in the previous section confirms the presence of the ionophore group in the sample and the incorporation of the several co-precursors. Furthermore, the elemental analysis results from Table 48 reveal that the sample features less nitrogen and hydrogen than expected. This might be due to an incomplete hydrolysis of some precursors, not considered for the theoretical scenarios presented in Table 48, which is also suggested in the NMR spectra of Figure 43. This is in fact possible as POPTMS has much less time for hydrolysis than the remaining co-precursors and it explains the higher amount of carbon in the sample, compared to the other elements.

Table 48 - Chemical composition of sample P.

Hypothesis	wt% C	wt% H	wt% N
Complete condensation	28.0	4.60	5.68
Incomplete condensation 1 OH	25.7	5.15	5.20
Incomplete condensation 2 OH	23.7	5.62	4.80
Experimental	24.7 ± 0.5	4.56 ± 0.07	3.04 ± 0.02

6.3.2. Adsorption Performance

The study of the removal of the cations under focus was initiated with the removal of copper and lead. These results are compiled in Figure 45 and Table 49.

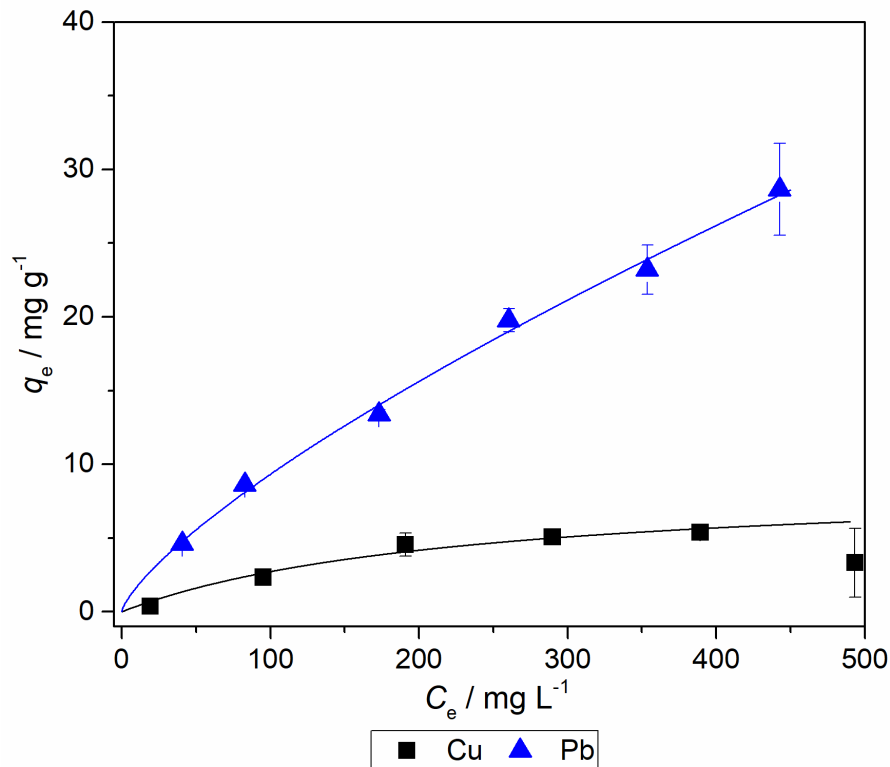


Figure 45 - Copper and lead sorption isotherms for sample P.

Table 49 - Isotherm adsorption models fit parameters for sorption on sample P.

	Langmuir model				Freundlich model				Max. Exp. $q_e / \text{mg g}^{-1}$
	$q_{\text{max}} / \text{mg g}^{-1}$	$K_L \times 10^3 / \text{L mg}^{-1}$	AIC	BIC	$1/n_F$	$K_F / \text{mg g}^{-1} (\text{L/mg})^{1/n}$	AIC	BIC	
Cu	8.9	4.4	2.9	-9.8	0.60	0.16	8.1	-4.5	5.4
Pb	72	1.4	9.9	1.7	0.75	0.30	5.0	-3.2	28.7

The aforementioned data reveals that the adsorption performance of sample P is very reduced, in particular with the sorption of copper. This result was unexpected as azole modified materials were shown to have a selective behavior towards the sorption of copper, therefore interacting and removing it well. A Langmuir type isotherm was obtained for copper, which indicates that adsorption occurred in active surface sites, while for lead the same type of behavior was not obtained. To better understand the underwhelming performance, an investigation on both the adsorbent's surface (zeta potential) and the chemical speciation of copper (different starting pH with a concentration of 200 mg L^{-1}) was carried out and the results are shown in Figure 46.

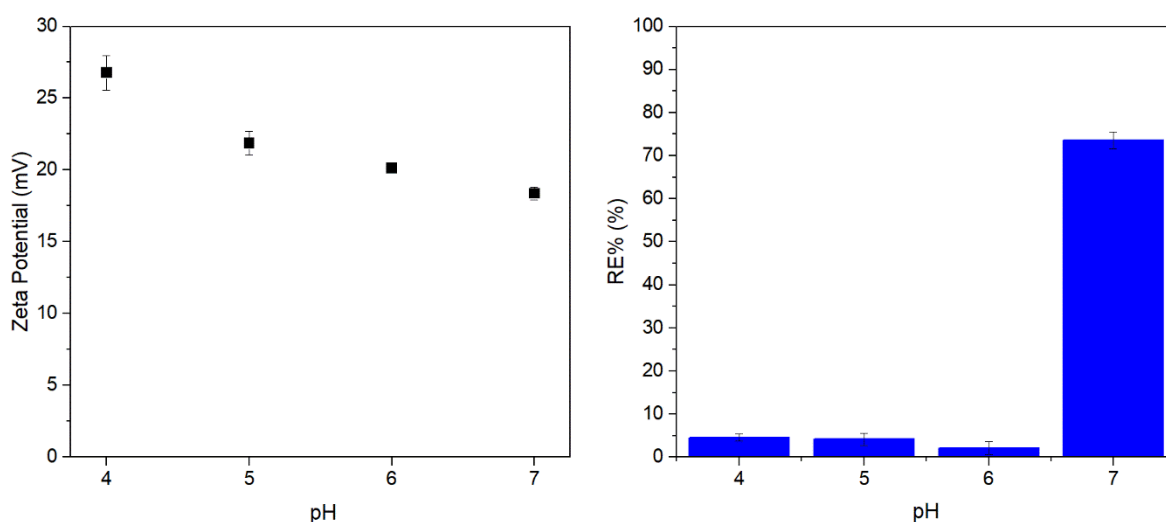


Figure 46 - Zeta potential of sample P (left) and copper removal (right) at different pH values.

Figure 46 reveals that the surface of adsorbent P is positively charged despite silica having a negative surface charge [527, 528]. That might be a consequence of the surface chemistry modifications, as it is described elsewhere [547-549]. It is known that if the sorption of cations is driven by electrostatic forces or hydrogen bonding, the adsorbent surface must be negatively charged [210]; however, cation complexation (inner-sphere complexation) seems to be insensitive to the surface's charge [210]. The tertiary amines are expected to complex with metal cations.

The results of the geometry optimization of POPTMS are presented in Figure 47 and Table C. 1 and can provide further insight on the sorptive behavior of aerogel P. The azole ring of the precursor is smaller (estimated at 2.2 Å across) than the hydrated cations (Table 2). Furthermore, the donor atoms in this heterocycle are quite close (N-N bond length of 1.3 Å) and seem to be difficult to access due to the alkyl chain (C and second N, atoms 17 and 8 respectively *vide* Figure C.2, are distanced by 2.4 Å). The oxygen atoms in the alkyl chain could also interact with the cations, being 3.1 Å apart, but these are not as efficient in doing so. Thus, it can be stated that in sample P the azole groups are not easily accessible to metal ions; therefore, it is plausible that the latter would position themselves in the space shaped by the C-N-N chain. Steric hindrance from neighboring methylene or methine groups may avert the cations to place themselves in ways, such as stacked on the azole ring. Moreover, the adsorption of cations in their “free” hydrated state, at pH values up to 5, is not favored in this sample due to electrostatic repulsion. At pH 7, copper is hydrolyzed (CuOH^+ , $\text{Cu}_2(\text{OH})_2^{2+}$ and $\text{Cu}_3(\text{OH})_4^{2+}$), Figure 2, and the adsorption enhancement is due to an electrostatic interaction between the sorbent and less positively charge density of complexed copper ions or even to its precipitation.

Given the lackluster adsorption performance found, sample P was not considered a suitable candidate for the adsorption of metallic cations or the recovery of copper.

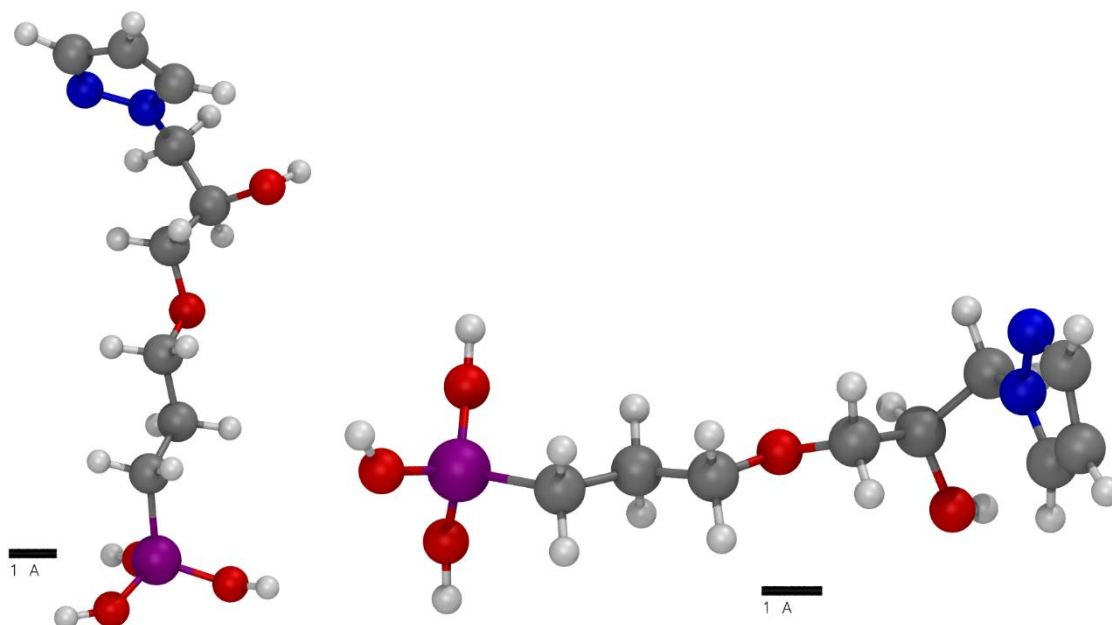
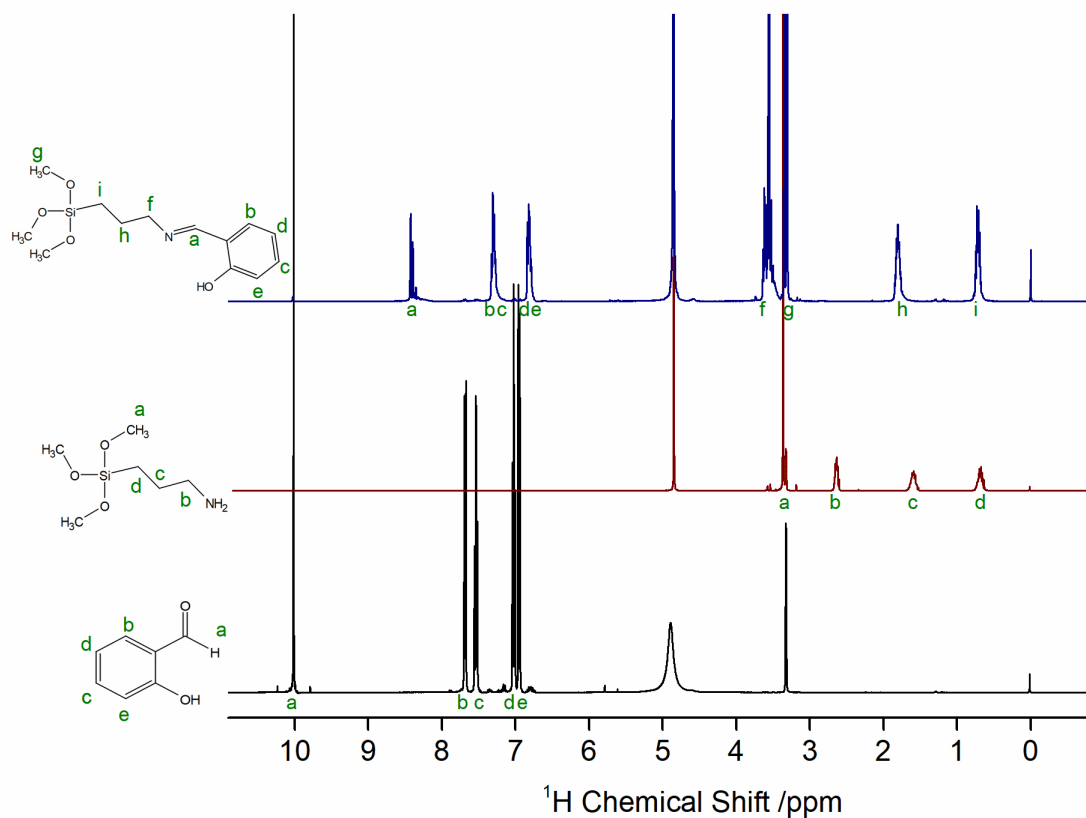


Figure 47 - Representation of the computed optimum structure of the hydrolyzed POPTMS co-precursor.

6.4. Schiff Base Modified Silica Adsorbent

6.4.1. Schiff Base Reaction

The formation of HSPTMS, via the reaction illustrated in Figure 42, was studied and the NMR spectra are presented in Figure 48. The formation of HSPTMS can be observed, namely, by the disappearance of the aldehyde group from salicylaldehyde (peak a, ~10 ppm) and the amine group in APTMS (peak b, ~2.7 ppm) in the product, and the appearance of a new proton associated with the azomethine (HC=N) bond (peak a, ~8.4 ppm). Protons associated with the methoxy groups and propyl chain did not suffer changes in their chemical environment, while the ones associated with the aromatic ring (peaks b-e in the salicylaldehyde and HSPTMS spectra) suffered some alterations, due to a new chemical environment.


 Figure 48 - ^1H NMR spectra for salicylaldehyde, APTMS and HSPTMS.

6.4.2. Characteristics of the Adsorbent

The obtained modified silica aerogel and its porous morphology are depicted in Figure 49. The physical/structural properties of the adsorbent are summarized in Table 50.

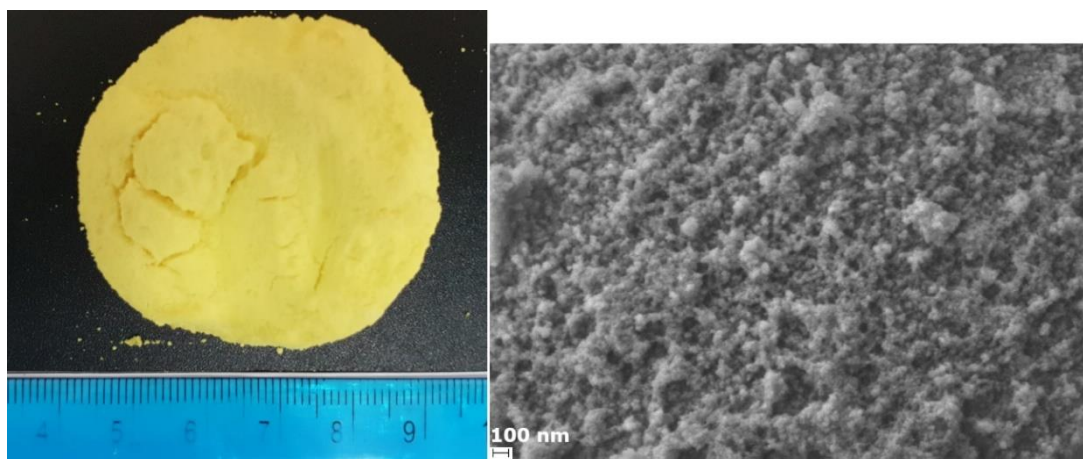


Figure 49 - Photograph (left) and micrograph at 30kx magnification (right) of the Schiff base modified aerogel.

Table 50 - Physical/structural properties of the Schiff base modified aerogel.

Bulk Density / g cm^{-3}	Porosity /%	Linear Shrinkage /%	S_{BET} / $\text{m}^2 \text{g}^{-1}$	V_{pore} / $\text{cm}^3 \text{g}^{-1}$	D_{pore} / nm
0.22 ± 0.04	85 ± 3	10 ± 3	27.7 ± 0.3	3.9 ± 0.8	563 ± 122

The ORMOSIL aerogel samples feature a distinctive bright yellow color, due to the presence of the hemi-salen. Despite being dried by evaporation of the solvent, the gel remained a monolith with small radial shrinkage, resulting in a bulk density and porosity similar to that of amine modified silica aerogels, and contrasting to their xerogel counterparts (Section 5.4.). For the Schiff base modified aerogel, hydrogen bonding with solvent molecules does not counter the effect of non-hydrolysable apolar groups in the network, resulting in low capillary stresses during solvent evaporation and low shrinkages in the final material. This result can be due to: the presence of the azomethine imine (fully substituted nitrogen) instead of a primary or secondary amine in amine modified gels; and the high pore radius. The same result was also achieved with thiol modified silica xerogels (Chapter 4). The specific surface area is small, which is due to the predominant macroporous nature of the material, as observable in Figure 49.

The FE-SEM image depicted in Figure 49 confirms the high porosity of the sample, revealing numerous voids with a wide distribution of pore sizes. Additionally, the secondary silica particles are very small and seem to be poorly individualized, surely due to the extended aging period. This microstructure is similar to that of the amine modified aerogels from Chapter 5. The evaluated structural properties allow to conclude that the prepared sample can be considered an aerogel, according to the different proposals for this definition [340, 344, 353, 361].

The FTIR spectra and the C, H, N composition of the aerogel are presented in Figure 50 and Table 51, respectively. The interpretation of the experimental results obtained by elemental analysis relies on theoretical assumptions regarding the condensation of hydrolyzed precursor molecules in the sol, previously detailed in Section 4.1.3..

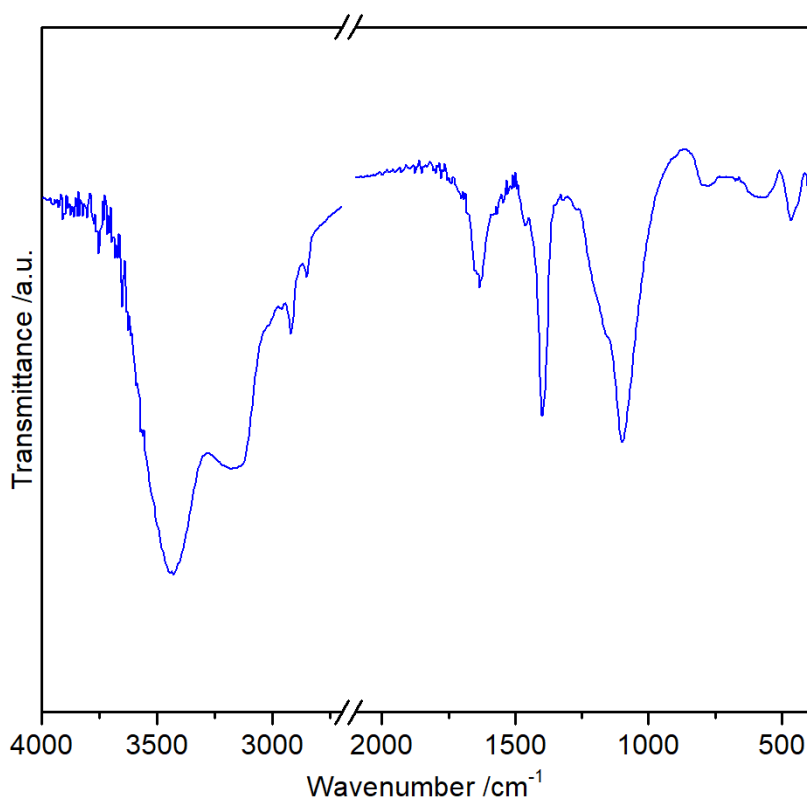


Figure 50 - Infrared spectrum of the Schiff base modified adsorbent.

The FTIR spectrum of the adsorbent reveals the formation of the silica matrix and the incorporation of the Schiff base in its structure. Bands associated with siloxane bonds are visible at 577, 1099 and 1162sh cm^{-1} ; bands associated with the ortho substituted benzene ring are visible at 1464 and 3100 cm^{-1} and bonded hydroxyl groups generate a broad band at 3431 cm^{-1} . Some band are resultant from the overlap of different functional groups that vibrate at similar frequencies. The bands at 465 and 791 cm^{-1} are the result of overlapping vibrations from siloxane bonds and the benzene ring, while the band at $\sim 1632 \text{ cm}^{-1}$ results from the overlapping of multiple bond stretching of the benzene group, the azomethine bond and hydroxyl groups. These bonds limit the conclusions gained from this analysis. The remaining peaks are due to the methyl and methylene groups in the precursors MTMS and HSPTMS.

Table 51 - C, H and N content of the Schiff base modified aerogel.

Sample/Hypothesis	wt% C	wt% H	wt% N
Complete Condensation	27.0	3.7	2.4
Incomplete Condensation 1OH	25.1	4.5	2.2
Incomplete Condensation 2OH	22.9	5.1	2.0
Experimental Values	24 ± 2	3.6 ± 0.1	2.5 ± 0.1

Analyzing the carbon content of the sample, the elemental analysis reveals that condensation is not complete, suggesting that the one hydroxyl group incomplete condensation hypothesis is the most likely. This result can be justified by the fact that HSPTMS co-precursor may undergo incomplete hydrolysis, in comparison to the remaining co-precursors, due to its slower reactivity and to it being added just before the base. Furthermore, the large organic group in this co-precursor is likely to hinder the formation of siloxane bridges. The nitrogen content in the sample is superior to the predicted, which can be related with the presence of ammonia residues even after the washing stage, as found before in samples without nitrogen-containing precursors (Chapter 5). The experimental value obtained indicates that there are 1.8 mmol of hemi-salen groups per gram of adsorbent, or 3.9×10^{19} active sites per square meter. It was verified experimentally by EDS that the distribution of the co-precursors in the aerogel matrix is not homogenous, as expected. Nitrogen was not detected with statistical significance in some portions of sample and in others, reached 4 wt%. The hydrogen content is inferior to the predicted, but this element is also more affected by the randomness of the network ramification. The excess of salicylaldehyde seems to be completely removed by the washing stage, as the carbon content would exceed the predictions if otherwise.

The addition of the hemi-salen groups caused the silica surface to feature a positive charge (24 ± 1 mV), at the conditions for cation adsorption, instead of a negative charge found in non-modified silica aerogels. Positive zeta potentials were also reported for amine-modified silicas [547-549]. In fact, it is known that inner-sphere complexation, mechanism in which the cation is sorbed by losing its hydration shell and forming chemical bonds with the adsorbent, is insensitive to the surface charge of the adsorbent [210]. By contrast, if the sorption of cations is due to electrostatic forces or hydrogen bonding, it is only verified on a negatively charged adsorbent surface [210].

6.4.3. Adsorption Performance

The experimental data and the best isotherm fit are presented in Figure 51. The fit parameters for the studied models are reported in Table 52.

Nickel removal, cation for which some salens were shown to be ionophores, was the highest observed out of the four cations studied. From the statistically point of view, the BET model represented the data the best for nickel, copper and lead, as the data points seem to follow a type II isotherm (gas isotherm classification) [550] or an L3 isotherm (solid-liquid isotherm classification) [199], which is less defined in nickel sorption. Thus, the adsorption on the Schiff base modified ORMOSIL aerogel is suggested to occur in multilayers of adsorbate deposited on the surface of the adsorbent. However, understanding how metal ions can form multilayers by sorption onto an ionophore-containing surface is not straightforward. In fact, the adsorption of metal ions from aqueous media is generally controlled by adsorbent surface chemistry and surface

area [202] and occurs in the form of coordination bonds [205, 206, 212-217, 280]. The interaction of Lewis bases-modified adsorbents with the heavy metal cations may be explained by the Pearson acid-base concept. Thus, the results reported in this section follow a different trend compared to amine modified silica aerogels (Chapter 5) or similar materials for which the Langmuir model fitted to the data the best in most situations [280, 497-499]. However, by the way the data is presented in the literature, I cannot conclude if testing higher cation concentrations would produce an isotherm shaped like a BET curve. Even so, it should be highlighted that a multilayer-like sorption for metal ions has been previously reported [551-554]. Different hypothesis for this observation can be raised and are discussed as following.

The sorption isotherms can be due to a combination of different factors: the macroporous nature of the adsorbent [550] and the affinity between sorbate layers, as relevant as cation-adsorbent interactions [199], assuming that multilayers are present. That is, adsorption is not an exclusive result of the interaction with active surface sites. Multilayer sorption is commonplace in the adsorption of organic pollutants due to van der Waals or π - π bonding; however, cations would repel each other. Some anions may interact with the adsorbed cation layer [530]; based on that, Jorgetto *et al.* [555] proposed that the BET isotherm reflects multiple adsorbate layers due to the electrostatic interactions between alternating layers of cations and counter-ions in solution. However, this situation does not seem so likely with the nitrate anions used in this work [530]. In fact, energy dispersive X-rays analysis conducted with the loaded adsorbent particles was not able to detect the presence of cations at the surface, with one exception for copper referred later.

To obtain further insight on this matter, the hybrid Langmuir-Henry model, Table 52, was analyzed. This considers the possibility of the structure of water molecules inside the aerogel's pores to be different than in the liquid water (bulk) allowing the dissolution of different amount of electrolyte, in addition to adsorption at active surface sites. If that is occurring, the hybrid Langmuir-Henry model would fit better to experimental data, which is not the case. Lead is the only cation for which the plateau corresponding to the monolayer sorption capacity is well-defined, resembling a Langmuir curve, suggesting that the cation-adsorbent interactions are strong in this case and, AIC and BIC do not agree on the preferred model; however, it can be observed that the data resembles the BET curve.

Based on the previous observations I must conclude that in spite of the BET model represented the data the best for nickel, copper and lead, the adsorption of these cations does not occur in multilayers. As such, the increase in sorption capacity after a plateau (saturation of active sites) may simply reflect changes in the adsorbent's surface/active site availability or the occurrence of metal nucleation induced by the salen-metal initial interaction [556-558]. EDS spectra support this conclusion, since some copper was quantified using a large area of sample.

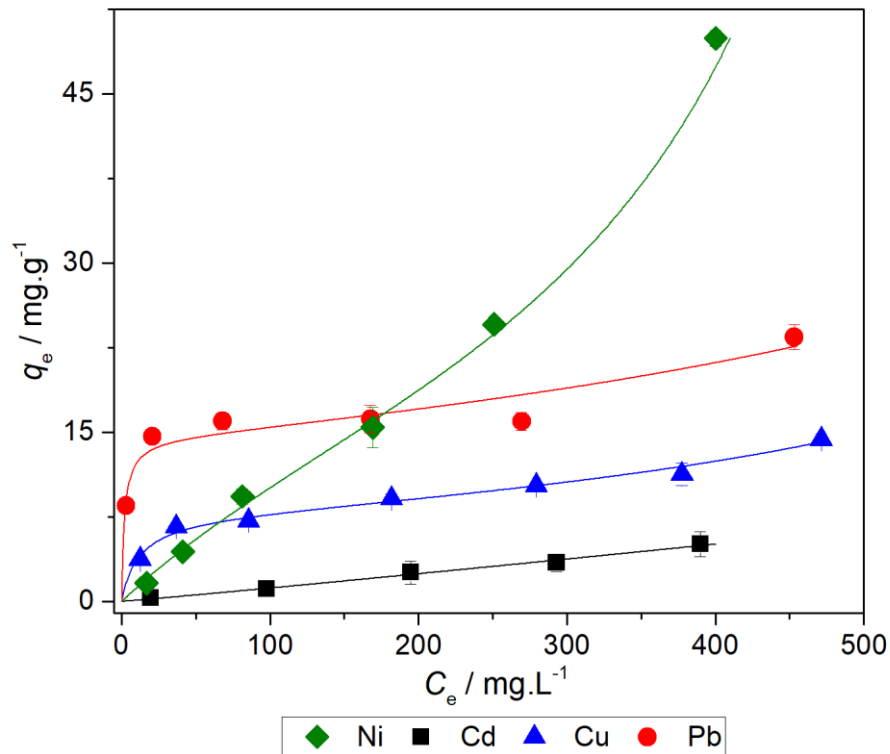


Figure 51 - Adsorption isotherms onto adsorbent SI in single-metal solutions.

Table 52 - Fit parameters for the isotherm models and maximum uptake by Schiff base modified aerogel.

	BET model				Freundlich model				Langmuir-Henry model				Max q_e exp/ mg g ⁻¹
	$q_m /$ mg g ⁻¹	$K_L \times 10^3 /$ L mg ⁻¹	$K_S \times 10^3 /$ L mg ⁻¹	AIC BIC	$1/n_F$	$K_F / \text{mg g}^{-1}$ (L mg ⁻¹) ^{1/n_F}	AIC BIC		$q_m /$ mg g ⁻¹	$K_L /$ L mg ⁻¹	$K_H \times$ 10 ³ / L g ⁻¹	AIC BIC	
Ni	19 ± 2	7 ± 2	1.6 ± 0.0	18 -3	1.3 ± 0.1	(2 ± 1) x10 ⁻²	21 13		a)	a)	a)	a) a)	49.9
Cd	4 ± 2	4 ± 3	1.2 ± 0.3	22 -19	1.1 ± 0.1	(9 ± 4) x10 ⁻³	-6 -18		a)	a)	a)	a) a)	5.1
Cu	7.6 ± 0.4	87 ± 24	0.99 ± 0.08	5 -8	0.33 ± 0.04	1.7 ± 0.4	7 1		6.6 ± 0.9	0.12 ± 0.07	15 ± 3	11 -2	14.4
Pb	14 ± 1	524 ± 268	0.8 ± 0.2	30 10	0.16 ± 0.04	8 ± 2	23 15		14 ± 2	0.5 ± 0.3	17 ± 6	32 12	23.4

a) The model did not fit to the data.

A different but related question that shall be addressed is the interaction mechanism between metal ions and the Schiff base. At the highest equilibrium concentration, the Schiff base:Ni ratio is 2:1, meaning that not all potential sorption sites are occupied. In Chapter 5, the existence of multiple types of surface groups available for adsorption generated a L4 isotherm for copper. The adsorption occurs due to strong interactions with the adsorbent's surface, since non-specific interactions, like electrostatic interactions with the positively charged surface of the modified silica aerogel, cannot occur. Thus, complexation of cations by the Schiff base occurs with partial loss of hydration water [210].

I propose that the hemi-salen groups interact differently with the cations, because of the latter's hydrated radius and the proximity of adjacent Schiff base groups. To help support this hypothesis the geometry optimization of POPTMS in water was conducted, and its results are in Figure 52 and Table C. 2. The azomethine nitrogen and the hydroxyl group in the Schiff base are relatively close (distance estimated at 2.4 Å, Figure 52), compared to the cation's hydrated radius (3.9 Å in the smallest direction for copper due to Jahn-Teller distortion; 4.1 Å for nickel; 4.6 Å for cadmium and 5.1 Å for lead [48]). So, considering a single hemi-salen group, it is possible that the bigger cations are not complexed by both atoms, as they would retain a large radius even after partial loss of the hydration shell. The Schiff base could then act as two different active sites, for cadmium and lead, resulting in a weaker interaction between the phases. This justifies the cadmium isotherm and the reduced removal of cadmium and lead. The Freundlich model fitted to the cadmium sorption data the best, as a linear trend (Henry's law) is observed. This shows that cadmium sorption is due mainly to pore diffusion rather than interactions between solid and liquid phases. A different hypothesis considers two adjacent hemi-salen groups complexing the metal together, in what would be a tetradentate salen ligand [542, 543, 559]. It is easily understandable that the distance between these groups will determine the cation size that acts as the coordination center. In this situation, potentially all of the cations tested can be sorbed, but because the distribution of the active sites in the adsorbent is not uniform, the distance between surface groups cannot be determined.

The removal observed is very reduced when compared to the mercapto-amine aerogels of Chapter 4 or the amine-modified aerogels of Chapter 5 but is higher than non-modified aerogels, Sections 5.2. and 5.5.. The cumulative effect of the ionophore ligand, for which cation radius is important, and the impossibility of electrostatic interactions help to justify this observation. A silica aerogel not modified with Lewis bases groups (A_B *vide* Chapter 5) is not a good heavy metal sorbent, and only interacts with lead (the most labile) under the same conditions (uptake for copper of 2.5 mg g⁻¹; 15.7 mg g⁻¹ for lead; 1.6 mg g⁻¹ for cadmium and 1.4 mg g⁻¹ for nickel). The here presented Schiff base ORMOSIL aerogel is much more efficient in nickel removal than the salen modified silica gel (uptake capacity of 4 mg g⁻¹) reported by Kursunlu *et al.* [498]. When modifying mesoporous silica with salen, Enache and co-authors found that the sorption of lead increased a little (20% for MCM and up to 5% for HMS) up to 99 mg g⁻¹ [497]. The sorption of lead increased 49% with the incorporation of the salen reported in this work. The nickel uptake reported in this work is also superior to that of some amine-modified silicas (28 mg g⁻¹) [315] but is inferior to that of EDTA-modified silica (74 mg g⁻¹) [300] or poly(sodium 4-styrenesulfonate)-modified zeolitic imidazolate framework-8 (330 mg g⁻¹) [560]. The Schiff base silica aerogel is a better nickel sorbent than natural minerals, zeolites, sawdust and biochar adsorbents [561-563] and other materials [564, 565].

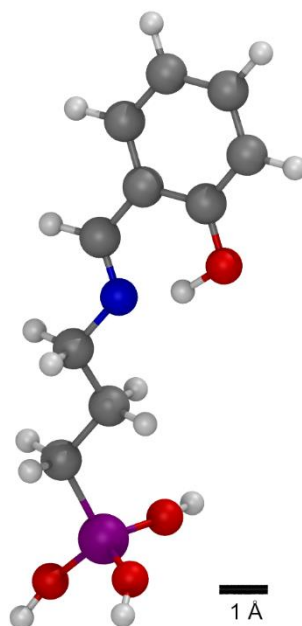


Figure 52 - Representation of the optimized structure of the hydrolyzed HSPTMS co-precursor.

6.4.4. Kinetics, Competitive Sorption and Selectivity

The HM sorption by the prepared adsorbent was studied in binary mixtures, as a kinetic test. The total molar uptake results are presented in Table 53 and Figure 53. The kinetic curves for copper and nickel sorption isolated and in binary mixtures are reported in Table 54 and Figure 54.

Table 53 - Fitting parameters of the kinetic models for the total sorption onto SI in binary mixtures.

	Modified pseudo-second order model					Pseudo-first order model			
	$q_0 \times 10^2$ /mmol g ⁻¹	$q_e \times 10$ /mmol g ⁻¹	k_2 /g mmol ⁻¹ h ⁻¹	AIC	BIC	$q_e \times 10$ /mmol g ⁻¹	k_1 / h ⁻¹	AIC	BIC
Ni+Cd	9 ± 1	2.3 ± 0.2	0.8 ± 0.3	-10	-51	2.5 ± 0.3	0.9 ± 0.4	-32	-40
Ni+Cu	a)	3.7 ± 0.3	142 ± 68	-59	-63	3.6 ± 0.1	23 ± 7	-55	-59
Ni+Pb	7 ± 2	2.8 ± 0.3	0.4 ± 0.2	-9	-50	2.6 ± 0.2	0.3 ± 0.1	-38	-46
Cu+Cd	a)	1.7 ± 0.4	32 ± 29	-27	-39	1.6 ± 0.2	8 ± 6	-24	-37
Cu+Pb	a)	1.3 ± 0.2	51 ± 32	-47	-55	1.3 ± 0.1	4 ± 1	-46	-54

a) Negligible value.

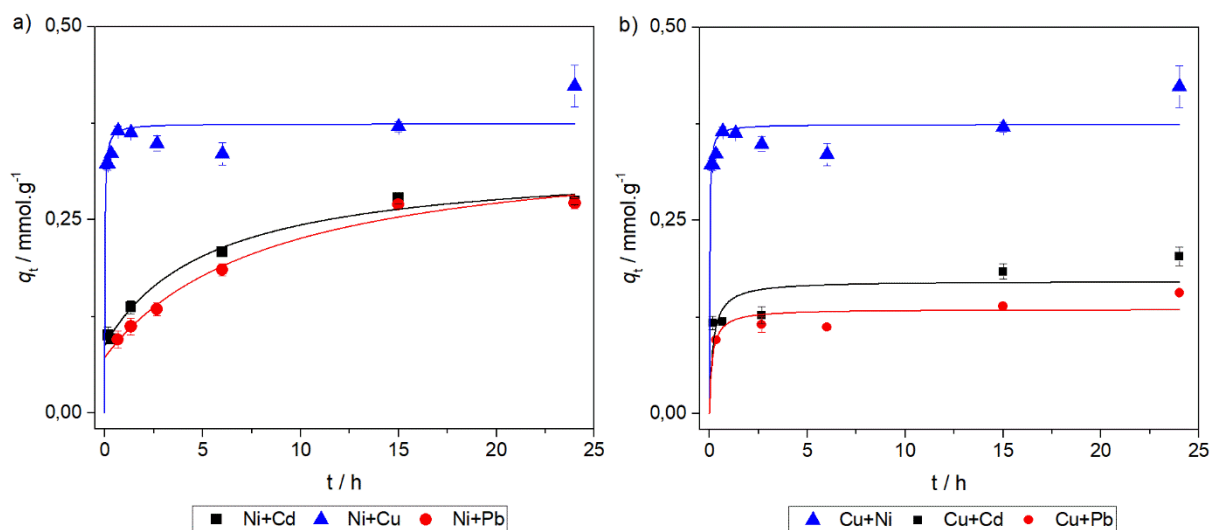


Figure 53 - Adsorption kinetics for the total uptake in binary mixtures of (a) nickel and (b) copper.

Table 54 - Fitting parameters of the kinetic models for the sorption of nickel and copper isolated and in the presence of interfering ions, onto Sl.

	Modified pseudo-second order model					Pseudo-first order model			
	q_0 /mg g ⁻¹	q_e /mg g ⁻¹	k_2 /g mg ⁻¹ h ⁻¹	AIC	BIC	q_e /mg g ⁻¹	k_1 / h ⁻¹	AIC	BIC
Ni	4.7 ± 0.8	17 ± 3	(5 ± 3) x10 ⁻³	24	4	16 ± 2	0.3 ± 0.1	25	19
Ni (w/ Cd)	3.7 ± 0.6	15 ± 2	(8 ± 3) x10 ⁻³	18	-2	14 ± 1	0.3 ± 0.1	20	14
Ni (w/ Cu)	a)	15 ± 2	(5 ± 3) x10 ⁻²	21	8	13 ± 1	0.5 ± 0.2	24	12
Ni (w/ Pb)	a)	14 ± 1	(2.3 ± 0.7) x10 ⁻²	9	1	13 ± 1	0.3 ± 0.1	14	6
Cu	a)	5.5 ± 0.4	1.0 ± 0.3	2	-11	5.4 ± 0.2	2.8 ± 0.6	5	-8
Cu (w/ Ni)	b)	b)	b)	b)	b)	b)	b)	b)	b)
Cu (w/ Cd)	a)	10 ± 1	0.13 ± 0.07	17	5	9 ± 1	0.8 ± 0.3	21	9
Cu (w/ Pb)	a)	8.0 ± 0.8	0.7 ± 0.3	5	-4	7.5 ± 0.4	4 ± 1	10	1

a) Negligible value; b) System is always at equilibrium – Figure54(b).

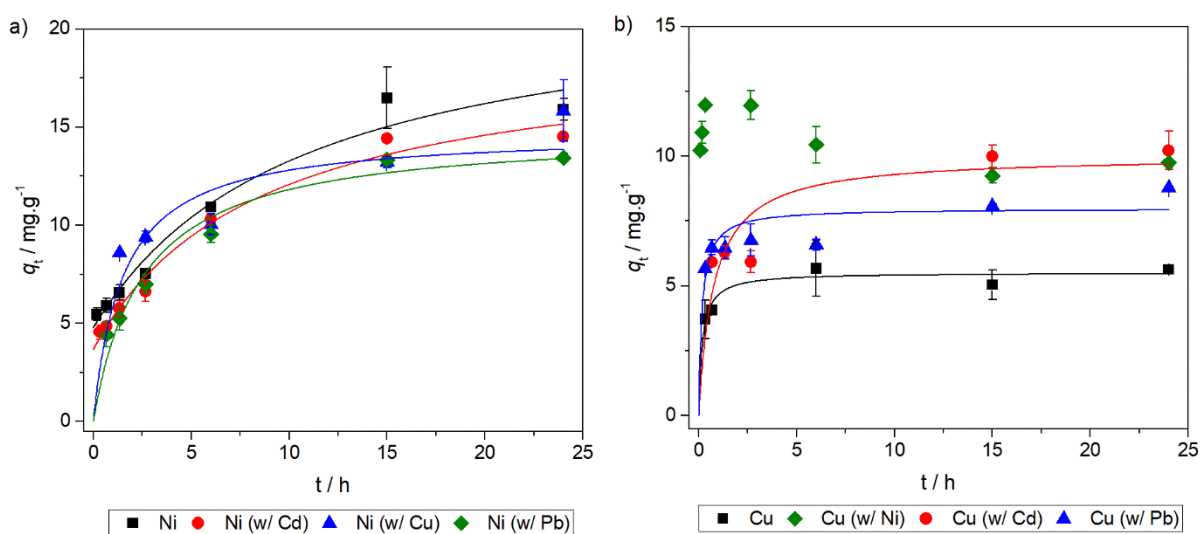


Figure 54 - Adsorption kinetics for (a) nickel and (b) copper, isolated and in binary mixtures.

The plots from Figure 53 and Figure 54 illustrate that a significant amount of adsorbates is sorbed in a short period of time. From there on, the adsorption process continues slowly, which is more pronounced when nickel is present. On the majority of datasets, the modified pseudo-second order kinetic model is reduced to pseudo-second order model, as there is no relevant initial sorption. The fit quality criteria, AIC and BIC agree that this model is clearly better than the pseudo-first order model, which indicates that the adsorption of the different sorbates is controlled by the surface reaction, *i.e.* the interaction with active surface sites. When an initial uptake is significant, AIC penalizes the modified pseudo-second order model for having more parameters (Table 53 and Table 54) while BIC considers this model more adequate than the pseudo-first order one. Figure 53 and 54 clearly show that the kinetic data follows the pseudo-second order trend, and so this model was chosen as the most adequate. Figure 51 elucidates that, on the concentrations tested for the kinetic tests, we are near the BET curve knee and thus, the insight provided by the kinetic tests does not allow to disprove the existence of multilayers since the BET theory assumes that the first layer is Langmuir-like and so it is reduced to the Langmuir equation when there is only one sorbed layer [231, 232].

When copper and nickel are mixed, the sorption of copper (Figure 54b) is almost instantaneous and remains somewhat constant, while nickel sorption increases over time and seems that it has not reached equilibrium after 24 hours (Figure 54a). Figure 53 shows that the mixtures of cadmium and lead with nickel have a higher uptake than those with copper. Figure 54 clarifies this observation by revealing that nickel sorption is not affected by the presence of these interfering cations (considering the equilibrium uptakes and their error in Table 54), hence the equilibrium found has no statistically significant change for all situations presented, and its uptake is higher than that of copper. With copper (Figure 54b), interfering cations have a synergistic effect on the former's adsorption, enhancing it, and its equilibrium uptake is affected by the interferents.

The observation that nickel sorption is unaffected by the presence of interferents is a clear indication of selectivity of the material towards this cation. Furthermore, this selectivity could not be achieved by mere non-specific interactions between phases, meaning that the hemi-salen ligands in the aerogel are strongly binding this cation, corroborating the idea of strong interactions for some cations. This is most likely the reason for the different shape of the nickel isotherm.

The recovery of nickel, achieved with the desorption tests with both desorption agents (HCl and HNO₃) was of 7%, meaning that the recovery of the sorbed cation is not likely to be achieved without the degradation of the adsorbent, as a consequence of strong adsorbent-adsorbate interactions. Thus, it is not easy to regenerate and reuse this adsorbent.

The selectivity coefficients in the binary mixtures are reported in Table 55. The selectivity coefficients confirm that nickel is sorbed preferentially, in the presence of the other tested cations,

as expected. In the absence of nickel, a selectivity towards copper is verified as expected from salen ligands.

Table 55 - Selectivity coefficients of the Schiff base-modified aerogel.

Cation	$\alpha_{\text{Cu,i}}$	$\alpha_{\text{Ni,i}}$
Cd	3.7	9.4
Cu	1.0	1.8
Pb	7.5	5.4
Ni	0.6	1.0

6.5. Conclusion

The development of two ORMOSIL materials based on ionophores was successfully achieved. The preparation of a silica precursor with the copper ionophore was achieved by the reaction of pyrazole with GLYMO, and the precursor with the nickel ionophore was obtained after reacting salicylaldehyde with APTMS. The modification of silica was confirmed by NMR analysis.

The azole modified aerogel, adsorbent P, is not as porous as other modified aerogels presented in previous chapters but is still very porous. When tested for copper and lead adsorption, it became evident that the adsorption performance was lacking and the material did not interact properly with copper, for which it is supposed to be selective. Further investigations revealed that the adsorbent's surface features a significant positive potential. Thus, the only interactions with the cations that are insensitive to this electrostatic repulsion is complexation, as occurs with other sorbents in this thesis. Because the sorptive performance is reduced, it is concluded that this material does not feature the ideal characteristics to remove metallic cations via sorption.

The preparation of a selective adsorbent for nickel, by incorporating a salen ionophore in a silica network, resulted in a bright yellow adsorbent. The modified aerogel was dried via ambient pressure drying but remained a highly porous (85%) monolith, with a reduced linear shrinkage (10%). The small specific surface area obtained is a result of the macroporous structure of the material. The isotherm studies revealed that the BET curve fits the sorption of the majority of the tested cations, although different interactions with surface sites at higher sorbate concentrations seem more likely than the formation of multilayers. Nickel was the most sorbed cation. Kinetic studies evidenced a very fast initial uptake, which is sometimes reflected by what can be considered as an initial boost to the sorptive process, that slows down as active sites become occupied. The adsorption of binary mixtures revealed a high affinity for both copper and nickel. The selectivity coefficients calculated indicate that the prepared adsorbent removes nickel ~9 times more than cadmium, ~5 times more than lead and ~2 times more than copper, confirming the fitness of this

material for the recovery of nickel from solutions with other metals. However, it is clear that copper is only the preferred sorbate in the absence of nickel, as copper uptake decreases slightly in the presence of nickel as time increases and, nickel uptake is not affected by the presence of the other tested species in solution.

Chapter 7

Final Conclusions and Future Work



Different aerogel/xerogel adsorbents were prepared and are described in this thesis, confirming that adsorption is a suitable process to remove divalent cations from solution. These adsorbent formulations show that surface chemistry plays a key role on the formation of active sites for adsorption. It must be highlighted that non-modified silica-based aerogels/xerogels were not good adsorbents. The adsorbent surface area was also shown to be important, as aerogels can be more efficient than xerogels (Table 36), even though in some cases this property does not make a significant impact (Table 26, Table 36). Thus, the different results allow to conclude that the surface chemistry is the most important characteristic of the sorbent, as even xerogels or aerogels with low surface area (as low as $2 \text{ m}^2 \text{ g}^{-1}$) are able to remove the studied cations (Table 28). However not all formulations led to efficient sorbents. Amine groups were shown to be better than thiol ones, and so the results from Chapter 5 focus on the former. Some functional groups (Table 36, Table 49), despite featuring electron donor atoms, did not interact properly with the cations. This could have been due to steric hindrance in the functional group, the relation between the ion's radius and the size of the functional group, and the strength of the Lewis bases.

Surface chemistry can however be limiting of adsorbent's reuse. The strong interactions between functional groups at the surface of the adsorbent and cations can impair desorption and reuse, a result verified in this thesis (*e.g.*, 7% nickel desorption from Sl). Nevertheless, the recovery of copper from A_A+3A was quite successful in adsorption-desorption cycles (complete desorption in the first cycle). Further analysis concluded that chemical regeneration of the adsorbent induced its partial degradation (Section 5.12.). Additional procedure optimization and testing of more conditions (*e.g.*, smaller contact times, chelating agents as desorption agents) might inhibit the degradation of the adsorbent by chemical regeneration. Moreover, different functional groups, such as sulfonate, used in ion exchange resins, might allow the synthesis of good performing and reusable silica-based adsorbents.

The ionic radius is of utmost importance, as found with adsorbents A_A+3A, P and Sl. The ionic radius affects the charge density and stability of the hydration shell. Lead is the more labile of the studied cations, hence it was easily removed by all adsorbents. However, copper and nickel are the most stable in solution and their removal is difficult and reflects stronger interactions between the phases (Section 5.9.). Besides, the cation's size, compared to that of the functional group, also affects their ability to interact with each other. This was particularly relevant for adsorbents P and Sl, as some ions are too big to be coordinated by the multiple electron donor atoms present in the azole and hemi-salen, respectively, resulting in a weaker interaction between the phases. Another relevant aspect regarding adsorbents P and Sl is the possible steric hindrance of the electron donor atoms in the silica precursor. The limited interaction with the cations could

possibly be overcome if these atoms are present at the end of the silane's organic group, which could improve the obtained adsorbent without new classes of ligands.

The removal of the four cations under focus was achieved by different adsorbents prepared in this thesis, however, A₂A+3A was considered the best sorbent for a universal solution as it is great when removing an isolated metal (Langmuir adsorption capacity of 60 mg g⁻¹ for copper, 347 mg g⁻¹ for lead, 83 mg g⁻¹ for cadmium and 66 mg g⁻¹ for nickel). It was found that, in binary mixtures, this material favors the removal of copper (Figure 35) up to six hours of contact time. Although mixtures of more than two divalent cations were not tested, potentially, an effluent can be treated in different ways depending on its composition. If it has neither copper nor nickel it can be treated with A₂A+3A for twenty-four hours to remove all pollutants. Copper can be removed from an effluent by employing A₂A+A up to six hours, and then the resulting effluent can be further treated with another batch of A₂A+3A to remove the remaining cations. An additional step for nickel separation can be performed with adsorbent SI. More work needs to be conducted in this regard, namely, testing real effluents, testing cations of other valences (like sodium) or common cations in tap water (calcium, magnesium) as interferences, and performing continuous adsorption tests with column setups.

Copper desorption was successful, and this cation can be recovered in a useful way via electrodeposition (Section 5.11.). Even so, the electrodeposition process can be further studied and improved upon, namely increasing the surface area of the electrode, using a better power source allowing to work with higher current intensities, and reaching longer times. The selective removal of nickel was possible with adsorbent SI, that showed little affinity to other cations. Thus, these other cations did not affect the removal of nickel. Due to the strong interaction with nickel, its recovery was not possible without the destruction of the aerogel matrix. The regeneration of this sample might be possible by dissolving ligands, in organic solvents if needed, whose affinity for nickel is greater than that of the salen. To improve on the reusability of selective adsorbents, further ionophores, preferably non-salen, like porphyrins and crown ethers must be tested. It must be noted that the majority of reported nickel ionophores are Schiff bases and thus, vastly different results should not be expected. Furthermore, nickel sensors based on Schiff bases are limited to very dilute concentrations, which may hint that their reversible adsorption/desorption behavior is not verified at higher concentrations. Ligands with lower metal-ligand formation constants than Schiff bases but whose electron donor atoms are similarly distanced, might interact selectively with nickel due to steric hindrance, in an easier to reverse process. This might partly explain the selectivity and reversibility of A₂A+3A's sorption of copper.

References



1. Panagos, P., Van Liedekerke, M., Yigini, Y., and Montanarella, L., *Contaminated Sites in Europe: Review of the Current Situation Based on Data Collected through a European Network*. Journal of Environmental and Public Health, 2013. **2013**: p. 11.
2. Radivojević, M., Rehren, T., Kuzmanović-Cvetković, J., Jovanović, M., and Northover, J.P., *Tainted ores and the rise of tin bronzes in Eurasia, c. 6500 years ago*. Antiquity, 2013. **87**(338): p. 1030-1045.
3. The Editors of Encyclopaedia Britannica, *Bronze Age*, in *Encyclopædia Britannica* 2020, Encyclopædia Britannica, inc. .
4. Guerreiro, C., Ortiz, A.G., de Leeuw, F., Viana, M., and Horálek, J., *Air quality in Europe — 2016 report*. 2016, European Environment Agency: Denmark.
5. The International Council on Mining and Metals, *Trends in the mining and metals industry in Mining's contribution to sustainable development: the series*. 2012.
6. Cutler, C.P., *Use of Metals in Our Society*, in *Metal Allergy: From Dermatitis to Implant and Device Failure*, J.K. Chen and Thyssen, J.P., Editors. 2018, Springer International Publishing: Cham. p. 3-16.
7. Bolan, N.S., Choppala, G., Kunhikrishnan, A., Park, J., and Naidu, R., *Microbial Transformation of Trace Elements in Soils in Relation to Bioavailability and Remediation*, in *Reviews of Environmental Contamination and Toxicology*, M.D. Whitacre, Editor. 2013, Springer: New York, NY. p. 1-56.
8. Adriano, D.C., *Trace Elements in Terrestrial Environments: Biogeochemistry, Bioavailability, and Risks of Metals*. 2nd Edition ed. 2001: Springer.
9. Adriano, D.C., Wenzel, W.W., Vangronsveld, J., and Bolan, N.S., *Role of assisted natural remediation in environmental cleanup*. Geoderma, 2004. **122**(2-4): p. 121-142.
10. Kabata-Pendias, A., *Trace Elements in Soils and Plants*. 4th Edition ed. 2011, USA: CRC Press.
11. Bolan, N., Kunhikrishnan, A., Thangarajan, R., Kumpiene, J., Park, J., Makino, T., Kirkham, M.B., and Scheckel, K., *Remediation of heavy metal(loid)s contaminated soils--to mobilize or to immobilize?* J Hazard Mater, 2014. **266**: p. 141-66.
12. Amundsen, P.-A., Staldvik, F.J., Lukin, A.A., Kashulin, N.A., Popova, O.A., and Reshetnikov, Y.S., *Heavy metal contamination in freshwater fish from the border region between Norway and Russia*. Science of The Total Environment, 1997. **201**(3): p. 211-224.
13. European Environment Agency, *Indicator Assessment: Heavy metal emissions*, in *EEA Indicators*. 2019: Denmark.
14. Oorts, K., *Copper*, in *Heavy Metals in Soils: Trace Metals and Metalloids in Soils and their Bioavailability*, J.B. Alloway, Editor. 2013, Springer: Dordrecht. p. 367-394.
15. Alloway, B.J., *Introduction*, in *Heavy Metals in Soils: Trace Metals and Metalloids in Soils and their Bioavailability*, B.J. Alloway, Editor. 2013, Springer Netherlands: Dordrecht. p. 3-9.
16. Clavadetscher, J., Hoffmann, S., Lilienkamp, A., Mackay, L., Yusop, R.M., Rider, S.A., Mullins, J.J., and Bradley, M., *Copper Catalysis in Living Systems and In Situ Drug Synthesis*. Angewandte Chemie International Edition, 2016. **55**(50): p. 15662-15666.
17. Su, L., Dong, J., Liu, L., Sun, M., Qiu, R., Zhou, Y., and Yin, S.-F., *Copper Catalysis for Selective Heterocoupling of Terminal Alkynes*. Journal of the American Chemical Society, 2016. **138**(38): p. 12348-12351.
18. Lang, F., Zewge, D., Houppis, I.N., and Volante, R.P., *Amination of aryl halides using copper catalysis*. Tetrahedron Letters, 2001. **42**(19): p. 3251-3254.
19. Steinnes, E., *Lead*, in *Heavy Metals in Soils: Trace Metals and Metalloids in Soils and their Bioavailability*, J.B. Alloway, Editor. 2013, Springer Dordrecht. p. 395-409.
20. European Chemicals Agency. *Lead in shot, bullets and fishing weights* 2019. Accessed on April 2021. Available from: <https://echa.europa.eu/hot-topics/lead-in-shot-bullets-and-fishing-weights>.

21. Das, S., 3 - *Review of restricted substances in apparel*, in *Product Safety and Restricted Substances in Apparel*, S. Das, Editor. 2013, Woodhead Publishing India. p. 14-28.
22. Occupational Safety & Health Administration. *Cadmium*. Accessed on April 2021. Available from: <https://www.osha.gov/cadmium>.
23. European Chemicals Agency. *Substances restricted under REACH* 2021. Accessed on April 2021. Available from: <https://echa.europa.eu/substances-restricted-under-reach>.
24. Tasker, S.Z., Standley, E.A., and Jamison, T.F., *Recent advances in homogeneous nickel catalysis*. *Nature*, 2014. **509**(7500): p. 299-309.
25. World Bank Group, *Commodity Markets Outlook April*. 2020: Washington.
26. Duda-Chodak, A. and Blaszczyk, U., *The Impact of Nickel on Human Health*. *Journal of Elementology*, 2008. **13**(4): p. 685-696.
27. Gonnelli, C. and Renella, G., *Chromium and Nickel*, in *Heavy Metals in Soils: Trace Metals and Metalloids in Soils and their Bioavailability*, J.B. Alloway, Editor. 2013, Springer: Dordrecht. p. 313-333.
28. World Bank Group, *Commodity Markets Outlook January*. 2017: Washington.
29. Diederer, A.M., *Metal minerals scarcity: A call for managed austerity and the elements of hope*. 2009, The Hague Centre for Strategic Studies.
30. European Commission. *EU Circular Economy Action Plan*. 2020. Accessed on October 2020. Available from: <https://ec.europa.eu/environment/circular-economy/>.
31. World Bank Group, *World Bank Commodities Price Data (The Pink Sheet), 2-October-2020*. 2020: Washington.
32. Duffus, J.H., "Heavy Metals"—*a meaningless term?* *Pure and Applied Chemistry*, 2002. **74**: p. 793–807.
33. Mihaly-Cozmuta, L., Mihaly-Cozmuta, A., Peter, A., Nicula, C., Tutu, H., Silipas, D., and Indrea, E., *Adsorption of heavy metal cations by Na-clinoptilolite: Equilibrium and selectivity studies*. *Journal of Environmental Management*, 2014. **137**: p. 69-80.
34. Baes, C.F. and Mesmer, R.S., *The Hydrolysis of Cations*. 1976: John Wiley & Sons.
35. Powell Kipton, J., Brown Paul, L., Byrne Robert, H., Gajda, T., Hefter, G., Sjöberg, S., and Wanner, H., *Chemical speciation of environmentally significant metals with inorganic ligands Part 2: The Cu²⁺-OH⁻, Cl⁻, CO₃²⁻, SO₄²⁻, and PO₄³⁻ systems (IUPAC Technical Report)*. *Pure and Applied Chemistry*, 2007. **79**(5): p. 895.
36. Powell Kipton, J., Brown Paul, L., Byrne Robert, H., Gajda, T., Hefter, G., Leuz, A.-K., Sjöberg, S., and Wanner, H., *Chemical speciation of environmentally significant metals with inorganic ligands. Part 3: The Pb²⁺ + OH⁻, Cl⁻, CO₃²⁻, SO₄²⁻, and PO₄³⁻ systems (IUPAC Technical Report)*. *Pure and Applied Chemistry*, 2009. **81**(12): p. 2425.
37. Powell Kipton, J., Brown Paul, L., Byrne Robert, H., Gajda, T., Hefter, G., Leuz, A.-K., Sjöberg, S., and Wanner, H., *Chemical speciation of environmentally significant metals with inorganic ligands. Part 4: The Cd²⁺ + OH⁻, Cl⁻, CO₃²⁻, SO₄²⁻, and PO₄³⁻ systems (IUPAC Technical Report)*. *Pure and Applied Chemistry*, 2011. **83**(5): p. 1163.
38. Tchounwou, P.B., Yedjou, C.G., Patlolla, A.K., and Sutton, D.J., *Heavy metal toxicity and the environment*. *Experientia supplementum* (2012), 2012. **101**: p. 133-164.
39. Manahan, S.E., *Toxicological Chemistry and Biochemistry*. Third Edition ed. 2003, New York: Lewis Publishers.
40. Campbell, P.G.C., *Cadmium—A Priority Pollutant*. *Environmental Chemistry*, 2006. **3**: p. 387-388.
41. Smolders, E. and Mertens, J., *Cadmium*, in *Heavy Metals in Soils: Trace Metals and Metalloids in Soils and their Bioavailability*, J.B. Alloway, Editor. 2013, Springer: Dordrecht. p. 283-311.
42. Martínez, C.E. and Motto, H.L., *Solubility of lead, zinc and copper added to mineral soils*. *Environmental Pollution*, 2000. **107**: p. 153-158.
43. Uriu-Adams, J.Y. and Keen, C.L., *Copper, oxidative stress, and human health*. *Mol Aspects Med*, 2005. **26**(4-5): p. 268-98.
44. Khodadoust, A.P., Reddy, K.R., and Maturi, K., *Removal of Nickel and Phenanthrene from Kaolin Soil Using Different Extractants*. *Environmental Engineering Science*, 2004. **21**: p. 691-704.
45. Moreira, F.R. and Moreira, J.C., *Os efeitos do chumbo sobre o organismo humano e seu significado para a saúde*. *Rev Panam Salud Publica*, 2004. **15**: p. 119-129.
46. Mertens, J. and Smolders, E., *Zinc*, in *Heavy Metals in Soils: Trace Metals and Metalloids in Soils and their Bioavailability*, J.B. Alloway, Editor. 2013, Springer: Dordrecht. p. 465-493.
47. Plum, L.M., Rink, L., and Haase, H., *The essential toxin: impact of zinc on human health*. *Int J Environ Res Public Health*, 2010. **7**(4): p. 1342-65.
48. Persson, I., *Hydrated metal ions in aqueous solution: How regular are their structures?* *Pure and Applied Chemistry*, 2010. **82**(10): p. 1901-1917.

49. *APPENDIX 2 - Charge Densities of Selected Ions*, in *Descriptive Inorganic Chemistry*, G. Rayner-Canham and Overton, T., Editors. 2014, W. H. Freeman and Company: New York.
50. Smith, D.W., *Ionic hydration enthalpies*. Journal of Chemical Education, 1977. **54**(9): p. 540.
51. Kirpichtchikova, T.A., Manceau, A., Spadini, L., Panfili, F., Marcus, M.A., and Jacquet, T., *Speciation and solubility of heavy metals in contaminated soil using X-ray microfluorescence, EXAFS spectroscopy, chemical extraction, and thermodynamic modeling*. Geochimica et Cosmochimica Acta, 2006. **70**(9): p. 2163-2190.
52. World Health Organization, *Guidelines for drinking-water quality, 4th edition, incorporating the 1st addendum*, 2017.
53. Bolan, N.S., Adriano, D.C., and Naidu, R., *Role of phosphorus in (Im)mobilization and bioavailability of heavy metals in the soil-plant system*. Rev Environ Contam Toxicol, 2003. **177**(177): p. 1-44.
54. Wuana, R.A. and Okieimen, F.E., *Heavy Metals in Contaminated Soils: A Review of Sources, Chemistry, Risks and Best Available Strategies for Remediation*. ISRN Ecology, 2011. **2011**: p. 1-20.
55. Young, S.D., *Chemistry of Heavy Metals and Metalloids in Soils*, in *Heavy Metals in Soils: Trace Metals and Metalloids in Soils and their Bioavailability*, J.B. Alloway, Editor. 2013, Springer: Dordrecht. p. 51-95.
56. Mahimairaja, S., Bolan, N.S., Adriano, D.C., and Robinson, B., *Arsenic Contamination and its Risk Management in Complex Environmental Settings*. Advances in Agronomy, 2005. **86**: p. 1-82.
57. Bolan, N.S., Adriano, D.C., Mani, P.A., and Duraisamy, A., *Immobilization and phytoavailability of cadmium in variable charge soils. II. Effect of lime addition*. Plant and Soil, 2003. **251**(2): p. 187-198.
58. Fu, F. and Wang, Q., *Removal of heavy metal ions from wastewaters: A review*. Journal of Environmental Management, 2011. **92**(3): p. 407-418.
59. Mulligan, C.N., Yong, R.N., and Gibbs, B.F., *Remediation technologies for metal-contaminated soils and groundwater: an evaluation*. Engineering Geology, 2001. **60**(1): p. 193-207.
60. Asad, S.A., Farooq, M., Afzal, A., and West, H., *Integrated phytobial heavy metal remediation strategies for a sustainable clean environment - A review*. Chemosphere, 2019. **217**: p. 925-941.
61. Song, Y., Kirkwood, N., Maksimović, Č., Zheng, X., O'Connor, D., Jin, Y., and Hou, D., *Nature based solutions for contaminated land remediation and brownfield redevelopment in cities: A review*. Science of The Total Environment, 2019. **663**: p. 568-579.
62. Pratush, A., Kumar, A., and Hu, Z., *Adverse effect of heavy metals (As, Pb, Hg, and Cr) on health and their bioremediation strategies: a review*. International Microbiology, 2018. **21**(3): p. 97-106.
63. Suman, J., Uhlik, O., Viktorova, J., and Macek, T., *Phytoextraction of Heavy Metals: A Promising Tool for Clean-Up of Polluted Environment?* Frontiers in Plant Science, 2018. **9**(1476).
64. Peng, W., Li, X., Xiao, S., and Fan, W., *Review of remediation technologies for sediments contaminated by heavy metals*. Journal of Soils and Sediments, 2018. **18**(4): p. 1701-1719.
65. Alloway, B.J., *Sources of Heavy Metals and Metalloids in Soils*, in *Heavy Metals in Soils: Trace Metals and Metalloids in Soils and their Bioavailability*, B.J. Alloway, Editor. 2013, Springer Netherlands: Dordrecht. p. 11-50.
66. Council of the European Union, *Directive 2008/50/EC of the European Parliament and of the Council of 21 May 2008 on ambient air quality and cleaner air for Europe*, 2008/50/EC, 2008.
67. Hunt, P.R., Olejnik, N., and Sprando, R.L., *Toxicity ranking of heavy metals with screening method using adult Caenorhabditis elegans and propidium iodide replicates toxicity ranking in rat*. Food and Chemical Toxicology, 2012. **50**(9): p. 3280-3290.
68. Jones, M.M., Schoenheit, J.E., and Weaver, A.D., *Pretreatment and heavy metal LD50 values*. Toxicology and Applied Pharmacology, 1979. **49**(1): p. 41-44.
69. Council of the European Union, *DIRECTIVE (EU) 2020/2184 OF THE EUROPEAN PARLIAMENT AND OF THE COUNCIL of 16 December 2020 on the quality of water intended for human consumption (recast)*, 2020/2184, Brussels. 2020.
70. United States Environmental Protection Agency, *2018 Edition of the Drinking Water Standards and Health Advisories Tables*, EPA 822-F-18-001, Washington, D.C. 2018.
71. Water and Air Quality Bureau - Healthy Environments and Consumer Safety Branch, *Guidelines for Canadian Drinking Water Quality—Summary Table*, Ottawa, Ontario. 2017.
72. Ministry of Health of China, *Standards for drinking water, National Standard of the People's Republic of China*, GB 5749-2006, Ministry of Health of China, 2006.
73. JECFA, *Joint FAO/WHO Expert Committee on Food Additives Database*. 2017.
74. Pescod, M.B., *Wastewater treatment and use in agriculture - FAO irrigation and drainage paper 47*. 1992, Rome: Food And Agriculture Organization Of The United Nations
75. Ministério do Ambiente, *Decreto-Lei n.º 236/98 de 1 de Agosto*, Diário da República — I Série-A N.º 176, 1998.

76. Canadian Council of Ministers of the Environment, *Canadian Water Quality Guidelines for the Protection of Agricultural Water Uses - Summary Table*, 1999.
77. Pourrut, B., Shahid, M., Dumat, C., Winterton, P., and Pinelli, E., *Lead Uptake, Toxicity, and Detoxification in Plants*. Reviews of Environmental Contamination and Toxicology, 2011. **vol. 213**: p. pp. 113-136.
78. Council of the European Communities, *Council Directive of 12 June 1986 on the protection of the environment, and in particular of the soil, when sewage sludge is used in agriculture*, 86/278/EEC, Brussels. 1986.
79. Canadian Council of Ministers of the Environment, *Canadian Soil Quality Guidelines for the Protection of Environmental and Human Health - Summary Table*, 1999.
80. Ingersoll, C.G., MacDonald, D.D., Wang, N., Crane, J.L., Field, L.J., Haverland, P.S., Kemble, N.E., Lindskoog, R.A., Severn, C., and Smorong, D.E., *Prediction of sediment toxicity using consensus-based freshwater sediment quality guidelines* 2000, U.S. Environmental Protection Agency.
81. National Oceanic and Atmospheric Administration's Office of Response and Restoration, *Screening Quick Reference Tables*. 2008.
82. Canadian Council of Ministers of the Environment, *Canadian Sediment Quality Guidelines for the Protection of Aquatic Life - Summary Table*, 2001.
83. Antunes, I.M.H.R., Neiva, A.M.R., Albuquerque, M.T.D., Carvalho, P.C.S., Santos, A.C.T., and Cunha, P.P., *Potential toxic elements in stream sediments, soils and waters in an abandoned radium mine (central Portugal)*. Environmental Geochemistry and Health, 2018. **40**(1): p. 521-542.
84. Neiva, A.M.R., de Carvalho, P.C.S., Antunes, I.M.H.R., da Silva Cabral Pinto, M.M., dos Santos, A.C.T., Cunha, P.P., and Costa, M.M., *Spatial variability of soils and stream sediments and the remediation effects in a Portuguese uranium mine area*. Chemie der Erde - Geochemistry, 2016. **76**(4): p. 501-518.
85. Fernández, M.R., Martín, G., Corzo, J., de la Linde, A., García, E., López, M., and Sousa, M., *Design and Testing of a New Diatom-Based Index for Heavy Metal Pollution*. Archives of Environmental Contamination and Toxicology, 2018. **74**(1): p. 170-192.
86. de la Torre, M.L., Grande, J.A., Valente, T., Santisteban, M., and Cerón, J.C., *Hydrochemical changes in a reservoir that receives water contaminated by acid mine drainage*. Hydrology Research, 2015. **46**(3): p. 303.
87. Aziz, F., Ouazzani, N., and Mandi, L., *Assif El Mal River: source of human water consumption and a transfer vector of heavy metals*. Desalination and Water Treatment, 2014. **52**(13-15): p. 2863-2874.
88. Monterroso, C., Rodríguez, F., Chaves, R., Diez, J., Becerra-Castro, C., Kidd, P.S., and Macías, F., *Heavy metal distribution in mine-soils and plants growing in a Pb/Zn-mining area in NW Spain*. Applied Geochemistry, 2014. **44**: p. 3-11.
89. Sterckeman, T., Douay, F., Proix, N., and Fourier, H., *Vertical distribution of Cd, Pb and Zn in soils near smelters in the North of France*. Environmental Pollution, 2000. **107**(3): p. 377-389.
90. Sterckeman, T., Douay, F., Proix, N., Fourier, H., and Perdrix, E., *Assessment of the Contamination of Cultivated Soils by Eighteen Trace Elements Around Smelters in the North of France*. Water, Air, and Soil Pollution, 2002. **135**(1): p. 173-194.
91. Šajn, R., Aliu, M., Stafilov, T., and Alijagić, J., *Heavy metal contamination of topsoil around a lead and zinc smelter in Kosovska Mitrovica/Mitrovičë, Kosovo/Kosovë*. Journal of Geochemical Exploration, 2013. **134**: p. 1-16.
92. Nahmani, J., Hodson, M.E., and Black, S., *Effects of metals on life cycle parameters of the earthworm Eisenia fetida exposed to field-contaminated, metal-polluted soils*. Environmental Pollution, 2007. **149**(1): p. 44-58.
93. Vaněk, A., Borůvka, L., Drábek, O., Mihaljevič, M., and Komárek, M., *Mobility of lead, zinc and cadmium in alluvial soils heavily polluted by smelting industry*. Plant, Soil and Environment, 2005. **51**(7): p. 316-321.
94. Komárek, M., Chrastrný, V., and Štichová, J., *Metal/metalloid contamination and isotopic composition of lead in edible mushrooms and forest soils originating from a smelting area*. Environment International, 2007. **33**(5): p. 677-684.
95. Rieuwerts, J.S., Farago, M.E., Cikrt, M., and Bencko, V., *Differences in Lead Bioavailability Between a Smelting and a Mining Area*. Water, Air, and Soil Pollution, 2000. **122**(1): p. 203-229.
96. Ji, H., Li, H., Zhang, Y., Ding, H., Gao, Y., and Xing, Y., *Distribution and risk assessment of heavy metals in overlying water, porewater, and sediments of Yongding River in a coal mine brownfield*. Journal of Soils and Sediments, 2018. **18**(2): p. 624-639.
97. Price, P. and Wright, I.A., *Water Quality Impact from the Discharge of Coal Mine Wastes to Receiving Streams: Comparison of Impacts from an Active Mine with a Closed Mine*. Water, Air, & Soil Pollution, 2016. **227**(5): p. 155.
98. Li, H. and Ji, H., *Chemical speciation, vertical profile and human health risk assessment of heavy metals in soils from coal-mine brownfield, Beijing, China*. Journal of Geochemical Exploration, 2017. **183**: p. 22-32.

99. Oke, S. and Vermeulen, D., *Geochemical Modeling and Remediation of Heavy Metals and Trace Elements from Artisanal Mines Discharge*. Soil and Sediment Contamination: An International Journal, 2017. **26**(1): p. 84-95.
100. Abraham, J., Dowling, K., and Florentine, S., *Assessment of potentially toxic metal contamination in the soils of a legacy mine site in Central Victoria, Australia*. Chemosphere, 2018. **192**: p. 122-132.
101. Atibu, E.K., Lacroix, P., Sivalingam, P., Ray, N., Giuliani, G., Mulaji, C.K., Otamonga, J.-P., Mpiana, P.T., Slaveykova, V.I., and Poté, J., *High contamination in the areas surrounding abandoned mines and mining activities: An impact assessment of the Dilala, Luilu and Mpingiri Rivers, Democratic Republic of the Congo*. Chemosphere, 2018. **191**: p. 1008-1020.
102. Narendrula, R., Nkongolo, K.K., Beckett, P., and Spiers, G., *Total and bioavailable metals in two contrasting mining regions (Sudbury in Canada and Lubumbashi in DR-Congo): relation to genetic variation in plant populations*. Chemistry and Ecology, 2013. **29**(2): p. 111-127.
103. Atibu, E.K., Devarajan, N., Laffite, A., Giuliani, G., Salumu, J.A., Muteb, R.C., Mulaji, C.K., Otamonga, J.-P., Elongo, V., Mpiana, P.T., and Poté, J., *Assessment of trace metal and rare earth elements contamination in rivers around abandoned and active mine areas. The case of Lubumbashi River and Tshamilemba Canal, Katanga, Democratic Republic of the Congo*. Chemie der Erde - Geochemistry, 2016. **76**(3): p. 353-362.
104. Podolský, F., Ettler, V., Šebek, O., Ježek, J., Mihaljevič, M., Kříbek, B., Sracek, O., Vaněk, A., Penížek, V., Majer, V., Mapani, B., Kamona, F., and Nyambe, I., *Mercury in soil profiles from metal mining and smelting areas in Namibia and Zambia: distribution and potential sources*. Journal of Soils and Sediments, 2015. **15**(3): p. 648-658.
105. Kříbek, B., Majer, V., Veselovský, F., and Nyambe, I., *Discrimination of lithogenic and anthropogenic sources of metals and sulphur in soils of the central-northern part of the Zambian Copperbelt Mining District: A topsoil vs. subsurface soil concept*. Journal of Geochemical Exploration, 2010. **104**(3): p. 69-86.
106. Li, Z., Ma, Z., van der Kuip, T.J., Yuan, Z., and Huang, L., *A review of soil heavy metal pollution from mines in China: Pollution and health risk assessment*. Science of The Total Environment, 2014. **468-469**: p. 843-853.
107. Li, Y., Fang, F., Wu, M., Kuang, Y., and Wu, H., *Heavy metal contamination and health risk assessment in soil-rice system near Xinqiao mine in Tongling city, Anhui province, China*. Human and Ecological Risk Assessment: An International Journal, 2018. **24**(3): p. 743-753.
108. Long, J., Tan, D., Deng, S., and Lei, M., *Pollution and ecological risk assessment of antimony and other heavy metals in soils from the world's largest antimony mine area, China*. Human and Ecological Risk Assessment: An International Journal, 2018. **24**(3): p. 679-690.
109. Hu, X.-F., Jiang, Y., Shu, Y., Hu, X., Liu, L., and Luo, F., *Effects of mining wastewater discharges on heavy metal pollution and soil enzyme activity of the paddy fields*. Journal of Geochemical Exploration, 2014. **147**: p. 139-150.
110. Liu, G., Tao, L., Liu, X., Hou, J., Wang, A., and Li, R., *Heavy metal speciation and pollution of agricultural soils along Jishui River in non-ferrous metal mine area in Jiangxi Province, China*. Journal of Geochemical Exploration, 2013. **132**: p. 156-163.
111. Liao, J., Chen, J., Ru, X., Chen, J., Wu, H., and Wei, C., *Heavy metals in river surface sediments affected with multiple pollution sources, South China: Distribution, enrichment and source apportionment*. Journal of Geochemical Exploration, 2017. **176**: p. 9-19.
112. Candeias, C., Melo, R., Ávila, P.F., Ferreira da Silva, E., Salgueiro, A.R., and Teixeira, J.P., *Heavy metal pollution in mine-soil-plant system in S. Francisco de Assis – Panasqueira mine (Portugal)*. Applied Geochemistry, 2014. **44**: p. 12-26.
113. Magiera, T., Zawadzki, J., Szuszkiewicz, M., Fabijańczyk, P., Steinnes, E., Fabian, K., and Miszczak, E., *Impact of an iron mine and a nickel smelter at the Norwegian/Russian border close to the Barents Sea on surface soil magnetic susceptibility and content of potentially toxic elements*. Chemosphere, 2018. **195**: p. 48-62.
114. Andrade, M.G.d., Melo, V.d.F., Gabardo, J., Souza, L.C.d.P., and Reissmann, C.B., *Metais pesados em solos de área de mineração e metalurgia de chumbo: I - Fitoxtração*. Revista Brasileira de Ciência do Solo, 2009. **33**: p. 1879-1888.
115. Akopyan, K., Petrosyan, V., Grigoryan, R., and Melkom Melkomian, D., *Assessment of residential soil contamination with arsenic and lead in mining and smelting towns of northern Armenia*. Journal of Geochemical Exploration, 2018. **184**: p. 97-109.
116. Gallini, L., Ajmone-Marsan, F., and Scalenghe, R., *The contamination legacy of a decommissioned iron smelter in the Italian Alps*. Journal of Geochemical Exploration, 2018. **186**: p. 121-128.
117. Audry, S., Schäfer, J., Blanc, G., and Jouanneau, J.-M., *Fifty-year sedimentary record of heavy metal pollution (Cd, Zn, Cu, Pb) in the Lot River reservoirs (France)*. Environmental Pollution, 2004. **132**(3): p. 413-426.

118. Müller, G., *Schadstoffe in Sedimenten - Sedimente als Schadstoffe*. Mitteilungen der Österreichischen Geologischen Gesellschaft, 1986. **79**: p. 107-126.
119. Fernandes, C., Fontainhas-Fernandes, A., Cabral, D., and Salgado, M.A., *Heavy metals in water, sediment and tissues of *Liza saliens* from Esmoriz-Paramos lagoon, Portugal*. Environmental Monitoring and Assessment, 2008. **136**(1): p. 267-275.
120. Oliveira, A. and Pampulha, M.E., *Effects of long-term heavy metal contamination on soil microbial characteristics*. J Biosci Bioeng, 2006. **102**(3): p. 157-61.
121. Inácio, M., Neves, O., Pereira, V., and Ferreira da Silva, E., *Levels of selected potential harmful elements (PHEs) in soils and vegetables used in diet of the population living in the surroundings of the Estarreja Chemical Complex (Portugal)*. Applied Geochemistry, 2014. **44**: p. 38-44.
122. Clemente, R., Dickinson, N.M., and Lepp, N.W., *Mobility of metals and metalloids in a multi-element contaminated soil 20 years after cessation of the pollution source activity*. Environmental Pollution, 2008. **155**(2): p. 254-261.
123. Guillén, M.T., Delgado, J., Albanese, S., Nieto, J.M., Lima, A., and De Vivo, B., *Heavy metals fractionation and multivariate statistical techniques to evaluate the environmental risk in soils of Huelva Township (SW Iberian Peninsula)*. Journal of Geochemical Exploration, 2012. **119-120**: p. 32-43.
124. Cecchi, M., Dumat, C., Alric, A., Felix-Faure, B., Pradere, P., and Guisresse, M., *Multi-metal contamination of a calcic cambisol by fallout from a lead-recycling plant*. Geoderma, 2008. **144**(1): p. 287-298.
125. Spahić, M.P., Sakan, S., Cvetković, Ž., Tančić, P., Trifković, J., Nikić, Z., and Manojlović, D., *Assessment of contamination, environmental risk, and origin of heavy metals in soils surrounding industrial facilities in Vojvodina, Serbia*. Environmental Monitoring and Assessment, 2018. **190**(4): p. 208.
126. Dragović, R., Gajić, B., Dragović, S., Đorđević, M., Đorđević, M., Mihailović, N., and Onjia, A., *Assessment of the impact of geographical factors on the spatial distribution of heavy metals in soils around the steel production facility in Smederevo (Serbia)*. Journal of Cleaner Production, 2014. **84**: p. 550-562.
127. Stafilov, T., Šajin, R., Pančevski, Z., Boev, B., Frontasyeva, M.V., and Strelkova, L.P., *Heavy metal contamination of topsoils around a lead and zinc smelter in the Republic of Macedonia*. Journal of Hazardous Materials, 2010. **175**(1): p. 896-914.
128. Zhao, Y.-F., Shi, X.-Z., Huang, B., Yu, D.-S., Wang, H.-J., Sun, W.-X., ÖBoern, I., and Blombäck, K., *Spatial Distribution of Heavy Metals in Agricultural Soils of an Industry-Based Peri-Urban Area in Wuxi, China*. Pedosphere, 2007. **17**(1): p. 44-51.
129. Wei, C., Shenglu, Z., Guoliang, W., Bo, S., and Xiang, G., *Spatial Variability Characteristic of Soil Heavy Metals Due to Industry Development of Typical Regions in Yangtze River Delta of China*. in 2009 International Conference on Energy and Environment Technology. 2009.
130. Bade, R., Oh, S., and Shin, W.S., *Diffusive gradients in thin films (DGT) for the prediction of bioavailability of heavy metals in contaminated soils to earthworm (*Eisenia foetida*) and oral bioavailable concentrations*. Science of The Total Environment, 2012. **416**: p. 127-136.
131. Gutiérrez-Ruiz, M.E., Cenicerós-Gómez, A.E., Villalobos, M., Romero, F., and Santiago, P., *Natural arsenic attenuation via metal arsenate precipitation in soils contaminated with metallurgical wastes: II. Cumulative evidence and identification of minor processes*. Applied Geochemistry, 2012. **27**(11): p. 2204-2214.
132. Hsu, L.-C., Huang, C.-Y., Chuang, Y.-H., Chen, H.-W., Chan, Y.-T., Teah, H.Y., Chen, T.-Y., Chang, C.-F., Liu, Y.-T., and Tzou, Y.-M., *Accumulation of heavy metals and trace elements in fluvial sediments received effluents from traditional and semiconductor industries*. Scientific Reports, 2016. **6**: p. 34250.
133. Hang, X., Wang, H., Zhou, J., Du, C., and Chen, X., *Characteristics and accumulation of heavy metals in sediments originated from an electroplating plant*. Journal of Hazardous Materials, 2009. **163**(2): p. 922-930.
134. John, M., Heuss-Aßbichler, S., Ullrich, A., and Rettenwander, D., *Purification of heavy metal loaded wastewater from electroplating industry under synthesis of delafossite (ABO₂) by "Lt-delafossite process"*. Water Research, 2016. **100**: p. 98-104.
135. Orescanin, V., Mikelic, L., Lulic, S., Nad, K., Mikulic, N., Rubcic, M., and Pavlovic, G., *Purification of Electroplating Wastewaters Utilizing Waste By-Product Ferrous Sulfate and Wood Fly Ash*. Journal of Environmental Science and Health, Part A, 2004. **39**(9): p. 2437-2446.
136. Anirudhan, T.S. and Sreekumari, S.S., *Adsorptive removal of heavy metal ions from industrial effluents using activated carbon derived from waste coconut buttons*. Journal of Environmental Sciences, 2011. **23**(12): p. 1989-1998.
137. Frank, V. and Harangozó, M., *Heavy metals in industrial wastewater determined by radionuclide X-ray fluorescence analysis and their effects on *Allium cepa* root tip cells*. Journal of Radioanalytical and Nuclear Chemistry, 1994. **187**(2): p. 137-141.
138. Ayeni, O., *Assessment of heavy metals in wastewater obtained from an industrial area in Ibadan, Nigeria*. RMZ – M&G, 2014. **61**: p. 19-24.

139. Rawat, M., Moturi, M.C.Z., and Subramanian, V., *Inventory compilation and distribution of heavy metals in wastewater from small-scale industrial areas of Delhi, India*. Journal of Environmental Monitoring, 2003. **5**(6): p. 906-912.
140. Ma, W., Sun, P., Song, Y., Zhang, Y., and Yin, J., *Removal Of Heavy Metals From Electroplating Wastewater By Anaerobic Bacteria*. AIP Conference Proceedings, 2010. **1251**(1): p. 109-112.
141. Pandey, S.N., *Accumulation of heavy metals (Cd, Cr, Cu, Ni and Zn) in Raphanus sativus L. and Spinacia oleracea L. plants irrigated with industrial effluent*. Journal of Environmental Biology, 2006. **27**(2): p. 381-384.
142. Ogunleye, I.O. and Izuagie, A.A., *Determination of heavy metal contents in some industrial effluents from Ondo State, Nigeria*. Journal of Environmental Chemistry and Ecotoxicology, 2013. **5**(8): p. 216-2179.
143. Ahmed, A.H. and Hanafy, R., *Effects of Industrial Effluents Polluting the Ismailia Water Canal on Growth and Metabolic Responses of Pisum sativum Seedlings*. Egyptian Journal of Botany, 2017. **57**(3): p. 583-594.
144. Kumar Sharma, R., Agrawal, M., and Marshall, F., *Heavy metal contamination of soil and vegetables in suburban areas of Varanasi, India*. Ecotoxicology and Environmental Safety, 2007. **66**(2): p. 258-266.
145. Gupta, N., Khan, D.K., and Santra, S.C., *An Assessment of Heavy Metal Contamination in Vegetables Grown in Wastewater-Irrigated Areas of Titagarh, West Bengal, India*. Bulletin of Environmental Contamination and Toxicology, 2008. **80**(2): p. 115-118.
146. Karadede-Akin, H. and Ünlü, E., *Heavy Metal Concentrations in Water, Sediment, Fish and Some Benthic Organisms from Tigris River, Turkey*. Environmental Monitoring and Assessment, 2007. **131**(1): p. 323-337.
147. Diagomanolin, V., Farhang, M., Ghazi-Khansari, M., and Jafarzadeh, N., *Heavy metals (Ni, Cr, Cu) in the Karoon waterway river, Iran*. Toxicology Letters, 2004. **151**(1): p. 63-67.
148. Salati, S. and Moore, F., *Assessment of heavy metal concentration in the Khoshk River water and sediment, Shiraz, Southwest Iran*. Environmental Monitoring and Assessment, 2010. **164**(1): p. 677-689.
149. Kaushik, A., Kansal, A., Santosh, Meena, Kumari, S., and Kaushik, C.P., *Heavy metal contamination of river Yamuna, Haryana, India: Assessment by Metal Enrichment Factor of the Sediments*. Journal of Hazardous Materials, 2009. **164**(1): p. 265-270.
150. Bhardwaj, R., Gupta, A., and Garg, J.K., *Evaluation of heavy metal contamination using environmetrics and indexing approach for River Yamuna, Delhi stretch, India*. Water Science, 2017. **31**(1): p. 52-66.
151. Krishna, A.K., Satyanarayanan, M., and Govil, P.K., *Assessment of heavy metal pollution in water using multivariate statistical techniques in an industrial area: A case study from Patancheru, Medak District, Andhra Pradesh, India*. Journal of Hazardous Materials, 2009. **167**(1): p. 366-373.
152. Javed, M. and Usmani, N., *Assessment of heavy metal (Cu, Ni, Fe, Co, Mn, Cr, Zn) pollution in effluent dominated rivulet water and their effect on glycogen metabolism and histology of Mastacembelus armatus*. SpringerPlus, 2013. **2**(1): p. 390.
153. Gaur, V.K., Gupta, S.K., Pandey, S.D., Gopal, K., and Misra, V., *Distribution of heavy metals in sediment and water of river Gomti*. Environmental Monitoring and Assessment, 2005. **102**(1): p. 419-433.
154. Singh, K.P., Mohan, D., Singh, V.K., and Malik, A., *Studies on distribution and fractionation of heavy metals in Gomti river sediments—a tributary of the Ganges, India*. Journal of Hydrology, 2005. **312**(1): p. 14-27.
155. Ali, M.M., Ali, M.L., Islam, M.S., and Rahman, M.Z., *Preliminary assessment of heavy metals in water and sediment of Karnaphuli River, Bangladesh*. Environmental Nanotechnology, Monitoring & Management, 2016. **5**: p. 27-35.
156. Wang, Z., Sun, R., Zhang, H., and Chen, L., *Analysis and assessment of heavy metal contamination in surface water and sediments: a case study from Luan River, Northern China*. Frontiers of Environmental Science & Engineering, 2015. **9**(2): p. 240-249.
157. Pekey, H., Karakaş, D., and Bakog'lu, M., *Source apportionment of trace metals in surface waters of a polluted stream using multivariate statistical analyses*. Marine Pollution Bulletin, 2004. **49**(9): p. 809-818.
158. Shanbehzadeh, S., Vahid Dastjerdi, M., Hassanzadeh, A., and Kiyanizadeh, T., *Heavy Metals in Water and Sediment: A Case Study of Tembi River*. Journal of Environmental and Public Health, 2014. **2014**: p. 5.
159. Malvandi, H., *Preliminary evaluation of heavy metal contamination in the Zarrin-Gol River sediments, Iran*. Marine Pollution Bulletin, 2017. **117**(1): p. 547-553.
160. Islam, M.S., Ahmed, M.K., Raknuzzaman, M., Habibullah -Al- Mamun, M., and Islam, M.K., *Heavy metal pollution in surface water and sediment: A preliminary assessment of an urban river in a developing country*. Ecological Indicators, 2015. **48**: p. 282-291.
161. Wang, Y., Wang, P., Bai, Y., Tian, Z., Li, J., Shao, X., Mustavich, L.F., and Li, B.-L., *Assessment of surface water quality via multivariate statistical techniques: A case study of the Songhua River Harbin region, China*. Journal of Hydro-environment Research, 2013. **7**(1): p. 30-40.

162. Alves, R.I.d.S., Tonani, K.A.d.A., Nikaido, M., Cardoso, O.d.O., Trevilato, T.M.B., and Segura-Muñoz, S.I., *Evaluation of heavy metal levels in surface water and sediments of Monte Alegre Stream and tributaries, Ribeirão Preto, SP, Brazil*. *Ambiente e Água - An Interdisciplinary Journal of Applied Science*, 2010. **5**(3): p. 11.
163. Buccolieri, A., Buccolieri, G., Cardellicchio, N., Dell'Atti, A., Di Leo, A., and Maci, A., *Heavy metals in marine sediments of Taranto Gulf (Ionian Sea, Southern Italy)*. *Marine Chemistry*, 2006. **99**(1): p. 227-235.
164. Micó, C., Peris, M., Sánchez, J., and Recatalá, L., *Heavy metal content of agricultural soils in a Mediterranean semiarid area: the Segura River Valley (Alicante, Spain)*. *Spanish Journal of Agricultural Research*, 2006. **4**: p. 363-372.
165. Micó, C., Peris, M., Recatalá, L., and Sanchez, J., *Baseline values for heavy metals in agricultural soils in an European Mediterranean region*. *Sci Total Environ*, 2007. **378**(1-2): p. 13-7.
166. Chen, X. and Lu, X., *Contamination characteristics and source apportionment of heavy metals in topsoil from an area in Xi'an city, China*. *Ecotoxicology and Environmental Safety*, 2018. **151**: p. 153-160.
167. Cheng, H., Li, M., Zhao, C., Li, K., Peng, M., Qin, A., and Cheng, X., *Overview of trace metals in the urban soil of 31 metropolises in China*. *Journal of Geochemical Exploration*, 2014. **139**: p. 31-52.
168. Smith, L., *Chapter Twelve - Historical Perspectives on Water Purification*, in *Chemistry and Water*, S. Ahuja, Editor. 2017, Elsevier. p. 421-468.
169. Tankersley, K.B., Dunning, N.P., Carr, C., Lentz, D.L., and Scarborough, V.L., *Zeolite water purification at Tikal, an ancient Maya city in Guatemala*. *Scientific Reports*, 2020. **10**(1): p. 18021.
170. Kurniawan, T.A., Chan, G.Y.S., Lo, W.-H., and Babel, S., *Physico-chemical treatment techniques for wastewater laden with heavy metals*. *Chemical Engineering Journal*, 2006. **118**(1): p. 83-98.
171. Mirbagheri, S.A. and Hosseini, S.N., *Pilot plant investigation on petrochemical wastewater treatment for the removal of copper and chromium with the objective of reuse*. *Desalination*, 2005. **171**(1): p. 85-93.
172. Aziz, H.A., Adlan, M.N., and Ariffin, K.S., *Heavy metals (Cd, Pb, Zn, Ni, Cu and Cr(III)) removal from water in Malaysia: Post treatment by high quality limestone*. *Bioresource Technology*, 2008. **99**(6): p. 1578-1583.
173. SUEZ Water Technologies & Solutions. *MetClear* Metals Solutions*. Accessed on June 2020. Available from: <https://www.suezwatertechnologies.com/products/wastewater-treatments/heavy-metals-removal>.
174. Shammas, N.K., *Coagulation and Flocculation*, in *Physicochemical Treatment Processes*, L.K. Wang, Hung, Y.-T., and Shammas, N.K., Editors. 2005, Humana Press: Totowa, NJ. p. 103-139.
175. Al-Saydeh, S.A., El-Naas, M.H., and Zaidi, S.J., *Copper removal from industrial wastewater: A comprehensive review*. *Journal of Industrial and Engineering Chemistry*, 2017. **56**: p. 35-44.
176. Petrov, S. and Nenov, V., *Removal and recovery of copper from wastewater by a complexation-ultrafiltration process*. *Desalination*, 2004. **162**: p. 201-209.
177. Ferella, F., Prisciandaro, M., De Michelis, I., and Veglio, F., *Removal of heavy metals by surfactant-enhanced ultrafiltration from wastewaters*. *Desalination*, 2007. **207**(1): p. 125-133.
178. Barakat, M.A. and Schmidt, E., *Polymer-enhanced ultrafiltration process for heavy metals removal from industrial wastewater*. *Desalination*, 2010. **256**(1): p. 90-93.
179. Cobzaru, C. and Inglezakis, V., *Chapter Ten - Ion Exchange*, in *Progress in Filtration and Separation*, S. Tarleton, Editor. 2015, Academic Press: Oxford. p. 425-498.
180. Dąbrowski, A., Hubicki, Z., Podkościelny, P., and Robens, E., *Selective removal of the heavy metal ions from waters and industrial wastewaters by ion-exchange method*. *Chemosphere*, 2004. **56**(2): p. 91-106.
181. Valverde, J.L., de Lucas, A., Carmona, M., González, M., and Rodríguez, J.F., *Equilibrium data of the exchange of Cu²⁺, Cd²⁺ and Zn²⁺ ions for H⁺ on the cationic exchanger Lewatit TP-207*. *Journal of Chemical Technology & Biotechnology*, 2004. **79**(12): p. 1371-1375.
182. Pehlivan, E. and Altun, T., *Ion-exchange of Pb²⁺, Cu²⁺, Zn²⁺, Cd²⁺, and Ni²⁺ ions from aqueous solution by Lewatit CNP 80*. *Journal of Hazardous Materials*, 2007. **140**(1-2): p. 299-307.
183. Pehlivan, E. and Cetin, S., *Sorption of Cr(VI) ions on two Lewatit-anion exchange resins and their quantitative determination using UV-visible spectrophotometer*. *Journal of Hazardous Materials*, 2009. **163**(1): p. 448-453.
184. Kress, N., *Chapter 2 - Desalination Technologies*, in *Marine Impacts of Seawater Desalination*, N. Kress, Editor. 2019, Elsevier. p. 11-34.
185. Kanani, N., *Chapter 5 - Electrodeposition Considered at the Atomistic Level*, in *Electroplating*, N. Kanani, Editor. 2004, Elsevier: Oxford. p. 141-177.
186. Gubicza, J., *Chapter 1 - Processing Methods of Nanomaterials*, in *Defect Structure and Properties of Nanomaterials (Second Edition)*, J. Gubicza, Editor. 2017, Woodhead Publishing. p. 1-25.

187. Chowdhury, S., Mazumder, M.A.J., Al-Attas, O., and Husain, T., *Heavy metals in drinking water: Occurrences, implications, and future needs in developing countries*. Science of The Total Environment, 2016. **569-570**: p. 476-488.
188. Burakov, A.E., Galunin, E.V., Burakova, I.V., Kucherova, A.E., Agarwal, S., Tkachev, A.G., and Gupta, V.K., *Adsorption of heavy metals on conventional and nanostructured materials for wastewater treatment purposes: A review*. Ecotoxicology and Environmental Safety, 2018. **148**: p. 702-712.
189. Qu, X., Alvarez, P.J.J., and Li, Q., *Applications of nanotechnology in water and wastewater treatment*. Water Research, 2013. **47**(12): p. 3931-3946.
190. Lu, F. and Astruc, D., *Nanomaterials for removal of toxic elements from water*. Coordination Chemistry Reviews, 2018. **356**: p. 147-164.
191. Heidari, A., Younesi, H., Mehraban, Z., and Heikkinen, H., *Selective adsorption of Pb(II), Cd(II), and Ni(II) ions from aqueous solution using chitosan-MAA nanoparticles*. International Journal of Biological Macromolecules, 2013. **61**: p. 251-263.
192. Shaheen, S.M., Derbalah, A.S., and Moghanm, F.S., *Removal of Heavy Metals from Aqueous Solution by Zeolite in Competitive Sorption System*. International Journal of Environmental Science and Development, 2012. **3**(4): p. 362-367.
193. Gorny, J., Dumoulin, D., Alaimo, V., Lesven, L., Noiriell, C., Madé, B., and Billon, G., *Passive sampler measurements of inorganic arsenic species in environmental waters: A comparison between 3-mercapto-silica, ferrihydrite, Metsorb®, zinc ferrite, and zirconium dioxide binding gels*. Talanta, 2019. **198**: p. 518-526.
194. Măicăneanu, A., Bedelea, H., Ardelean, M., Burcă, S., and Stanca, M., *Haneş and Valea Vinului (Romania) closed mines Acid Mine Drainages (AMDs) – Actual condition and passive treatment remediation proposal*. Chemosphere, 2013. **93**(7): p. 1400-1405.
195. Motsi, T., Rowson, N.A., and Simmons, M.J.H., *Adsorption of heavy metals from acid mine drainage by natural zeolite*. International Journal of Mineral Processing, 2009. **92**(1): p. 42-48.
196. Delkash, M., Ebrazi Bakhshayesh, B., and Kazemian, H., *Using zeolitic adsorbents to cleanup special wastewater streams: A review*. Microporous and Mesoporous Materials, 2015. **214**: p. 224-241.
197. Sposito, G., *The Chemistry of Soils*. 1989, Oxford: Oxford University Press.
198. Foo, K.Y. and Hameed, B.H., *Insights into the modeling of adsorption isotherm systems*. Chemical Engineering Journal, 2010. **156**(1): p. 2-10.
199. Piccin, J.S., Cadaval, T.R.S.A., de Pinto, L.A.A., and Dotto, G.L., *Adsorption Isotherms in Liquid Phase: Experimental, Modeling, and Interpretations*, in *Adsorption Processes for Water Treatment and Purification*, A. Bonilla-Petriciolet, Mendoza-Castillo, D.I., and Reynel-Ávila, H.E., Editors. 2017, Springer International Publishing: Cham. p. 19-51.
200. Naylor, T.d., *20 - Permeation Properties A2 - Allen, Geoffrey*, in *Comprehensive Polymer Science and Supplements*, J.C. Bevington, Editor. 1989, Pergamon: Amsterdam. p. 643-668.
201. Plazinski, W. and Rudzinski, W., *Kinetics of Adsorption at Solid/Solution Interfaces Controlled by Intraparticle Diffusion: A Theoretical Analysis*. The Journal of Physical Chemistry C, 2009. **113**(28): p. 12495-12501.
202. Cao, X., Ma, L., Gao, B., and Harris, W., *Dairy-Manure Derived Biochar Effectively Sorbs Lead and Atrazine*. Environmental Science & Technology, 2009. **43**(9): p. 3285-3291.
203. Mohan, D., Pittman, C.U., Bricka, M., Smith, F., Yancey, B., Mohammad, J., Steele, P.H., Alexandre-Franco, M.F., Gómez-Serrano, V., and Gong, H., *Sorption of arsenic, cadmium, and lead by chars produced from fast pyrolysis of wood and bark during bio-oil production*. Journal of Colloid and Interface Science, 2007. **310**(1): p. 57-73.
204. Shen, Z., Zhang, Y., Jin, F., McMillan, O., and Al-Tabbaa, A., *Qualitative and quantitative characterisation of adsorption mechanisms of lead on four biochars*. Science of The Total Environment, 2017. **609**(Supplement C): p. 1401-1410.
205. Benhamou, A., Baudu, M., Derriche, Z., and Basly, J.P., *Aqueous heavy metals removal on amine-functionalized Si-MCM-41 and Si-MCM-48*. Journal of Hazardous Materials, 2009. **171**(1): p. 1001-1008.
206. Bois, L., Bonhommé, A., Ribes, A., Pais, B., Raffin, G., and Tessier, F., *Functionalized silica for heavy metal ions adsorption*. Colloids and Surfaces A: Physicochemical and Engineering Aspects, 2003. **221**(1): p. 221-230.
207. Adapa, S. and Malani, A., *Role of hydration energy and co-ions association on monovalent and divalent cations adsorption at mica-aqueous interface*. Scientific Reports, 2018. **8**(1): p. 12198.
208. Stewart, B., Kogej, K., Luisa Ramos, M., Valente, A.J.M., and Burrows, H.D., *Binding of divalent and higher valent metal ions to surfactants and polyelectrolytes*. Current Opinion in Colloid & Interface Science, 2017. **32**: p. 76-83.
209. Burrows, H.D., Costa, D., Ramos, M.L., Miguel, M.d.G., Teixeira, M.H., Pais, A.A.C.C., Valente, A.J.M., Bastos, M., and Bai, G., *Does cation dehydration drive the binding of metal ions to polyelectrolytes in*

- water? What we can learn from the behaviour of aluminium(III) and chromium(III). *Physical Chemistry Chemical Physics*, 2012. **14**(22): p. 7950-7953.
210. Bradl, H., Kim, C., Kramar, U., and StÜben, D., *Interactions of heavy metals*, in *Heavy Metals in the Environment: Origin, Interaction and Remediation*, H.B. Bradl, Editor. 2005, Elsevier. p. 28-164.
 211. Ruthven, D.M., *Fundamentals of Adsorption Equilibrium and Kinetics in Microporous Solids*, in *Adsorption and Diffusion*, H.G. Karge and Weitkamp, J., Editors. 2008, Springer Berlin Heidelberg: Berlin, Heidelberg. p. 1-43.
 212. Cheng, Q., Huang, Q., Khan, S., Liu, Y., Liao, Z., Li, G., and Ok, Y.S., *Adsorption of Cd by peanut husks and peanut husk biochar from aqueous solutions*. *Ecological Engineering*, 2016. **87**(Supplement C): p. 240-245.
 213. Deng, J., Liu, Y., Liu, S., Zeng, G., Tan, X., Huang, B., Tang, X., Wang, S., Hua, Q., and Yan, Z., *Competitive adsorption of Pb(II), Cd(II) and Cu(II) onto chitosan-pyromellitic dianhydride modified biochar*. *Journal of Colloid and Interface Science*, 2017. **506**(Supplement C): p. 355-364.
 214. de Mello Ferreira Guimarães, A., Ciminelli, V.S.T., and Vasconcelos, W.L., *Smectite organofunctionalized with thiol groups for adsorption of heavy metal ions*. *Applied Clay Science*, 2009. **42**(3): p. 410-414.
 215. Liang, X., Xu, Y., Sun, G., Wang, L., Sun, Y., and Qin, X., *Preparation, characterization of thiol-functionalized silica and application for sorption of Pb²⁺ and Cd²⁺*. *Colloids and Surfaces A: Physicochemical and Engineering Aspects*, 2009. **349**(1): p. 61-68.
 216. Wu, S., Li, F., Xu, R., Wei, S., and Li, G., *Synthesis of thiol-functionalized MCM-41 mesoporous silicas and its application in Cu(II), Pb(II), Ag(I), and Cr(III) removal*. *Journal of Nanoparticle Research*, 2010. **12**(6): p. 2111-2124.
 217. Wang, F., Pan, Y., Cai, P., Guo, T., and Xiao, H., *Single and binary adsorption of heavy metal ions from aqueous solutions using sugarcane cellulose-based adsorbent*. *Bioresource Technology*, 2017. **241**(Supplement C): p. 482-490.
 218. Vareda, J.P., Valente, A.J., and Durães, L., *Heavy metals in Iberian soils: Removal by current adsorbents/amendments and prospective for aerogels*. *Advances in Colloid and Interface Science*, 2016. **237**: p. 28-42.
 219. Lagergreen, S., *Zur Theorie der sogenannten Adsorption gelöster Stoffe*. *Zeitschrift für Chemie und Industrie der Kolloide*, 1907. **2**(1): p. 15-15.
 220. Lagoa, R. and Rodrigues, J.R., *Kinetic analysis of metal uptake by dry and gel alginate particles*. *Biochemical Engineering Journal*, 2009. **46**(3): p. 320-326.
 221. Ho, Y.S. and McKay, G., *Sorption of dye from aqueous solution by peat*. *Chemical Engineering Journal*, 1998. **70**(2): p. 115-124.
 222. Wilczak, A. and Keinath, T.M., *Kinetics of sorption and desorption of copper(II) and lead (II) on activated carbon*. *Water Environment Research*, 1993. **65**(3): p. 238-244.
 223. Chiron, N., Guilet, R., and Deydier, E., *Adsorption of Cu(II) and Pb(II) onto a grafted silica: isotherms and kinetic models*. *Water Research*, 2003. **37**(13): p. 3079-3086.
 224. Wu, F.-C., Tseng, R.-L., and Juang, R.-S., *Initial behavior of intraparticle diffusion model used in the description of adsorption kinetics*. *Chemical Engineering Journal*, 2009. **153**(1-3): p. 1-8.
 225. Qiu, H., Lv, L., Pan, B.-c., Zhang, Q.-j., Zhang, W.-m., and Zhang, Q.-x., *Critical review in adsorption kinetic models*. *Journal of Zhejiang University SCIENCE A*, 2009. **10**(5): p. 716-724.
 226. Bulut, E., Özacar, M., and Şengil, İ.A., *Adsorption of malachite green onto bentonite: Equilibrium and kinetic studies and process design*. *Microporous and Mesoporous Materials*, 2008. **115**(3): p. 234-246.
 227. Langmuir, I., *The Constitution and Fundamental Properties of Solids and Liquids. Part I. Solids*. *Journal of the American Chemical Society*, 1916. **38**(11): p. 2221-2295.
 228. Ayawei, N., Ebelegi, A.N., and Wankasi, D., *Modelling and Interpretation of Adsorption Isotherms*. *Journal of Chemistry*, 2017. **2017**: p. 11.
 229. Freundlich, H.M.F., *Over the adsorption in solution*. *The Journal of Physical Chemistry*, 1906. **57**: p. 385-471.
 230. Brunauer, S., Emmett, P.H., and Teller, E., *Adsorption of Gases in Multimolecular Layers*. *Journal of the American Chemical Society*, 1938. **60**(2): p. 309-319.
 231. Ebadi, A., Soltan Mohammadzadeh, J.S., and Khudiev, A., *What is the correct form of BET isotherm for modeling liquid phase adsorption?* *Adsorption*, 2009. **15**(1): p. 65-73.
 232. Hammond, K.D. and Conner, W.C., *Chapter One - Analysis of Catalyst Surface Structure by Physical Sorption*, in *Advances in Catalysis*, B.C. Gates and Jentoft, F.C., Editors. 2013, Academic Press. p. 1-101.
 233. Lima, E.C., Hosseini-Bandegharai, A., Moreno-Piraján, J.C., and Anastopoulos, I., *A critical review of the estimation of the thermodynamic parameters on adsorption equilibria. Wrong use of equilibrium constant in the*

- Van't Hoof equation for calculation of thermodynamic parameters of adsorption.* Journal of Molecular Liquids, 2019. **273**: p. 425-434.
234. Liu, Y., *Is the Free Energy Change of Adsorption Correctly Calculated?* Journal of Chemical & Engineering Data, 2009. **54**(7): p. 1981-1985.
235. Havlík, T., *Chapter 7 - Kinetics of Heterogeneous Reactions of Leaching Processes*, in *Hydrometallurgy*, T. Havlík, Editor. 2008, Woodhead Publishing. p. 184-241.
236. Speight, J.G., *Chapter 5 - Sorption, Dilution, and Dissolution*, in *Reaction Mechanisms in Environmental Engineering*, J.G. Speight, Editor. 2018, Butterworth-Heinemann. p. 165-201.
237. Ali, Z., Khan, A., and Ahmad, R., *The use of functionalized aerogels as a low level chromium scavenger.* Microporous and Mesoporous Materials, 2015. **203**: p. 8-16.
238. Alothman, Z.A. and Apblett, A.W., *Metal ion adsorption using polyamine-functionalized mesoporous materials prepared from bromopropyl-functionalized mesoporous silica.* Journal of Hazardous Materials, 2010. **182**(1): p. 581-590.
239. Fan, H.-T., Su, Z.-J., Fan, X.-L., Guo, M.-M., Wang, J., Gao, S., and Sun, T., *Sol-gel derived organic-inorganic hybrid sorbent for removal of Pb²⁺, Cd²⁺ and Cu²⁺ from aqueous solution.* Journal of Sol-Gel Science and Technology, 2012. **64**(2): p. 418-426.
240. Fatimah, I. and Yudha, S.P., *N-[β-(Trimethoxysilyl)propyl] ethylenediamine Functionalized Saponite as Adsorbent of Nickel from Aqueous Solution.* Engineering Journal, 2017. **21**(2): p. 107-121.
241. Bleam, W., *Chapter 8 - Surface Chemistry and Adsorption*, in *Soil and Environmental Chemistry (Second Edition)*, W. Bleam, Editor. 2017, Academic Press. p. 385-443.
242. Dinker, M.K., Ajithkumar, T.G., and Kulkarni, P.S., *l-Proline Functionalized Dicationic Framework of Bifunctional Mesoporous Organosilica for the Simultaneous Removal of Lead and Nitrate Ions.* ACS Sustainable Chemistry & Engineering, 2017. **5**(5): p. 4188-4196.
243. He, X., Cheng, L., Wang, Y., Zhao, J., Zhang, W., and Lu, C., *Aerogels from quaternary ammonium-functionalized cellulose nanofibers for rapid removal of Cr(VI) from water.* Carbohydrate Polymers, 2014. **111**: p. 683-7.
244. Hokkanen, S., Repo, E., Suopajarvi, T., Liimatainen, H., Niinimaa, J., and Sillanpää, M., *Adsorption of Ni(II), Cu(II) and Cd(II) from aqueous solutions by amino modified nanostructured microfibrillated cellulose.* Cellulose, 2014. **21**(3): p. 1471-1487.
245. Anis, S.F., Khalil, A., Saepurahman, Singaravel, G., and Hashaikeh, R., *A review on the fabrication of zeolite and mesoporous inorganic nanofibers formation for catalytic applications.* Microporous and Mesoporous Materials, 2016. **236**: p. 176-192.
246. Erdem, E., Karapinar, N., and Donat, R., *The removal of heavy metal cations by natural zeolites.* Journal of Colloid and Interface Science, 2004. **280**(2): p. 309-314.
247. Egashira, R., Tanabe, S., and Habaki, H., *Adsorption of heavy metals in mine wastewater by Mongolian natural zeolite.* Procedia Engineering, 2012. **42**: p. 49-57.
248. Álvarez-Ayuso, E., García-Sánchez, A., and Querol, X., *Purification of metal electroplating waste waters using zeolites.* Water Research, 2003. **37**(20): p. 4855-4862.
249. Mihajlović, M.T., Lazarević, S.S., Janković-Častvan, I.M., Jokić, B.M., Janačković, Đ.T., and Petrović, R.D., *A comparative study of the removal of lead, cadmium and zinc ions from aqueous solutions by natural and Fe(III)-modified zeolite.* Chemical Industry and Chemical Engineering Quarterly, 2014. **20**(2): p. 283-293.
250. Choi, H.-J., Yu, S.-W., and Kim, K.H., *Efficient use of Mg-modified zeolite in the treatment of aqueous solution contaminated with heavy metal toxic ions.* Journal of the Taiwan Institute of Chemical Engineers, 2016. **63**: p. 482-489.
251. Hamidpour, M., Kalbasi, M., Afyuni, M., Shariatmadari, H., Holm, P.E., and Hansen, H.C., *Sorption hysteresis of Cd(II) and Pb(II) on natural zeolite and bentonite.* Journal of Hazardous Materials, 2010. **181**(1-3): p. 686-91.
252. Wang, C., Li, J., Sun, X., Wang, L., and Sun, X., *Evaluation of zeolites synthesized from fly ash as potential adsorbents for wastewater containing heavy metals.* Journal of Environmental Sciences, 2009. **21**(1): p. 127-136.
253. Ibrahim, H.S., Jamil, T.S., and Hegazy, E.Z., *Application of zeolite prepared from Egyptian kaolin for the removal of heavy metals: II. Isotherm models.* Journal of Hazardous Materials, 2010. **182**(1): p. 842-847.
254. El-Kamash, A.M., Zaki, A.A., and El Geleel, M.A., *Modeling batch kinetics and thermodynamics of zinc and cadmium ions removal from waste solutions using synthetic zeolite A.* Journal of Hazardous Materials, 2005. **127**(1): p. 211-220.
255. Yavuz, Ö., Altunkaynak, Y., and Güzel, F., *Removal of copper, nickel, cobalt and manganese from aqueous solution by kaolinite.* Water Research, 2003. **37**(4): p. 948-952.

256. Ijagbemi, C.O., Baek, M.-H., and Kim, D.-S., *Montmorillonite surface properties and sorption characteristics for heavy metal removal from aqueous solutions*. Journal of Hazardous Materials, 2009. **166**(1): p. 538-546.
257. Etcı, Ö., Bektaş, N., and Öncel, M.S., *Single and binary adsorption of lead and cadmium ions from aqueous solution using the clay mineral beidellite*. Environmental Earth Sciences, 2010. **61**(2): p. 231-240.
258. Mobasherpour, I., Salahi, E., and Pazouki, M., *Comparative of the removal of Pb²⁺, Cd²⁺ and Ni²⁺ by nano crystallite hydroxyapatite from aqueous solutions: Adsorption isotherm study*. Arabian Journal of Chemistry, 2012. **5**(4): p. 439-446.
259. Roszkopfová, O., Galamboš, M., Pivarčiová, L., Čaplovičová, M., and Rajec, P., *Adsorption of nickel on synthetic hydroxyapatite from aqueous solutions*. Journal of Radioanalytical and Nuclear Chemistry, 2012. **295**(1): p. 459-465.
260. Ghassabzadeh, H., Mohadespour, A., Torab-Mostaedi, M., Zaheri, P., Maragheh, M.G., and Taheri, H., *Adsorption of Ag, Cu and Hg from aqueous solutions using expanded perlite*. Journal of Hazardous Materials, 2010. **177**(1): p. 950-955.
261. Manatunga, D.C., de Silva, Rohini M., de Silva, K.M.N., and Ratnaweera, R., *Natural polysaccharides leading to super adsorbent hydroxyapatite nanoparticles for the removal of heavy metals and dyes from aqueous solutions*. RSC Advances, 2016. **6**(107): p. 105618-105630.
262. Bulut, Y., Akçay, G., Elma, D., and Serhatlı, I.E., *Synthesis of clay-based superabsorbent composite and its sorption capability*. Journal of Hazardous Materials, 2009. **171**(1): p. 717-723.
263. Paulino, A.T., Guilherme, M.R., Reis, A.V., Tambourgi, E.B., Nozaki, J., and Muniz, E.C., *Capacity of adsorption of Pb²⁺ and Ni²⁺ from aqueous solutions by chitosan produced from silkworm chrysalides in different degrees of deacetylation*. Journal of Hazardous Materials, 2007. **147**(1-2): p. 139-147.
264. Pivarčiová, L., Roszkopfová, O., Galamboš, M., and Rajec, P., *Sorption of nickel on chitosan*. Journal of Radioanalytical and Nuclear Chemistry, 2014. **300**(1): p. 361-366.
265. Popuri, S.R., Vijaya, Y., Boddu, V.M., and Abburi, K., *Adsorptive removal of copper and nickel ions from water using chitosan coated PVC beads*. Bioresource Technology, 2009. **100**(1): p. 194-199.
266. Thuan, L.V., Chau, T.B., Ngan, T.T.K., Vu, T.X., Nguyen, D.D., Nguyen, M.-H., Thao, D.T.T., To Hoai, N., and Sinh, L.H., *Preparation of cross-linked magnetic chitosan particles from steel slag and shrimp shells for removal of heavy metals*. Environmental Technology, 2018. **39**(14): p. 1745-1752.
267. Aliabadi, M., Irani, M., Ismaeili, J., Piri, H., and Parnian, M.J., *Electrospun nanofiber membrane of PEO/Chitosan for the adsorption of nickel, cadmium, lead and copper ions from aqueous solution*. Chemical Engineering Journal, 2013. **220**: p. 237-243.
268. Yang, J.-S., Park, Y.-T., Baek, K., and Choi, J., *Removal of Metal Ions From Aqueous Solutions Using Sawdust Modified with Citric Acid or Tartaric Acid*. Separation Science and Technology, 2010. **45**(12-13): p. 1963-1974.
269. Gupta, V.K. and Nayak, A., *Cadmium removal and recovery from aqueous solutions by novel adsorbents prepared from orange peel and Fe₂O₃ nanoparticles*. Chemical Engineering Journal, 2012. **180**: p. 81-90.
270. Jiang, S., Huang, L., Nguyen, T.A.H., Ok, Y.S., Rudolph, V., Yang, H., and Zhang, D., *Copper and zinc adsorption by softwood and hardwood biochars under elevated sulphate-induced salinity and acidic pH conditions*. Chemosphere, 2016. **142**: p. 64-71.
271. Bogusz, A., Oleszczuk, P., and Dobrowolski, R., *Application of laboratory prepared and commercially available biochars to adsorption of cadmium, copper and zinc ions from water*. Bioresource Technology, 2015. **196**: p. 540-549.
272. Vilvanathan, S. and Shanthakumar, S., *Ni²⁺ and Co²⁺ adsorption using Tectona grandis biochar: kinetics, equilibrium and desorption studies*. Environmental Technology, 2017: p. 1-15.
273. Chen, P.-p., Zhang, H.-p., Liu, H.-d., Luo, X.-g., Lin, X.-y., Lu, X., and Tang, Y., *Cost effective biochar gels with super capabilities for heavy metal removal*. RSC Advances, 2016. **6**(79): p. 75430-75439.
274. Li, R., Liang, W., Huang, H., Jiang, S., Guo, D., Li, M., Zhang, Z., Ali, A., and Wang, J.J., *Removal of cadmium(II) cations from an aqueous solution with aminothiurea chitosan strengthened magnetic biochar*. Journal of Applied Polymer Science, 2018. **135**(19): p. 46239.
275. Boparai, H.K., Joseph, M., and O'Carroll, D.M., *Kinetics and thermodynamics of cadmium ion removal by adsorption onto nano zerovalent iron particles*. Journal of Hazardous Materials, 2011. **186**(1): p. 458-465.
276. Kim, K.-J. and Park, J.-W., *Stability and reusability of amine-functionalized magnetic-cored dendrimer for heavy metal adsorption*. Journal of Materials Science, 2017. **52**(2): p. 843-857.
277. Maleki, A., Hayati, B., Najafi, F., Gharibi, F., and Joo, S.W., *Heavy metal adsorption from industrial wastewater by PAMAM/TiO₂ nanohybrid: Preparation, characterization and adsorption studies*. Journal of Molecular Liquids, 2016. **224**: p. 95-104.
278. Yang, R.-X., Wang, T.-T., and Deng, W.-Q., *Extraordinary Capability for Water Treatment Achieved by a Perfluorinated Conjugated Microporous Polymer*. Scientific Reports, 2015. **5**(1): p. 10155.

279. He, J., Li, Y., Wang, C., Zhang, K., Lin, D., Kong, L., and Liu, J., *Rapid adsorption of Pb, Cu and Cd from aqueous solutions by β -cyclodextrin polymers*. Applied Surface Science, 2017. **426**: p. 29-39.
280. Murugesan, A., Ravikumar, L., SathyaSelvaBala, V., SenthilKumar, P., Vidhyadevi, T., Kirupha, S.D., Kalaivani, S.S., Krithiga, S., and Sivanesan, S., *Removal of Pb(II), Cu(II) and Cd(II) ions from aqueous solution using polyazomethineamides: Equilibrium and kinetic approach*. Desalination, 2011. **271**(1): p. 199-208.
281. Li, B., Zhou, F., Huang, K., Wang, Y., Mei, S., Zhou, Y., and Jing, T., *Highly efficient removal of lead and cadmium during wastewater irrigation using a polyethylenimine-grafted gelatin sponge*. Scientific Reports, 2016. **6**(1): p. 33573.
282. Mittal, H., Maity, A., and Sinha Ray, S., *The Adsorption of Pb²⁺ and Cu²⁺ onto Gum Ghatti-Grafted Poly(acrylamide-co-acrylonitrile) Biodegradable Hydrogel: Isotherms and Kinetic Models*. The Journal of Physical Chemistry B, 2015. **119**(5): p. 2026-2039.
283. Macedo, T.R. and Airoidi, C., *New inorganic-organic lamellar derivatives synthesized from H-RUB-18 and thermodynamics of cation sorption*. New Journal of Chemistry, 2009. **33**(10): p. 2081-2089.
284. Wang, H., Zhou, A., Peng, F., Yu, H., and Yang, J., *Mechanism study on adsorption of acidified multivalled carbon nanotubes to Pb(II)*. Journal of Colloid and Interface Science, 2007. **316**(2): p. 277-283.
285. Kabbashi, N.A., Atieh, M.A., Al-Mamun, A., Mirghami, M.E.S., Alam, M.D.Z., and Yahya, N., *Kinetic adsorption of application of carbon nanotubes for Pb(II) removal from aqueous solution*. Journal of Environmental Sciences, 2009. **21**(4): p. 539-544.
286. Vuković, G.D., Marinković, A.D., Čolić, M., Ristić, M.Đ., Aleksić, R., Perić-Grujić, A.A., and Uskoković, P.S., *Removal of cadmium from aqueous solutions by oxidized and ethylenediamine-functionalized multi-walled carbon nanotubes*. Chemical Engineering Journal, 2010. **157**(1): p. 238-248.
287. Kobya, M., Demirbas, E., Senturk, E., and Ince, M., *Adsorption of heavy metal ions from aqueous solutions by activated carbon prepared from apricot stone*. Bioresource Technology, 2005. **96**(13): p. 1518-1521.
288. Al-Omair, M.A. and El-Sharkawy, E.A., *Removal of Heavy Metals Via Adsorption on Activated Carbon Synthesized from Solid Wastes*. Environmental Technology, 2007. **28**(4): p. 443-451.
289. Tang, C., Shu, Y., Zhang, R., Li, X., Song, J., Li, B., Zhang, Y., and Ou, D., *Comparison of the removal and adsorption mechanisms of cadmium and lead from aqueous solution by activated carbons prepared from *Typha angustifolia* and *Salix matsudana**. RSC Advances, 2017. **7**(26): p. 16092-16103.
290. Hayati, B., Maleki, A., Najafi, F., Daraei, H., Gharibi, F., and McKay, G., *Synthesis and characterization of PAMAM/CNT nanocomposite as a super-capacity adsorbent for heavy metal (Ni²⁺, Zn²⁺, As³⁺, Co²⁺) removal from wastewater*. Journal of Molecular Liquids, 2016. **224**: p. 1032-1040.
291. Hayati, B., Maleki, A., Najafi, F., Daraei, H., Gharibi, F., and McKay, G., *Super high removal capacities of heavy metals (Pb²⁺ and Cu²⁺) using CNT dendrimer*. Journal of Hazardous Materials, 2017. **336**: p. 146-157.
292. Ma, Y.-X., Kou, Y.-L., Xing, D., Jin, P.-S., Shao, W.-J., Li, X., Du, X.-Y., and La, P.-Q., *Synthesis of magnetic graphene oxide grafted polymaleicamide dendrimer nanohybrids for adsorption of Pb(II) in aqueous solution*. Journal of Hazardous Materials, 2017. **340**: p. 407-416.
293. Zhang, L., Hu, X., Yu, C., Crawford, R., and Yu, A., *Preparation of sinapinaldehyde modified mesoporous silica materials and their application in selective extraction of trace Pb(II)*. International Journal of Environmental Analytical Chemistry, 2013. **93**(12): p. 1274-1285.
294. Guo, Y., Liu, D., Zhao, Y., Gong, B., Guo, Y., and Huang, W., *Synthesis of chitosan-functionalized MCM-41-A and its performance in Pb(II) removal from synthetic water*. Journal of the Taiwan Institute of Chemical Engineers, 2017. **71**: p. 537-545.
295. Anbia, M., Kargosha, K., and Khoshbooei, S., *Heavy metal ions removal from aqueous media by modified magnetic mesoporous silica MCM-48*. Chemical Engineering Research and Design, 2015. **93**: p. 779-788.
296. Dinh Du, P., Hieu, N.T., To, T.C., Bach, L.G., Tinh, M.X., Xuan Mau, T., and Quang Khieu, D., *Aminopropyl Functionalised MCM-41: Synthesis and Application for Adsorption of Pb(II) and Cd(II)*. Advances in Materials Science and Engineering, 2019. **2019**: p. 8573451.
297. Ghorbani, M., Nowee, S.M., Ramezani, N., and Raji, F., *A new nanostructured material amino functionalized mesoporous silica synthesized via co-condensation method for Pb(II) and Ni(II) ion sorption from aqueous solution*. Hydrometallurgy, 2016. **161**: p. 117-126.
298. Soltani, R., Dinari, M., and Mohammadnezhad, G., *Ultrasonic-assisted synthesis of novel nanocomposite of poly(vinyl alcohol) and amino-modified MCM-41: A green adsorbent for Cd(II) removal*. Ultrasonics Sonochemistry, 2018. **40**: p. 533-542.
299. Košak, A., Lobnik, A., and Bauman, M., *Adsorption of Mercury(II), Lead(II), Cadmium(II) and Zinc(II) from Aqueous Solutions using Mercapto-Modified Silica Particles*. International Journal of Applied Ceramic Technology, 2015. **12**(2): p. 461-472.

300. Kumar, R., Barakat, M.A., Daza, Y.A., Woodcock, H.L., and Kuhn, J.N., *EDTA functionalized silica for removal of Cu(II), Zn(II) and Ni(II) from aqueous solution*. Journal of Colloid and Interface Science, 2013. **408**: p. 200-205.
301. Hatay, I., Gup, R., and Ersoz, M., *Silica gel functionalized with 4-phenylacetophynone 4-aminobenzoylhydrazone: Synthesis of a new chelating matrix and its application as metal ion collector*. Journal of Hazardous Materials, 2008. **150**(3): p. 546-53.
302. Oliveira, F.J.V.E., da Silva Filho, E.C., Melo, M.A., and Airoidi, C., *Modified coupling agents based on thiourea, immobilized onto silica. Thermodynamics of copper adsorption*. Surface Science, 2009. **603**(14): p. 2200-2206.
303. Pawlaczyk, M. and Schroeder, G., *Adsorption studies of Cu(II) ions on dendrimer-grafted silica-based materials*. Journal of Molecular Liquids, 2019. **281**: p. 176-185.
304. Li, M., Li, M.-y., Feng, C.-g., and Zeng, Q.-x., *Preparation and characterization of multi-carboxyl-functionalized silica gel for removal of Cu (II), Cd (II), Ni (II) and Zn (II) from aqueous solution*. Applied Surface Science, 2014. **314**: p. 1063-1069.
305. Silva, A.L.P., Sousa, K.S., Germano, A.F.S., Oliveira, V.V., Espínola, J.G.P., Fonseca, M.G., Airoidi, C., Arakaki, T., and Arakaki, L.N.H., *A new organofunctionalized silica containing thioglycolic acid incorporated for divalent cations removal—A thermodynamic cation/basic center interaction*. Colloids and Surfaces A: Physicochemical and Engineering Aspects, 2009. **332**(2): p. 144-149.
306. Gomes, E.C.C., de Sousa, A.F., Vasconcelos, P.H.M., Melo, D.Q., Diógenes, I.C.N., de Sousa, E.H.S., do Nascimento, R.F., San Gil, R.A.S., and Longhinotti, E., *Synthesis of bifunctional mesoporous silica spheres as potential adsorbent for ions in solution*. Chemical Engineering Journal, 2013. **214**: p. 27-33.
307. Liu, Y., Lou, Z., Sun, Y., Zhou, X., Baig, S.A., and Xu, X., *Influence of complexing agent on the removal of Pb(II) from aqueous solutions by modified mesoporous SiO₂*. Microporous and Mesoporous Materials, 2017. **246**: p. 1-13.
308. Hao, S., Zhong, Y., Pepe, F., and Zhu, W., *Adsorption of Pb²⁺ and Cu²⁺ on anionic surfactant-templated amino-functionalized mesoporous silicas*. Chemical Engineering Journal, 2012. **189-190**: p. 160-167.
309. Hao, S., Verlotta, A., Aprea, P., Pepe, F., Caputo, D., and Zhu, W., *Optimal synthesis of amino-functionalized mesoporous silicas for the adsorption of heavy metal ions*. Microporous and Mesoporous Materials, 2016. **236**: p. 250-259.
310. Chen, F., Wu, Q., Lü, Q., Xu, Y., and Yu, Y., *Synthesis and characterization of bifunctional mesoporous silica adsorbent for simultaneous removal of lead and nitrate ions*. Separation and Purification Technology, 2015. **151**: p. 225-231.
311. Agaba, A., Cheng, H., Zhao, J., Zhang, C., Tebyetekerwa, M., Rong, L., Sui, X., and Wang, B., *Precipitated silica agglomerates reinforced with cellulose nanofibrils as adsorbents for heavy metals*. RSC Advances, 2018. **8**(58): p. 33129-33137.
312. Wu, S., Li, F., Wang, H., Fu, L., Zhang, B., and Li, G., *Effects of poly (vinyl alcohol) (PVA) content on preparation of novel thiol-functionalized mesoporous PVA/SiO₂ composite nanofiber membranes and their application for adsorption of heavy metal ions from aqueous solution*. Polymer, 2010. **51**(26): p. 6203-6211.
313. Prakash, S., Kumar, M., Tripathi, B.P., and Shahi, V.K., *Sol-gel derived poly(vinyl alcohol)-3-(2-aminoethylamino) propyl trimethoxysilane: Cross-linked organic-inorganic hybrid beads for the removal of Pb(II) from aqueous solution*. Chemical Engineering Journal, 2010. **162**(1): p. 28-36.
314. Qu, Q., Gu, Q., Gu, Z., Shen, Y., Wang, C., and Hu, X., *Efficient removal of heavy metal from aqueous solution by sulfonic acid functionalized nonporous silica microspheres*. Colloids and Surfaces A: Physicochemical and Engineering Aspects, 2012. **415**: p. 41-46.
315. Faghihian, H., Nourmoradi, H., and Shokouhi, M., *Removal of copper (II) and nickel (II) from aqueous media using silica aerogel modified with amino propyl triethoxysilane as an adsorbent: equilibrium, kinetic, and isotherms study*. Desalination and Water Treatment, 2013. **52**(1-3): p. 305-313.
316. Faghihian, H., Nourmoradi, H., and Shokouhi, M., *Performance of silica aerogels modified with amino functional groups in Pb(II) and Cd(II) removal from aqueous solutions*. Polish Journal of Chemical Technology, 2012. **14**(1): p. 50-56.
317. Štandeker, S., Veronovski, A., Novak, Z., and Knez, Ž., *Silica aerogels modified with mercapto functional groups used for Cu(II) and Hg(II) removal from aqueous solutions*. Desalination, 2011. **269**(1-3): p. 223-230.
318. Pouredal, H.R. and Kazemi, M., *Characterization of modified silica aerogel using sodium silicate precursor and its application as adsorbent of Cu²⁺, Cd²⁺, and Pb²⁺ ions*. International Journal of Industrial Chemistry, 2012. **3**(1): p. 20.
319. Huang, Y.-D., Gao, X.-D., Gu, Z.-Y., and Li, X.-M., *Amino-terminated SiO₂ aerogel towards highly-effective lead (II) adsorbent via the ambient drying process*. Journal of Non-Crystalline Solids, 2016. **443**: p. 39-46.

320. Duan, X., Qi, G., Wang, P., and Giannelis, E.P., *A Highly Efficient and Selective Polysilsesquioxane Sorbent for Heavy Metal Removal*. ChemPhysChem, 2012. **13**(10): p. 2536-2539.
321. Maatar, W. and Boufi, S., *Poly(methacrylic acid-co-maleic acid) grafted nanofibrillated cellulose as a reusable novel heavy metal ions adsorbent*. Carbohydrate Polymers, 2015. **126**: p. 199-207.
322. Chaisuwan, T., Komalwanich, T., Luangsukrerak, S., and Wongkasemjit, S., *Removal of heavy metals from model wastewater by using polybenzoxazine aerogel*. Desalination, 2010. **256**(1-3): p. 108-114.
323. Mo, L., Pang, H., Tan, Y., Zhang, S., and Li, J., *3D multi-wall perforated nanocellulose-based polyethylenimine aerogels for ultrahigh efficient and reversible removal of Cu(II) ions from water*. Chemical Engineering Journal, 2019. **378**: p. 122157.
324. Tian, C., She, J., Wu, Y., Luo, S., Wu, Q., and Qing, Y., *Reusable and cross-linked cellulose nanofibrils aerogel for the removal of heavy metal ions*. Polymer Composites, 2018. **39**(12): p. 4442-4451.
325. Deze, E.G., Papageorgiou, S.K., Favvas, E.P., and Katsaros, F.K., *Porous alginate aerogel beads for effective and rapid heavy metal sorption from aqueous solutions: Effect of porosity in Cu²⁺ and Cd²⁺ ion sorption*. Chemical Engineering Journal, 2012. **209**: p. 537-546.
326. Jiao, C., Xiong, J., Tao, J., Xu, S., Zhang, D., Lin, H., and Chen, Y., *Sodium alginate/graphene oxide aerogel with enhanced strength-toughness and its heavy metal adsorption study*. International Journal of Biological Macromolecules, 2016. **83**: p. 133-41.
327. Goel, J., Kadirvelu, K., Rajagopal, C., and Garg, V.K., *Investigation of adsorption of lead, mercury and nickel from aqueous solutions onto carbon aerogel*. Journal of Chemical Technology & Biotechnology, 2005. **80**(4): p. 469-476.
328. Kadirvelu, K., Goel, J., and Rajagopal, C., *Sorption of lead, mercury and cadmium ions in multi-component system using carbon aerogel as adsorbent*. Journal of Hazardous Materials, 2008. **153**(1-2): p. 502-7.
329. Wang, X., Jiang, S., Cui, S., Tang, Y., Pei, Z., and Duan, H., *Magnetic-controlled aerogels from carboxylated cellulose and MnFe₂O₄ as a novel adsorbent for removal of Cu(II)*. Cellulose, 2019. **26**(8): p. 5051-5063.
330. van Berkel, P.M., Driessen, W.L., Reedijk, J., Sherrington, D.C., and Zitsmanis, A., *Metal-ion binding affinity of azole-modified oxirane and thiirane resins*. Reactive and Functional Polymers, 1995. **27**(1): p. 15-28.
331. van Berkel, P.M., Dijkstra, D.J., Driessen, W.L., Reedijk, J., and Sherrington, D.C., *Selective and rapid uptake of Cu(II) by bis(benzimidazole) modified oxirane and thiirane resins*. Reactive and Functional Polymers, 1995. **28**(1): p. 39-54.
332. Verweij, P.D., Dugué, T., Driessen, W.L., Reedijk, J., Rowatt, B., and Sherrington, D.C., *Metal uptake by N,N'-bis(2-benzimidazolylmethyl) amine immobilized on poly(glycidyl methacrylate-co-ethylene glycol dimethacrylate)*. Reactive Polymers, 1991. **14**(3): p. 213-227.
333. Yan, H., Dai, J., Yang, Z., Yang, H., and Cheng, R., *Enhanced and selective adsorption of copper(II) ions on surface carboxymethylated chitosan hydrogel beads*. Chemical Engineering Journal, 2011. **174**(2-3): p. 586-594.
334. Dam, H.A. and Kim, D., *Selective Copper(II) Sorption Behavior of Surface-Imprinted Core-Shell-Type Polymethacrylate Microspheres*. Industrial & Engineering Chemistry Research, 2009. **48**(12): p. 5679-5685.
335. Dudler, V., Lindoy, L.F., Sallin, D., and Schlaepfer, C.W., *An Oxygen-Nitrogen Donor Macrocyclic Immobilized on Silica Gel. A Reagent Showing High Selectivity for Copper(II) in the Presence of Cobalt(II), Nickel(II), Zinc(II) or Cadmium(II)*. Australian Journal of Chemistry, 1987. **40**(9): p. 1557-1563.
336. Yang, Z., Wang, Y., and Tang, Y., *Preparation and adsorption properties of metal ions of crosslinked chitosan azacrown ethers*. Journal of Applied Polymer Science, 1999. **74**(13): p. 3053-3058.
337. Im, H.-J., Yang, Y., Allain, L.R., Barnes, C.E., Dai, S., and Xue, Z., *Functionalized Sol-Gels for Selective Copper(II) Separation*. Environmental Science & Technology, 2000. **34**(11): p. 2209-2214.
338. Ebraheem, K.A.K. and Hamdi, S.T., *Synthesis and properties of a copper selective chelating resin containing a salicylaldehyde group*. Reactive and Functional Polymers, 1997. **34**(1): p. 5-10.
339. Nosrati, A., Larsson, M., Lindén, J.B., Zihao, Z., Addai-Mensah, J., and Nydén, M., *Polyethylenimine functionalized mesoporous diatomite particles for selective copper recovery from aqueous media*. International Journal of Mineral Processing, 2017. **166**: p. 29-36.
340. Kistler, S.S., *Coherent expanded aerogels and jellies*. Nature, 1931. **127**: p. 741.
341. Gurav, J.L., Jung, I.-K., Park, H.-H., Kang, E.S., and Nadargi, D.Y., *Silica Aerogel: Synthesis and Applications*. Journal of Nanomaterials, 2010. **2010**: p. 1-11.
342. IUPAC, *Compendium of Chemical Terminology, 2nd ed. (the "Gold Book")*, ed. A.D. McNaught and Wilkinson, A. 1997, Oxford Blackwell Scientific Publications.
343. Eychmüller, A., Ziegler, C., Wolf, A., Liu, W., Herrmann, A.-K., and Gaponik, N., *Modern Inorganic Aerogels*. Angewandte Chemie International Edition, 2017: p. n/a-n/a.

344. Leventis, N., Sadekar, A., Chandrasekaran, N., and Sotiriou-Leventis, C., *Click Synthesis of Monolithic Silicon Carbide Aerogels from Polyacrylonitrile-Coated 3D Silica Networks*. Chemistry of Materials, 2010. **22**(9): p. 2790-2803.
345. Stöcker, C. and Baiker, A., *Zirconia aerogels: effect of acid-to-alkoxide ratio, alcoholic solvent and supercritical drying method on structural properties*. Journal of Non-Crystalline Solids, 1998. **223**(3): p. 165-178.
346. Baumann, T.F., Gash, A.E., Chinn, S.C., Sawvel, A.M., Maxwell, R.S., and Satcher, J.H., *Synthesis of High-Surface-Area Alumina Aerogels without the Use of Alkoxide Precursors*. Chemistry of Materials, 2005. **17**(2): p. 395-401.
347. Dutoit, D.C.M., Schneider, M., and Baiker, A., *Titania aerogels prepared by low-temperature supercritical drying. Influence of extraction conditions*. Journal of Porous Materials, 1995. **1**(2): p. 165-174.
348. Innerlohinger, J., Weber, H.K., and Kraft, G., *Aerocellulose: Aerogels and Aerogel-like Materials made from Cellulose*. Macromolecular Symposia, 2006. **244**(1): p. 126-135.
349. Williams, J.C., Nguyen, B.N., McCorkle, L., Scheiman, D., Griffin, J.S., Steiner, S.A., and Meador, M.A.B., *Highly Porous, Rigid-Rod Polyamide Aerogels with Superior Mechanical Properties and Unusually High Thermal Conductivity*. ACS Applied Materials & Interfaces, 2017. **9**(2): p. 1801-1809.
350. Zhang, X.M., Liu, J.G., and Yang, S.Y., *Synthesis and characterization of flexible and high-temperature resistant polyimide aerogel with ultra-low dielectric constant*. Express Polymer Letters, 2016. **10**(10): p. 789-798.
351. Pierre, A.C., *History of Aerogels*, in *Aerogels Handbook*, M.A. Aegerter, Leventis, N., and Koebel, M.M., Editors. 2011, Springer New York: New York, NY. p. 3-18.
352. Soleimani Dorcheh, A. and Abbasi, M.H., *Silica aerogel; synthesis, properties and characterization*. Journal of Materials Processing Technology, 2008. **199**(1-3): p. 10-26.
353. Vareda, J.P., Lamy-Mendes, A., and Durães, L., *A reconsideration on the definition of the term aerogel based on current drying trends*. Microporous and Mesoporous Materials, 2018. **258**(Supplement C): p. 211-216.
354. Pierre, A.C. and Rigacci, A., *SiO₂ Aerogels*, in *Aerogels Handbook*, M.A. Aegerter, Leventis, N., and Koebel, M.M., Editors. 2011, Springer New York: New York, NY. p. 21-45.
355. Maleki, H., Durães, L., and Portugal, A., *An overview on silica aerogels synthesis and different mechanical reinforcing strategies*. Journal of Non-Crystalline Solids, 2014. **385**: p. 55-74.
356. Zhang, G., Dass, A., Rawashdeh, A.-M.M., Thomas, J., Council, J.A., Sotiriou-Leventis, C., Fabrizio, E.F., Ilhan, F., Vassilaras, P., Scheiman, D.A., McCorkle, L., Palczar, A., Johnston, J.C., Meador, M.A., and Leventis, N., *Isocyanate-crosslinked silica aerogel monoliths: preparation and characterization*. Journal of Non-Crystalline Solids, 2004. **350**: p. 152-164.
357. Woignier, T., Phalippou, J., Despetis, F., and Calas-Etienne, S., *Aerogel Processing*, in *Handbook of Sol-Gel Science and Technology: Processing, Characterization and Applications*, L. Klein, Aparicio, M., and Jitianu, A., Editors. 2018, Springer International Publishing: Cham. p. 985-1011.
358. Matias, T., Varino, C., de Sousa, H.C., Braga, M.E.M., Portugal, A., Coelho, J.F.J., and Durães, L., *Novel flexible, hybrid aerogels with vinyl- and methyltrimethoxysilane in the underlying silica structure*. Journal of Materials Science, 2016. **51**(14): p. 6781-6792.
359. *Critical Constants Of Inorganic Compounds*, in *CRC Handbook of Chemistry and Physics 97th Ed*, W.M. Haynes, Lide, D.R., and Bruno, T.J., Editors. 2017, CRC Press: Florida, USA.
360. Pei, X., Zhai, W., and Zheng, W., *Preparation and Characterization of Highly Cross-Linked Polyimide Aerogels Based on Polyimide Containing Trimethoxysilane Side Groups*. Langmuir, 2014. **30**(44): p. 13375-13383.
361. Hüsing, N. and Schubert, U., *Aerogels*, in *Ullmann's Encyclopedia of Industrial Chemistry*, C. Ley, Editor. 2000, Wiley-VCH Verlag GmbH & Co. KGaA.
362. Kumar, A., Rana, A., Sharma, G., Sharma, S., Naushad, M., Mola, G.T., Dhiman, P., and Stadler, F.J., *Aerogels and metal-organic frameworks for environmental remediation and energy production*. Environmental Chemistry Letters, 2018. **16**(3): p. 797-820.
363. Maleki, H., Duraes, L., Garcia-Gonzalez, C.A., Del Gaudio, P., Portugal, A., and Mahmoudi, M., *Synthesis and biomedical applications of aerogels: Possibilities and challenges*. Adv Colloid Interface Sci, 2016. **236**: p. 1-27.
364. García-González, C.A., Budtova, T., Durães, L., Erkey, C., Del Gaudio, P., Gurikov, P., Koebel, M., Liebner, F., Neagu, M., and Smirnova, I., *An Opinion Paper on Aerogels for Biomedical and Environmental Applications*. Molecules, 2019. **24**(9): p. 1815.
365. Randall, J.P., Meador, M.A., and Jana, S.C., *Tailoring mechanical properties of aerogels for aerospace applications*. ACS Applied Materials & Interfaces, 2011. **3**(3): p. 613-26.
366. Koebel, M., Rigacci, A., and Achard, P., *Aerogel-based thermal superinsulation: an overview*. Journal of Sol-Gel Science and Technology, 2012. **63**(3): p. 315-339.
367. Baetens, R., Jelle, B.P., and Gustavsen, A., *Aerogel insulation for building applications: A state-of-the-art review*. Energy and Buildings, 2011. **43**(4): p. 761-769.

368. Cuce, E. and Riffat, S.B., *A state-of-the-art review on innovative glazing technologies*. Renewable and Sustainable Energy Reviews, 2015. **41**: p. 695-714.
369. Pavan, C., Delle Piane, M., Gullo, M., Filippi, F., Fubini, B., Hoet, P., Horwell, C.J., Huaux, F., Lison, D., Lo Giudice, C., Martra, G., Montfort, E., Schins, R., Sulpizi, M., Wegner, K., Wyart-Remy, M., Ziemann, C., and Turci, F., *The puzzling issue of silica toxicity: are silanols bridging the gaps between surface states and pathogenicity?* Particle and Fibre Toxicology, 2019. **16**(1): p. 32.
370. Zhang, H., Dunphy, D.R., Jiang, X., Meng, H., Sun, B., Tarn, D., Xue, M., Wang, X., Lin, S., Ji, Z., Li, R., Garcia, F.L., Yang, J., Kirk, M.L., Xia, T., Zink, J.I., Nel, A., and Brinker, C.J., *Processing Pathway Dependence of Amorphous Silica Nanoparticle Toxicity: Colloidal vs Pyrolytic*. Journal of the American Chemical Society, 2012. **134**(38): p. 15790-15804.
371. Murugadoss, S., Lison, D., Godderis, L., Van Den Brule, S., Mast, J., Brassinne, F., Sebaihi, N., and Hoet, P.H., *Toxicology of silica nanoparticles: an update*. Archives of Toxicology, 2017. **91**(9): p. 2967-3010.
372. Occupational Safety and Health Administration, *1910 - Occupational Safety and Health Standards, in 1910 Subpart Z - Toxic and Hazardous Substances; TABLE Z-3 Mineral Dusts*.
373. Health and Safety Executive, *EH40/2005 Workplace exposure limits*. 2020.
374. Del Castillo, A.M.P., *Nanomaterials and workplace health & safety: What are the issues for workers?* 2013, European Trade Union Institute, : Brussels.
375. Merget, R., Bauer, T., Küpper, H., Philippou, S., Bauer, H., Breitstadt, R., and Bruening, T., *Health hazards due to the inhalation of amorphous silica*. Archives of Toxicology, 2002. **75**(11): p. 625-634.
376. Iler, R.K., *THE CHEMISTRY OF SILICA: Solubility, Polymerization, Colloid and Surface Properties, and Biochemistry*. 1979, New York: John Wiley & Sons.
377. He, Q., Zhang, Z., Gao, Y., Shi, J., and Li, Y., *Intracellular Localization and Cytotoxicity of Spherical Mesoporous Silica Nano- and Microparticles*. Small, 2009. **5**(23): p. 2722-2729.
378. Engelbrecht, F.M. and Burger, F.J., *The toxicity of silicic acid*. South African Journal of Laboratory and Clinical Medicine, 1961. **7**: p. 16-21.
379. Brunner, T.J., Wick, P., Manser, P., Spohn, P., Grass, R.N., Limbach, L.K., Bruinink, A., and Stark, W.J., *In Vitro Cytotoxicity of Oxide Nanoparticles: Comparison to Asbestos, Silica, and the Effect of Particle Solubility*. Environmental Science & Technology, 2006. **40**(14): p. 4374-4381.
380. Croissant, J.G., Butler, K.S., Zink, J.I., and Brinker, C.J., *Synthetic amorphous silica nanoparticles: toxicity, biomedical and environmental implications*. Nature Reviews Materials, 2020. **5**(12): p. 886-909.
381. Croissant, J.G., Fatieiev, Y., Almalik, A., and Khashab, N.M., *Mesoporous Silica and Organosilica Nanoparticles: Physical Chemistry, Biosafety, Delivery Strategies, and Biomedical Applications*. Advanced Healthcare Materials, 2018. **7**(4): p. 1700831.
382. Sani, N.S., Malek, N.A.N.N., Jemon, K., Kadir, M.R.A., and Hamdan, H., *Preparation and characterization of hydroxyapatite incorporated silica aerogel and its effect on normal human dermal fibroblast cells*. Journal of Sol-Gel Science and Technology, 2019. **90**(2): p. 422-433.
383. Meera, K.M.S., Sankar, R.M., Jaisankar, S.N., and Mandal, A.B., *Mesoporous and biocompatible surface active silica aerogel synthesis using choline formate ionic liquid*. Colloids and Surfaces B: Biointerfaces, 2011. **86**(2): p. 292-297.
384. Ayers, M.R. and Hunt, A.J., *Synthesis and properties of chitosan-silica hybrid aerogels*. Journal of Non-Crystalline Solids, 2001. **285**(1): p. 123-127.
385. Veres, P., Király, G., Nagy, G., Lázár, I., Fábíán, I., and Kalmár, J., *Biocompatible silica-gelatin hybrid aerogels covalently labeled with fluorescein*. Journal of Non-Crystalline Solids, 2017. **473**: p. 17-25.
386. Ge, J., Li, M., Zhang, Q., Yang, C.Z., Wooley, P.H., Chen, X., and Yang, S.-Y., *Silica Aerogel Improves the Biocompatibility in a Poly-ε-Caprolactone Composite Used as a Tissue Engineering Scaffold*. International Journal of Polymer Science, 2013. **2013**: p. 402859.
387. Yin, W., Venkitachalam, S.M., Jarrett, E., Staggs, S., Leventis, N., Lu, H., and Rubenstein, D.A., *Biocompatibility of surfactant-templated polyurea-nanoencapsulated macroporous silica aerogels with plasma platelets and endothelial cells*. Journal of Biomedical Materials Research Part A, 2010. **92A**(4): p. 1431-1439.
388. Stergar, J. and Maver, U., *Review of aerogel-based materials in biomedical applications*. Journal of Sol-Gel Science and Technology, 2016. **77**(3): p. 738-752.
389. Nagy, G., Király, G., Veres, P., Lázár, I., Fábíán, I., Bánfalvi, G., Juhász, I., and Kalmár, J., *Controlled release of methotrexate from functionalized silica-gelatin aerogel microparticles applied against tumor cell growth*. International Journal of Pharmaceutics, 2019. **558**: p. 396-403.
390. Wang, X., Wang, J., Feng, S., Zhang, Z., Wu, C., Zhang, X., and Kang, F., *Nano-Porous Silica Aerogels as Promising Biomaterials for Oral Drug Delivery of Paclitaxel*. Journal of Biomedical Nanotechnology, 2019. **15**(7): p. 1532-1545.

391. Qin, L., He, Y., Zhao, X., Zhang, T., Qin, Y., and Du, A., *Preparation, Characterization, and In Vitro Sustained Release Profile of Resveratrol-Loaded Silica Aerogel*. *Molecules*, 2020. **25**(12): p. 2752.
392. Sabri, F., Cole, J.A., Scarbrough, M.C., and Leventis, N., *Investigation of Polyurea-Crosslinked Silica Aerogels as a Neuronal Scaffold: A Pilot Study*. *PLOS ONE*, 2012. **7**(3): p. e33242.
393. Sani, N.S., Malek, N.A.N.N., Jemon, K., Kadir, M.R.A., and Hamdan, H., *In vitro bioactivity and osteoblast cell viability studies of hydroxyapatite-incorporated silica aerogel*. *Journal of Sol-Gel Science and Technology*, 2020. **96**(1): p. 166-177.
394. Sani, N.S., Malek, N.A.N.N., Jemon, K., Kadir, M.R.A., and Hamdan, H., *Effect of mass concentration on bioactivity and cell viability of calcined silica aerogel synthesized from rice husk ash as silica source*. *Journal of Sol-Gel Science and Technology*, 2017. **82**(1): p. 120-132.
395. Tiryaki, E., Başaran Elalınış, Y., Karakuzu İkizler, B., and Yücel, S., *Novel organic/inorganic hybrid nanoparticles as enzyme-triggered drug delivery systems: Dextran and Dextran aldehyde coated silica aerogels*. *Journal of Drug Delivery Science and Technology*, 2020. **56**: p. 101517.
396. Slomberg, D.L. and Schoenfish, M.H., *Silica Nanoparticle Phytotoxicity to Arabidopsis thaliana*. *Environmental Science & Technology*, 2012. **46**(18): p. 10247-10254.
397. Clément, L., Zenerino, A., Hurel, C., Amigoni, S., Taffin de Givenchy, E., Guittard, F., and Marmier, N., *Toxicity assessment of silica nanoparticles, functionalised silica nanoparticles, and HASE-grafted silica nanoparticles*. *Science of The Total Environment*, 2013. **450-451**: p. 120-128.
398. Karunakaran, G., Suriyaprabha, R., Manivasakan, P., Rajendran, V., and Kannan, N., *Influence of Nano and Bulk SiO₂ and Al₂O₃ Particles on PGPR and Soil Nutrient Contents*. *Current Nanoscience*, 2014. **10**(4): p. 604-612.
399. Book, F., Ekvall, M.T., Persson, M., Lönnnerud, S., Lammel, T., Sturve, J., and Backhaus, T., *Ecotoxicity screening of seven different types of commercial silica nanoparticles using cellular and organismic assays: Importance of surface and size*. *NanoImpact*, 2019. **13**: p. 100-111.
400. Ríos, F., Fernández-Arteaga, A., Fernández-Serrano, M., Jurado, E., and Lechuga, M., *Silica micro- and nanoparticles reduce the toxicity of surfactant solutions*. *Journal of Hazardous Materials*, 2018. **353**: p. 436-443.
401. Canesi, L., Ciacci, C., Vallotto, D., Gallo, G., Marcomini, A., and Pojana, G., *In vitro effects of suspensions of selected nanoparticles (C60 fullerene, TiO₂, SiO₂) on Mytilus hemocytes*. *Aquatic Toxicology*, 2010. **96**(2): p. 151-158.
402. Casado, M.P., Macken, A., and Byrne, H.J., *Ecotoxicological assessment of silica and polystyrene nanoparticles assessed by a multitrophic test battery*. *Environment International*, 2013. **51**: p. 97-105.
403. Lee, S.-W., Kim, S.-M., and Choi, J., *Genotoxicity and ecotoxicity assays using the freshwater crustacean Daphnia magna and the larva of the aquatic midge Chironomus riparius to screen the ecological risks of nanoparticle exposure*. *Environmental Toxicology and Pharmacology*, 2009. **28**(1): p. 86-91.
404. Perdigoto, M.L.N., Martins, R.C., Rocha, N., Quina, M.J., Gando-Ferreira, L., Patrício, R., and Durães, L., *Application of hydrophobic silica based aerogels and xerogels for removal of toxic organic compounds from aqueous solutions*. *Journal of Colloid and Interface Science*, 2012. **380**(1): p. 134-140.
405. Maleki, H., *Recent advances in aerogels for environmental remediation applications: A review*. *Chemical Engineering Journal*, 2016. **300**: p. 98-118.
406. Torres, R.B., Vareda, J.P., Lamy-Mendes, A., and Durães, L., *Effect of different silylation agents on the properties of ambient pressure dried and supercritically dried vinyl-modified silica aerogels*. *The Journal of Supercritical Fluids*, 2019. **147**: p. 81-89.
407. Obrey, K.A.D., Wilson, K.V., and Loy, D.A., *Enhancing mechanical properties of silica aerogels*. *Journal of Non-Crystalline Solids*, 2011. **357**(19): p. 3435-3441.
408. Yantasee, W., Warner, C.L., Sangvanich, T., Addleman, R.S., Carter, T.G., Wiacek, R.J., Fryxell, G.E., Timchalk, C., and Warner, M.G., *Removal of Heavy Metals from Aqueous Systems with Thiol Functionalized Superparamagnetic Nanoparticles*. *Environmental Science & Technology*, 2007. **41**(14): p. 5114-5119.
409. Alfarra, A., Frackowiak, E., and Béguin, F., *The HSAB concept as a means to interpret the adsorption of metal ions onto activated carbons*. *Applied Surface Science*, 2004. **228**(1-4): p. 84-92.
410. Cui, L., Wu, J., and Ju, H., *Electrochemical sensing of heavy metal ions with inorganic, organic and bio-materials*. *Biosensors and Bioelectronics*, 2015. **63**: p. 276-286.
411. Brodbelt, J.S., Kempen, E., and Reyzer, M., *Determination of Binding Selectivities by Electrospray Ionization Mass Spectrometry*. *Structural Chemistry*, 1999. **10**(3): p. 213-220.
412. Blair, S.M., Brodbelt, J.S., Marchand, A.P., Kumar, K.A., and Chong, H.-S., *Evaluation of Binding Selectivities of Caged Crown Ligands toward Heavy Metals by Electrospray Ionization/Quadrupole Ion Trap Mass Spectrometry*. *Analytical Chemistry*, 2000. **72**(11): p. 2433-2445.

413. Tsybizova, A., Tarábek, J., Buchta, M., Holý, P., and Schröder, D., *Electrospray ionization mass spectrometric investigations of the complexation behavior of macrocyclic thiacyclic ethers with bivalent transitional metals (Cu, Co, Ni and Zn)*. *Rapid Communications in Mass Spectrometry*, 2012. **26**(19): p. 2287-2294.
414. Mondal, B., Lohar, S., Pal, S., Maji, A., and Chattopadhyay, P., *A new chemosensor selective for Cu²⁺ ions through fluorescence quenching approach applicable to real samples*. *Journal of the Indian Chemical Society*, 2015. **92**: p. 1-8.
415. Yang, Z., She, M., Zhang, J., Chen, X., Huang, Y., Zhu, H., Liu, P., Li, J., and Shi, Z., *Highly sensitive and selective rhodamine Schiff base "off-on" chemosensors for Cu²⁺ imaging in living cells*. *Sensors and Actuators B: Chemical*, 2013. **176**: p. 482-487.
416. Bing, Q., Wang, L., Li, D., and Wang, G., *A new high selective and sensitive turn-on fluorescent and ratiometric absorption chemosensor for Cu²⁺ based on benzimidazole in aqueous solution and its application in live cell*. *Spectrochimica Acta Part A: Molecular and Biomolecular Spectroscopy*, 2018. **202**: p. 305-313.
417. Nouri Moghadam, F., Amirnasr, M., Meghdadi, S., Eskandari, K., Buchholz, A., and Plass, W., *A new fluorene derived Schiff-base as a dual selective fluorescent probe for Cu²⁺ and CN⁻*. *Spectrochimica Acta Part A: Molecular and Biomolecular Spectroscopy*, 2019. **207**: p. 6-15.
418. Gündüz, Z.Y., Gündüz, C., Özpınar, C., and Urucu, O.A., *A novel Schiff-base as a Cu(II) ion fluorescent sensor in aqueous solution*. *Spectrochimica Acta Part A: Molecular and Biomolecular Spectroscopy*, 2015. **136**: p. 1679-1683.
419. Shao, N., Zhang, Y., Cheung, S., Yang, R., Chan, W., Mo, T., Li, K., and Liu, F., *Copper Ion-Selective Fluorescent Sensor Based on the Inner Filter Effect Using a Spiropyran Derivative*. *Analytical Chemistry*, 2005. **77**(22): p. 7294-7303.
420. Luo, H.-Y., Zhang, X.-B., Jiang, J.-H., Li, C.-Y., Peng, J., Shen, G.-L., and Yu, R.-Q., *An Optode Sensor for Cu²⁺ with High Selectivity Based on Porphyrin Derivative Appended with Bipyridine*. *Analytical Sciences*, 2007. **23**(5): p. 551-555.
421. Aksuner, N., Henden, E., Yilmaz, I., and Cukurovali, A., *A highly sensitive and selective fluorescent sensor for the determination of copper(II) based on a schiff base*. *Dyes and Pigments*, 2009. **83**(2): p. 211-217.
422. Gholivand, M.B., Niroomandi, P., Yari, A., and Joshagani, M., *Characterization of an optical copper sensor based on N,N'-bis(salicylidene)-1,2-phenylenediamine*. *Analytica Chimica Acta*, 2005. **538**(1): p. 225-231.
423. Peralta-Domínguez, D., Rodríguez, M., Ramos-Ortiz, G., Maldonado, J.L., Meneses-Nava, M.A., Barbosa-García, O., Santillan, R., and Farfán, N., *A Schiff base derivative from cinnamaldehyde for colorimetric detection of Ni²⁺ in water*. *Sensors and Actuators B: Chemical*, 2015. **207**: p. 511-517.
424. Goswami, S., Chakraborty, S., Paul, S., Halder, S., and Maity, A.C., *A simple quinoxaline-based highly sensitive colorimetric and ratiometric sensor, selective for nickel and effective in very high dilution*. *Tetrahedron Letters*, 2013. **54**(37): p. 5075-5077.
425. Kang, J.H., Lee, S.Y., Ahn, H.M., and Kim, C., *A novel colorimetric chemosensor for the sequential detection of Ni²⁺ and CN⁻ in aqueous solution*. *Sensors and Actuators B: Chemical*, 2017. **242**: p. 25-34.
426. Biswas, S., Acharyya, S., Sarkar, D., Gharami, S., and Mondal, T.K., *Novel pyridyl based azo-derivative for the selective and colorimetric detection of nickel(II)*. *Spectrochimica Acta Part A: Molecular and Biomolecular Spectroscopy*, 2016. **159**: p. 157-162.
427. Yari, A., Gholivand, M.B., and Rahhedayat, F., *Development and characterization of a new nickel(II) ion selective optode based on 2-amino-1-cyclopentene-dithiocarboxylic acid*. *Measurement*, 2011. **44**(9): p. 1691-1696.
428. Wang, L., Ye, D., and Cao, D., *A novel coumarin Schiff-base as a Ni(II) ion colorimetric sensor*. *Spectrochimica Acta Part A: Molecular and Biomolecular Spectroscopy*, 2012. **90**: p. 40-44.
429. Chowdhury, B., Karar, M., Paul, S., Joshi, M., Choudhury, A.R., and Biswas, B., *Salen Type Ligand as a Selective and Sensitive Nickel(II) ion Chemosensor: A Combined Investigation with Experimental and Theoretical Modelling*. *Sensors and Actuators B: Chemical*, 2018. **276**: p. 560-566.
430. Ganjali, M.R., Hosseini, M., Motalebi, M., Sedaghat, M., Mizani, F., Faridbod, F., and Norouzi, P., *Selective recognition of Ni²⁺ ion based on fluorescence enhancement chemosensor*. *Spectrochimica Acta Part A: Molecular and Biomolecular Spectroscopy*, 2015. **140**: p. 283-287.
431. Aksuner, N., Henden, E., Yilmaz, I., and Cukurovali, A., *A novel optical chemical sensor for the determination of nickel(II) based on fluorescence quenching of newly synthesized thiazolo-triazol derivative and application to real samples*. *Sensors and Actuators B: Chemical*, 2012. **166-167**: p. 269-274.
432. Awual, M.R., Eldesoky, G.E., Yaita, T., Naushad, M., Shiwaku, H., AlOthman, Z.A., and Suzuki, S., *Schiff based ligand containing nano-composite adsorbent for optical copper(II) ions removal from aqueous solutions*. *Chemical Engineering Journal*, 2015. **279**: p. 639-647.
433. Ma, D.-L., Ma, V.P.-Y., Chan, D.S.-H., Leung, K.-H., He, H.-Z., and Leung, C.-H., *Recent advances in luminescent heavy metal complexes for sensing*. *Coordination Chemistry Reviews*, 2012. **256**(23): p. 3087-3113.

434. Paderni, D., Giorgi, L., Fusi, V., Formica, M., Ambrosi, G., and Micheloni, M., *Chemical sensors for rare earth metal ions*. Coordination Chemistry Reviews, 2020: p. 213639.
435. Abbaspour, A. and Kamyabi, M.A., *Copper(II)-selective electrode based on dithioacetal*. Analytica Chimica Acta, 2002. **455**(2): p. 225-231.
436. Gholivand, M.B. and Nozari, N., *Copper(II)-selective electrode using 2,2'-dithiodianiline as neutral carrier*. Talanta, 2001. **54**(4): p. 597-602.
437. Kamata, S., Murata, H., Kubo, Y., and Bhale, A., *Copper(II)-selective membrane electrodes based on o-xyllylene bis(dithiocarbamates) as neutral carriers*. Analyst, 1989. **114**(9): p. 1029-1031.
438. Kamata, S., Bhale, A., Fukunaga, Y., and Murata, H., *Copper(II)-selective electrode using thiuram disulfide neutral carriers*. Analytical Chemistry, 1988. **60**(22): p. 2464-2467.
439. Paul, A., Nair, R.R., Chatterjee, P.B., and Srivastava, D.N., *Fabrication of a Cu(II)-Selective Electrode in the Polyvinyl Chloride Matrix Utilizing Mechanochemically Synthesized Rhodamine 6g as an Ionophore*. ACS Omega, 2018. **3**(11): p. 16230-16237.
440. Jeong, D.-C., Lee, H.-K., and Jeon, S.-W., *Highly Copper(II)-selective PVC Membrane Based on a Schiff Base Complex of N,N'-Bis-pyridin-2-ylmethylene-naphthalene-1,8-diamine as an Ionophore*. Bulletin of the Korean Chemical Society, 2006. **27**(10): p. 1593-1596.
441. Zamani, H.A., Rajabzadeh, G., Ganjali, M.R., and Khatami, S.M., *Highly Selective and Sensitive Copper(II) Membrane Sensors Based on 6-Methyl-4-(1-phenylmethylidene)amino-3-thioxo-1,2,4-triazin-5-one as a New Neutral Ionophore*. Electroanalysis, 2005. **17**(24): p. 2260-2265.
442. Mittal, S.K., Kumar, A., Gupta, N., Kaur, S., and Kumar, S., *8-hydroxyquinoline based neutral tripodal ionophore as a copper (II) selective electrode and the effect of remote substituents on electrode properties*. Analytica Chimica Acta, 2007. **585**(1): p. 161-170.
443. Gupta, V.K., Jain, A.K., Maheshwari, G., Lang, H., and Ishtaiwi, Z., *Copper(II)-selective potentiometric sensors based on porphyrins in PVC matrix*. Sensors and Actuators B: Chemical, 2006. **117**(1): p. 99-106.
444. Hasani, B., Zamani, A., Mofakhar, M.K., Mostafavi, M., Yafatian, M.R., and Ghorbanloo, M., *Ionophore Properties of Schiff Base Compounds as Ion Sensing Molecules for Fabricating Cu(II) Ion-Selective Electrodes*. Journal of Analytical Chemistry, 2018. **73**(1): p. 82-90.
445. Mashhadizadeh, M.H., Mostafavi, A., Razavi, R., and Shamsipur, M., *Highly selective Cu(II) PVC membrane electrode based on 3,6,9,14-tetrathiabicyclo[9.2.1]tetradeca-11,13-diene as a suitable neutral ionophore*. Sensors and Actuators B: Chemical, 2002. **86**(2): p. 222-228.
446. Kopylovich, M.N., Mahmudov, K.T., and Pombeiro, A.J.L., *Poly(vinyl) chloride membrane copper-selective electrode based on 1-phenyl-2-(2-hydroxyphenylhydrazo)butane-1,3-dione*. Journal of Hazardous Materials, 2011. **186**(2): p. 1154-1162.
447. Chandra, S., Tomar, P.K., Kumar, A., Malik, A., and Singh, A., *Fabrication of copper-selective PVC membrane electrode based on newly synthesized copper complex of Schiff base as carrier*. Journal of Saudi Chemical Society, 2016. **20**: p. S293-S299.
448. Shamsipur, M., Avanes, A., Javanbakht, M., Ganjali, M.R., and Sharghi, H., *A 9,10-anthraquinone derivative having two propenyl arms as a neutral ionophore for highly selective and sensitive membrane sensors for copper(II) ion*. Analytical Sciences, 2002. **18**(8): p. 875-9.
449. Jain, A.K., Gupta, V.K., Singh, L.P., and Raisoni, J.R., *Chelating ionophore based membrane sensors for copper(II) ions*. Talanta, 2005. **66**(5): p. 1355-1361.
450. Ghanei-Motlagh, M., Taher, M.A., Saheb, V., Fayazi, M., and Sheikhshoae, I., *Theoretical and practical investigations of copper ion selective electrode with polymeric membrane based on N,N'-(2,2-dimethylpropane-1,3-diyl)-bis(dihydroxyacetophenone)*. Electrochimica Acta, 2011. **56**(15): p. 5376-5385.
451. Demir, S., Yilmaz, H., Dilimulati, M., and Andac, M., *Spectral and thermal characterization of salophen type Schiff base and its implementation as solid contact electrode for quantitative monitoring of copper(II) ion*. Spectrochimica Acta Part A: Molecular and Biomolecular Spectroscopy, 2015. **150**: p. 523-532.
452. Pouya, F., Arabi, M., and Absalan, G., *Application of 2-(benzyliminomethyl)-6-methoxy-4-(4-methoxyphenyl-azo)phenol in construction of ion-selective PVC membrane electrode for determination of copper (II) in mineral water sample*. Applied Organometallic Chemistry, 2018. **32**(2): p. e4040.
453. Fakhari, A.R., Raji, T.A., and Naeimi, H., *Copper-selective PVC membrane electrodes based on salens as carriers*. Sensors and Actuators B: Chemical, 2005. **104**(2): p. 317-323.
454. Sadeghi, S., Eslahi, M., Naseri, M.A., Naeimi, H., Sharghi, H., and Shameli, A., *Copper Ion Selective Membrane Electrodes Based on Some Schiff Base Derivatives*. Electroanalysis, 2003. **15**(15-16): p. 1327-1333.
455. Zamani, H.A., Rajabzadeh, G., Firouz, A., and Ganjali, M.R., *Determination of copper(II) in wastewater by electroplating samples using a PVC-membrane copper(II)-selective electrode*. Journal of Analytical Chemistry, 2007. **62**(11): p. 1080-1087.

456. Brinić, S., Buzuk, M., Bralić, M., and Generalić, E., *Solid-contact Cu(II) ion-selective electrode based on 1,2-di-(o-salicylaldiminophenylthio)ethane*. Journal of Solid State Electrochemistry, 2012. **16**(4): p. 1333-1341.
457. Gupta, K.C. and Jeanne D'Arc, M., *Effect of concentration of ion exchanger, plasticizer and molecular weight of cyanocopolymers on selectivity and sensitivity of Cu(II) ion selective electrodes*. Analytica Chimica Acta, 2001. **437**(2): p. 199-216.
458. Karimipour, G., Ghaedi, M., Behfar, M., Andikaey, Z., Kowkabi, S., and Orojloo, A.H., *Synthesis and Application of New Porphyrin Derivatives for Preparation of Copper Selective Electrodes: Influence of Carbon Nanotube on Their Responses*. IEEE Sensors Journal, 2012. **12**(8): p. 2638-2647.
459. Afkhami, A., Khoshsafar, H., Madrakian, T., and Shirzadmehr, A., *A new nano-composite electrode as a copper (II) selective potentiometric sensor*. Journal of the Iranian Chemical Society, 2014. **11**(5): p. 1373-1380.
460. Ali, T.A., Mohamed, G.G., El-Dessouky, M.M.I., Abou El-Ella, S.M., and Mohamed, R.T.F., *Modified Screen-Printed Electrode for Potentiometric Determination of Copper(II) in Water Samples*. Journal of Solution Chemistry, 2013. **42**(6): p. 1336-1354.
461. Czirok, J.B., Jágerszki, G., Tóth, K., Révész, Á., Drahos, L., and Bitter, I., *Click synthesis of triazole-linked calix[4]arene ionophores. Potentiometric and ESI-MS screening of ion-selectivity*. Journal of Inclusion Phenomena and Macrocyclic Chemistry, 2014. **78**(1): p. 207-215.
462. Singh, A.K., Sharma, C.L., Baniwal, S., and Panwar, A., *Nickel(II)-Selective Membrane Electrode Based on Macrocyclic Ligand*. Electroanalysis, 2001. **13**(14): p. 1209-1214.
463. Mashhadizadeh, M.H., Sheikshoae, I., and Saeid-Nia, S., *Nickel(II)-selective membrane potentiometric sensor using a recently synthesized Schiff base as neutral carrier*. Sensors and Actuators B: Chemical, 2003. **94**(3): p. 241-246.
464. Mashhadizadeh, M.H. and Momeni, A., *Nickel(II) selective membrane potentiometric sensor using a recently synthesized mercapto compound as neutral carrier*. Talanta, 2003. **59**(1): p. 47-53.
465. Mazloum, M., Niassary, M.S., and Amini, M.K., *Pentacyclooctaaza as a neutral carrier in coated-wire ion-selective electrode for nickel(II)*. Sensors and Actuators B: Chemical, 2002. **82**(2): p. 259-264.
466. Girish Kumar, K., Poduval, R., John, S., and Augustine, P., *A PVC plasticized membrane sensor for nickel ions*. Microchimica Acta, 2006. **156**(3): p. 283-287.
467. Singh, L.P. and Bhatnagar, J.M., *PVC Based Selective Sensors for Ni²⁺ Ions Using Carboxylated and Methylated Porphine*. Sensors, 2003. **3**(9).
468. Shamsipur, M. and Kazemi, S.Y., *A PVC-Based Dibenzo[di]aza-15-crown-4 Membrane Potentiometric Sensor for Ni(II)*. Electroanalysis, 2000. **12**(18): p. 1472-1475.
469. Yari, A., Azizi, S., and Kakanejadifard, A., *An electrochemical Ni(II)-selective sensor-based on a newly synthesized dioxime derivative as a neutral ionophore*. Sensors and Actuators B: Chemical, 2006. **119**(1): p. 167-173.
470. Gupta, V.K., Prasad, R., and Kumar, A., *Dibenzocyclamnickel(II) as Ionophore in PVC-Matrix for Ni²⁺-Selective Sensor*. Sensors, 2002. **2**(10).
471. Gupta, V.K., Prasad, R., Kumar, P., and Mangla, R., *New nickel(II) selective potentiometric sensor based on 5,7,12,14-tetramethyldibenzo[di]azaannulene in a poly(vinyl chloride) matrix*. Analytica Chimica Acta, 2000. **420**(1): p. 19-27.
472. Jain, A.K., Gupta, V.K., Singh, R.D., Khurana, U., and Singh, L.P., *Nickel(II)-selective sensors based on heterogeneous membranes of macrocyclic compounds*. Sensors and Actuators B: Chemical, 1997. **40**(1): p. 15-20.
473. Gupta, V.K., Goyal, R.N., Agarwal, S., Kumar, P., and Bachheti, N., *Nickel(II)-selective sensor based on dibenzo-18-crown-6 in PVC matrix*. Talanta, 2007. **71**(2): p. 795-800.
474. Mousavi, M.F., Alizadeh, N., Shamsipur, M., and Zohari, N., *A new PVC-based 1,10-dibenzyl-1,10-diaza-18-crown-6 selective electrode for detecting nickel(II)ion*. Sensors and Actuators B: Chemical, 2000. **66**(1): p. 98-100.
475. Gupta, V.K., Jain, A.K., Ishtaiwi, Z., Lang, H., and Maheshwari, G., *Ni²⁺ selective sensors based on meso-tetrakis-{4-[tris-(4-allyl dimethylsilyl-phenyl)-silyl]-phenyl}porphyrin and (sal)2trien in poly(vinyl chloride) matrix*. Talanta, 2007. **73**(5): p. 803-811.
476. Elsaid, F.A.G., Hamza, S., Rizk, N., Matter, H.A.B., and Amerah, E.A.S., *Ni²⁺ Selective Membrane Sensors Based on Sulfamethoxazole Diazonium Resorcinol in Poly (Vinyl Chloride) (PVC) Matrix*. Arabian Journal for Science and Engineering, 2013. **38**(7): p. 1681-1689.
477. Jain, A.K., Gupta, V.K., Ganeshpure, P.A., and Raison, J.R., *Ni(II)-selective ion sensors of salen type Schiff base chelates*. Analytica Chimica Acta, 2005. **553**(1): p. 177-184.
478. Gupta, V.K., Singh, A.K., and Pal, M.K., *Ni(II) selective sensors based on Schiff bases membranes in poly(vinyl chloride)*. Analytica Chimica Acta, 2008. **624**(2): p. 223-231.

479. Tomar, P.K., Chandra, S., Malik, A., and Kumar, A., *Nickel analysis in real samples by Ni²⁺ selective PVC membrane electrode based on a new Schiff base*. Materials Science and Engineering: C, 2013. **33**(8): p. 4978-4984.
480. Ganjali, M.R., Alahdadi, I., Aghazadeh, M., and Pourbasheer, E., *All Solid State (ASS) Polymeric Membrane Sensor (PMS) for the Monitoring of Nanomolar Nickel Concentration*. International Journal of Electrochemical Science, 2015. **10**: p. 6913-6923.
481. Gupta, V.K., Jain, A.K., Singh, L.P., and Khurana, U., *Porphyryns as carrier in PVC based membrane potentiometric sensors for nickel(II)*. Analytica Chimica Acta, 1997. **355**(1): p. 33-41.
482. Ma, Y.-H., Yuan, R., Chai, Y.-Q., Wu, X., Zhou, W., Liu, X.-L., and Deng, F., *New Ni(II) Ion-Selective Electrode Based on the N-S Schiff Base Ligand as Neutral Carrier in PVC Matrix*. Analytical Letters, 2009. **42**(15): p. 2411-2429.
483. Matsushita, A.F.Y., Tapia, M.J., Pais, A.A.C.C., and Valente, A.J.M., *Luminescent Properties of Lanthanoid-Poly(Sodium Acrylate) Composites: Insights on the Interaction Mechanism*. Polymers, 2020. **12**(6): p. 1314.
484. Berhanu, A.L., Gaurav, Mohiuddin, I., Malik, A.K., Aulakh, J.S., Kumar, V., and Kim, K.-H., *A review of the applications of Schiff bases as optical chemical sensors*. TrAC Trends in Analytical Chemistry, 2019. **116**: p. 74-91.
485. Al Zoubi, W., Al-Hamdani, A.A.S., and Kaseem, M., *Synthesis and antioxidant activities of Schiff bases and their complexes: a review*. Applied Organometallic Chemistry, 2016. **30**(10): p. 810-817.
486. Slassi, S., El-Ghayoury, A., Aarjane, M., Yamni, K., and Amine, A., *New copper(II) and zinc(II) complexes based on azo Schiff base ligand: Synthesis, crystal structure, photoisomerization study and antibacterial activity*. Applied Organometallic Chemistry, 2020. **34**(4): p. e5503.
487. Pessoa, J.C. and Correia, I., *Salan vs. salen metal complexes in catalysis and medicinal applications: Virtues and pitfalls*. Coordination Chemistry Reviews, 2019. **388**: p. 227-247.
488. Erxleben, A., *Transition metal salen complexes in bioinorganic and medicinal chemistry*. Inorganica Chimica Acta, 2018. **472**: p. 40-57.
489. Wang, J. and Zhuang, S., *Cesium separation from radioactive waste by extraction and adsorption based on crown ethers and calixarenes*. Nuclear Engineering and Technology, 2020. **52**(2): p. 328-336.
490. Mohammadzadeh Kakhki, R. and Rakhshanipour, M., *Application of nanoparticle modified with crown ether in colorimetric determinations*. Arabian Journal of Chemistry, 2019. **12**(8): p. 3096-3107.
491. Pettinari, C., Marchetti, F., and Drozdov, A., *1.11 - Higher Denticity Ligands*, in *Comprehensive Coordination Chemistry II*, J.A. McCleverty and Meyer, T.J., Editors. 2003, Pergamon: Oxford. p. 211-251.
492. Min Park, J., Lee, J.H., and Jang, W.-D., *Applications of porphyrins in emerging energy conversion technologies*. Coordination Chemistry Reviews, 2020. **407**: p. 213157.
493. Younis, S.A., Lim, D.-K., Kim, K.-H., and Deep, A., *Metalloporphyrinic metal-organic frameworks: Controlled synthesis for catalytic applications in environmental and biological media*. Advances in Colloid and Interface Science, 2020. **277**: p. 102108.
494. Zhang, X., Wasson, M.C., Shayan, M., Berdichevsky, E.K., Ricardo-Noordberg, J., Singh, Z., Papazyan, E.K., Castro, A.J., Marino, P., Ajoyan, Z., Chen, Z., Islamoglu, T., Howarth, A.J., Liu, Y., Majewski, M.B., Katz, M.J., Mondloch, J.E., and Farha, O.K., *A historical perspective on porphyrin-based metal-organic frameworks and their applications*. Coordination Chemistry Reviews, 2020: p. 213615.
495. Giancane, G. and Valli, L., *State of art in porphyrin Langmuir-Blodgett films as chemical sensors*. Advances in Colloid and Interface Science, 2012. **171-172**: p. 17-35.
496. Awual, M.R., Yaita, T., El-Safty, S.A., Shiwaku, H., Suzuki, S., and Okamoto, Y., *Copper(II) ions capturing from water using ligand modified a new type mesoporous adsorbent*. Chemical Engineering Journal, 2013. **221**: p. 322-330.
497. Enache, D.F., Vasile, E., Simonescu, C.M., Culita, D., Vasile, E., Oprea, O., Pandele, A.M., Razvan, A., Dumitru, F., and Nechifor, G., *Schiff base-functionalized mesoporous silicas (MCM-41, HMS) as Pb(II) adsorbents*. RSC Advances, 2018. **8**(1): p. 176-189.
498. Kursunlu, A.N., Guler, E., Dumrul, H., Kocyigit, O., and Gubbuk, I.H., *Chemical modification of silica gel with synthesized new Schiff base derivatives and sorption studies of cobalt (II) and nickel (II)*. Applied Surface Science, 2009. **255**(21): p. 8798-8803.
499. Qiao, W., Zhang, P., Sun, L., Ma, S., Xu, W., Xu, S., and Niu, Y., *Adsorption performance and mechanism of Schiff base functionalized polyamidoamine dendrimer/silica for aqueous Mn(II) and Co(II)*. Chinese Chemical Letters, 2020. **31**(10): p. 2742-2746.
500. Durães, L., Maia, A., and Portugal, A., *Effect of additives on the properties of silica based aerogels synthesized from methyltrimethoxysilane (MTMS)*. The Journal of Supercritical Fluids, 2015. **106**: p. 85-92.

501. Posada, D. and Buckley, T.R., *Model Selection and Model Averaging in Phylogenetics: Advantages of Akaike Information Criterion and Bayesian Approaches Over Likelihood Ratio Tests*. Systematic Biology, 2004. **53**(5): p. 793-808.
502. Durães, L., Ochoa, M., Portugal, A., Duarte, N., Dias, J.P., Rocha, N., and Hernandez, J., *Tailored Silica Based Xerogels and Aerogels for Insulation in Space Environments*. Advances in Science and Technology, 2010. **63**: p. 41-46.
503. Howard, A.G. and Khdary, N.H., *Spectrofluorimetric determination of surface-bound thiol groups and its application to the analysis of thiol-modified silicas*. Analyst, 2004. **129**(9): p. 860-863.
504. Jung, H.-S., Moon, D.-S., and Lee, J.-K., *Quantitative Analysis and Efficient Surface Modification of Silica Nanoparticles*. Journal of Nanomaterials, 2012. **2012**: p. 8.
505. Reichenauer, G. and Scherer, G.W., *Nitrogen sorption in aerogels*. Journal of Non-Crystalline Solids, 2001. **285**(1-3): p. 167-174.
506. Reichenauer, G. and Scherer, G.W., *Effects upon Nitrogen Sorption Analysis in Aerogels*. Journal of Colloid and Interface Science, 2001. **236**(2): p. 385-386.
507. Lamy-Mendes, A., Girão, A.V., Silva, R.F., and Durães, L., *Polysilsesquioxane-based silica aerogel monoliths with embedded CNTs*. Microporous and Mesoporous Materials, 2019. **288**: p. 109575.
508. Lee, J.Y., Chen, C.H., Cheng, S., and Li, H.Y., *Adsorption of Pb(II) and Cu(II) metal ions on functionalized large-pore mesoporous silica*. International Journal of Environmental Science and Technology, 2016. **13**(1): p. 65-76.
509. Soliman, E.M., *Synthesis and Metal Collecting Properties of Mono, Di, Tri and Tetramine Based on Silica Gel Matrix*. Analytical Letters, 1997. **30**(9): p. 1739-1751.
510. Burnham, K.P. and Anderson, D.R., *Multimodel inference: understanding AIC and BIC in model selection*. Sociological methods & research, 2004. **33**(2): p. 261-304.
511. Mazerolle, M., *Improving data analysis in herpetology: using Akaike's Information Criterion (AIC) to assess the strength of biological hypotheses*. Amphibia-Reptilia, 2006. **27**(2): p. 169-180.
512. Matias, T., Marques, J., Quina, M.J., Gando-Ferreira, L., Valente, A.J.M., Portugal, A., and Durães, L., *Silica-based aerogels as adsorbents for phenol-derivative compounds*. Colloids and Surfaces A: Physicochemical and Engineering Aspects, 2015. **480**: p. 260-269.
513. Burke, A.M., Hanrahan, J.P., Healy, D.A., Sodeau, J.R., Holmes, J.D., and Morris, M.A., *Large pore bi-functionalised mesoporous silica for metal ion pollution treatment*. Journal of Hazardous Materials, 2009. **164**(1): p. 229-234.
514. Cui, X., Fang, S., Yao, Y., Li, T., Ni, Q., Yang, X., and He, Z., *Potential mechanisms of cadmium removal from aqueous solution by Canna indica derived biochar*. Science of The Total Environment, 2016. **562**(Supplement C): p. 517-525.
515. Han, H., Wei, W., Jiang, Z., Lu, J., Zhu, J., and Xie, J., *Removal of cationic dyes from aqueous solution by adsorption onto hydrophobic/hydrophilic silica aerogel*. Colloids and Surfaces A: Physicochemical and Engineering Aspects, 2016. **509**: p. 539-549.
516. Harlick, P.J.E. and Sayari, A., *Applications of Pore-Expanded Mesoporous Silicas. 3. Triamine Silane Grafting for Enhanced CO₂ Adsorption*. Industrial & Engineering Chemistry Research, 2006. **45**(9): p. 3248-3255.
517. Begag, R., Krutka, H., Dong, W., Mihalcik, D., Rhine, W., Gould, G., Baldic, J., and Nahass, P., *Superhydrophobic amine functionalized aerogels as sorbents for CO₂ capture*. Greenhouse Gases: Science and Technology, 2013. **3**(1): p. 30-39.
518. Kong, Y., Jiang, G., Wu, Y., Cui, S., and Shen, X., *Amine hybrid aerogel for high-efficiency CO₂ capture: Effect of amine loading and CO₂ concentration*. Chemical Engineering Journal, 2016. **306**: p. 362-368.
519. Duan, Y., Jana, S.C., Lama, B., and Espe, M.P., *Reinforcement of Silica Aerogels Using Silane-End-Capped Polyurethanes*. Langmuir, 2013. **29**(20): p. 6156-6165.
520. Wang, Z., Zhou, Q., Guo, H., Yang, P., and Lu, W., *Determination of water solubility in supercritical CO₂ from 313.15 to 473.15 K and from 10 to 50 MPa by in-situ quantitative Raman spectroscopy*. Fluid Phase Equilibria, 2018. **476**: p. 170-178.
521. Tadanaga, K. and Minami, T., *Measurements of Gas Adsorption and Permeability of Sol-Gel Materials*, in *Handbook of Sol-Gel Science and Technology: Processing, Characterization and Applications*, L. Klein, Aparicio, M., and Jitianu, A., Editors. 2018, Springer International Publishing: Cham. p. 1411-1423.
522. Reichenauer, G., *Structural Characterization of Aerogels*, in *Aerogels Handbook*, M.A. Aegerter, Leventis, N., and Koebel, M.M., Editors. 2011, Springer New York: New York, NY. p. 449-498.
523. Issa, A.A. and Luyt, A.S., *Kinetics of Alkoxysilanes and Organoalkoxysilanes Polymerization: A Review*. Polymers, 2019. **11**(3): p. 537.

524. Al-Oweini, R. and El-Rassy, H., *Synthesis and characterization by FTIR spectroscopy of silica aerogels prepared using several $\text{Si}(\text{OR})_4$ and $\text{R}'\text{Si}(\text{OR}')_3$ precursors*. Journal of Molecular Structure, 2009. **919**(1-3): p. 140-145.
525. Itagaki, A., Nakanishi, K., and Hirao, K., *Phase Separation in Sol-Gel System Containing Mixture of 3- and 4-Functional Alkoxysilanes*. Journal of Sol-Gel Science and Technology, 2003. **26**(1): p. 153-156.
526. Díaz, M., Palop, J.A., Sanmartín, C., and Lizarraga, E., *Thermal stability and decomposition of urea, thiourea and selenourea analogous diselenide derivatives*. Journal of Thermal Analysis and Calorimetry, 2017. **127**(2): p. 1663-1674.
527. Icenhower, J. and Dove, P.M., *Water behavior at silica surfaces*, in *Adsorption on Silica Surfaces*, E. Papirer, Editor. 2000, Marcel Dekker: New York. p. 277-295.
528. Kosmulski, M., *Surface charge and zeta potential of silica in mixtures of organic solvents and water*, in *Adsorption on Silica Surfaces* E. Papirer, Editor. 2000, Marcel Dekker: New York. p. 343-67.
529. Klonkowski, A.M., Grobelna, B., Widernik, T., Jankowska-Frydel, A., and Mozgawa, W., *The Coordination State of Copper(II) Complexes Anchored and Grafted onto the Surface of Organically Modified Silicates*. Langmuir, 1999. **15**(18): p. 5814-5819.
530. Lam, K.F., Chen, X., McKay, G., and Yeung, K.L., *Anion Effect on Cu^{2+} Adsorption on NH_2 -MCM-41*. Industrial & Engineering Chemistry Research, 2008. **47**(23): p. 9376-9383.
531. Pan, A., Biswas, T., Rakshit, A.K., and Moulik, S.P., *Enthalpy-Entropy Compensation (EEC) Effect: A Revisit*. The Journal of Physical Chemistry B, 2015. **119**(52): p. 15876-15884.
532. Wang, X.-S., Huang, J., Hu, H.-Q., Wang, J., and Qin, Y., *Determination of kinetic and equilibrium parameters of the batch adsorption of $\text{Ni}(\text{II})$ from aqueous solutions by Na-mordenite*. Journal of Hazardous Materials, 2007. **142**(1): p. 468-476.
533. Wang, X.S., Hu, H.Q., and Sun, C., *Removal of Copper (II) Ions from Aqueous Solutions using Na-mordenite*. Separation Science and Technology, 2007. **42**(6): p. 1215-1230.
534. Agarwal, B., Balomajumder, C., and Thakur, P.K., *Simultaneous co-adsorptive removal of phenol and cyanide from binary solution using granular activated carbon*. Chemical Engineering Journal, 2013. **228**(Supplement C): p. 655-664.
535. Afolabi, F.O., Musonge, P., and Bakare, B.F., *Bio-sorption of copper and lead ions in single and binary systems onto banana peels*. Cogent Engineering, 2021. **8**(1): p. 1886730.
536. Jiang, J., Xu, R.-k., and Li, S.-z., *Effect of Ionic Strength and Mechanism of $\text{Cu}(\text{II})$ Adsorption by Goethite and $\gamma\text{-Al}_2\text{O}_3$* . Journal of Chemical & Engineering Data, 2010. **55**(12): p. 5547-5552.
537. Hu, X.-j., Liu, Y.-g., Wang, H., Zeng, G.-m., Hu, X., Guo, Y.-m., Li, T.-t., Chen, A.-w., Jiang, L.-h., and Guo, F.-y., *Adsorption of copper by magnetic graphene oxide-supported β -cyclodextrin: Effects of pH, ionic strength, background electrolytes, and citric acid*. Chemical Engineering Research and Design, 2015. **93**: p. 675-683.
538. Wang, S., Vincent, T., Faur, C., and Guibal, E., *Modeling competitive sorption of lead and copper ions onto alginate and greenly prepared algal-based beads*. Bioresource Technology, 2017. **231**: p. 26-35.
539. Fan, H.-T., Sun, X.-T., Zhang, Z.-G., and Li, W.-X., *Selective Removal of Lead(II) from Aqueous Solution by an Ion-Imprinted Silica Sorbent Functionalized with Chelating N-Donor Atoms*. Journal of Chemical & Engineering Data, 2014. **59**(6): p. 2106-2114.
540. Panayotova, M. and Velikov, B., *Kinetics of heavy metal ions removal by use of natural zeolite*. Journal of Environmental Science and Health, Part A, 2002. **37**(2): p. 139-147.
541. Moore, B.D., Sherrington, D.C., and Zitsmanis, A., *Conversion of a glycidyl methacrylate resin into a thiirane analogue and subsequent immobilisation of aliphatic amine andazole ligands*. Journal of Materials Chemistry, 1992. **2**(12): p. 1231-1236.
542. Antony, R., Marimuthu, R., Vishnoi, P., and Murugavel, R., *Ethoxysilane appended $\text{M}(\text{II})$ complexes and their $\text{SiO}_2/\text{MCM-41}$ supported forms as catalysts for efficient oxidation of secondary alcohols*. Inorganica Chimica Acta, 2018. **469**: p. 173-182.
543. Bhunia, S. and Koner, S., *Tethering of nickel(II) Schiff-base complex onto mesoporous silica: An efficient heterogeneous catalyst for epoxidation of olefins*. Polyhedron, 2011. **30**(11): p. 1857-1864.
544. Kühne, T.D., Iannuzzi, M., Del Ben, M., Rybkin, V.V., Seewald, P., Stein, F., Laino, T., Khaliullin, R.Z., Schütt, O., Schiffmann, F., Golze, D., Wilhelm, J., Chulkov, S., Bani-Hashemian, M.H., Weber, V., Borštnik, U., Taillefumier, M., Jakobovits, A.S., Lazzaro, A., Pabst, H., Müller, T., Schade, R., Guidon, M., Andermatt, S., Holmberg, N., Schenter, G.K., Hehn, A., Bussy, A., Belleflamme, F., Tabacchi, G., Glöß, A., Lass, M., Bethune, I., Mundy, C.J., Plessl, C., Watkins, M., VandeVondele, J., Krack, M., and Hutter, J., *CP2K: An electronic structure and molecular dynamics software package - Quickstep: Efficient and accurate electronic structure calculations*. The Journal of Chemical Physics, 2020. **152**(19): p. 194103.

545. Grimme, S., Bannwarth, C., and Shushkov, P., *A Robust and Accurate Tight-Binding Quantum Chemical Method for Structures, Vibrational Frequencies, and Noncovalent Interactions of Large Molecular Systems Parametrized for All spd-Block Elements (Z = 1–86)*. Journal of Chemical Theory and Computation, 2017. **13**(5): p. 1989-2009.
546. Grimme, S., Antony, J., Ehrlich, S., and Krieg, H., *A consistent and accurate ab initio parametrization of density functional dispersion correction (DFT-D) for the 94 elements H-Pu*. The Journal of Chemical Physics, 2010. **132**(15): p. 154104.
547. Soto-Cantu, E., Cueto, R., Koch, J., and Russo, P.S., *Synthesis and Rapid Characterization of Amine-Functionalized Silica*. Langmuir, 2012. **28**(13): p. 5562-5569.
548. Sheng, W., Wei, W., Li, J., Qi, X., Zuo, G., Chen, Q., Pan, X., and Dong, W., *Amine-functionalized magnetic mesoporous silica nanoparticles for DNA separation*. Applied Surface Science, 2016. **387**: p. 1116-1124.
549. Hsiao, I.L., Fritsch-Decker, S., Leidner, A., Al-Rawi, M., Hug, V., Diabaté, S., Grage, S.L., Meffert, M., Stoeger, T., Gerthsen, D., Ulrich, A.S., Niemeyer, C.M., and Weiss, C., *Biocompatibility of Amine-Functionalized Silica Nanoparticles: The Role of Surface Coverage*. Small, 2019. **15**(10): p. 1805400.
550. Thommes, M., Kaneko, K., Neimark, A.V., Olivier, J.P., Rodriguez-Reinoso, F., Rouquerol, J., and Sing, K.S.W., *Physisorption of gases, with special reference to the evaluation of surface area and pore size distribution (IUPAC Technical Report)*. Pure and Applied Chemistry, 2015. **87**(9-10): p. 1051-1069.
551. Šćiban, M., Radetić, B., Kevresan, Z., and Klasnja, M., *Adsorption of heavy metals from electroplating wastewater by wood sawdust*. Bioresource technology, 2007. **98**(2): p. 402-409.
552. Teow, Y.H., Kam, L.M., and Mohammad, A.W., *Synthesis of cellulose hydrogel for copper (II) ions adsorption*. Journal of Environmental Chemical Engineering, 2018. **6**(4): p. 4588-4597.
553. Danesh, N., Ghorbani, M., and Marjani, A., *Separation of copper ions by nanocomposites using adsorption process*. Scientific Reports, 2021. **11**(1): p. 1676.
554. Batool, S., Idrees, M., Hussain, Q., and Kong, J., *Adsorption of copper (II) by using derived-farmyard and poultry manure biochars: Efficiency and mechanism*. Chemical Physics Letters, 2017. **689**: p. 190-198.
555. Jorgetto, A.d.O., da Silva, A.C.P., Wondracek, M.H.P., Silva, R.I.V., Velini, E.D., Saeki, M.J., Pedrosa, V.A., and Castro, G.R., *Multilayer adsorption of Cu(II) and Cd(II) over Brazilian Orchid Tree (Pata-de-vaca) and its adsorptive properties*. Applied Surface Science, 2015. **345**: p. 81-89.
556. Bhadbhade, M.M. and Srinivas, D., *Effects on molecular association, chelate conformation, and reactivity toward substitution in copper Cu(5-X-salen) complexes, salen²⁻ = N,N'-ethylenebis(salicylideneaminato), X = H, CH₃O, and Cl: synthesis, x-ray structures, and EPR investigations*. Inorganic Chemistry, 1993. **32**(24): p. 5458-5466.
557. Mohammadkish, M. and Bagheri, F., *Synthesis and characterization of [Cu(salen)]₂ coordination nano-assembly by a green and simple method*. Zeitschrift für Kristallographie - Crystalline Materials, 2017. **232**(6): p. 407-414.
558. Dong, H., Tao, W., Bi, J., Milway, V., Xu, Z., Zhang, S., Meng, X., Bi, W., Li, J., and Li, M., *Self-assembly of copper and cobalt complexes with hierarchical size and catalytic properties for hydroxylation of phenol*. Nanoscale Research Letters, 2011. **6**(1): p. 484.
559. Nikoorazm, M., Ghorbani-Choghamarani, A., Mahdavi, H., and Esmacili, S.M., *Efficient oxidative coupling of thiols and oxidation of sulfides using UHP in the presence of Ni or Cd salen complexes immobilized on MCM-41 mesoporous as novel and recoverable nanocatalysts*. Microporous and Mesoporous Materials, 2015. **211**: p. 174-181.
560. Ji, C., Zhang, J., Jia, R., Zhang, W., Lv, L., and Pan, B., *Sorption enhancement of nickel(II) from wastewater by ZIF-8 modified with poly (sodium 4-styrenesulfonate): Mechanism and kinetic study*. Chemical Engineering Journal, 2021. **414**: p. 128812.
561. Vareda, J.P., Valente, A.J.M., and Durães, L., *Assessment of heavy metal pollution from anthropogenic activities and remediation strategies: A review*. Journal of Environmental Management, 2019. **246**: p. 101-118.
562. Yang, L., He, L., Xue, J., Wu, L., Ma, Y., Li, H., Peng, P., Li, M., and Zhang, Z., *Highly efficient nickel (II) removal by sewage sludge biochar supported α -Fe₂O₃ and α -FeOOH: Sorption characteristics and mechanisms*. PLOS ONE, 2019. **14**(6): p. e0218114.
563. Šuránek, M., Melichová, Z., Kureková, V., Kljajević, L., and Nenadović, S., *Removal of Nickel from Aqueous Solutions by Natural Bentonites from Slovakia*. Materials, 2021. **14**(2).
564. Siddiqui, M.N., Ali, I., Asim, M., and Chanbasha, B., *Quick removal of nickel metal ions in water using asphalt-based porous carbon*. Journal of Molecular Liquids, 2020. **308**: p. 113078.
565. Veneu, D.M., Yokoyama, L., Cunha, O.G.C., Schneider, C.L., and Monte, M.B.d.M., *Nickel sorption using Bioclastic Granules as a sorbent material: equilibrium, kinetic and characterization studies*. Journal of Materials Research and Technology, 2019. **8**(1): p. 840-852.

566. Becker, T., Schlaak, M., and Strasdeit, H., *Adsorption of nickel(II), zinc(II) and cadmium(II) by new chitosan derivatives*. *Reactive and Functional Polymers*, 2000. **44**(3): p. 289-298.
567. Amemiya, S., *7 - Potentiometric Ion-Selective Electrodes*, in *Handbook of Electrochemistry*, C.G. Zoski, Editor. 2007, Elsevier: Amsterdam. p. 261-294.

Annex I

Distribution of Heavy Metals in Different Locations



The content of this annex is based on the author's published work *Assessment of heavy metal pollution from anthropogenic activities and remediation strategies: A review*.

Table I. 1 - Heavy metal concentration in watercourses of sites affected by mines (minimum and maximum values).

Site [Ref.]	Concentration in water / $\mu\text{g L}^{-1}$							
	Arsenic	Cadmium	Chromium	Copper	Lead	Mercury	Nickel	Zinc
Alto da Várzea, Portugal [83]	1.3 - 32.8	b.d.l. - 4.3	b.d.l. - 8.2	b.d.l. - 77.2	b.d.l. - 50.7	--	b.d.l. - 10.8	b.d.l. - 23.3
S. Francisco Assis, Portugal [112]	1.0 - 7.8	b.d.l. - 0.36	--	2.5 - 10.3	0.2 - 23.1	--	--	5.0 - 319.3
Iberian Pyrite Belt, Spain [85]	0.31 - 3604	b.d.l. - 2119	b.d.l. - 389	1.08 - 222700	b.d.l. - 1607	--	b.d.l. - 13682	b.d.l. - 683503
Meca river, Spain [86]	130	800	--	9200	360	--	220	4090
Assif El Mal, Morocco [87]	--	--	--	80 - 1320	48 - 64	--	31 - 38	3040 - 5980
Yongding River, China [96]	--	--	0.74 - 1.44	0.54 - 2.46	0.10 - 0.42	--	1.59 - 7.95	3.25 - 34.7
Yiyang, China [109]	--	b.d.l. - 40	80 - 660	b.d.l. - 90	b.d.l. - 30	--	10 - 600	3 - 4100
Sidney basin, Australia [97]	b.d.l. - 10	0.1 - 0.2	--	b.d.l. - 13	b.d.l. - 7	--	45 - 220	13 - 400
Anka, Nigeria^a [99]	9736 - 13630	168 - 243	b.d.l.	53 - 210	48 - 153	--	--	--

b.d.l. - below detection limit; a Values refer to mine discharge water.

Environmental Cleaning and Recovery of Heavy Metals via Functionalization of Silica Aerogels

Table I. 2 - Heavy metal concentration in soils and sediments of sites affected by mines (minimum and maximum values).

Site [Ref.]	Concentration / mg kg ⁻¹							
	Arsenic	Cadmium	Chromium	Copper	Lead	Mercury	Nickel	Zinc
Soil								
Alto da Várzea, Portugal [83]	67.9 - 130	n.d.	3.6 - 22.6	10.2 - 17.8	17.0 - 39.8	--	3.4 - 6.6	b.d.l. - 141
Senhora das Fontes, Portugal [84]	50.9 - 375	b.d.l. - 4.0	10.5 - 93.1	b.d.l. - 92.1	11.0 - 48.8	--	9.7 - 119	8.6 - 160
S. Francisco Assis, Portugal [112]	223.6	1.3	37.8	163.7	58.6	--	24.7	323.2
Rubiais, Spain [88]	--	2 - 95	3 - 21	21 - 160	46 - 6100	0.2 - 24.8	5 - 41	340 - 52000
United Kingdom [92]	--	b.d.l. - 347	--	22.9 - 77.5	348 - 42700	--	--	321 - 53400
Douai, France [89]	--	0.045 - 305	--	--	7.8 - 5410	--	--	30 - 31175
Cultivated soils Douai, France [90]	6.2 - 29.0	1.86 - 21.25	34.8 - 69.5	15.5 - 46.2	101 - 1131.8	0.12 - 0.65	9.6 - 39.5	149.8 - 2167.0
Litavka River valley, Czech Rep. [93]	--	3.0 - 67.5	--	--	15 - 4705	--	--	333 - 8728
Pribram, Czech Republic [94]	126 - 252	0.12 - 11.9	--	105 - 488	934 - 36234	--	--	15.8 - 519
Pribram, Czech Republic [95]	115 - 204	2.8 - 43.5	--	12 - 146	278 - 4660	--	--	252 - 5740
Sør-Varanger, Norway [113]	0.6 - 12.3	0.1 - 2.9	5.1 - 56.9	9.9 - 1124.4	5.3 - 142.6	--	8.9 - 1858.8	14.8 - 816.2
Kosovska Mitrovica, Kosovo [91]	2.1 - 3900	0.10 - 47	7.0 - 1100	9.0 - 1600	34 - 35000	0.020 - 11	7.6 - 2600	32 - 12000
Assif El Mal, Morocco [87]	--	--	--	53.9 - 117	74.1 - 165.8	--	4.8 - 15.5	533 - 2042
Kolwezi, DR Congo [101]	0.80 - 66.3	1.00 - 51.3	5.30 - 264.7	51.8 - 175859.5	6.10 - 1164.6	--	5.8 - 793.2	26.9 - 10398
Lubumbashi, DR Congo [102]	20 - 101	0.9 - 19.8	--	11600 - 14200	21 - 809	--	6.0 - 33.5	178 - 1250
Lubumbashi, DR Congo [103]	35 - 94	20 - 40	42 - 141	6438 - 14385	114 - 2609	0.2	26 - 70	133 - 869
Copperbelt Province, Zambia [104]	0.85 - 85.2	0.02 - 1.25	--	2.89 - 37800	2.95 - 419	0.0055 - 0.39	--	11.8 - 549
Copperbelt Province, Zambia [105]	b.d.l. - 254.9	--	1.6 - 595.0	6.0 - 41900	b.d.l. - 503	0.002 - 0.441	b.d.l. - 132	b.d.l. - 450

Table I.2 - Heavy metal concentration in soils and sediments of sites affected by mines (minimum and maximum values) (continued).

Site [Ref.]	Concentration/ mg kg ⁻¹							
	Arsenic	Cadmium	Chromium	Copper	Lead	Mercury	Nickel	Zinc
Soil								
Northern Namibia [104]	0.94 - 2370	0.11 - 511	--	3.07 - 4970	9.21 - 8170	0.0038 - 4.39	--	10.9 - 9740
Sudbury, Canada [102]	2 - 46	0.3 - 2	--	52 - 1330	18 - 176	--	54 - 1600	32 - 86
Tongling, China [107]	--	1.18 - 25.97	28.25 - 155.07	50.46 - 788.94	41.45 - 337.10	--	8.44 - 37.41	87.42 - 756.99
Xikuangshan, China [108]	5.60 - 352.22	0.10 - 130.63	--	9.25 - 352.60	4.13 - 654.40	--	--	51.83 - 5080
Beijing, China [98]	--	0.14 - 0.90	20.72 - 74.90	17.60 - 145.0	16.60 - 152.65	--	18.90 - 56.07	52.39 - 153.00
Dexing, China [110]	10 - 210	0.5 - 2.6	60 - 95	29 - 429	40 - 540	--	20 - 53	73 - 450
Yiyang, China [109]	--	0.4 - 10.6	23.1 - 55.3	22.4 - 215.1	22.1 - 74.4	--	14.1 - 40.2	91.3 - 484.5
China ^a [106]	0.063 - 11299 (195.5)	n.d. - 292.8 (11.0)	1.0 - 684.0 (84.28)	n.d. - 5024 (211.9)	n.d. - 29702 (641.3)	0.001 - 72.25 (3.82)	1 - 1499 (106.6)	n.d. - 75300.9 (1163)
Maldon, Australia [100]	19 - 185	0.03 - 0.37	23 - 57	14 - 59	12 - 76	0.1 - 9	7 - 23	22 - 328
Adrianópolis, Brazil [114]	--	1.9 - 22.1	8.9 - 27.8	57.1 - 894.8	234.8 - 9678.2	--	16.5 - 38.4	57.1 - 894.8
Alaverdi, Armenia [115]	24 - 1064	--	--	--	9 - 3703	--	--	--
Akhtala, Armenia [115]	9 - 276	--	--	--	15 - 12562	--	--	--
Villadossola, Italy [116]	5.3 - 6.1	0.3 - 1.3	44 - 101	28 - 72	32 - 92	--	36 - 44	52 - 143

Environmental Cleaning and Recovery of Heavy Metals via Functionalization of Silica Aerogels

Table I.2 - Heavy metal concentration in soils and sediments of sites affected by mines (minimum and maximum values) (concluded).

Site [Ref.]	Concentration/ mg kg ⁻¹							
	Arsenic	Cadmium	Chromium	Copper	Lead	Mercury	Nickel	Zinc
Sediment								
Alto da Várzea, Portugal [83]	41.6 - 515	n.d.	b.d.l. - 51.6	b.d.l. - 23.4	13.1 - 81.1	--	b.d.l. - 21.9	42.1 - 109
Senhora das Fontes, Portugal [84]	35.8 - 153	b.d.l. - 3.8	3.3 - 44.7	b.d.l. - 54.8	9.3 - 89.0	--	b.d.l. - 36.9	b.d.l. - 197
Lot River, France [117]	--	0.33 - 294	--	16.7 - 264	27.9 - 1280	--	--	81.5 - 10000
Assif El Mal, Morocco [87]	--	--	--	6.69 - 9.99	39.1 - 51.0	--	12.2 - 23.3	2018 - 3796
Yongding River, China [96]	--	--	25.9 - 70.6	12.4 - 49.1	12.6 - 135	--	21.2 - 174	39.6 - 161
Maba river, China [111]	40 - 1103	1.6 - 45.7	40 - 65.3	40 - 857	80 - 167	1.0 - 5.5	16 - 41.5	220 - 3523
Kolwezi, DR Congo [101]	0.70 - 34.7	1.10 - 28.9	5.70 - 252.9	115.50 - 209826.7	6.40 - 899.3	--	3.60 - 204.3	25.90 - 300.5
Lubumbashi, DR Congo [103]	17 - 159	b.d.l. - 158	42 - 121	4314 - 40152	70 - 10321	0.2 - 1.1	28 - 142	173 - 5463
Anka, Nigeria^b [99]	b.d.l. - 2896	n.d.	164.41 - 665.67	5582 - 6539	170597 - 262964	--	--	--

n.d. - not detected; b.d.l. - below detection limit; ^a Mean values in parenthesis; ^b Values refer to mine sediments.

Table I. 3 - Heavy metal concentration in watercourses in sites affected by industries (minimum and maximum values).

Site [Ref.]	Concentration in water / $\mu\text{g L}^{-1}$							
	Arsenic	Cadmium	Chromium	Copper	Lead	Mercury	Nickel	Zinc
Esmoriz-Paramos lagoon, Portugal [119]	--	--	b.d.l.	b.d.l. - 30	b.d.l. - 38	--	--	b.d.l. - 699
Tigris river, Turkey [146]	--	b.d.l.	--	58 - 92	b.d.l.	--	200 -400	70 - 130
Karoon river, Iran [147]	--	--	0.7 - 118.3	0.5 - 70.3	--	--	4.3 - 122.0	--
Khoshk river, Iran [148]	--	b.d.l. - 180	100 - 550	10 - 60	20 - 130	--	10 - 200	50 - 2730
Yamuna river, India [149]	--	10 - 20	0 - 8	--	--	--	20 - 210	--
Yamuna river, India [150]	--	1.7 - 433.0	2.6 - 1983.0	18.4 - 17642.4	6.8 - 1112.1	--	1.4 - 2748.1	15.4 - 28520.9
Yamuna river, India [139]	--	170 - 200	90 - 110	120 - 150	110 - 360	--	1060	50 - 120
Patancheru, India [151]	5.5 - 116.5	--	4.2 - 46.8	--	0.2 - 13.8	--	4.9 - 54.1	32.8 - 364.8
Kasimpur, India [152]	--	--	100	860	--	--	120	300
Gomti river, India [153]	--	b.d.l.	b.d.l. - 316	b.d.l. - 45	2 - 86	--	7 - 186	22 - 160
Gomti river, India [154]	--	b.d.l.	1.0 - 5.7	b.d.l.	22 - 39	--	9 - 17	11 - 32
Karnaphuli River, Bangladesh [155]	13.31 - 53.87	2.54 - 18.34	46.09 - 112.43	--	5.29 - 27.45	--	--	--
The Luan River Basin, China [156]	--	0.8 - 1.1	7.9 - 89.3	3.7 - 29.4	6.5 - 15.1	--	1.34 - 13.9	55.8 - 176.3
Jiangsu, China [133]	--	--	10 - 854	40 - 4500	--	--	181 - 3800	9 - 354
Taichung, Taiwan [132]	--	b.d.l.	b.d.l. - 52.3	b.d.l. - 61	b.d.l. - 0.39	--	b.d.l. - 33	b.d.l. - 15

b.d.l. - below detection limit.

Environmental Cleaning and Recovery of Heavy Metals via Functionalization of Silica Aerogels

Table I. 4 - Heavy metal concentration in soils and sediments in sites affected by industries (minimum and maximum values).

Site [Ref.]	Concentration/ mg kg ⁻¹							
	Arsenic	Cadmium	Chromium	Copper	Lead	Mercury	Nickel	Zinc
Soil								
Estarreja, Portugal [120]	1558	1.1	1.2	132.9	270.8	109.0	1.6	165.5
Estarreja, Portugal [121]	2.9 - 532.3	--	--	--	--	0.03 - 13.65	--	16 - 199
Huelva, Spain [123]	8.9 - 2066	0.16 - 18.4	6.50 - 112	269 - 10000	68.6 - 5469	--	6.0 - 48.7	74.6 - 4707
Bazoches-les Gallérandes, France [124]	3.01 - 28.08	--	14.54 - 92.67	3.94 - 34.23	3.59 - 1932.58	--	7.43 - 40.79	7.96 - 86.90
Avenmouth, United Kingdom [92]	--	54.5	--	161	1740	--	--	3630
Prescot, United Kingdom [122]	18 - 143	4.0 - 44	--	184 - 1123	311 - 575	--	--	92 - 176
Vojvodina, Serbia [125]	1.9 - 23	0.18 - 0.71	11 - 195	6.5 - 140	8 - 70	0.02 - 0.53	6 - 61	20 - 770
Smederevo, Serbia [126]	--	0.22 - 4.61	0.01 - 115	7.12 - 183	20 - 140	--	40.0 - 170	8.40 - 150
Veles, Macedonia [127]	1.3 - 110	0.3 - 600	17 - 1800	11 - 1700	13 - 15000	0.01 - 12	7.3 - 600	22 - 27000
Varanasi, India [144]	--	0.55 - 8.85	13.40 - 679.89	2.55 - 203.45	0.46 - 44.50	--	2.00 - 34.45	14.23 - 387.78
Titagarh, India [145]	--	22.20 - 51.00	118.05 - 190.40	22.00 - 166.50	99.30 - 168.30	--	44.72 - 133.80	182.00 - 285.00
Wuxi, China [128]	9.9 - 22.1	0.003 - 0.370	26.4 - 96.2	26.7 - 151.6	17.0 - 162.1	0.066 - 0.266	--	29.7 - 445.3
Yixing, China [129]	--	0.09 - 0.37	43.34 - 67.83	15.31 - 38.11	35.56 - 53.66	--	--	--
South Korea [130]	127.4 - 67954	--	--	88.96 - 28024	186.48 - 122248	--	--	784.56 - 3962
Monterey, Mexico [131]	114 - 6043	b.d.l. - 344	--	b.d.l. - 726	212 - 31420	--	--	323 - 12280

Table I.4 - Heavy metal concentration in soils and sediments in sites affected by industries (minimum and maximum values) (concluded).

Site [Ref.]	Concentration/ mg kg ⁻¹							
	Arsenic	Cadmium	Chromium	Copper	Lead	Mercury	Nickel	Zinc
Sediment								
Esmoriz-Paramos lagoon, Portugal [119]	--	--	b.d.l. - 255	6 - 232	7 - 299	--	--	15 - 545
Tigris river, Turkey [146]	--	b.d.l.	--	25.39 - 194.53	b.d.l.	--	36.68 - 170.83	17.09 - 66.26
Khoshk river, Iran [148]	--	0.1 - 2	114 - 253	19.7 - 63.4	29.6 - 199.1	--	95.9 - 123.6	33.9 - 101.1
Yamuna river, India [149]	--	0.82 - 4.6	6.8 - 35	--	--	--	45.2 - 49.9	--
Yamuna river, India [139]	--	23	68	56	12	--	25	76
Gomti river, India [153]	--	0.14 - 20.71	3.87 - 60.97	2.23 - 118.5	4.68 - 111.2	--	4.74 - 64.92	11.2 - 249.32
Gomti river, India [154]	--	1.10 - 8.38	2.22 - 19.13	b.d.l. - 35.03	27.28 - 75.33	--	6.53 - 29.76	11.40 - 101.73
Karnaphuli River, Bangladesh [155]	11.56 - 31.53	0.63 - 3.21	39.18 - 160.32	--	21.98 - 73.42	--	--	--
The Luan River Basin, China [156]	--	0.7 - 1.3	61.6 - 275.4	4.8 - 37.5	11.5 - 54.4	--	4.1 - 58.8	58.7 - 278.6
Jiangsu, China [133]	--	1.44 - 2.33	345 - 9671	440 - 9797	17.2 - 106	--	251 - 2846	391 - 1483
Taichung, Taiwan [132]	--	b.d.l. - 6.3	13.3 - 360	10 - 280	10 - 62	--	16.6 - 322	50 - 950

b.d.l. - below detection limit.

Environmental Cleaning and Recovery of Heavy Metals via Functionalization of Silica Aerogels

Table I. 5 - Heavy metal concentration in watercourses in sites affected by several sources of pollution (minimum and maximum values).

Site [Ref.]	Concentration in water / $\mu\text{g L}^{-1}$							
	Arsenic	Cadmium	Chromium	Copper	Lead	Mercury	Nickel	Zinc
Dil Deresi, Turkey [157]	10 - 290	3 - 15	16 - 110	11 - 94	11 - 370	--	--	150 - 4100
Tembi river, Iran [158]	--	70 - 350	130 - 580	260 - 710	590 - 1910	--	160 - 830	110 - 510
Korotoa river, Bangladesh [160]	10 - 92	0.9 - 22	33 - 126	23 - 119	8 - 64	--	9.3 - 71	--
Songhua river, China [161]	0.10 - 3.80	--	0.2 - 18.0 ^a	0.50 - 37.00	0.50 - 28.00	--	--	2.00 - 397.00
Monte Alegro watercourse, Brazil [162]	--	0.02 - 0.06	0.17 - 0.59	1.00 - 6.08	7.10 - 18.80	--	--	16.65 - 26.15

^a Defined as Cr(VI) content.

Table I. 6 - Heavy metal concentration in soils and sediments in sites affected by several sources of pollution (minimum and maximum values).

Site [Ref.]	Concentration/ mg kg ⁻¹							
	Arsenic	Cadmium	Chromium	Copper	Lead	Mercury	Nickel	Zinc
Soil								
Segura river valley, Spain [164]	--	0.15 - 0.88	21.1 - 42.5	16.1 - 30.6	8.9 - 34.5	--	16.4 - 32.0	33.4 - 80.7
Alicante, Spain [165]	--	0.34	26.5	22.5	22.8	--	20.9	52.8
Xi'an city, China [166]	3.10 - 14.5	--	--	21.20 - 85.0	19.80 - 157.1	--	19.60 - 85.1	54.30 - 464.8
China [167]	1.1 - 160.0	0.023 - 90.90	8 - 1341	3.5 - 1440	3.4 - 2521	0.003 - 15.4	4.0 - 348.9	13 - 2180
Sediment								
Gulf of Taranto, Italy [163]	--	--	75.2 - 102.8	42.4 - 52.3	44.7 - 74.8	0.04 - 0.41	47.9 - 60.7	86.8 - 129.0
Zarrin-Gol River, Iran [159]	10.69 - 29.98	--	30.41 - 50.11	--	--	--	10.09 - 13.84	26.22 - 39.81
Tembi river, Iran [158]	--	10 - 40	11 - 74	37 - 100	141 - 270	--	52 - 150	21 - 74
Korotoa river, Bangladesh [160]	2.6 - 52	0.26 - 2.8	55 - 183	35 - 118	36 - 83	--	37 - 163	--
Monte Alegro watercourse, Brazil [162]	--	0.13 - 0.43	60.98 - 587	432 - 1569	216 - 696	--	--	739 - 1724

Annex II

Copper and Nickel Ionophores



The content of this annex is based on the author's published work *Ligands as copper and nickel ionophores: Applications and implications on wastewater treatment*.

Selected works of copper and nickel selective ligands are discussed in the following subsections. These fall onto four main types of works, as briefly described below.

The first two types of studies deal with the study of the ionophore molecule, evaluating the binding affinity towards the cation. These include the thermodynamic assessment on the ligand-cation complex through computation of the formation constant (K) [411-413], and the development of colorimetric chemosensors, evaluating modifications occurring in fluorescence intensities and/or absorbance upon complexation [414-432]. Some works take advantage of these ionophores to develop optodes. In fact, the development of chemosensors for metal ions is recurrent [433, 434]. An important parameter described is the selectivity (α), a measure in the response of a given cation in the presence of interferents.

The third type of studies evaluates the selectivity of modified materials for adsorption tests. Mixed metal solutions are, in general, used to evaluate the effect of interferents on adsorption performance. Selectivity (α) can be calculated by the ratio of the distribution coefficients (K_d), although in some works other methods are used [335, 336, 339].

The final category of papers, the most common one, regards the preparation of potentiometric ion-selective membranes electrodes (ISE). These are based on the incorporation of the ligand in the polymeric membrane, followed by the evaluation of its efficiency as a sensor. The selectivity of the sensor's response to interferents is reported as the potentiometric selectivity (α_{pot}) [477].

Copper ionophores

Copper selective ionophores or modified materials are discussed here. Table II.1 presents works in which the binding of the ligand and the ion was studied, and Table II.2 features works with modified materials and ion-sensing electrodes. The ligands discussed in Tables II.1 and II.2 are presented, respectively, in Figures II.1 and II.3.

Environmental Cleaning and Recovery of Heavy Metals via Functionalization of Silica Aerogels

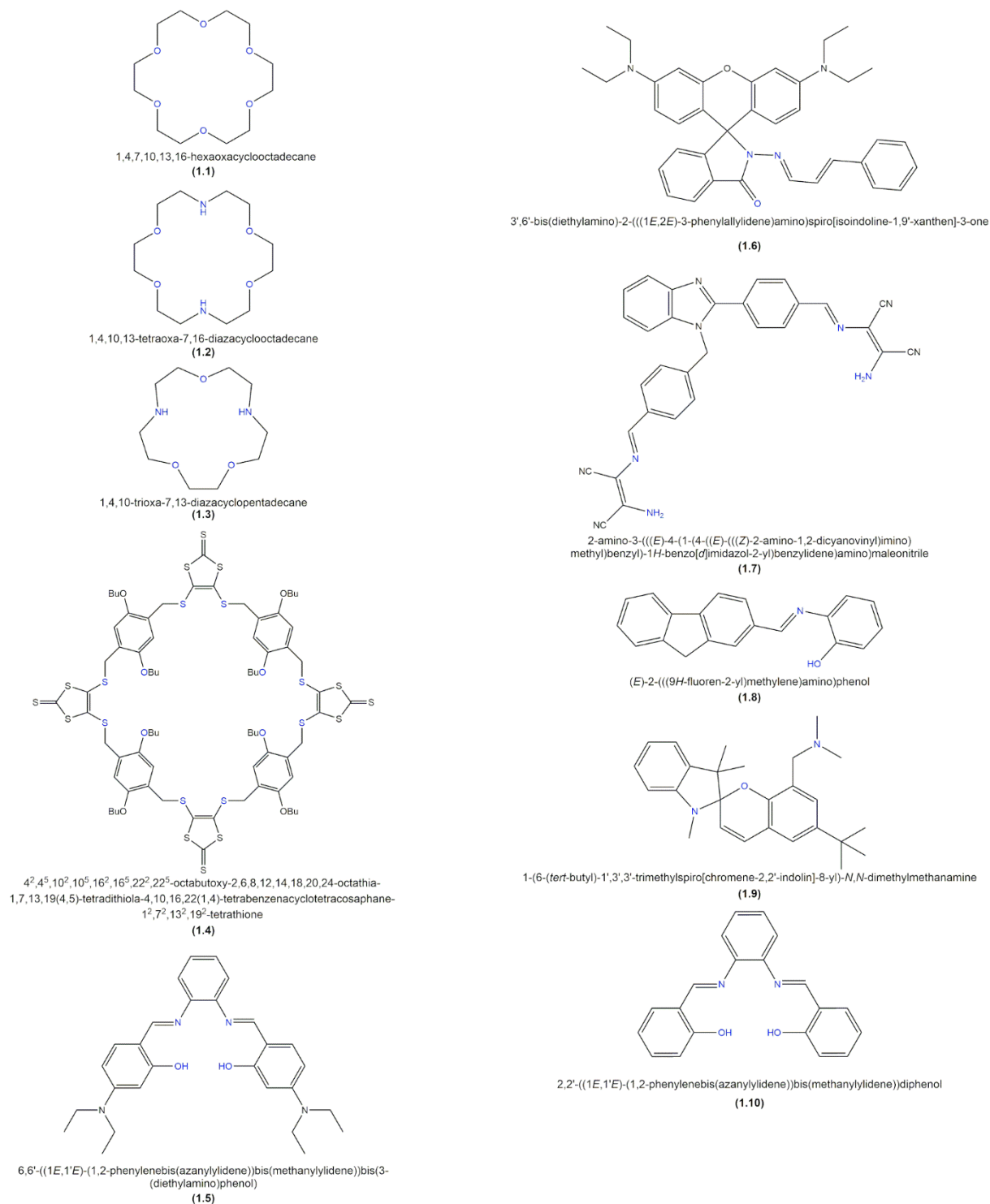


Figure II. 1 - Representation of molecular structures of selected copper ligands. Proposed functional groups responsible for cation interaction are presented in blue.

Table II. 1 - Selected studies where the interaction of ligands with copper and interferents is evaluated.

Ligand Molecule	Ligand Family	Relevant Results	Ref.
(1.1)	Crown ether	Evaluated in methanol: log <i>K</i> 2.47 Cu(II) 2.22 Zn (II) 3.41 Co(II) 4.35 Na(I) 6.08 K(I)	[411]
(1.2)	Crown ether (aza modified)	Evaluated in methanol: log <i>K</i> 8.48 Cu(II) 3.56 Co(II) 1.50 Na(I) 1.80 K(I)	[411]
(1.3)	Crown ether (aza modified)	Evaluated in methanol: Selective to Cu(II) in comparison to Cd(II), Hg(I) and Pb(II) as chlorides. Not selective for perchlorates and nitrates	[412]
(1.4)	Crown ethers (thia modified)	Evaluated in methanol/dichloromethane: log <i>K</i> 8.6 Cu(II) 4.8 Na(I)	[413]
(1.5)	Schiff base	$\alpha > 17200$ (Co(II), Ni(II), Zn(II)) Evaluated in HEPES buffer/ethanol: log <i>K</i> 4.2 Cu(II)	[414]
(1.6)	Schiff base	Evaluated in ethanol-PBS: log <i>K</i> 4.9 Cu(II)	[415]
(1.7)	Schiff base	Evaluated in acetonitrile-tris buffer: log <i>K</i> 8.4 Cu(II)	[416]
(1.8)	Schiff base	Evaluated in acetonitrile: log <i>K</i> 5.5 Cu(II)	[417]
(1.9)	Spiropyran	Evaluated in ethanol: log <i>K</i> 6.8 Cu(II) 5.5 Co(II) 4.8 Zn(II)	[419]
(1.10)	Schiff base	Evaluated in acetonitrile: log <i>K</i> 8.4 Cu(II)	[422]

The results for binding studies via electrospray ionization process mass spectroscopy (ESI-MS) for copper ligands are summarized in Table II.1 [411-413]. The works show that modified crown ethers tend to bind more strongly with copper than with other tested cations. However, when other salts, with different anions, are used this tendency was not maintained [412]. In fact, anions are known to affect the adsorption of cations on active sites [530, 566]. Furthermore, the number of cation interferents studied is limited.

Copper fluorescent ionophores were studied by several authors [414-421]. Some fluorescence images are depicted in Figure II.2. The majority of these are Schiff bases. The salen studied by Mondal *et al.* [414] as a chemosensor in HEPES buffer/ethanol was subject to a quenching effect by copper, which is not affected by the presence of other metal ions. Similar results were obtained by Yang *et al.* [415] in ethanol–PBS, by Bing *et al.* [416] in acetonitrile-tris and by Nouri Moghadam *et al.* [417] in acetonitrile. In these works, the fluorescence intensity, and absorbance when evaluated, of the ligand-Cu(II) complex was not significantly disrupted by the presence of interferents. The ligand studied by Bing *et al.* [416], a Schiff base derived from benzimidazole, has its fluorescence intensity and absorbance quenched by some interferents. Nevertheless, these properties are vastly different when copper is present in a cation mixture. The ligand tested by Gündüz *et al.* [418] showed a very strong fluorescence response to copper in a DMSO/water mixture, compared to other metals, in spite of these not being tested as interferents. Matsushita *et al.* [483] verified that the fluorescence of europium(III)/poly(sodium acrylate) and terbium(III)/poly(sodium acrylate) composites was quenched by their interaction with other cations. It was concluded that the composites could be used for the detection of copper, as this analyte quenched the fluorescence of the composite almost entirely, a result not obtained for remaining ions.

Several authors used chemosensing ligands to develop optodes. Shao *et al.* [419] studied a spiropyran derivate as a fluorescent ligand. The association constants between the ligand and several cations (Table II.1) as well as selectivity were evaluated, and it was found that the ligand is highly selective for copper. Luo *et al.* [420] used a porphyrin derivate with a bipyridine as the ionophore and reported that the influence of interferents on the fluorescence of the optode had a maximum offset of 5%. Aksuner *et al.* [421] used a fluorescent Schiff base and the membrane's operation is based on quenching upon copper binding in water. Several interferents were tested and it was reported that these alter the fluorescence of the ligand, in the presence of copper, by a maximum of 7%. For the membrane developed by Gholivand *et al.* [422] the presence of an interferent in the sample only changed the absorbance by up to 5%, demonstrating the potential of the salen ionophore. A Schiff-base immobilized silica [432] exhibited an increase at absorbance intensity after binding with copper only, and was also shown to be a selective adsorbent.

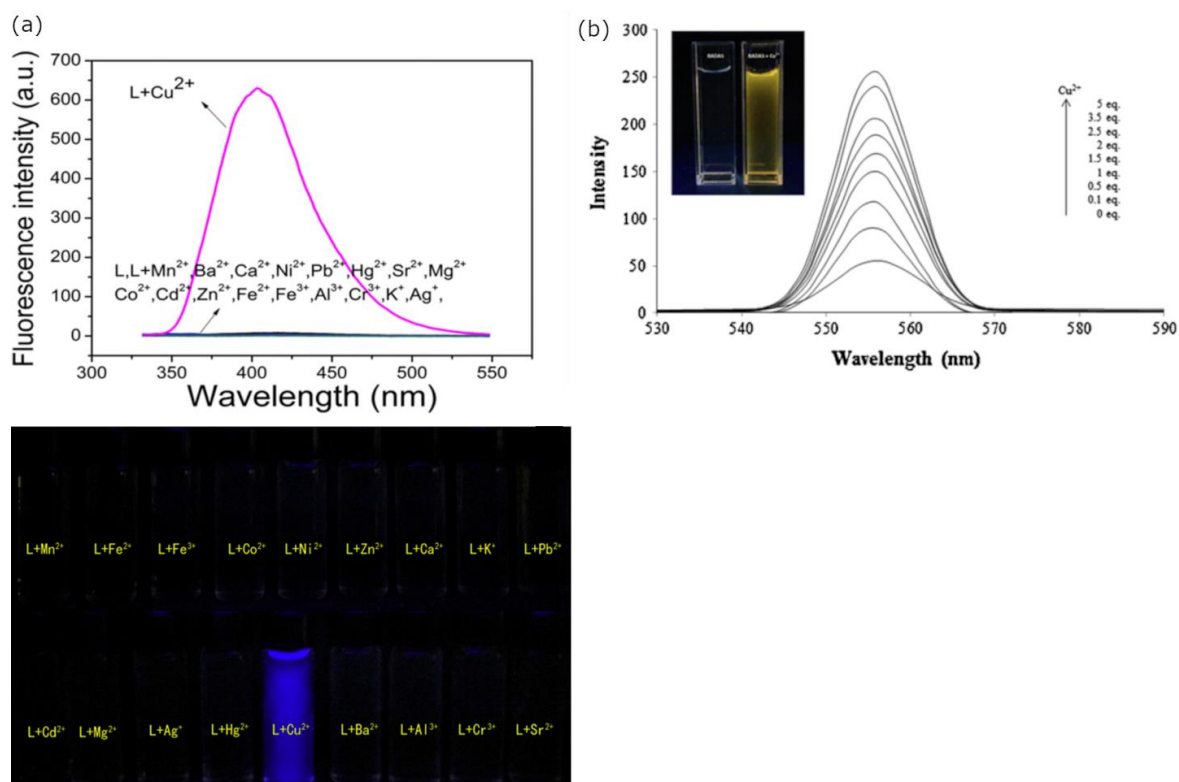
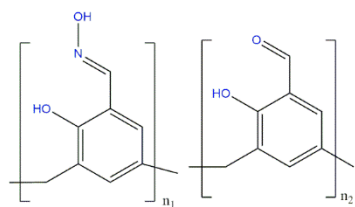


Figure II. 2 - Fluorescence spectra changes and images reported by (a) Bing *et al.* [416] and (b) Gündüz *et al.* [418].

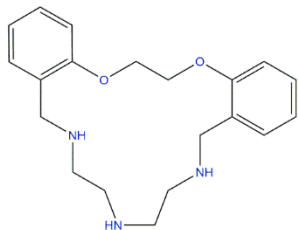
Many authors have reported the development of copper ISE [435-461], Table II.2. The electrodes are prepared with neutral ionophores (selective ligand) and are, most commonly, plasticized poly(vinyl chloride) liquid membranes [567]. The most common ionophores are Schiff bases [440, 441, 444, 447, 449-451, 453-455]. Other membrane components include anion excluders like sodium tetraphenylborate and solvent mediators such as chloronaphthalene, dioctyl phthalate, tri-*n*-butylphosphate and dibutyl(butyl)phosphonate [443, 449]. It was found that despite different ligands being used as ionophores, the optimization of the membrane compositions ensures good selectivity results. In fact, these components are quite important, since other membrane formulations reported in these studies do not achieve the same results.

Modified adsorbents compiled in Table II.2 were already discussed in Section 3.4..

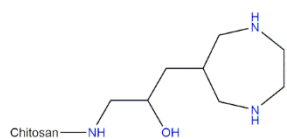
Environmental Cleaning and Recovery of Heavy Metals via Functionalization of Silica Aerogels



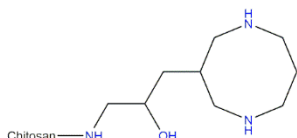
3-ethyl-2-hydroxy-5-methylbenzaldehyde compound with (*E*)-3-ethyl-2-hydroxy-5-methylbenzaldehyde oxime (1:1)
(3.1)



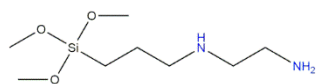
6,7,8,9,10,11,12,13,19,20-decahydro-5*H*-dibenzo[*e,p*][1,4]dioxo[8,11,14]triazacycloheptadecine
(3.2)



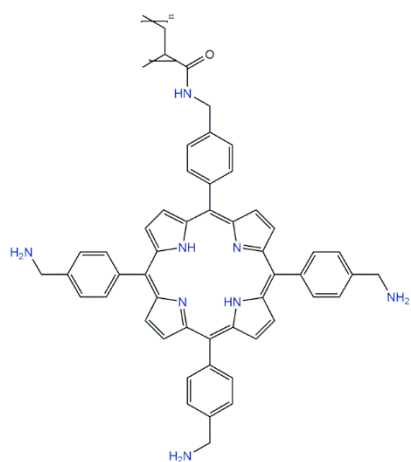
Chitosan—NH
1-amino-3-(1,4-diazepan-6-yl)propan-2-ol modified chitosan
(3.3)



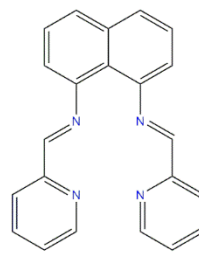
Chitosan—NH
1-amino-3-(1,5-diazocan-3-yl)propan-2-ol modified chitosan
(3.4)



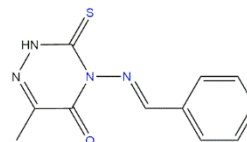
*N*¹-(3-(trimethoxysilyl)propyl)ethane-1,2-diamine
(3.5)



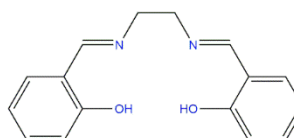
2-methyl-*N*-(4-(10,15,20-tris(4-(aminomethyl)phenyl)porphyrin-5-yl)benzyl)butanamide
(3.6)



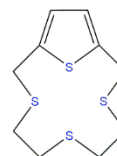
(1*E*,1'*E*)-*N,N'*-(naphthalene-1,8-diyl)bis(1-(pyridin-2-yl)methanimine)
(3.7)



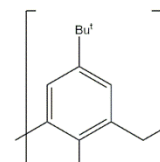
(*E*)-4-(benzylideneamino)-6-methyl-3-thioxo-3,4-dihydro-1,2,4-triazin-5(2*H*)-one
(3.8)



2,2'-((1*E*,1'*E*)-(ethane-1,2-diyldis(azanylylidene)bis(methanylylidene))diphenol
(3.9)



3,6,9-trithia-1(2,5)-thiophenacyclodecaphane
(3.10)



Hexanol
(3.11)

Figure II. 3 - Copper ionophores applied to modify materials/membrane sensors and representation of proposed functional groups responsible for cation interaction (in blue).

Table II. 2 - Selected works containing selective modified adsorbents or ISE towards copper.

Ligand Molecule	Ligand Family	Material	Relevant Results	Ref.
(3.1)	Oxime	Resin	Evaluated in sodium acetate/HCl: K_d 2771 Cu(II) 396 Cd(II) 283 Zn(II) 139 Ni(II)	[338]
chitosan and pyromellitic dianhydride	Carboxylic acid anhydride	Biochar	Evaluated in water: $a_{Cu,i}$ $7 < a < 21$ (Cd(II)) $13 < a < 47$ (Pb(II))	[213]
carboxymethylated chitosan	Carboxylic acid	Chitosan hydrogel beads	Evaluated in water: $a_{Cu,i}$ $3 < a < 19$ (Pb(II)) $0.5 < a < 4.9$ (Mg(II))	[333]
ethylene glycol dimethacrylate and copper methacrylates	Acrylate polymer	Core-shell-type metal ion-imprinted polymer microspheres	Evaluated in water: $a_{Cu,i}$ 12.19 (Ni(II)) 28.2 (Cd(II)) 10.2 (Mg(II))	[334]
(3.2)	Crown ether (aza modified)	Silica gel	Evaluated in methanol: $\log K$ 14.4 Cu(II) 10.0 Ni(II) 8.7 Cd(II) 7.6 Co(II) 7.5 (Zn(II)) Evaluated in water: competitive adsorption with Co(II), Zn(II) and Ni(II) shows that only Cu(II) is removed.	[335]
(3.3) and (3.4)	Crown ether (aza modified) crosslinked with chitosan	Chitosan	Evaluated in water: $a_{Cu,i}$ > 15.4 (Cd(II)) > 3.6 (Hg(II))	[336]
(3.5)	Amine	Silica gel	Evaluated in water: K_d 1540 Cu(II) 5.7 Cd(II) 10.2 Zn(II) $\log K$ for the di-amine chain 20.1	[337]
(3.6)	Porphyrin	Carbon nanotubes paste ISE	Evaluated in water: $\log a_{pot} < -3.2$	[458]
(3.7)	Schiff base	PVC membrane ISE	Evaluated in water: $\log a_{pot} < -3.6$	[440]
(3.8)	Schiff base	PVC membrane ISE	Evaluated in acetonitrile: $\log K$ 4.7 Cu(II) <2.5 for remaining cations Evaluated in water: $\log a_{pot} < -2$	[441]

Table II.2- Selected works containing selective modified adsorbents or ISE towards copper (concluded).

Ligand Molecule	Ligand Family	Material	Relevant Results	Ref.
(3.9)	Schiff base	PVC membrane ISE	Evaluated in water: $\log a_{\text{pot}} < -1.5$	[444]
(3.10)	Crown ethers (thia modified)	PVC membrane ISE	Evaluated in water: $\log a_{\text{pot}} < -1.6$	[445]
(3.11)	Azole	PVC membrane ISE	Evaluated in methanol/water: ESI-MS revealed higher binding affinity for Cu(II) Evaluated in water: $\log a_{\text{pot}} < -3.6$	[461]

The results summarized in Table II.1 reveal that the stability constants for copper-ligand complexes are fairly high in the majority of cases. Knowing the binding constant between the organic ligand and the ion, one can accurately draw more conclusions about the selectivity of the ligand. This result is dependent on the experimental conditions, such as the solvent. Two studies stand out: the crown ether presented by Brodbelt *et al.* [411] has a higher stability constant for other cations than for copper; and the reported constants by Shao *et al.* [419] are not so different for copper and cobalt. Furthermore, it seems that crown ethers' (and their aza modified counterparts) selectivity towards copper is not consistent across different works [335, 412], with the anions interfering significantly [412]. Despite not assessing the formation constant for other ions, in the remaining works described in Table II.1, the selectivity is shown in each study by the effect on the sensor's response by cation interferents.

The results summarized in Table II.2 reveal that the ligands can still act selectively when mobilized in modified adsorbents and in different media. However, despite good selectivity being reported, not many interferents are tested and there are several parameters that influence the properties of the adsorbent and the sorption conditions, leading to different results. Furthermore, it is possible to obtain selective results with much simpler ligands. Works dealing with ISEs show that a lot of ligands can act as selective copper ionophores. Although interferents are tested, the obtained potentiometric selectivity does not transfer well to the performance of a material modified with the ligand, since the membrane is composed by other elements.

In conclusion, Schiff bases seem to be the best kind of copper ionophores, as evidenced by their abundance in the literature and the multiple parameters studied (K , α_{pot}) that agree.

Nickel ionophores

In this section nickel selective ionophores are discussed. Table II.3 summarizes works in which the affinity constant for the ligand-nickel complex was studied and Table II.4 presents nickel ISEs. The ligands discussed in Tables II.3 and II.4 are presented, respectively, in Figures II.4 and II.6.

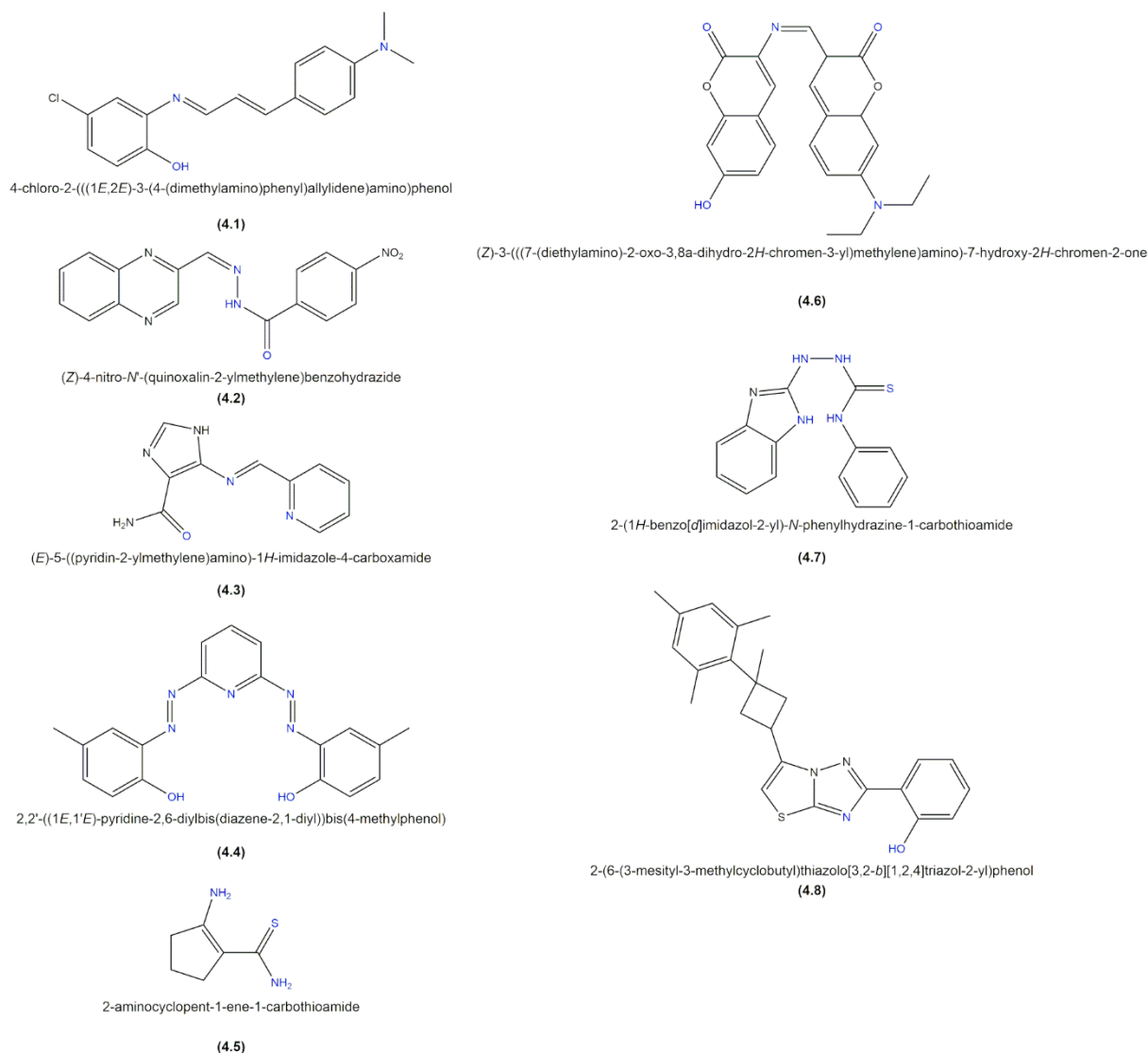


Figure II. 4 - Representative nickel ligands. Proposed functional groups responsible for cation interaction are presented in blue.

Table II. 3 - Selected studies where the interaction of ligands with nickel is evaluated.

Ligand Molecule	Ligand Family	Relevant Results	Ref.
(4.1)	Schiff base	Evaluated in water: log <i>K</i> 5.1 Ni(II)	[423]
(4.2)	Schiff base	Evaluated in acetonitrile: log <i>K</i> 5.4 Ni(II)	[424]
(4.3)	Schiff base	Evaluated in bis-tris buffer: log <i>K</i> 5.0 Ni(II)	[425]
(4.4)	Pyridyl derivative	Evaluated in methanol/water: log <i>K</i> 5.1 Ni(II)	[426]
(4.5)	Thioamide	Evaluated in acetonitrile: log <i>K</i> 11.8 Ni(II)	[427]
(4.6)	Schiff base	Evaluated in acetonitrile: log <i>K</i> 4.5 Ni(II)	[428]
(4.7)	Schiff base	Evaluated in acetonitrile/water: log <i>K</i> 5.9 Ni(II) 4.2 Cu(II)	[430]
(4.8)	Imine	Evaluated in water: log <i>K</i> 6.4 Ni(II)	[431]

Schiff bases [423-425] and a pyridyl derivative [426] were studied as colorimetric nickel sensors. The colorimetric detection of nickel, for some of these works, can be observed in Figure II.5. Changes in absorbance of specific wavelengths in the UV-VIS region were studied to determine the affinity of the ligand-nickel complex in the presence of interferents. The authors report clear differences in absorbance upon binding with nickel, even in the presence of interferents, showing that the latter do not bind significantly with the ligand. Based on one of these ionophores, Yari *et al.* [427] prepared a nickel selective optode, with a PVC membrane. Interferents only disrupted the measured absorbance by up to 6%.

Other authors studied the colorimetric sensing of nickel via fluorescence studies [428-430]. The Schiff base proposed by Wang *et al.* [428] did not show such a clear response towards mercury, cadmium, copper and iron, as seen by fluorescence, generating similar emission intensities in the presence of nickel. Chowdhury *et al.* [429] also proposed a Schiff base for this purpose that presents a shift on the fluorescence maximum emission intensity from 460 to 393 nm, in acetonitrile, upon binding with nickel. This behavior was not observed with other cations, highlighting the selectivity towards nickel and, consequently this ligand can be used as nickel chemosensor. For another ligand, the presence of interfering cations alongside nickel, did not quench its emission intensity [430]. Fluorescent ligands were also used to develop optical membrane sensors [431]. Once again, the

authors demonstrate that interferents do not alter the fluorescence intensity verified in the presence of nickel [431].

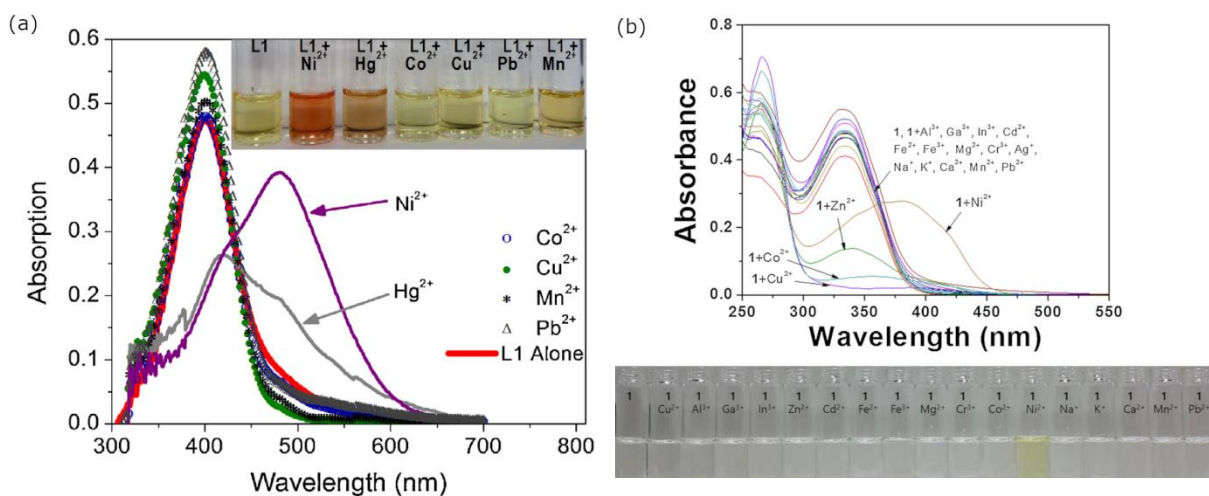


Figure II. 5 - Colorimetric detection of nickel and absorbance changes as reported by (a) Peralta-Domínguez *et al.* [423] and (b) Kang *et al.* [425].

Nickel ISE are also extensively studied in the literature [462-482], and selected works are summarized in Table II.4. These works are fairly similar to those mentioned in the previous section for copper.

Environmental Cleaning and Recovery of Heavy Metals via Functionalization of Silica Aerogels

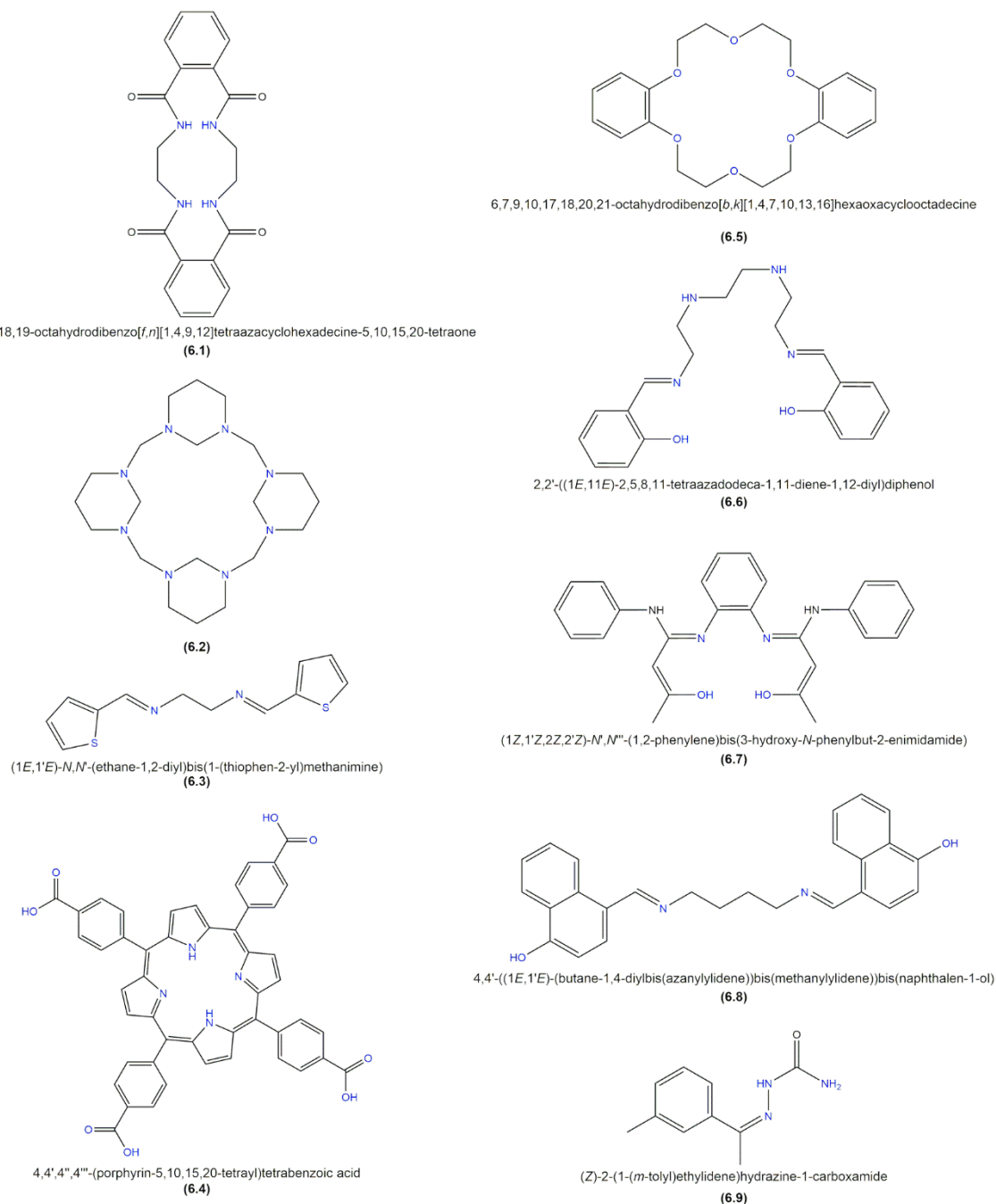


Figure II. 6 - Representation of nickel ionophores used to prepare membrane sensors and proposed functional groups responsible for cation interaction (in blue).

Table II. 4 - Selected works containing nickel ISE.

Ligand Molecule	Ligand Family	Material	Relevant Results	Ref.
(6.1)	Cyclic amide	PS membrane ISE	Evaluated in water: $\log a_{\text{pot}} < -0.5$	[462]
(6.2)	Crown ether (aza modified)	PVC membrane ISE	Evaluated in water: $\log a_{\text{pot}} < -2$	[465]
(6.3)	Imine	PVC membrane ISE	Evaluated in water: $\log a_{\text{pot}} < -2.7$	[466]
(6.4)	Porphyrin	PVC membrane ISE	Evaluated in water: $\log a_{\text{pot}} < -0.6$	[467]
(6.5)	Crown ether	PVC membrane ISE	Evaluated in water: $\log a_{\text{pot}} < -0.1$	[473]
(6.6)	Schiff base	PVC membrane ISE	Evaluated in water: $\log a_{\text{pot}} < -1.8$	[475]
(6.7)	Schiff base	PVC membrane ISE	$\log K$ 7.3 Ni(II) <4.2 for remainder ions Evaluated in water: $\log a_{\text{pot}} < -1.2$	[478]
(6.8)	Schiff base	PVC membrane ISE	$\log K$ 7.2 Ni(II) <3.3 for remainder ions Evaluated in water: $\log a_{\text{pot}} < -1.2$	[478]
(6.9)	Schiff base	PVC membrane ISE	$\log K$ 5.8 Ni(II) <4.6 for remainder ions Evaluated in water: $\log a_{\text{pot}} < -2.2$	[479]

The works discussed in this section reveal that Schiff bases are the most common nickel ionophores. In fact, very similar molecules like salens were found to be copper ionophores on ISEs. This reveals that small changes in the ligand molecule can lead to different results (evidenced by the formation constants [478]), but also that the composition of the ISE membrane is of utmost importance as it may justify why such similar ligands result in membranes selective to different cations. The Schiff bases of Table II.3 show similar values for the formation constant and these are different than the copper ionophores Schiff bases. Furthermore, crown ethers were also used as ionophores in nickel ISEs but the results are not consistent across different studies. This might explain the previous result with copper.

Appendix A

Thermogravimetric Data



Table A. 1 - Onset and end temperatures and mass loss for each thermal phenomenon in the aerogels of Chapter 5.

Sample	Phenomena #	$T_{\text{onset}} - T_{\text{end}} / ^\circ\text{C}$	Mass loss / %
A_B	1	55 – 77	0.6
	2	152 – 202	3.7
	3	340 – 424	5.1
	4	536 – 746	12.1
A_A	1	48 – 89	2.7
	2	439 – 629	30.5
A_3A	1	46 – 162	11.8
	2	350 – 510	25.2
A_A+3A	1	45 – 82	4.0
	2	333 – 574	31.0
A_TRIS	1	90 – 185	3.5
	2	467 – 549	26.5
A_U	1	135 – 219	20.3
	2	416 – 585	15.9

Appendix B

Desorption Data



Initially, the desorption from A_A+3A with different desorption agents was studied with copper, metal of interest to recover. The desorption agents and its concentrations were selected to replicate procedures from the literature. These tests were conducted by placing 20 mg of loaded particles with 3 mL of desorption agent and the mixture was magnetically stirred for three hours and left to rest overnight. The results are compiled in Table B. 1.

Table B. 1 - Desorption of copper from A_A+3A with different desorption agents.

Cation	Isotherm Initial Concentration /mg L⁻¹	Desorption Agent	Desorption /%	Sample Degradation
Cu	100	HNO ₃ 1M	70.1	+
Cu	100	HCl 1M	125.8	+
Cu	100	NaOH 0.1 M	71.6	+
Cu	100	EDTA 0.05 M	0.01	+

It was observed that with hydrochloric acid the blue loaded particles became white, while with sodium hydroxide and EDTA there was no change in this regard. Only with sodium hydroxide was the solution blue, due to the existence of hydroxides in solution. It was noticeable that the aerogel particles became much smaller and were not retained in a paper filter. To avoid this, magnetic stirring was no longer used. It is worth noting that the EDTA solution achieved no desorption, which indicates that the affinity of the cations towards the adsorbent is very high.

A desorption percentage superior to 100% was obtained in the test with hydrochloric acid, which could be attributed to an unaccounted amount of copper that precipitated in the particles upon drying, or due to the heterogeneity of the material, meaning that the particles employed could have uptaken more copper and the average uptake was used in the calculus.

The results of desorption tests from A_A+3A with multiple desorption agents conducted in a rotating shaker, with 20 mg of loaded particles and 3 mL of desorption agent, are given in Table B. 2. With the exception of EDTA, all prior desorption agents were further studied. Pertinent results are discussed in section 5.11..

Table B. 2 - Heavy metal desorption from A_A+3A after three hours with multiple desorption agents. Effect of concentration of the cation and regeneration agent.

Cation	Isotherm Initial Concentration /mg L⁻¹	Desorption Agent	Desorption /%	Sample Degradation
Cu	100	HCl 0.5 M	18.4	-
Pb	100	HCl 0.5 M	29.6	-
Cd	100	HCl 0.5 M	24.4	-
Ni	100	HCl 0.5 M	23.5	-
Cu	100	HCl 1 M	91.0	-
Cd	100	HCl 1 M	43.2	-
Ni	100	HCl 1 M	29.0	-
Cu	200	HCl 1M	57.6	-
Pb	200	HCl 1M	61.1	-
Cd	200	HCl 1M	27.5	-
Ni	200	HCl 1M	17.3	-
Cu	100	HNO3 0.5 M	21.1	-
Pb	100	HNO3 0.5 M	53.6	-
Cd	100	HNO3 0.5 M	30.8	-
Ni	100	HNO3 0.5 M	14.7	-
Cd	100	HNO3 1 M	21.5	-
Ni	100	HNO3 1 M	18.4	-
Cu	200	HNO3 1 M	32.4	-
Pb	200	HNO3 1 M	66.1	-
Cd	200	HNO3 1 M	15.7	-
Ni	200	HNO3 1 M	8.6	-
Cu	100	NaOH 0.5 M	5.5	+
Pb	100	NaOH 0.5 M	59.6	+
Cd	100	NaOH 0.5 M	0.1	+
Ni	100	NaOH 0.5 M	23.3	+
Cd	100	NaOH 1M	0.2	+
Ni	100	NaOH 1M	33.9	+
Cu	200	NaOH 1 M	75.1	+
Pb	200	NaOH 1 M	81.3	+
Cd	200	NaOH 1 M	2.0	+
Ni	200	NaOH 1 M	21.9	+

Appendix C

Simulation Details and Optimized Geometries Data



Additional data on the simulations carried out to optimize the geometry of POPTMS and HSPTMS precursors is found in this appendix. Figures C. 1 and C. 3 represent the initial simulation boxes, Figures C. 2 and C. 4 illustrate the atom numbering in the precursor molecule, and Tables C. 1 and C. 2 feature the cartesian coordinates for the optimized geometry of the precursor molecules.

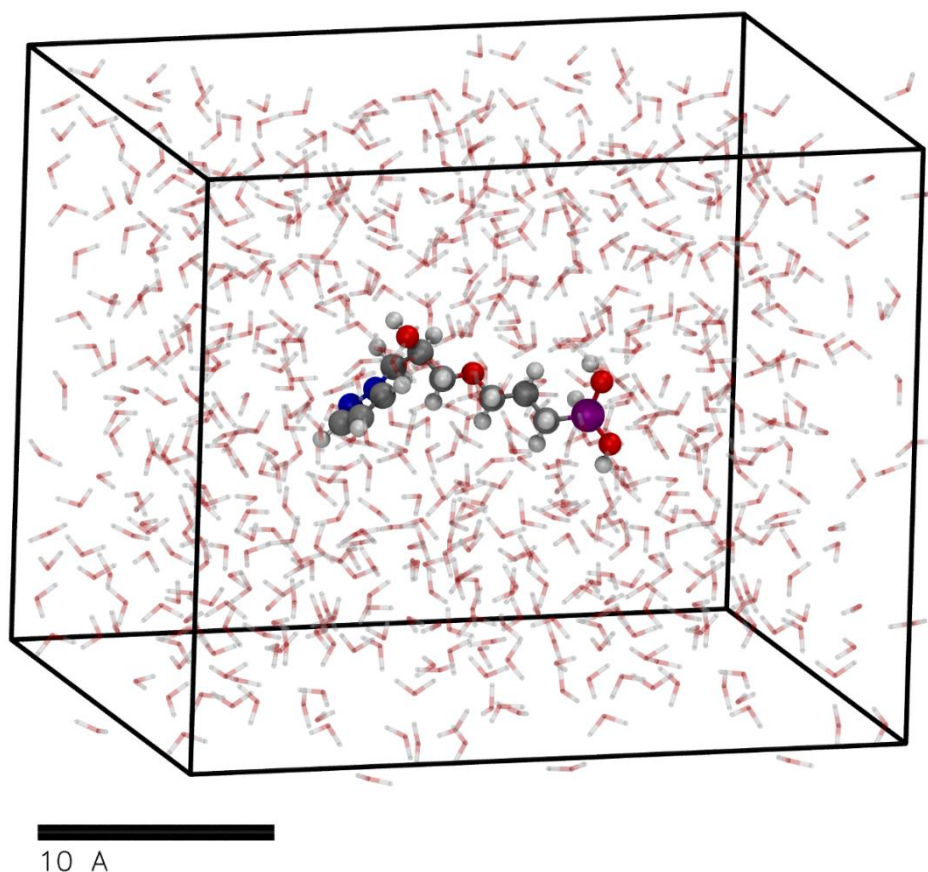


Figure C. 1 - Representation of the constructed simulation box used in the optimization of POPTMS. Dimensions: 2.5370 nm \times 3.1676 nm \times 2.5814 nm. The box contains 663 water molecules.

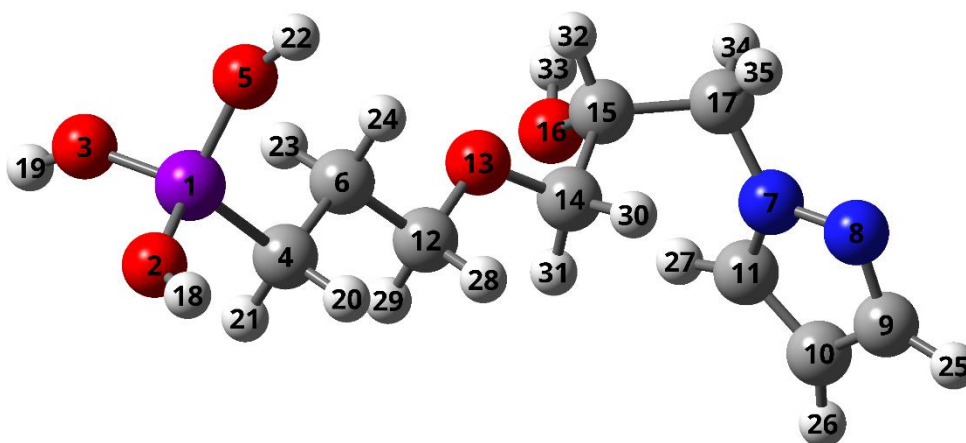


Figure C. 2 - Atom numbering in the POPTMS molecule.

Table C. 1 - Cartesian coordinates of the hydrolyzed POPTMS precursor.

Atom type (Number)	X / Å	Y / Å	Z / Å
Si (1)	10.448	19.391	11.764
O (2)	9.558	20.333	12.763
O (3)	10.212	19.892	10.230
C (4)	9.925	17.525	11.934
O (5)	12.051	19.524	12.000
C (6)	10.906	16.536	11.275
N (7)	12.261	10.067	11.806
N (8)	12.472	9.702	13.079
C (9)	11.494	8.855	13.385
C (10)	10.647	8.671	12.288
C (11)	11.175	9.465	11.288
C (12)	10.540	15.086	11.589
O (13)	11.559	14.268	11.023
C (14)	11.505	12.900	11.386
C (15)	12.501	12.158	10.478
O (16)	11.814	11.716	9.320
C (17)	13.198	10.966	11.163
H (18)	9.514	20.494	13.715
H (19)	9.591	19.911	9.498
H (20)	9.855	17.251	12.993
H (21)	8.918	17.335	11.532
H (22)	12.847	19.507	12.534
H (23)	10.908	16.687	10.190
H (24)	11.926	16.698	11.640
H (25)	11.440	8.415	14.367
H (26)	9.768	8.057	12.233
H (27)	10.850	9.641	10.276
H (28)	10.497	14.914	12.676
H (29)	9.555	14.840	11.160
H (30)	11.776	12.774	12.445
H (31)	10.501	12.477	11.233
H (32)	13.284	12.873	10.175
H (33)	12.446	11.463	8.611
H (34)	13.764	10.411	10.404
H (35)	13.882	11.326	11.933

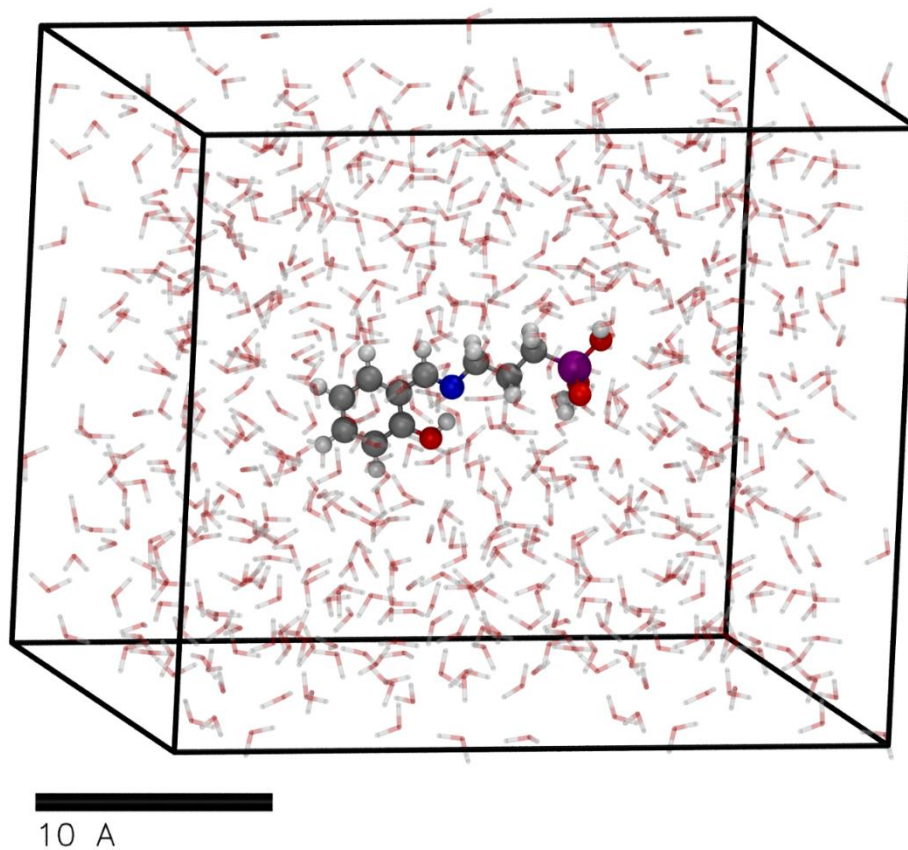


Figure C. 3 - Representation of the constructed simulation box used in the optimization of HSPTMS. Dimensions: 2.6520 nm \times 3.1410 nm \times 2.4120 nm. The box contains 632 water molecules.

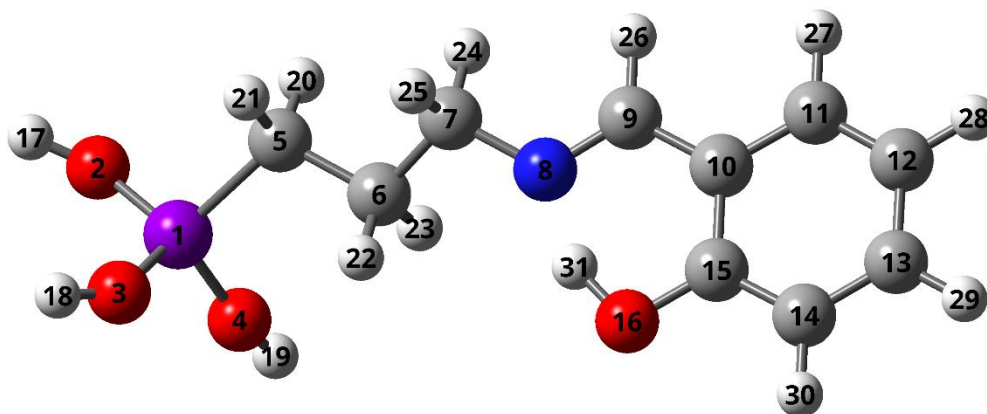


Figure C. 4 - Atom numbering in the HSPTMS molecule.

Table C. 2 - Cartesian coordinates of the hydrolyzed HSPTMS precursor.

Atom type (Number)	X / Å	Y / Å	Z / Å
Si (1)	13.960	19.172	9.061
O (2)	15.227	20.114	8.609
O (3)	12.896	19.988	10.008
O (4)	13.171	18.573	7.790
C (5)	14.645	17.662	10.099
C (6)	13.667	16.470	10.187
C (7)	14.198	15.391	11.131
N (8)	13.295	14.250	11.146
C (9)	13.764	13.065	11.341
C (10)	12.853	11.960	11.505
C (11)	13.318	10.653	11.718
C (12)	12.422	9.611	11.893
C (13)	11.048	9.852	11.831
C (14)	10.569	11.132	11.637
C (15)	11.457	12.194	11.425
O (16)	10.993	13.438	11.252
H (17)	15.668	20.921	8.889
H (18)	12.749	20.762	10.572
H (19)	12.944	18.204	6.937
H (20)	15.600	17.305	9.684
H (21)	14.887	17.982	11.124
H (22)	12.681	16.794	10.549
H (23)	13.521	16.043	9.188
H (24)	15.210	15.076	10.841
H (25)	14.237	15.785	12.155
H (26)	14.837	12.882	11.452
H (27)	14.388	10.474	11.789
H (28)	12.790	8.608	12.076
H (29)	10.349	9.027	11.960
H (30)	9.504	11.317	11.590
H (31)	11.887	14.029	11.164